The private life of small molecules:
Elucidating their molecular mechanisms in plants and in cycloadditions

Bram Denoo

Promoters:
Prof. Dr. Johan Winne
Prof. Dr. Annemieke Madder

Submitted to the Faculty of Sciences of Ghent University, in Fulfilment of the Requirements for the Degree of Doctor of Science: Chemistry

The greatest ideas are the simplest

Lord of The Flies

WILLIAM GOLDING

Acknowledgements

Alas, eleventy–one years is far too short a time to live among such excellent and admirable hobbits. I don't know half of you half as well as I should like, and I like less than half of you half as well as you deserve.

(BILBO BAGGINS in *The Lord of The Rings*)

It has now been six years since I started my PhD in the *department of organic chemistry*, as it was then called. Yet, it seems strange that such a long period of doing research has resulted in all but the 300 pages of this written work. Many of the experiences, if not most of them, cannot be written down but should be told and remembered which is what I would like to do in the following paragraphs.

A first very special word goes to my promotors Johan Winne and Annemieke Madder. Johan and I always had a kind of (profeesional) 'relationship' which has been, at least in my opinion, a rather peculiar one. I got to know Johan during my bachelor project and later during my master thesis and at that time he was not a professor yet, and thus still very active in the lab. Because of this, I have enjoyed the privilege of being thought and introduced into the realm of organic chemistry tips, tricks and cheats first–hand from the master himself. As I chose to pursue a PhD in chemistry I was warmly welcomed in the OBCR group of Annemieke Madder to engage into a collaborative research project in

biology; Johan joined as supervisor. As he later became a professor, I joined his brand new *Organic Synthesis group* to pursue more specific research questions in organic chemistry. I want to express my sincere gratitude to both Johan and Annemieke for the many years of sharing their experience and patience and for giving me the opportunity to work in their labs and become a scientist.

It must be said that one can only function in a somewhat decent condition when there are people around to support you. I have been in S4 for six years, so I have seen many different people come and go; an extensive recital of thank–you's and hope–we–see–each–other–in–the–future's should thus be appropriate. Yet, I do apologize for anyone not making the long shortlist while he or she might definitely have been a substantial part of the agreeable atmosphere that is ever so present everywhere in the department.

First and foremost, I would especially like to thank Jan Hullaert and Mien Christiaens, with whom the *organic synthesis group* was brought to life, for being such a nice people and excellent colleagues. Perhaps this is also the time for some apologies for the things Mien had to endure over the years — largely to be attributed to her horrendous taste in music. This brings me to another special thank you to Brenda, Kamil and Bram Ryckaert who where also excellent people to work with and talk to. I would go those six years all over again on the condition that I can work together with such a remarkable colleagues. Also, Duchan and Bart get the credits for being the nice colleagues whith whom I got to have very interesting (most often off–topic) discussions.

The OBCR group has seen many different faces over the years so this where I will cut the shortlist short. I would like to thank everybody from the OBCR group, though I would like to mention one person in particular. 'Meneer' Jos is the beating heart of the first floor and is always prepared to share a helping hand anytime he could spare one, or to give me five minutes of his time for a seemingly easy–to–solve 'issue'.

The six generations of chemistry students to which I had the pleasure of teaching the art of organic chemistry have been very enriching for me as a person. Each academic

year spawned at least a couple of students which will always hold a special place in my memory. Even more important was the very nice collaboration with 'polleman' Paul during the, sometimes agonizingly long, practical exercise sessions in S4. Paul has gotten and will always keep my deepest respect for being such a nice — almost renaissance — man who will, in the very near future, probably become a skilled chemist himself.

I would also like to thank Jan Goeman for the provided services and advices regarding anything which has a chromatographic column and mass spectrometer attached. Also, Tim ('Timmy') and Dieter do get quite some credits as every NMR spectrum that is written in this work would largely be impossible to obtain without their advice and expertise. The sometimes 'customshop' solutions that they have made possible have proven to be very valuable.

Wim Dejonghe, Kriril Mishev and Jenny Russinova are the odd ones out in this acknowledgements as they are the biologists whith whom I got the pleasure of working together. The entire biology part of this written part would have been impossible without their collaboration. I would like to thank them for the interesting years working together.

A final but very important message goes to my family in general but my wife and children in particular. Without her never–ending support and immeasurable patience, this work would have been lost before it had even begun. Also my two daughters have been very important during the course of this PhD although they do not understand one letter of what their father has been doing their entire life (at least up to this point). The importance of having people around you that you can trust and rely upon has become very clear to me, and I would like to wish for everybody, to be able to have the pleasure and honor to live and work with such a remarkable people.

Bram Denoo

Ghent, 2019

Preface

The main subjects of this work can be divided into two parts which in total contain 5 experimental, 2 theoretical and 2 concluding chapters. The first part focusses on interdisciplinary work on the interface between chemistry and biology. In this, the first chapter introduces the reader into the concepts and some of the background of *chemical biology* and *chemical genetics*. We give an overview of the methodology commonly applied in this field and we address some of the challenges from a chemical point of view. Chapter 2 is a first experimental chapter and describes early investigations into *chemical genetics* strategies to be applied in later research. The third and fourth chapter contain the published experimental accounts of collaborative research between the Organic Synthesis group of prof. dr. Johan Winne and the Plant Systems Biology group of prof. dr. Eugenia Russinova. The results described herein cover the usage of small organic molecules as a tool in biology research. We conclude the first part with a fifth concluding chapter.

The second main part of this work deals with more specific research questions regarding cycloaddition reactions. In this, the sixth chapter, reviews some of the mechanistic considerations to be made on cycloaddition reactions in general and describes some selected examples of known cycloadditions. Chapter 7 describes collaborative research between the Organic Synthesis group and the Center for Molecular Modeling. Herein we discuss the combination of experimental and theoretical efforts to establish a model that can rationalize some of the experimental observations we made in a specific cycloaddition reaction, developed in our lab. These results are currently under review for publication. The eighth chapter largely contains unpublished preliminary experimental work on allyl

cation cycloadditions. We end the second main part with a ninth concluding chapter.

A third part gives a detailed description of all the experiments that were performed to support the findings described in this work. We provide elaborate descriptions of experimental procedures as well as relevant experimental data.

Glossary

AA	Antimycin A.
AFCS	Alexa–Fluor Castasterone.
AIBN	Azobisisobutyronitrile.
ARF	ADP–Ribosylation Factor.
ATP	Adenosine Triphosphate.
BES1	BZR2/BRI1 EMS SUPPRESSOR1.
BFA	Brefeldin A.
BIN2	BRASSINOSTEROID INSENSITIVE 2.
BL	Brassinolide.
BRI1	BRASSINOSTEROID INSENSITIVE 1.
BRZ	Brassinazole.
BR	Brassinosteroid.
CCCP	Carbonyl Cyanide *m*-Chlorophenyl Hydrazone.
CETSA	Cellular Thermal Shift Assay.
CHC	Clathrin Heavy Chain.
CME	Clathrin Mediated Endocytosis.
COPI	Coatomer Complex I.
CS	Castasterone.
DARTS	Drug Affinity Responsive Target Stability.
DHDT	Dihydrodithiin.
EE	Early Endosome.

ES9	Endosidin 9.
$FADH_2$	Reduced Flavin Adenine Dinucleotide.
GAP	GTPase–Activating Protein.
GDP	Guanosine Diphosphate.
GEF	Guanine–nucleotide Exchange Factor.
GFP	Green Fluorescent Protein.
GTP	Guanosine Triphosphate.
HOMO	Highest Occupied Molecular Orbital.
IC_{50}	Half Maximal Inhibitory Concentration.
ISC	Intersystem Crossing.
LUMO	Lowest Unoccupied Molecular Orbital.
MO	Molecular Orbital.
MVB	Multivesicular Bodies.
NADH	Reduced Nicotinamide Adenine Dinucleotide.
PES	Potential Energy Surface.
PMO	Perturbation Molecular Orbital.
SAR	Structure Activity Relationship.
SCD	Secdin.
TGN	Trans–Golgi Network.
TICC	Target Identification by Chromatographic Co–elution.
TS	Transition State.
TyrA23	Tyrphostin A23.
TyrA51	Tyrphostin A51.
WH	Woodward–Hoffmann.

Contents

In biology, nothing is clear, everything is too complicated, everything is a mess, and just when you think you understand something, you peel off a layer and find deeper complications beneath. Nature is anything but simple

(R. Preston)

I

Small Molecules as Tools for Biology Research

Interrogating Brassinosteroid Signaling and Membrane Trafficking in Plants

1 Chemical Biology

1.1. Introduction

For some time now, biology has been studying life at the molecular level. Modern methods have created a pretty clear image of what is to be found in cells when it comes to small molecules and macromolecular structures. However, as new answers often do, scientists are faced with even more questions than the ones they started with:

> "With the dawn of the 21st century genomic sequencing became a widespread and readily available technology. As chemistry outraced the classical phenotypic analysis, all the genes are suddenly known, but most of their functions are not. The greatest challenge confronting all fields in biology is to establish correspondence between genes and discrete biologic functions."[1]

> "Beginning with the mechanistic assertion that living organisms are biological machines, it is incumbent on biologists to understand the workings of these machines. Acquiring a list of parts (proteins) with determinative importance in any particular biological function is often the first step in such understanding. Genetics can provide that list, and it is left to other disciplines (biochemistry, cell biology, and structural biology) to determine how the parts are shaped, where they reside within cells, and how they fit together."[2]

The typical reductionist approach in which cellular subprocesses are studied, has provided some profound insights into smaller parts of the cell machinery (e.g. transcription,

translation, etc.), but in many cases the knowledge of how they interact within the larger complex cellular operating system is still fragmented and remains highly speculative.

1.2. CHEMICAL BIOLOGY

Biological research has come a long way to understand life at the smallest level. Genetic methods have been of vital importance in understanding the way organisms function. Directed or random mutations are key steps to locate and to identify the function of genes. Although these methods are well established and relatively fast when applied in well–known systems, they suffer from some drawbacks. Genome mutations are, in general, hard to control in the sense that they can induce effects that are unpredictable and hard to rationalize. Therefore methods have been and are still being developed that are complementary to the well–established genetic methods.

Even before the era of Mendel and his *Drosophila* experiments,[3] scientists noticed that there is a very powerful way of controlling and influencing the function of genes and their downstream products in the body of proteins and enzymes. As early as the 18th century, scientist realized that chemicals in general can have a profound impact on the way an organism functions and behaves. One of the most notorious examples comes from the work of Joseph Priestley (1733-1802).[4] Inspired by the work of Benjamin Franklin on electricity, Priestley started experiments with gases, of which oxygen is the most known as Priestly is mostly identified with its discovery. To understand the chemistry of these gases, Priestly sought help in biology. He tested the gases on mice and evaluated the chemical properties with the rather brute criterion of observing the mice either being dead or alive, which can be regarded as a very primitive example of phenotypic screening. These series of experiments are regarded as a landmark in a discipline now called *Chemical Biology*. The journal *Nature Chemical Biology* defines the term as:

> "both the use of chemistry to advance a molecular understanding of biology and the harnessing of biology to advance chemistry"[5]

In a sense we can regard chemical biology as a platform for chemists and biologists to gain a more profound understanding of their research field. Simply put, biologists can exploit chemical reactivity to investigate biological systems (e.g. chemical modulation of genes or target identification) or chemists can learn about chemical properties of substances by investigating them in biological contexts (e.g. J. Priestly, *vide supra*).[6] A fine example of chemists gaining biology–driven knowledge about chemistry is found in so–called genome mining in which inactive genes, that were once active in natural product biosynthesis, are re–activated to map the evolutionary history of the natural product or to find new potential drug candidates.[7–10]

Chemical biology has advanced into a highly specialised branch of the life sciences, and requires tight collaborations between biologists and chemists, something which can surely be regarded as the very essence of this discipline.

1.3. The needle in the haystack: genetics and target identification

The human race is faced with large challenges when it comes to, for instance, food production and agriculture but also development of new potent drugs etc. Improving the existing biological systems will thus become inevitable to maintain a sustainable society. Understanding of biological processes is paramount, and will allow biology to evolve from a descriptive discipline into a branch of science that can predict and interfere with biological systems. However, the sheer complexity of cellular systems, populated with vast amounts of possible biological targets which are active in biological processes, makes it a daunting task to identify the relevant components and can literally be regarded as "finding the needle in the haystack".

1.3.1. The central dogma of molecular biology

The central dogma of molecular biology is mainly concerned with the direction of sequence information transfer. As Francis Crick stated:[11]

> "The central dogma of molecular biology deals with the detailed residue–by–residue transfer of sequential information. It states that such information cannot be transferred back from protein to either protein or nucleic acid."

Although contested many times (eg. epigenetics), this simple model explains how genetic information is transferred into functional biological catalysts (enzymes, receptors, ...). In short, the unique sequence encoded in the DNA strands is in a first stage transcribed into a corresponding RNA strand through the function of RNA polymerase. The information passed to the RNA is then translated by the ribosome to an amino acid sequence, also called the primary structure of the protein. From this primary structure follows the secondary structure: the local folding of peptide fragments into α–helices and β–sheets. As the amino–acid side chains interact with each other, the protein folds into a three–dimensional pattern called the tertiary structure. Supramolecular assembly of multiple amino–acid chains is then called the quaternary structure.

1.3.2. Unraveling biochemical pathways

Following Crick's definition stated above, any change in the genetic sequence should be transferred unidirectionally to the shape and function of proteins and enzymes and ultimately to the phenotype. As it is the function of proteins and enzymes we would like to understand, perturbation of its function by changing the corresponding genetic sequence or gene can indeed give us valuable information about the biological system.

Genetics can be divided into two different approaches:[12]

- **Forward classical genetics** starts by randomly mutating the genome followed by selection of phenotypes, showing interesting properties related to the process that is

studied. For example, if a growth–regulating pathway is studied, any phenotype in which growth is either impaired or enhanced, is interesting and will be investigated. Cross–breeding experiments are then applied to identify the gene responsible for the observed change in phenotype.

- **Reverse classical genetics** studies phenotypes that are induced by mutation of a specific gene for which the encoded protein is known as well as its function. This approach however, requires prior knowledge of the studied process.

These genetic methods however, involve some difficulties:

- **Organism viability:** the perturbations are done at the level of the gene, which means that one redesigns the genetic code of the organism. In doing so, there's no way back and any protein that is defectively or differently produced will be done so for the entire life span of the organism. In this way processes which might be vital for the organism can be disrupted, resulting in premature death, before any phenotypic properties can be investigated.
- **Gene redundancy:** redundancy means that there exists a set of genes coding for a homologues set of proteins of which each member has the same function.[13] This means that single–point mutations in one of the redundant genes are less likely to be translated into an aberrant phenotype; the non–mutated functional genes will take over. This can be considered as 'natural' protection against mutations and arises through gene duplication and divergent evolution.

An alternative method from the chemical biology toolbox is so–called *chemical genetics* which can be defined as:

> "The study of gene-product function in a cellular or organismal context using exogenous ligands"[14]

Instead of changing the function of proteins by altering their coding genes, small organic molecules are applied as ligands to proteins, perturbing their function and serving as 'the mutation'. Again two approaches exist:

- In **forward chemical genetics** a small molecule is administered to the organism. The change in phenotype is then correlated to the binding event to one or more proteins which are then identified with their corresponding gene by classical genetic experiments or the small molecule itself is applied as means to improve the organism's performance. In this case molecules are screened and selected for interesting phenotypes.
- **Reverse chemical genetics** starts from a known biological target, which is part of a biochemical pathway and possibly identified via classical genetic methods, for which a small molecule ligand is identified. This is the prevalent method in modern drug discovery.

One obvious advantage of chemical genetics is the reversibility of the effect. As the small organic molecules are metabolised or excreted, in the case of covalently bound ligands, ligand–bound proteins are degraded, the natural state of the organism is restored, which also addresses the issue of impaired viability due to mutation of essential genes. Problems with redundancy are also less likely as the small molecule will often target the entire set of homologous proteins since they are structurally related.

1.4. Target identification strategies

Strategies for the identification of cellular targets of biologically active small molecules can be roughly divided into four groups and depending on the expertise of the researchers as well as the facilities available, any of these methods or a combination thereof can be applied to identify a target. As the main focus of the methods described in the chapters to follow is chemistry oriented, we shall limit an in depth discussion to the direct biochemical approaches.

- Direct biochemical or affinity–based approaches,[15]
- classical genetics–based approaches,[16]

- phenotype–based approaches,
- computational approaches.

1.4.1. Affinity–based approaches

Affinity–based approaches are the more classical methods in the chemical biology toolbox. They rely on the direct interaction between the small molecule and its putative target, hence the name 'affinity–based'.

Any small–molecule affinity probe is essentially built up by three parts: the ligand (the small molecule of interest), a sorting unit (matrix or functional tag) and a linker (connecting the ligand with the sorting unit). The entire construct of ligand, linker and sorting unit is then called *affinity probe*. Affinity purification in general exists of incubating cell extracts with the affinity probe followed by purification and isolation of the protein target (target pull–down, fig. 1.1).

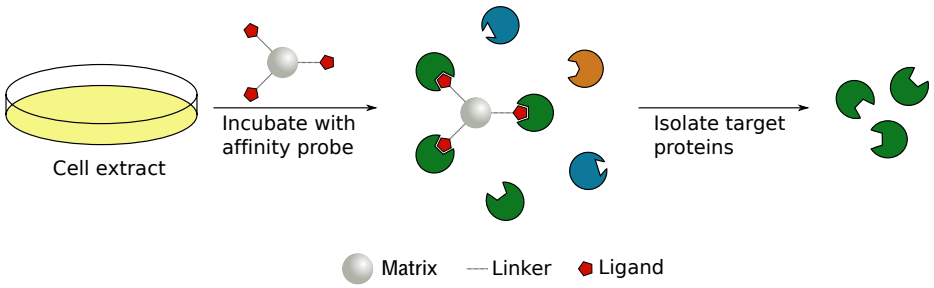

Figure 1.1. – General scheme for affinity purification

The construction of the so–called affinity probe faces researchers with some challenges. Once a hit compound is identified, this molecule has to be chemically modified in order to attach the linker and the sorting unit. The development of a functional affinity probe is dependent on a plethora of parameters each of which have to be monitored and controlled carefully.

A first point of attention is location of suitable chemosites where the linker, and subsequently the required sorting unit, should be attached. This is especially difficult in the case of small organic molecules of which there is no information about their structure activity relationship (SAR), which is aimed at finding the structural elements that are necessary for activity and which places in the molecule can be changed without losing activity. As a consequence, chemists are burdened with a lot of (sometimes lengthy) syntheses in order to establish SAR around a given molecule.

Once a suitable region of modification is identified, the next step is introduction of a suitable linker. Most of the time one finds dimers or trimers of ethylene glycol as these are found to be the most reliable. The most important factor that influences the applicability of an affinity probe is the linker length. Is the ligand attached to a solid phase bead or a biotin molecule, the sorting unit should extend far enough out of the active site where the ligand binds not to disturb the ligand–protein interaction. The presence of the linker itself, although necessary, might introduce some problems as well. Since the linker is a small molecule in itself, false positive targets arising from non–specific linker–protein interactions which are sometimes unrelated to the ligand–target binding, might impede the target identification by generating high background noise. Because of this, linker length and polarity (hydrophobicity/hydrophilicity) are parameters that should be tuned. Also, since we can regard the affinity probe as an above–average sized molecule, problems with solubility in the aqueous environment and bio–availability may arise. The relatively hydrophilic polyethylene glycol linkers can help to meet these requirements.

A final point to consider is the protein–ligand interaction strength. Since most small molecules exhibit their action via non–covalent interactions, binding strength can have a profound impact on the efficacy of the affinity, especially with regard to the detection. Weak interacting ligands will give weak read–outs in the pull–down experiment. Similarly, should the ligand target be a protein that is not abundant, the same issue arises. Therefore, SAR studies can meet the need for more active ligands but again at the cost of laborious syntheses of small molecules. Also, small organic ligands can bind multiple

targets at the same time. While this is most likely so for redundant proteins and highly desirable in that case, non–specific interactions with multiple (high abundance) targets again will raise the issue of high background noise and false positives. Elaborate SAR is paramount and the molecules should have as few targets as possible (Selectivity), be able to reach their target (Permeability), be active in low doses (Potency) and have the appropriate structural elements to exhibit its mode of action (Structure) (fig. 1.2).[17]

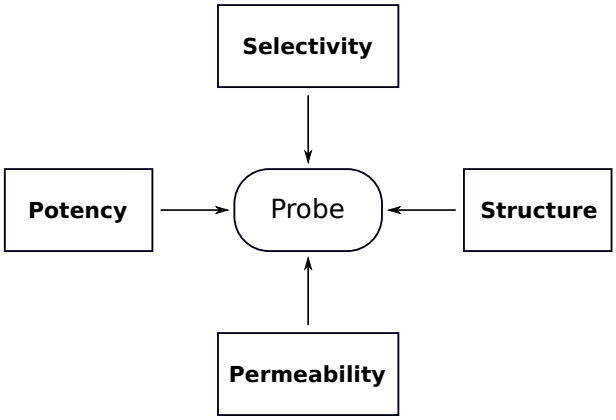

Figure 1.2. – The criteria to design a functional affinity–probe (adapted from Bunnage *et al.*[17])

1.4.1.1. Target pull–down techniques

The building of affinity probes can rely on quite some different techniques. The most direct possibility are *matrix–bound affinity probes* in which the ligand is connected directly via a linker to a solid–phase matrix like sugar–based sepharose or agarose beads. Incubation of cell extract with these solid–supported affinity probes, then allows the isolation of the target by gravity filtration of the target–bound beads. A more exotic matrix–bound probe was developed by Handa and co–workers by linking so–called Ferrite–Glycosidyl methacrylate (FG) beads to the ligand.[18] FG beads are magnetic and after incubation, targets can be isolated by magnetically removing the beads from the lysate. Handa and

co–workers identified the thalidomide–target cereblon (CRBL) by using a thalidomide analogue (**1.1**) to construct an FG–based affinity probe (**1.2**) (fig. 1.3). CRBL is part of a functional complex, which is inhibited by CRBL–binding of thalidomide, triggering the downstream down–regulation of *fibroblast growth factor 8* (*fgf8*), which is involved in limb growth.[19]

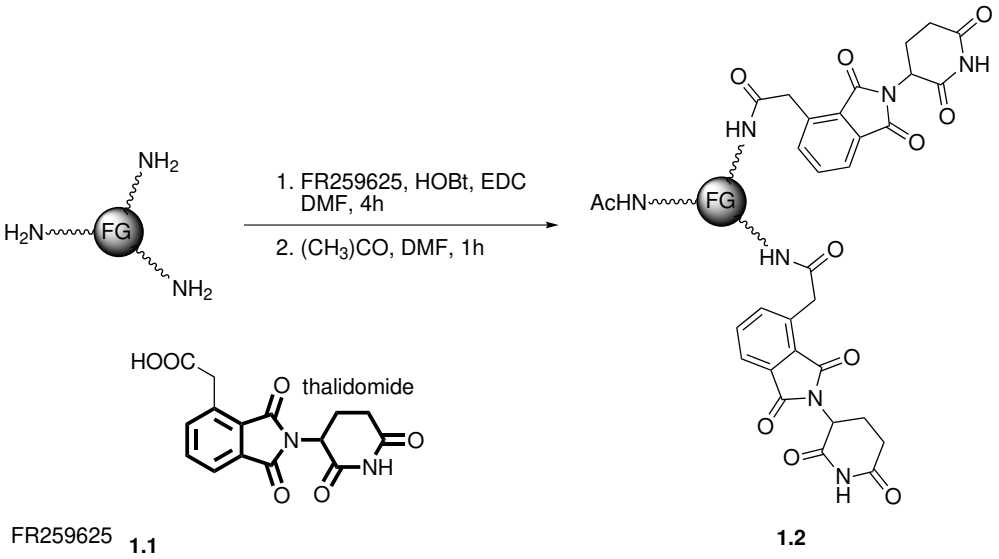

Figure 1.3. – FG–immobilised thalidomide probe

Also, the ligand can be connected to a so–called *functional tag* for visualising ligand–bound targets on Western blot; these include the incorporation of radioactive isotopes, which are most often incorporated into the ligand itself, or fluorescent groups (e.g. rhodamine, fluoresceine) which are generally connected via a linker.

Other functional tags allow for the direct target isolation, similar to the matrix–bound probes. The most representative method is incorporating biotin, which enables isolation of the target–bound affinity probe, by retention on an immobilised streptavidin or avidin column; two proteins that have a very strong interaction with biotin. An overview is given in fig. 1.4.

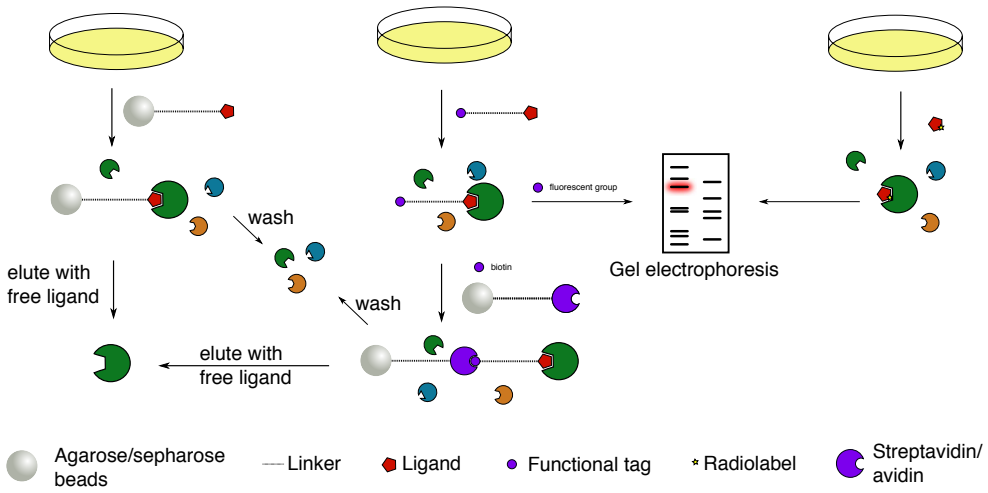

Figure 1.4. – Matrix–bound and functional tag–based affinity purification methods

We discussed earlier that modification of small molecule ligands requires careful tuning of different parameters such as linker length. Also, weak interactions or low abundant targets can offer big challenges when designing functional affinity probes. Some techniques can (at least partially) remediate these issues.

Problems with activity loss by introduction of a (bulky) linker can be solved by using so–called *bio–orthogonal linking*. The linker and sorting unit can then be attached to the small molecule in the biological system itself, minimizing any perturbing influences on the interaction event. The most commonly encountered examples are Huisgen (2+3)–dipolar cycloaddition of azides with alkynes and Staudinger ligation of triphenylphosphine with azides.

The problem of weak interacting ligands can either be solved by extensive SAR to generate a more active ligand, or by introduction of a group that covalently binds (cross–links) the sorting unit to the target protein, making the successful identification independent from the interaction strength.

One possible cross–linking method is *reactive–group labeling* which makes use of an affinity probe which is designed to contain a reactive chemical group (e.g. epoxide, to-

sylate) and for example a fluorescent group.[20,21] Upon ligand binding to the target protein, specific residues on the target protein surface can react with the reactive group and thereby covalently link the affinity probe which contains a fluorophore to the target protein. Subsequent visualisation then allows target identification.

Similarly photo–affinity tags like benzophenone or diazirine, allow the covalent linking of the entire construct (ligand–based probe) upon UV–irradiation (fig. 1.5). These groups produce very reactive radical or carbene intermediates which react with a whole array of functional groups on the protein surface. By this, the entire small molecule–probe is covalently attached to the target and, depending on the sorting unit, affinity purification can then be performed.

Although the covalent labeling methods can help in case of weak ligand–protein interactions or low–abundant targets, caution should be taken. These methods rely on highly reactive species and the risk of false positives arising from non–specific cross-linking is higher when using these techniques.

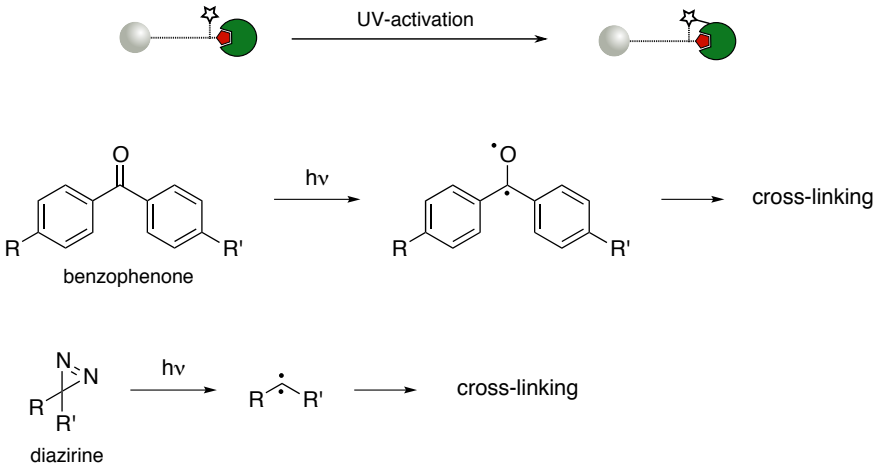

Figure 1.5. – Photo–affinity labeling of target proteins

1.4.1.2. Label–free methods

All of the techniques we described above, rely on the incorporation of an isolation tag. In this section we will describe some methods that are label–free, which means that they are still affinity–based but do not make use of an affinity matrix. For all these techniques, some idea of the possible target proteins must be known, obtained for example by affinity purification, therefore these methods are often applied in validation experiments.

A first big class of label–free techniques are based on the idea that the observable properties of proteins change when they are bound to a small molecule ligand. Based on this principle we can distinguish three methods that have been used in target identification research.

Cellular thermal shift assay or CETSA, is based upon the idea that ligand binding stabilizes the protein towards thermal denaturation.[22] This effect can be observed using living cells, heating them with or without compound treatment. The term 'thermal shift' then comes from the observation that the melting curve of a protein shifts when bound to a small molecule (fig. 1.6a).

A second method is *target identification by chromatographic co–elution* TICC and is based on a specific shift in retention time when comparing the unbound protein and/or ligand with the protein–ligand complex. The dynamics of the exchange should be slow to avoid coalescence of the peaks (fig. 1.6b).

The last possibility is *drug affinity responsive target stability* or DARTS and is based upon the observation that a protein's susceptibility to proteolytic digest decreases when bound to a small molecule.[23] The ligand binding event should be an overall stabilising process, making a bound protein less susceptible to protease digest (fig. 1.6c).

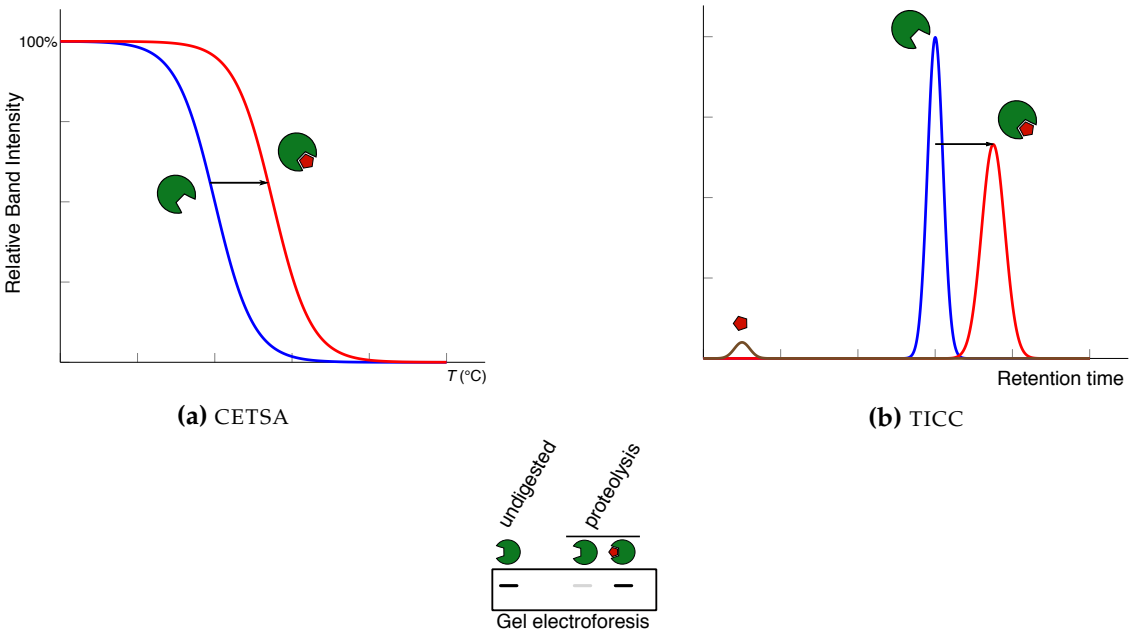

(a) CETSA **(b)** TICC

(c) DARTS

Figure 1.6. – Label–free methods for affinity–based target identification

1.4.2. Proteomics: from purification to identification

The techniques described in the previous sections are an essential part of cellular target identification. However, except for the label–free methods, the use of affinity probes only enables isolation of possible targets. By running a gel electrophoresis experiment, one can identify proteins of interest. Affinity probe pulldown and subsequent release of possible targets form the affinity matrix can point at possible targets for the molecule of interest. By extracting and digesting the relevant protein material, the resulting peptide mixture can be analyzed with HPLC–MS techniques to characterise the isolated proteins. The obtained sequence information is then compared with general protein sequence databases to identify the putative target. By multiple experimental repeats, a list of one or more possible targets is obtained which can then be experimentally validated (fig. 1.7).

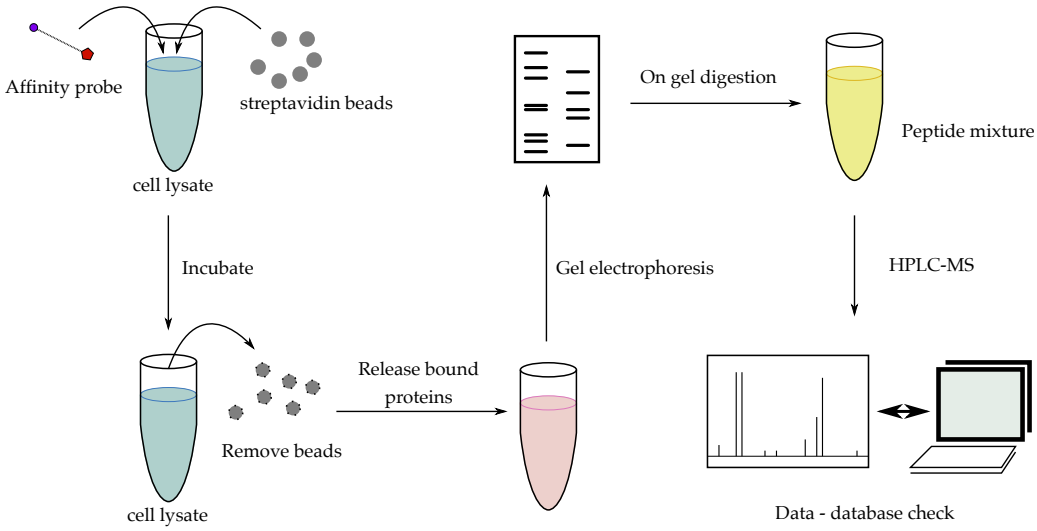

Figure 1.7. – Workflow for proteomics analysis

1.4.3. Other target identification techniques

Apart from the classical affinity–based techniques, we had mentioned three more possible methods that can be applied in target identification research. A first alternative are the so–called phenotypic methods which compare the biological/phentotypic profile of small molecules with that of known reference ligands. Just like the two other methods we will discuss, this is a rather indirect method as the target is not really isolated.

A second possibility is the use of classical genetics techniques. Assessing the small–molecule sensitivity of single–knockout mutant organisms can point to genetic loci which are involved in the studied pathways.[16] Most of the time, these methods are found to be used in conjunction with the affinity–based techniques, in order to validate the identified targets.

The last method, the computational approach, is in one aspect comparable to the phenotypic methods we described earlier. In general, these computational approaches can be divided into two classes. The ligand–based approach relies on pattern recognition

through connecting small molecule profiles to reference databases of small molecules with known modes of action ("landmark molecules"). The structure–based approach makes *in silico* predictions of ligand–target interactions.[16]

1.5. Chemical biology in plant research

The field of plant chemical biology has been expanding rapidly during the last decades. A lot of information of biological targets is known for mammalian systems,[24,25] mainly because of the advances in drug discovery. Although small organic molecules have been shown to be very valuable in plant biology research,[26] the number of identified targets is still rather limited.[27]

Plant chemical biology has mainly focussed on only a few target identification approaches. Genetic approaches are the most frequently encountered and an example is the identification of P-glycoprotein19 as a target of gravacin, a gravitropism inhibitor in *Arabidopsis* (fig. 1.8).[28] Phenotype based methods have for instance been applied in identifying two salicylic acid glucosyltransferases as targets of the imprimatin series of small molecules, which increase pathogen resistance in *Arabidopsis* (fig. 1.8).[29] Also *in silico* methods have been used to identify targets such as monogalactosyldiacylglycerol synthases — responsible for the biosynthesis of critical galactolipids in photosynthetic membranes — which are inhibited by galvestine–1 (fig. 1.8).[30]

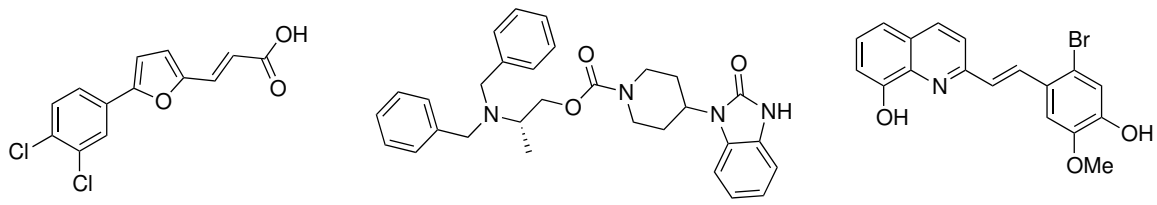

Gravacin Galvestine-1 ImprimatinA1

Figure 1.8. – Examples of small molecules for which a biological target is known in plants

Although these approaches have prove to be successful in a number of cases, it must be noted that affinity–based approaches are largely unexplored.[31]

1.6. Conclusions

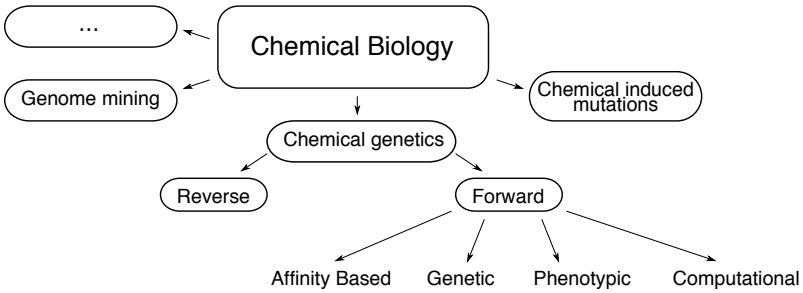

Figure 1.9. – Chemical Biology Flowchart

Despite the challenges encountered with affinity–based target identification, these method have proven their value in numerous occasions and are still developed further in order to speed up and facilitate biology research and by extension drug development. For reasons described before (section 1.3.2), affinity purification still is a method that is very often superior to the more classical forward genetic methods.

The success of affinity purification research largely depends on the joined efforts of chemists and biologists. One of the biggest challenges lies in the derivatization of small molecule ligands to collect SAR information and eventually construct affinity probes. Synthetic organic chemistry is a well established branch of science that can benefit from the knowledge of a large array of reliable and well–documented chemical transformations, allowing for the generation of a tremendous amount of different organic molecules, despite the sometimes lengthy parcours. Also, the creativity of many chemists and biologists allow for interesting and promising methods to be developed in the very near future.

Of particular interest for this work are affinity–based approaches plant chemical biology which will be the main focus of the chapters to follow.

2 Developing a generic derivatisation strategy

2.1. Introduction

In the previous chapter we discussed the possibilities of using small molecule ligands to dissect biochemical pathways. Essential is derivatisation of these ligands in order to obtain useful analogues and functional affinity probes. In order to achieve this, the researcher can adopt different strategies. Either the small organic molecule is armed directly with an appropriate chemical handle to which a linker and sorting unit can be attached ('diversity–oriented' or 'late stage' derivatisation) (fig. 2.1a), or the molecule is resynthesised during which strategic choices are to be made on how and when the necessary handles are introduced ('target–oriented' derivatisation) (fig. 2.1b).

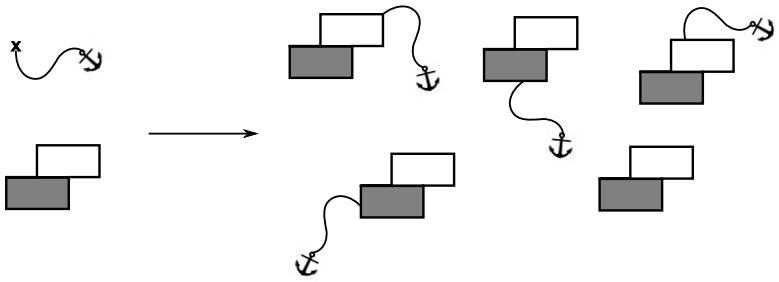

(a) Diversity–oriented/late stage derivatisation

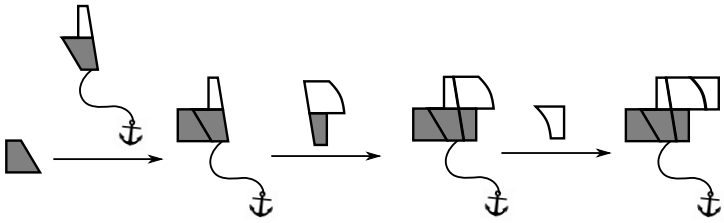

(b) Target–oriented derivatisation

Figure 2.1. – Different derivatisation strategies

As screening compounds are often produced by highly reliable synthesis steps in high–throughput combinatorial chemistry, using only a limited collection of possible reaction partners, using alternative building blocks is not always straightforward. However, establishing SAR becomes even more problematic when complex natural products are used. Modifications to the original carbon skeleton should then certainly rely on functionalities found in the molecule itself, since *de novo* synthesis of analogues with a slightly altered substitution pattern is time–consuming, often costly and quite challenging. The more direct strategy of harvesting the intrinsic reactivity of the ligands themselves, and derivatise them directly has gained quite some momentum in recent years as 'late stage' or 'CH–functionalisation' approaches.

2.1.1. *De novo* synthesis of small molecule probes

De novo synthesis of small molecule library members is the most general but also the most time–consuming method. This is especially the case if no previous SAR information on the initial hit compound is available, or if the compounds themselves are synthetically challenging (e.g. trapoxin fig. 2.2).[32,33]

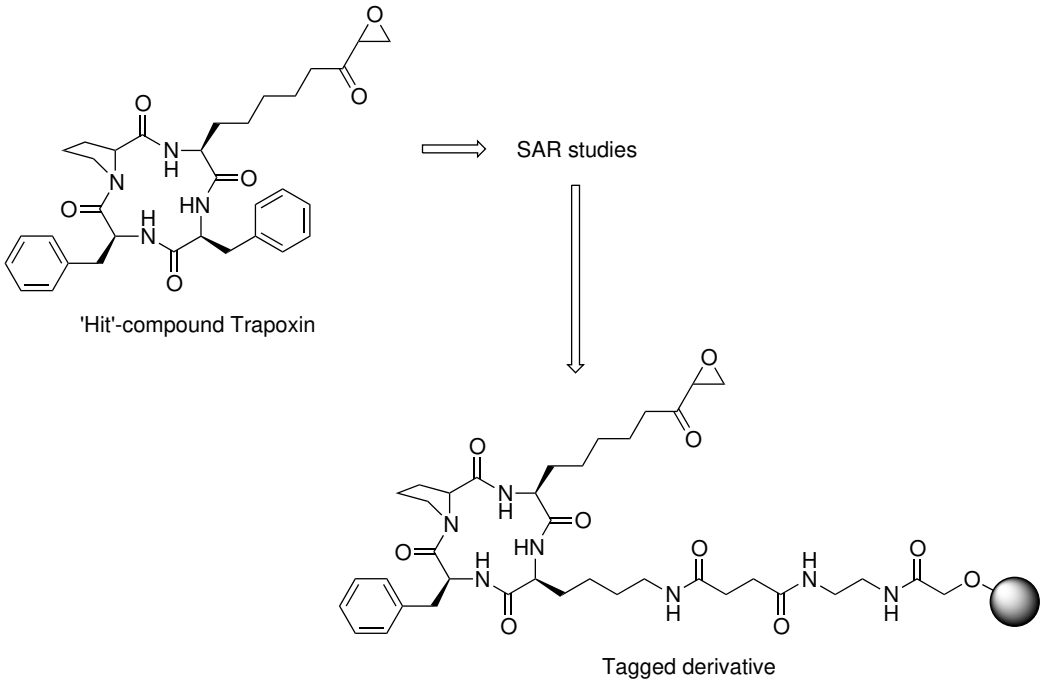

Figure 2.2. – Classical target–oriented derivatisation strategy

2.1.2. Tagged libraries

One of the best–known examples of direct "hit derivatisation" strategies is the use of tagged libraries. In this approach, all members of the libraries that are used in the biological screenings share a common substructure or functional group that can be exploited for direct site-selective derivatization.

The essence of a tagged library strategy lies in the incorporation of a protected linker moiety during library building. Interesting examples are found in the tagged libraries of triazine hits (fig. 2.3 and fig. 2.4).[33–35] This is only a minor variation on the classical strategy of derivatisation and although resynthesis and SAR–analysis is indeed avoided this way, this approach is limited to synthetic libraries and cannot be applied to natural product libraries. In a way, one could argue that instead of avoiding the problem of synthesis, it mostly moves it to the library synthesis stage. It does have the advantage of direct identification of suitable anchoring sites for linker attachment as they are already an integral part of the screened molecules.

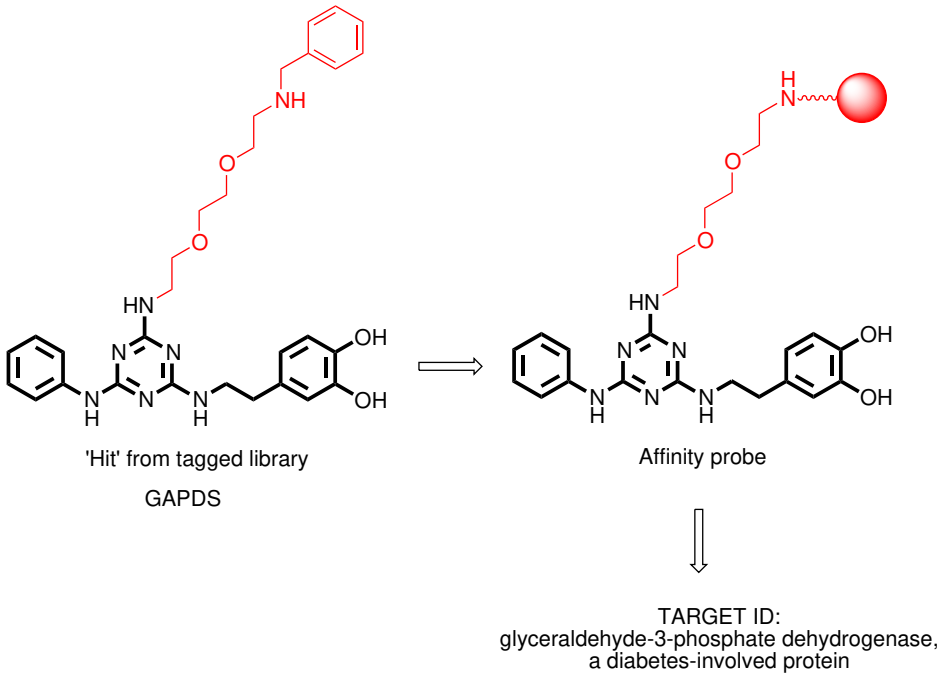

Figure 2.3. – Tagged–library approach for target identification: GAPDS target identification

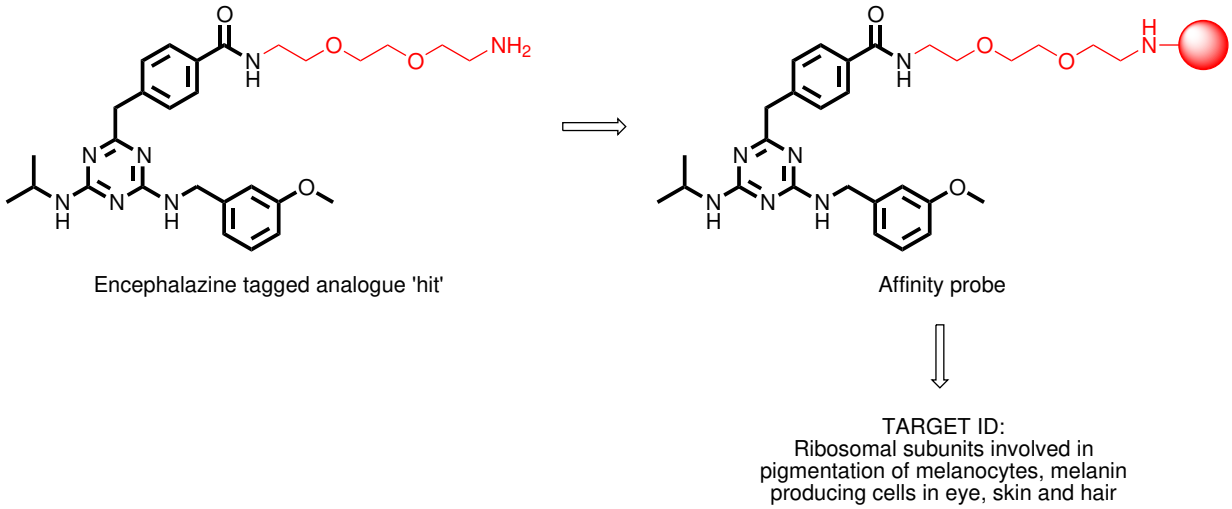

Figure 2.4. – Tagged–library approach for target identification: Encephalazine target identification

2.1.3. Functional group transformation

Another approach is the one in which libraries are built by harvesting the inherent reactivity of functional groups present in the molecule. This approach is especially well-suited for SAR–analysis of complex natural products. Fine examples are found in the works of Romo and co–workers where they develop methods to insert carbenes into OH–bonds (fig. 2.5),[36,37] as well as mild iodination techniques to derivatise aromatic substructures (fig. 2.6).[38]

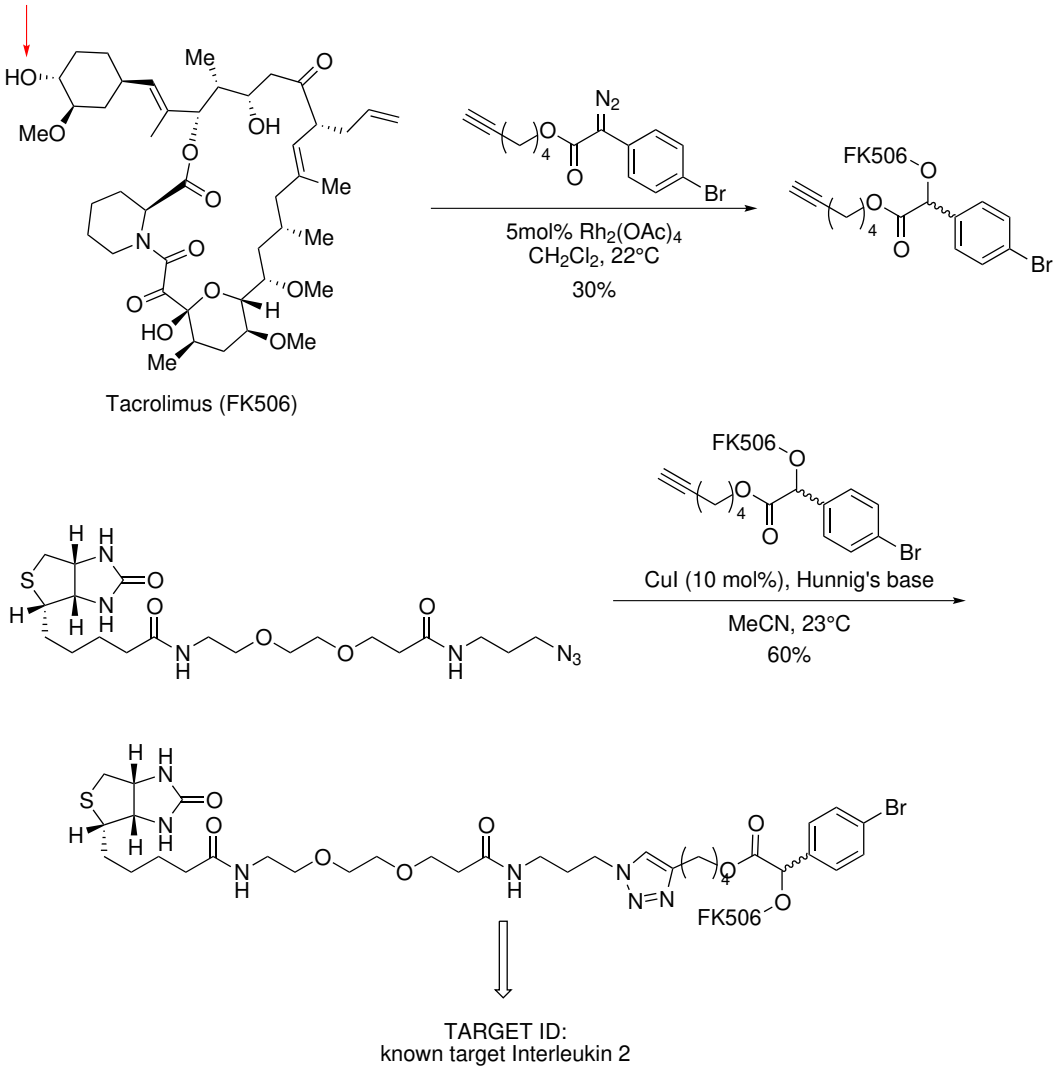

Figure 2.5. – Direct derivatisation strategies for natural product tagging: Diazo–reagents for OH–bond insertion

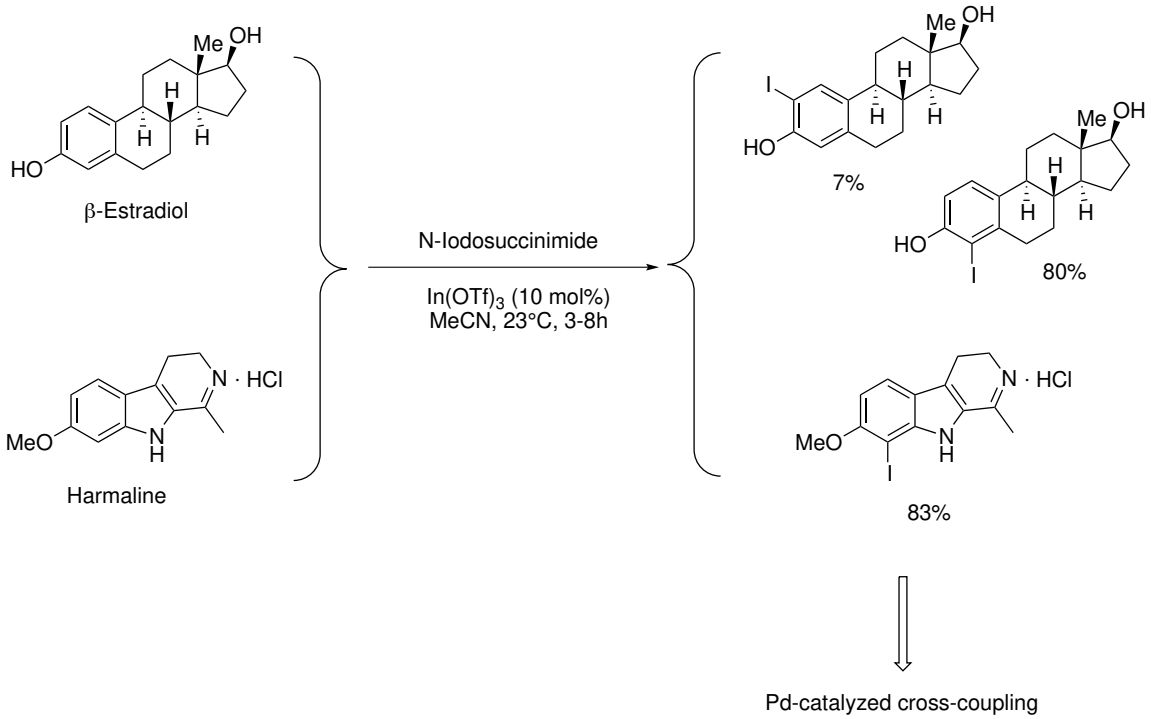

Figure 2.6. – Direct derivatisation strategies for natural product tagging: mild iodination of aromatic–group containing natural products

2.1.4. CH–activation methods

A still developing field in the area of organic synthesis, research into so-called CH–activation methods, seems particularly well–suited for application in a diversity–oriented derivatisation strategy.[39] CH–activation methods are intentionally aimed at provoking reactions at unfunctionalised CH–bonds. These modern synthetic methods rely on highly reactive species or intermediates which are directed somehow to favor one specific CH–bond in a molecule (usually via proximity, stereo–electronics or using specifically designed catalysts).

Recently, D. Romo and B. F. Cravatt presented a very interesting example by using this approach.[40] The 'random' insertion of a nitrenoid species into CH– and olefinic bonds is

applied, a CH–activation method which was originally developed by J. Du Bois and co-workers.[41,42] A reagent was used which contains a clickable alkyne group, a linker and a sulfamate group. Du Bois and co–workers had found that the sulfamate had superior characteristics regarding the nitrenoid formation and consecutive CH–insertion reactions. The procedure was optimized and applied on a range of natural products (cf. fig. 2.7) and by doing so, they successfully identified the target protein(s) of the known natural product eupalmerin acetate.

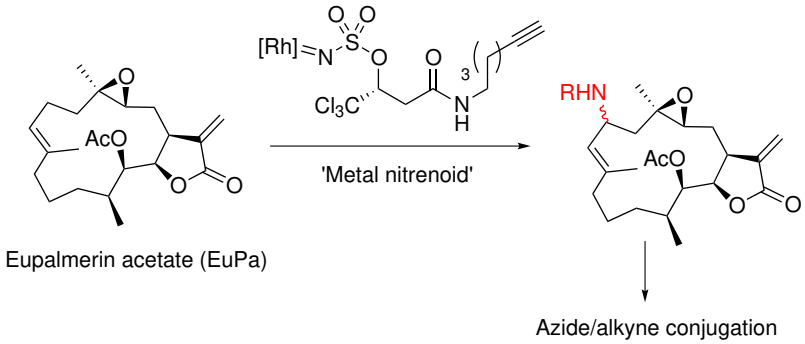

Figure 2.7. – Conjugation sequence for eupalmerin acetate as developed by D. Romo and B. F. Cravatt

2.1.5. "Random" photochemical immobilisation

An interesting approach has been described that is based on photo–affinity labeling.[43–45] The general idea is that a highly reactive species is generated photochemically on a solid support, in the presence of a solution of a biologically active small molecule (fig. 2.8). The reactive group is expected to react with the small molecule in an almost statistical manner, resulting in the solid support functionalized with the small molecule. Not all immobilized molecules will still be able to bind their biological target, but some should. Thus, the resulting solid support can be used as an affinity matrix for selective protein

isolation. In this way the process of SAR–evaluation is conveniently bypassed. However, this methodology is limited to one specific strategy for target identification, which is not very modular or "tunable".

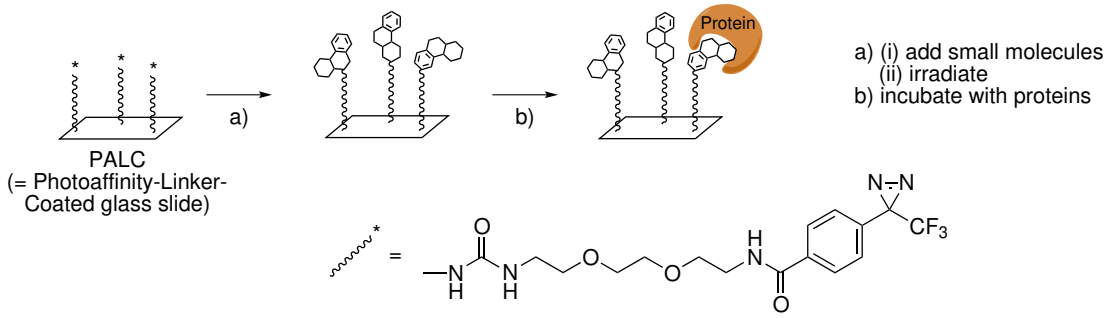

Figure 2.8. – Derivatized glass slides for target pull-down

2.2. Initial explorations: CH–functionalization reactions for diversity oriented derivatization

The group of E. Russinova identified several bioactive molecules which were of particular interest in plant biology, secdin and endosidin9 (fig. 2.9). There was large interest to generate SAR information around these molecules, as well as to develop functional affinity probes to dissect the involved biochemical pathways (see chapters 3 and 4). We chose to adopt a direct derivatisation strategy and we explored several possibilities in order to establish a generally applicable method to develop analogues and functional affinity probes.

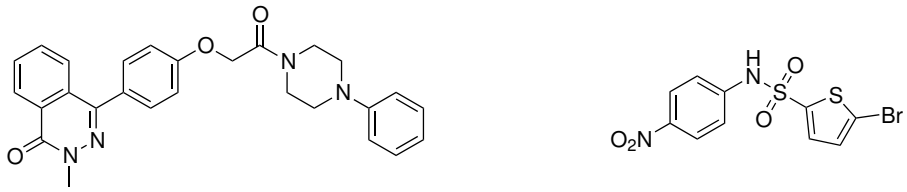

Figure 2.9. – Bio–active small molecules as basis for a generic derivatization strategy

For CH–activation methods in the context of diversity–oriented derivatization as outlined above, the prevalent issue of inherently hard–to–control regioselectivity can be regarded as an asset.[46] Indeed, whereas in classical synthesis projects CH–derivatisation should only occur at a limited number of positions, applied in this context, this method should target as many positions as possible. Therefore, a few state–of–the–art CH–functionalization strategies have been chosen as the initial methodologies of interest for this work.

2.2.1. Carbene insertion

One of the key challenges in CH–functionalization is the strong covalent character of the CH–bond, which makes it unsuitable for classical polarity–driven or ionic reactions. One way to circumvent this problem is to use the reactivity of radicals or even more so carbenes. These neutral but highly electron deficient species can be generated from relatively simple precursors without the need for a chain mechanism. These species are classically used in organic synthesis for the synthesis of cyclopropanes, as they readily undergo a cycloaddition with simple alkenes. However, by using transition metal catalysts, their extreme reactivity can be channeled towards other reaction types. The most interesting reaction is the insertion of a metallo–carbenoid species into a CH–bond. Carbenes can also be generated without transition metal catalysts, which usually gives very reactive species that behave as diradicals. Thus, photochemically generated carbenes can insert

into CH–bonds by way of a radical hydrogen abstraction and recombination of the two resulting radicals (cf. diazirine photo-affinity labeling).

The characteristic danger in synthesizing and using diazocompounds as well as the high cost of rhodium catalysts promoted us to explore alternatives. Moreover, photochemical methods proved to be rather difficult as reliability of UV–lamps is paramount in these type of reactions. Also thermal generation of carbenes did not yield any satisfying results as can be seen for example in the case of secdin (fig. 2.10). The starting molecule SCD was left intact, whereas the diazo compound was found to dimerize.

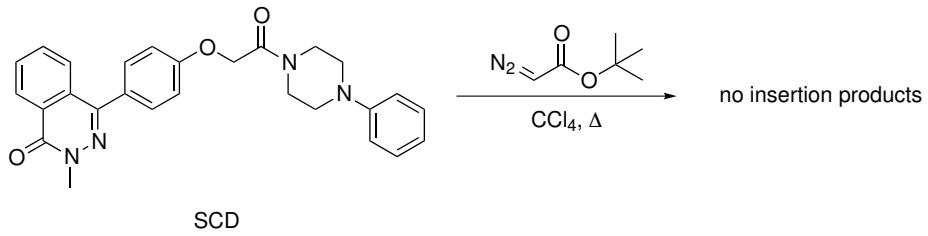

Figure 2.10. – Attempted thermal carbene insertion

2.2.2. Biomimetic CH–oxidation

The biosynthesis of many important natural products (nature's small molecule protein ligands) often involves late–stage and site–selective oxygenations. There are numerous enzymes which can convert unactivated CH–bonds into functionalized positions (alcohols, ketones, ...). However, such highly specific oxidations remain very challenging for synthetic chemists. A number of interesting methods have been described that approach these efficient enzymatic transformations.[47–51] These methods offer interesting opportunities to 'arm' bioactive small molecule ligands with a hydroxyl group or a ketone (aldehyde). Such functional groups can provide excellent handles for further derivatization.

In our lab, initial explorations of doing SAR around the plant hormone stigmasterol were performed (fig. 2.11). Our method of choice was biomimetic oxidation of the stigmasterol skeleton in order to find analogues of the well–known brassinosteroids brassinolide and castasterone, widely used in biology (chapter 3). Experimental tests proved even the intrinsic reactive sites of stigmasterol difficult to derivatise and therefore, no further effort was invested in the development of this method.

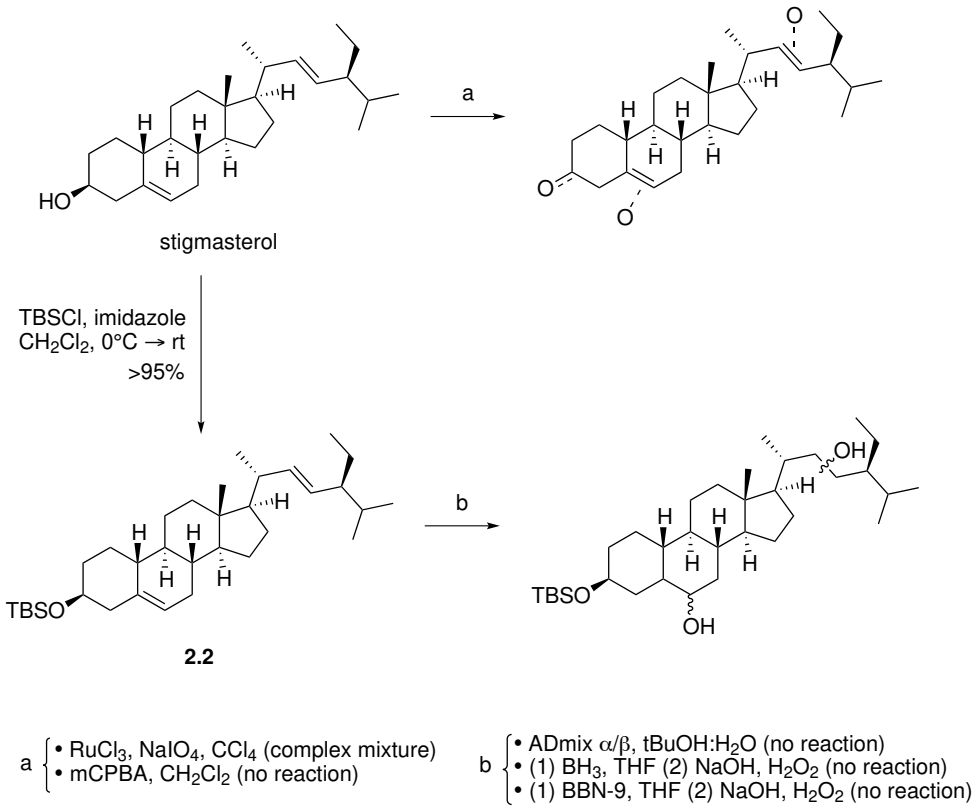

Figure 2.11. – Oxidative derivatisation of stigmasterol (Bachelor Project Andres Luttens)

2.2.3. Aromatic substitutions as CH activation

Several of the modern CH–functionalisation reactions are actually based on one of the oldest types of substitution reactions: the electrophilic aromatic substitution. Technically

this is not to be called CH–activation and the main issue in this type of transformations has been to overcome the regioselectivity of the reaction which is strictly dominated by the electronic characteristics of the arene ring. Because of the ubiquitous occurrence of aromatic rings in typical screening library members, this reaction might also be of use in a diversity–oriented derivatization strategy. The presence of halogens would be of interest as these enable substitution with several possible tags by palladium–catalysed cross–couplings. The necessary halogen atom could be introduced by standard electrophilic aromatic substitution reactions as can be seen for the bromination of **2.3** (fig. 2.12).

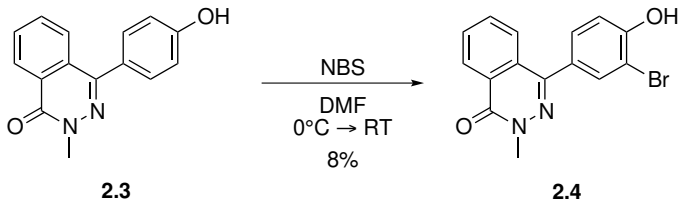

2.3 **2.4**

Figure 2.12. – Bromination of building block **2.3**

The introduced aryl bromide can be used in further derivatisation steps to introduce a linker and sorting group. Initial tests that were done in our lab for the derivatisation of **2.5** showed however some difficulties for replacement of the bromine atom, in particular in terms of chemoselectivity towards other functional groups. However, a Stille reaction with **2.6** proved this palladium–catalysed cross-coupling to be an efficient and reliable method to introduce an allyl tag on a relatively complex and functionalised compound.

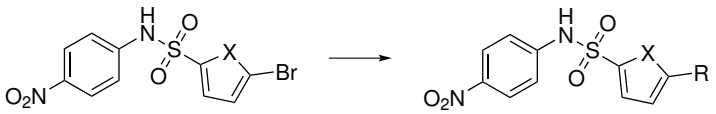

2.5 X: S
2.6 X: CH=CH

entry	X	Coupling partner	R	conditions	yield
1	S (**2.5**)	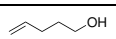	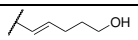	$Pd(PPh_3)_4$, base	complex mixture
2	S (**2.5**)	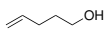	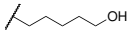	$Pd(PPh_3)_4$, 9-BBN	reduced nitro group
3	S (**2.5**)	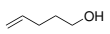	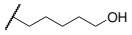	$Pd(PPh_3)_4$, $(Cy)_2BH$	reduced nitro group
4	CH=CH (**2.6**)			$Pd(PPh_3)_4$	69 %

Table 2.1. – Palladium–catalysed cross–couplings for derivatisation of **2.6** and **2.5** (entries 1 to 3: Bachelor Project Jan Hullaert, Bart Vanderstraeten, Tom De Saedeleer)

2.3. ALLYLATION: A SIMPLE DERIVATISATION

In the previous section we showed how a Stille reaction proved to be a very efficient method of introducing an allyl tag into library members of biologically interesting compounds. The value of the allyl–group can be assessed in multiple ways (fig. 2.13). An alkene is very versatile as it can serve as a reaction partner for many different chemical transformations including click–like transformations. Hydroboration, epoxidation or dihydroxylation are also possible transformations to diversify the introduced allyl group, and to obtain SAR–information for linker attachment.

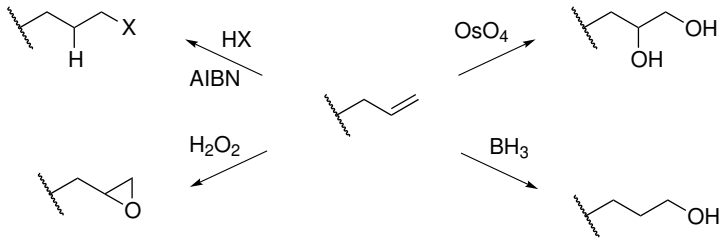

Figure 2.13. – Possible modifications of an allyl group

Moreover, introduction of allyl groups is not limited to halogen–substituted aryl groups. Indeed, substituting hydrogen atoms on oxygen or nitrogen is very straightforward and can be done under very mild conditions as is shown in fig. 2.14 for building block **2.3**. In theory, allylation could also be done directly on "naked" arenes via Friedel–Crafts chemistry.

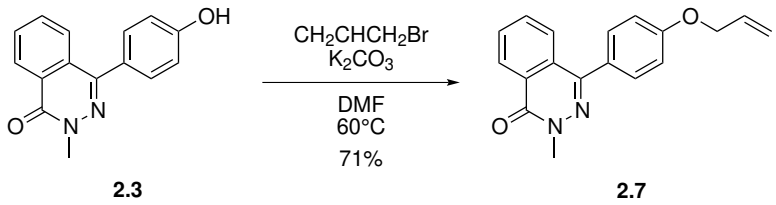

Figure 2.14. – Allyl substitution of oxygen

2.4. Hydrothiolation for 'clicking biotins'

When suitable reactions or synthetic protocols are found that allow the functionalization of a small molecule, a next step is developing strategies to prepare functional probes for target identification experiments. As we made the strategic choice to introduce an allyl group, suitable procedures to attach a linker and subsequently a biotin tag should be found. For this, the use of "click"–reactions seems appropriate. Substructures such as propargyl groups are very common for use in the Huisgen (3+2)–cycloaddition. The allyl group is especially suited for a radical hydrothiolation reaction which can also be termed a thiol–ene "click"–reaction (figs. 2.15 and 2.16).[52] Typically these reactions are performed at very high concentrations of thiol in methanol or ethanol with azobisisobutyronitrile (AIBN) as a radical initiator.

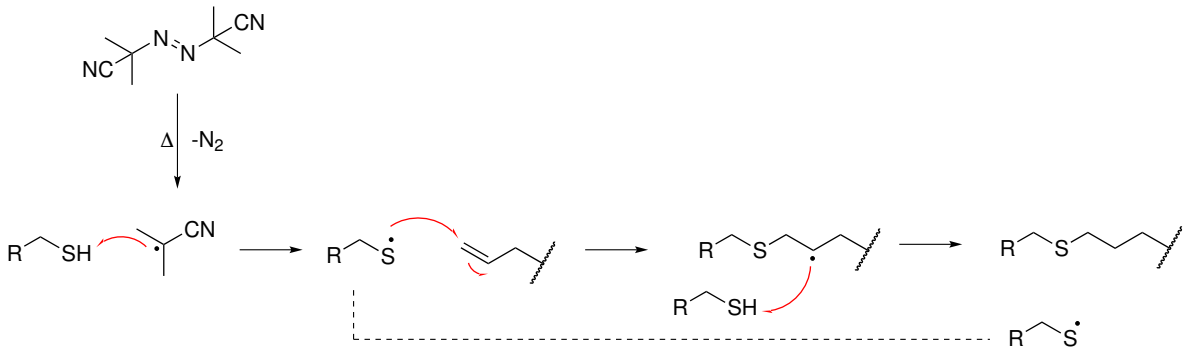

Figure 2.15. – Hydrothiolation mechanism

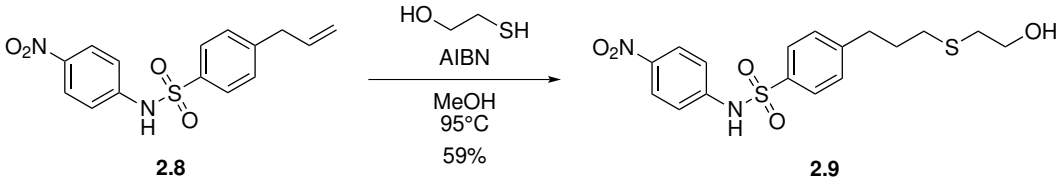

2.8 **2.9**

Figure 2.16. – Hydrothiolation of allylated compound **2.8**

The resulting alcohol can then be reacted with biotin under esterification conditions to yield a functional affinity probe. A more convergent approach we explored was the direct "clicking" of biotin to an allylated analogue (fig. 2.17). The biotin–based thiol compound **2.10** could be obtained by preparing the activated ester of biotin and reacting it with cysteamine hydrochloride. A O–allylation–hydrothiolation tandem applied to the secdin analogue **2.11** provided the affinity probe **2.12**.

Although this direct clicking of biotin is an attractive method, esterification in general is able to give higher yields. Applying high excess of the thiol in the hydrothiolation becomes rather difficult because of solubility reasons.

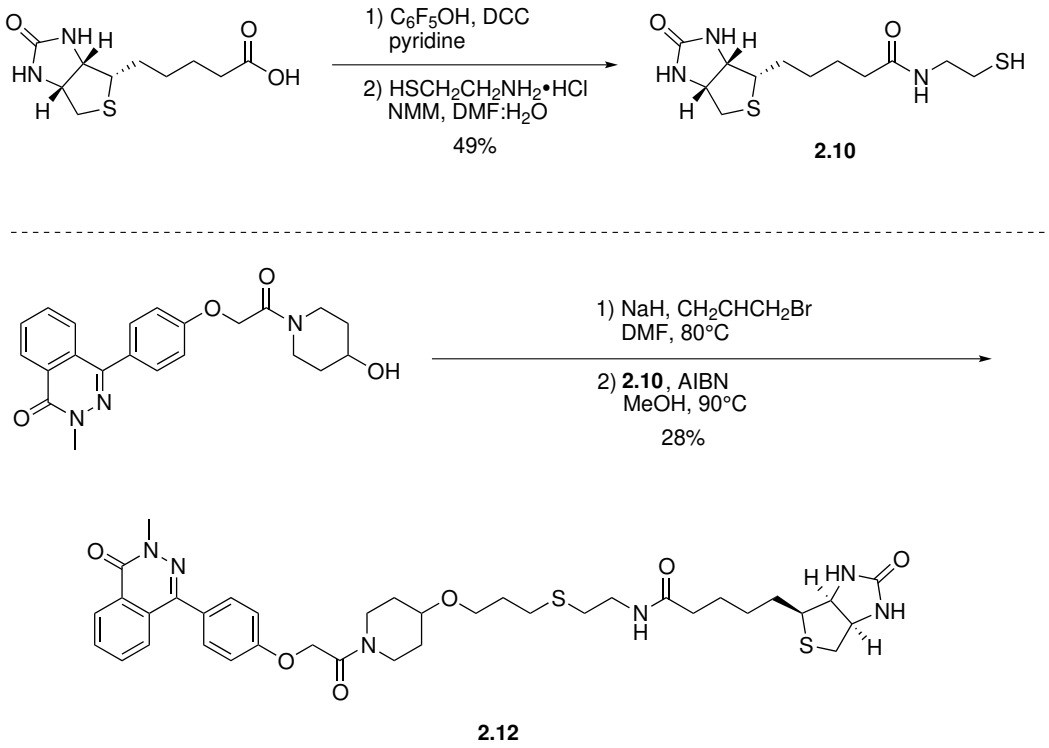

Figure 2.17. – Synthesis of biotin–based thiol **2.10**; O–allylation–hydrothiolation tandem applied to the secdin analogue **2.11**

We consider a hydrothiolation to be a good strategy as the allyl group and subsequent hydrothiolation products ar sterically less demanding than the triazoles typically found in Huisgen's cycloaddition, decreasing the risk of sterically induced binding problems. Also, the presence of a thioether allows for the introduction of a tunable linker. The sulfur is easily oxidized to a hydrophilic sulfone so any issues with water–solubility can easily be addressed.

2.5. Conclusions

In this chapter we discussed some state–of–the–art approaches for derivatisation of small molecules and subsequent SAR analysis and affinity probe construction. It became clear that indeed the transformations to directly introduce the required functionalities for the

relevant ligand, can be a major bottleneck and asks for efficient and reliable strategies. We explored some possibilities such as CH—activation (carbene insertion and CH–oxidation) but came to the conclusion that a suitable generic strategy would be to substitute an allyl group into the molecular structure and subsequently couple an OH–containing linker via a radical hydrothiolation; the hydroxyl then serves as a handle to attach biotin. A more convergent approach includes the use of thiol–containing biotin tags which can be "clicked" directly onto allyl groups. Since small molecule members of screening libraries generally contain quite some aromatic substructures, introduction of the allyl tag can easily be achieved by a palladium–catalysed Stille coupling. However, the attachment site should not be limited to carbon–halogen bonds but can surely be expanded to oxygen and nitrogen atoms. The required halogen atom is readily introduced by an aromatic substitution reaction.

3 Towards a selective endocytosis inhibitor in plants

nature chemical biology

Disruption of endocytosis through chemical inhibition of clathrin heavy chain function

Wim Dejonghe[1,2,16], Isha Sharma,[1,2] Bram Denoo,[3] Steven De Munck,[4,5] Qing Lu,[1,2] Kiril Mishev,[1,2,6] Haydar Bulut,[7] Evelien Mylle,[1,2] Riet De Rycke,[1,2,8] Mina Vasileva,[9] Daniel V. Savatin,[1,2] Wim Nerinckx,[10,11] An Staes,[10,12] Andrzej Drozdzecki,[13,14] Dominique Audenaert,[13,14] Klaas Yperman,[1,2] Annemieke Madder,[3] Jiří Friml,[9] Daniël Van Damme,[1,2] Kris Gevaert,[10,12] Volker Haucke,[15] Savvas N. Savvides,[4,5] Johan Winne,[3] Eugenia Russinova[1,2]

[1]Department of Plant Biotechnology and Bioinformatics, Ghent University, Ghent, Belgium. [2]Center for Plant Systems Biology, VIB, Ghent, Belgium. [3]Department of Organic and Macromolecular Chemistry, Ghent University, Ghent, Belgium. [4]Unit for Structural Biology, Department of Biochemistry and Microbiology, Ghent University, Ghent, Belgium. [5]Unit for Structural Biology, Center for Inflammation Research, VIB, Ghent, Belgium. [6]Institute of Plant Physiology and Genetics, Bulgarian Academy of Sciences, Sofia, Bulgaria. [7]Department of Biology, Ghemistry and Pharmacy, Freie Universität Berlin, Berlin, Germany. [8]Ghent University Expertise Centre for Transmission Electron Microscopy and VIB BioImaging Core, Ghent, Belgium. [9]Institute of Science and Technology, Klosterneuburg, Austria. [10]Center for Medical Biotechnology, VIB, Ghent, Belgium. [11]Department of Biochemistry and Microbiology, Ghent University, Ghent, Belgium. [12]Department of Biomolecular Medicine, Ghent University, Ghent, Belgium. [13]VIB Screening Core, Ghent, Belgium. [14]Expertise Centre for Bioassay Development and Screening, Ghent University, Ghent, Belgium. [15]Department of Molecular Pharmacology and Cell Biology, Leibniz Research Institute for Molecular Pharmacology, Berlin, Germany. [16]Present address: Department of Botany and Plant Sciences, Institute of Integrative Genome Biology, University of California, Riverside, CA, USA.

Author contribution: B.D. did synthesis of non–commercial analogues, development of affinity pull–down probes and SAR

3.1. INTRODUCTION

3.1.1. Brassinosteroids: structure, occurrence and biological activity

Brassinosteroids (BR) are plant hormones vitally important for growth and development and are found in many plant species throughout the plant kingdom (gymnosperms, monocotyledonous and dicotyledonous plants and algae).[53] Discovered at the end of the 1970's, research into the function and importance of these steroid hormones have made them applicable in agriculture some 20 years later.[53] BRs control traits such like biotic and abiotic stress resistance, senescence, seed yield, etc.[54,55] Applying brassinosteroids (BRs) to increase yields in plants has been done in two ways: the exogenous administration of BRs or analogues thereof and the genetic influencing of BR regulating mechanisms such as biosynthesis etc.[53,54] Synthetic analogues of BRs or natural BRs are quite costly and their variable activity has made their exogenous application a rather impractical method of controlling BR traits in plants.[55] In contrast, genetic control of the endogenous levels of BRs have been proven a viable strategy for increasing crop yields.[54,55]

The structure of brassinosteroids is very similar to the known steroidal hormones in animals. They comprise the typical tetracyclic core found in steroidal triterpenes such as mammalian cholesterol. Their biosynthesis, like all terpenoid biosyntheses, starts from mevalonate which is then transformed into metabolites of campesterol leading to more than 50 brassinosteroids of which castasterone and brassinolide are the most active known metabolites(fig. 3.1).[56,57]

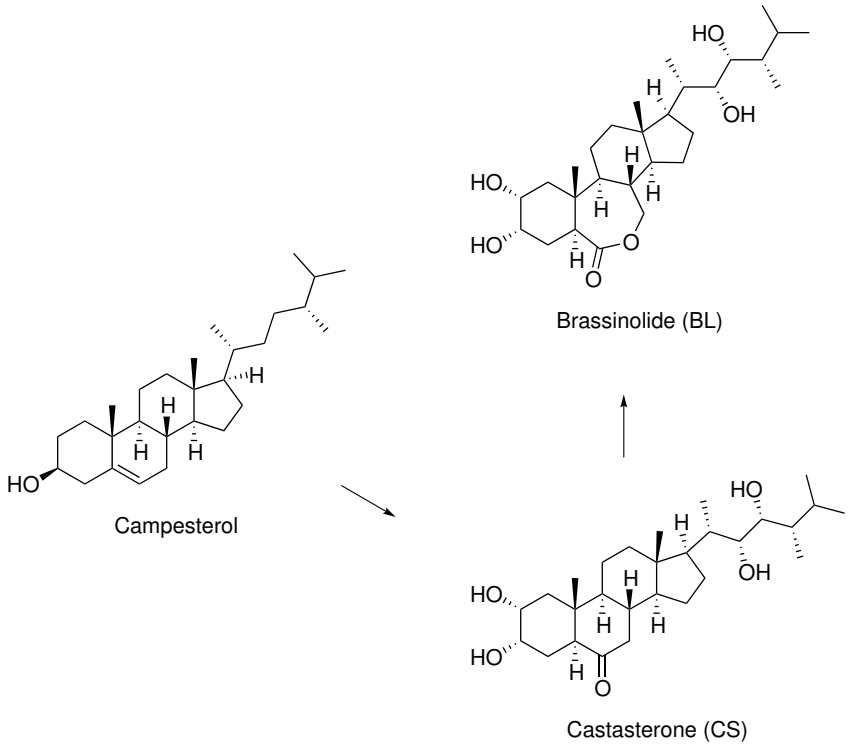

Figure 3.1. – Brassinosteroid biosysynthesis; brassinolide and castasterone structure

In order to be able to genetically influence the BR machinery, a profound understanding of the underlying mechanisms is of vital importance. A first step in this, is understanding how brassinosteroids regulate the transcription of genes in plants (fig. 3.2).[58–62] Central is the transmembrane leucine-rich repeat (LRR) receptor–like kinase BRASSINOSTEROID INSENSITIVE 1 (BRI1). In the BR unbound state, BRI1 is associated with BRI1 KINASE INHIBITOR1 (BKI1). The binding of BR activates the intracellular domain of BRI1 which phosphorylates BKI1. The phosphorylated BKI1 dissociates from the plasmamembrane and allows for the membrane–bound BRI1 ASSOCIATED KINASE1 (BAK1) to associate with BRI1. A series of autophosphorylation and transphosphorylation events activates the BRI1–BR–BAK1 complex having BRI1 catalyse the phosphorylation of BR SIGNALING KINASE 1 (BSK1). In turn the activated BSK1 activates BRI1 SUPPRESSOR1 (BSU1) through phosphorylation. BSU1 deactivates BIN2 which, in its phosphorylated state, acts as a negative BR pathway regulator through deactivation of the transcription factors BRASSINAZOLE RE-

SISTANT1 (BZR1) and BZR2/BRI1 EMS SUPPRESSOR1 (BES1). The inactive BZR1 and BES1 are normally actively retained in the cytosol and degraded whereas in their active state they are transported to the nucleus where they trigger the expression of BR-responsive genes.

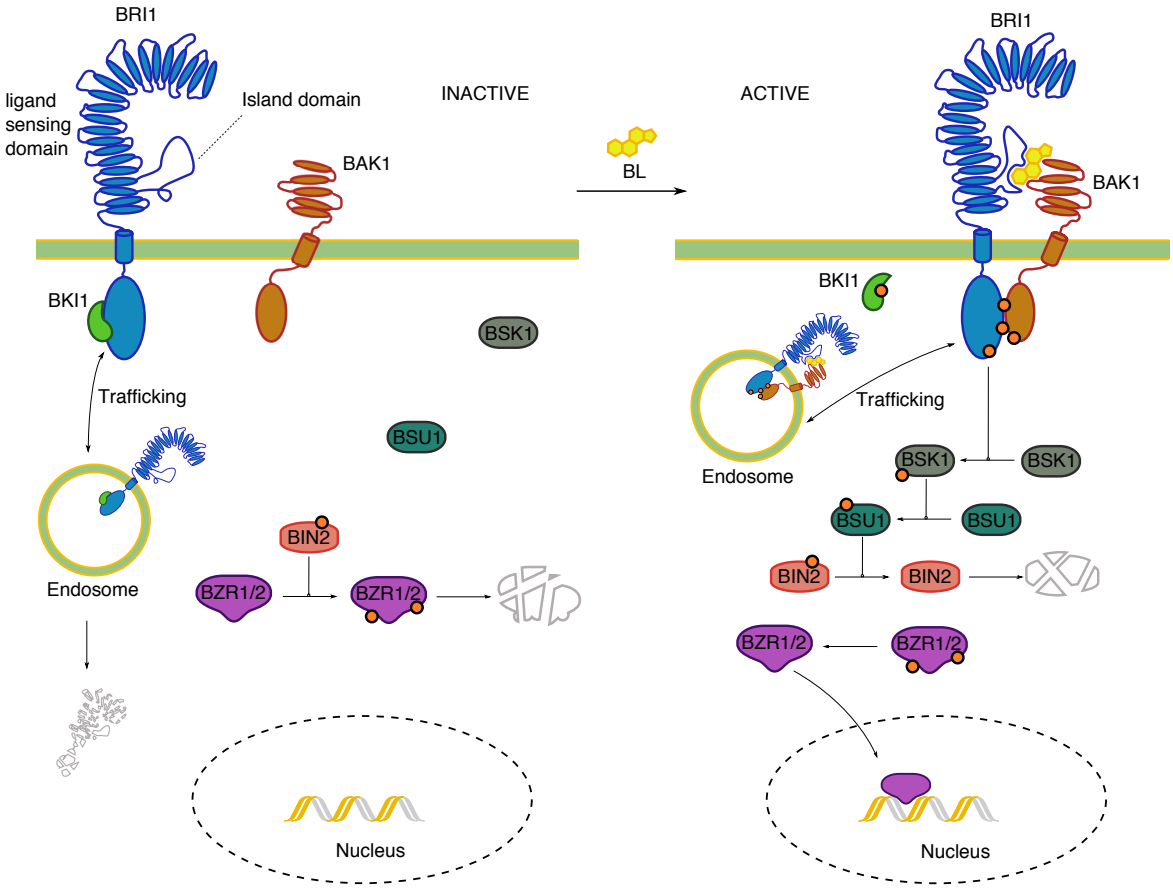

Figure 3.2. – Brassinosteroid signaling pathway

3.1.2. BR signaling and endomembrane trafficking

In fig. 3.2 both the inactive and activated receptor complex are indicated as travelling through the cell by endocytosis. They are transported to the endosome and recycled back to the plasmamembrane; a small portion is sorted for vacuolar degradation. Many plant

receptor–like kinases are actively transported through the cell and are mostly accumulated in the endosomes.[63] Endocytic mechanisms direct the relative rates of recycling and degradation and by doing so receptor availability at the plasmamembrane and subsequent signaling is regulated.[64] The exact details on the bidirectional feedbacks between endocytosis and signaling are still unclear and remain subject of further research.

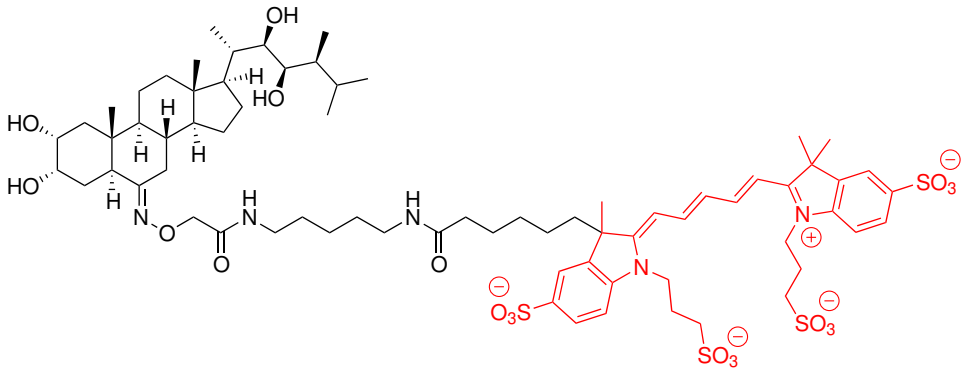

3.1

Figure 3.3. – Fluorescent analogue of CS AFCS

Irani *et al.* showed, by using a fluorescent analog of CS (**3.1**), called AFCS (Alexa Fluor Castasterone, fig. 3.3), in *Arabidopsis thaliana*, that the trafficking of BRI1 depends on clathrin–mediated endocytosis (CME).[65] The fluorescent brassinosteroid probe was prepared from castasterone and the far–red fluorescent Alexa Fluor®647, both coupled by a cadaverine linker. As it was unclear whether signaling by BRI1 activation was mainly initiated from the plasma membrane or perpetuated while trafficking through the cell, this investigation showed that the plasmamembrane bound BRI1 pool is responsible for the signaling activity.[65] Increasing the endosomal pool does not affect BR signaling, and reports do mention perpetuated signaling from endosomes.[66]

Localisation and tracking of the endocytic path of BRI1 and **3.1** showed that AFCS and its receptor follow a common trajectory from the plasmamembrane to the vacuole indicating that the BRI1 receptor is the main mediator of AFCS internalisation.[65] In fig. 3.4 we

clearly see that BRI1 and **3.1** are co–localised in different organelles which are visualised by organel–specific markers.[1]

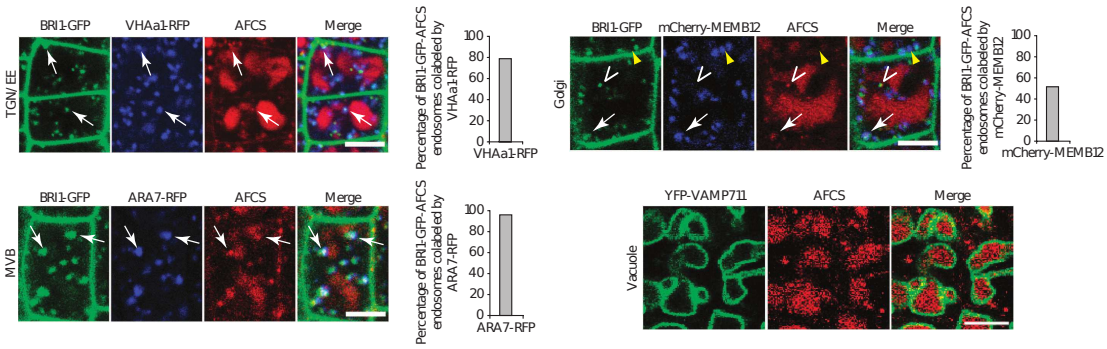

Figure 3.4. – Co–localisation of BRI1:GFP and **3.1** in *trans*–Golgi network/Early Endosomes (TGN/EE), Multi Vesicular Bodies (MVB), Golgi compartments and vacuole (reproduced from Irani *et al.*[65] with permission of Springer Nature; license number 4564220919399)

Overlap with the signals coming from BRI1 then allows the localisation of bound and unbound receptors in the cell. Increasing the endosomal pool of receptor did not affect BR signaling whereas blocking of CME, showed an increased response to brassinosteroid concentration.[65] As the receptor is retained at the plasmamembrane, the availability increases and so does the downstream response. This is monitored by the phosphorylation state of BES1, one of the transcription factors previously described. As the availability of the receptor increases so does the concentration of dephosphorylated BES1 (fig. 3.5).

Blocking of endocytosis is achieved by using the known molecule Tyrphostin A23 (**3.2**) (fig. 3.5). Western blotting indeed shows a shift from phosphorylated BES1 to its phosphorylated form, similar to the increased response of higher brassinolide concentration.

[1] the detailed description of these markers is beyond the scope of this dissertation.

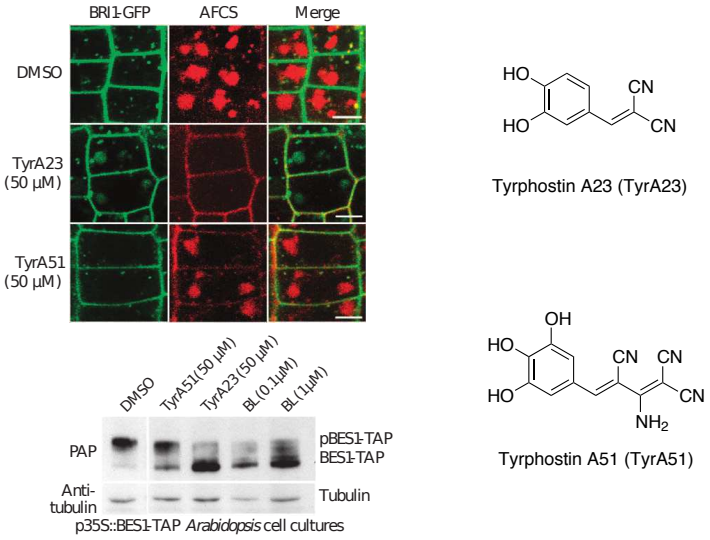

Figure 3.5. – Chemical structure of Tyrphostin A23 (TyrA23) and Tyrphostin A51 (TyrA51) (reproduced from Irani *et al.*[65] with permission of Springer Nature; license number 4564220919399)

To conclude, BRI1 traffics through the cell and is found to be the main mediator of AFCS internalisation.[65] The main mechanism by which internalization occurs is clathrin–mediated endocytosis (CME) and blocking of endocytosis is found to enhance te response to brassinosteroids.[65] The exact interplay between BR signaling and CME however is still unclear.

3.1.3. Clathrin mediated endocytosis (CME)

Clathrin mediated endocytosis (CME, fig. 3.6), as was described above, seems to play a crucial role in BR signaling. It is one of the endomembrane trafficking mechanisms in which coated vesicles are formed in order to facilitate endocytosis. The process occurs in different stages and starts by initiation of the endocytic site by assembly of modular endocytic adapter proteins, which are found in the cytosol, at the inner side of the donor membrane. It is the adaptor proteins that select which cargo is to be transported by vesicles, as different adapter proteins recognize different specific residues at the in-

ner side of the membranes. The binding of the adapter proteins is then followed by the recruitment of clathrin, a structural protein that expands the forming coat. The cargo is recruited and the donor membrane starts to invaginate; the forming vesicle is stabilised in an icosahedral cage build up by the polymerising clathrin. In the final stage, the tubule that still connects the almost finished vesicle to the plasmamembrane, is broken by dynamin which is recruited and forms a helix around the neck of the clathrin–coated pit. After release from the outer membrane, the clathrin cage falls apart releasing the vesicle which starts its way down to the early endosome/*trans*–Golgi network. The disassembled clathrin and adapter proteins can then be reused for new endocytosis events. For a more detailed discussion on the most recent findings we refer to a recent paper from Kaksonen *et al.*[67]

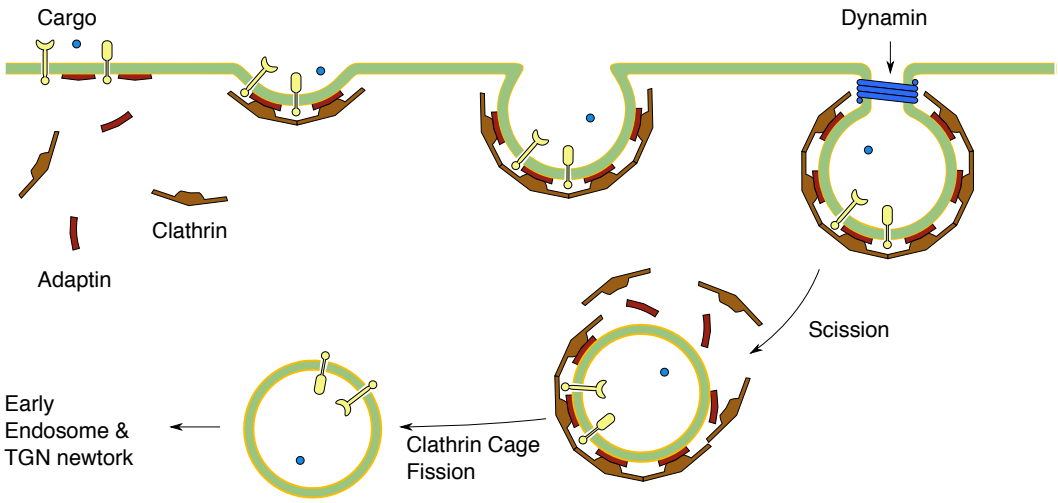

Figure 3.6. – Clathrin mediated endocytosis (CME)

3.2. Small molecules as modulators of endocytosis and brassinosteroid signaling

3.2.1. The brassinosteroid chemical toolbox

[68] The brassinosteroid signaling pathway has been extensively studied with the aid of small molecule perturbations.[68] The naturally occurring brassinolide (BL) and castasterone (CS) have served as a basis for the development of analogues in order shed further light on the molecular recognition patterns involved in the interactions of BR's and their receptor BRI1.[68] Further downstream, the small molecule bikinin (fig. 3.7) was identified as an inhibitor of some GSK3–like kinases among which is BIN2 (see fig. 3.2); inhibition leads to an enhanced BR signal response.[69]

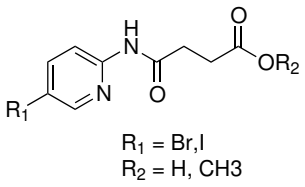

Figure 3.7. – Bikinin series

Other known small molecule perturbations mainly focus on the BR biosynthesis inhibition. The best known examples are the brassinazole (BRZ)[70–72] and the ketoconazole–containing YCZ series,[73] (fig. 3.8) which inhibit the hydroxylation of the C22–position during BR biosynthesis. Also, voriconazole was shown to inhibit a key–demethylation step in the biosynthesis of BR's (fig. 3.8).[74]

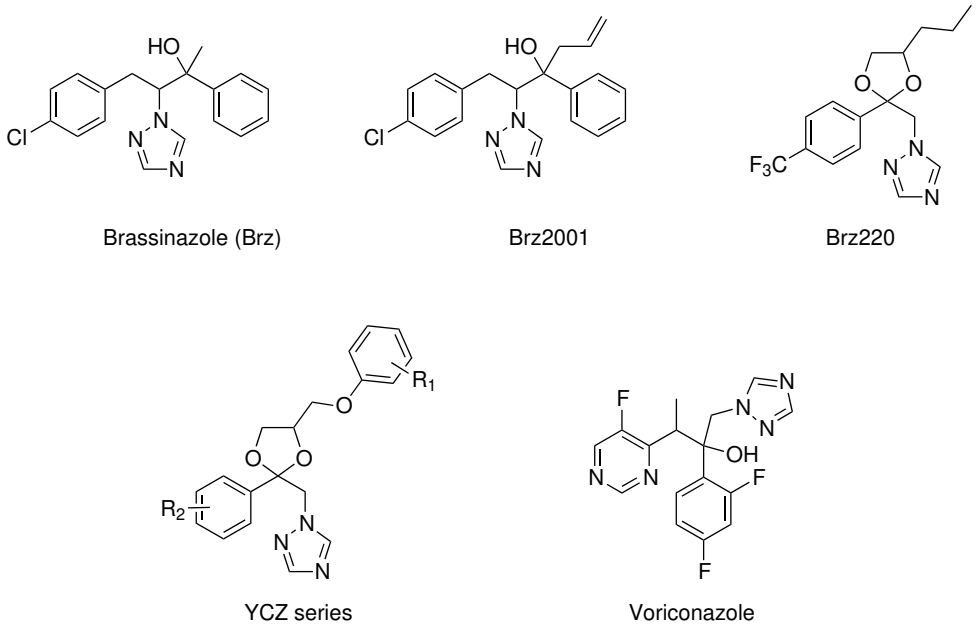

Figure 3.8. – Small molecule effectors of BR biosynthesis

3.2.2. Identification of small–molecule inhibitors of endocytosis

Small organic molecules have proven to be valuable tools in probing endomembrane trafficking processes (e.g. tyrphostin A23) as well as signaling processes (AFCS) (*vide supra*). To advance the further understanding of these pathways as well as the complex interplay between the two, development of new chemical tools can be of great value as to provide new insights. Moreover, as mentioned before, essential dynamic processes such like CME are very difficult to dissect by using classical genetic methods making a chemical genetics approach a very attractive strategy.

A large phenotypic screen, aimed at targeting endocytic processes, of a library comprising 46,418 compounds, had resulted in a subset of 360 molecules that inhibited tobacco pollen germination and growth. From those 360 compounds, 123 were found to affect the localization of a number of plasmamembrane markers, among which was the BRI1–

receptor. Based on availability, 51 compounds were tested using two different readouts in *Arabidopsis thaliana*.

A first of possible readouts included the assessment of FM4–64 uptake in cells. FM4–64 is a lipophilic dye (fig. 3.9) that selectively stains membranes by associating with the lipid tails of the phospholipid bilayer. It is commonly used as an endocytic tracer in plant biology as the trafficking of vesicles can be monitored through the staining of the vesicle membranes. Inhibition of FM4-64 uptake is an indication of defective CME.

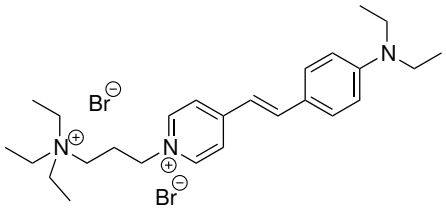

FM4-64

Figure 3.9. – Structure of the lipophilic dye FM4–64

A second test checks the BES1 phosphorylation state. The coupling of endocytosis and brassinosteroid signaling has been shown in section 3.1.2. There we also discussed that the concentration of the active (dephosphorylated) form of the transcription factor BES1 increased when endocytosis was blocked.

The subset of 51 molecules was thus also tested for BES1 dephosphorylation. From the aforementioned screens the small organic molecule endosidin 9 (ES9) was identified as it actively allowed plasmamembrane staining with FM4–64, showed inhibited internalization (cf. CME), increased the concentration of dephosphorylated BES1 and also showed internalization of AFCS (*vide supra*) indicating that the uptake inhibition was not a dye–related effect.[75]

3.2.3. Development of analogues and functional constructs: first generation SAR

The identification of ES9 as a potent inhibitor of endocytosis in plants, spurred us to obtain SAR–information on the molecular structure. Starting from the initial active hit compound ES9, a small collection of commercially available analogues was tested for their ability to block the uptake of FM4–64, after 30 minutes of compound treatment when dosed at 50 µM (fig. 3.10). The partial structure or possible hydrolysis products *N*-methylthiophene-2-sulfonamide and 4-nitroaniline lacked activity in this endocytosis inhibition assay, whereas removal of the bulky bromine–substituent on the thiophene ring, as in the simplified analogue ES9_2, gave retention of the FM–uptake blocking activity.

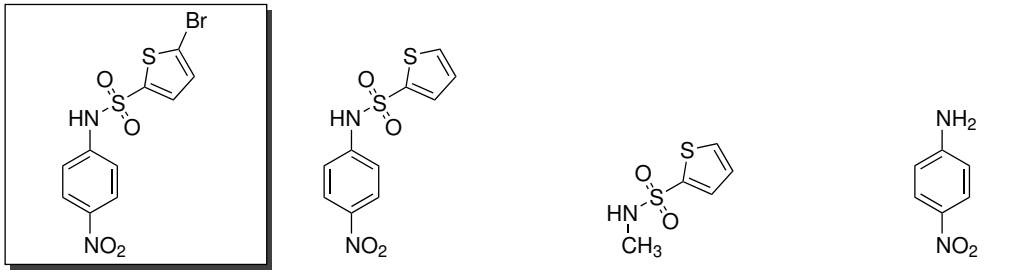

Figure 3.10. – Commercial analogues of ES9

Additional information was obtained by preparing a collection of non–commercial synthetic analogues. The sulfonamide core could easily be accessed by reacting the appropriate aniline together with an aryl–sulfonyl chloride in pyridine and stirring the mixture for 17 h. Extensive washing with an aqueous hydrochloric acid–solution allowed for the rapid (chromatography–free) assembly of analogue **2.6** (mentioned previously in chapter 2), and **3.3** (fig. 3.11a). The N–methyl analogue **3.4** could easily be prepared by

reacting the original hit molecule ES9 with methyl iodide and potassium carbonate in dimethylformamide (fig. 3.11b).

The blocking of FM–uptake was only retained for the analogue **2.6**, in which the thiophene–ring was replaced by its well–known phenyl bioisostere. Replacing the nitro–group by an acetyl–group (analogue **3.3**) as well as replacement of the acidic sulfonamide proton by a methyl group (analogue **3.4**), resulted in loss of activity.

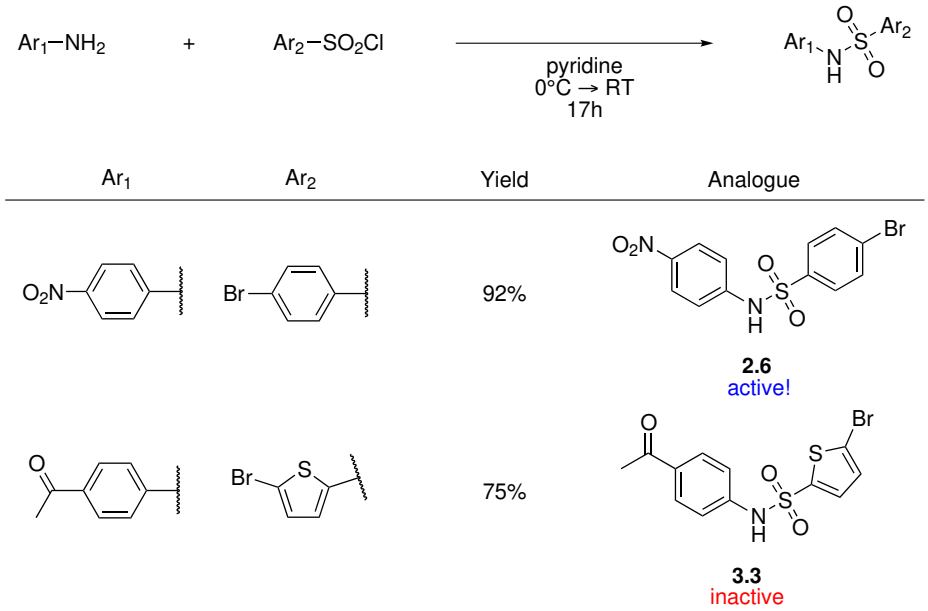

(a) Sulfonamide synthesis for ES9–analogues **2.6** and **3.3**

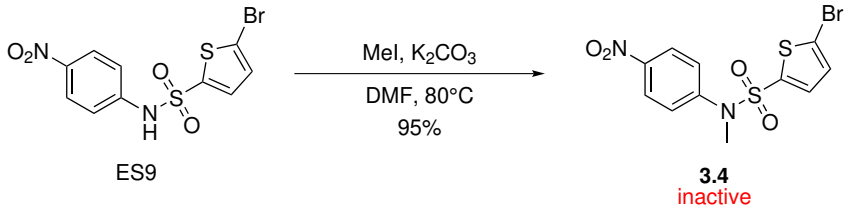

(b) Synthesis of analogue **3.4** by *N*–methylation of ES9

Figure 3.11. – Synthetic analogues of ES9

The primary aim of this SAR–analysis was not merely to gain insight in the structural features affecting the biological activity of ES9, but also to identify a suitable position for derivatisation with a linker and a biotin tag, to allow affinity purification in target identification experiments. The set of commercial analogues (fig. 3.10) showed retained activity for the analogue ES9_2, immediately suggesting the bromine occupied position to be a suitable anchoring place for introduction of a linker to attach a biotin label.

As was discussed in chapter 2, our strategy of choice would be the introduction of an allyl group for which we selected the Stille coupling as it is regarded as the most versatile transformation among the palladium catalyzed cross–couplings.[76] We also chose to build the affinity probe starting from the analogue **2.6** because the introduction of the allyl group on ES9 proved to be difficult as initial attempts showed little to no conversion. Also, the 5-bromothiophene-2-sulfonyl chloride building block, necessary for the construction of ES9, is quite expensive as compared to 4-bromobenzene-1-sulfonyl chloride from which the analogue **2.6** was prepared. Optimised conditions for the Stille reaction readily allowed the further derivatisation of the bromine-occupied position into the analogue **2.8** (fig. 3.12).

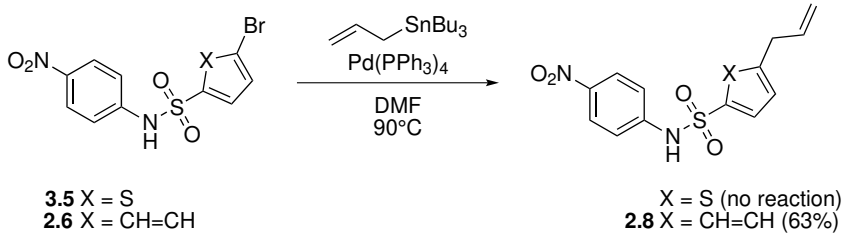

Figure 3.12. – Introduction of allyl tag

A radical hydrothiolation with mercaptoethanol as a reaction partner, resulted in the synthesis and identification of the still active analogue **2.9** with a hydroxyl–terminated linker. The derivative **2.9** retained its endocytosis blocking activity at 50 µM, indicating

that a suitable linker vector was found for introducing a biotin tag, which was accomplished by an optimised Steglich esterification between biotin and **2.9** leading to biotin–conjugate **3.6** (see fig. 3.13). As expected, due to the reduced cell permeability of large biotinylated compounds, this construct did not show activity in the endocytosis blocking assay, but was expected to retain binding affinity to its putative biomolecular targets.

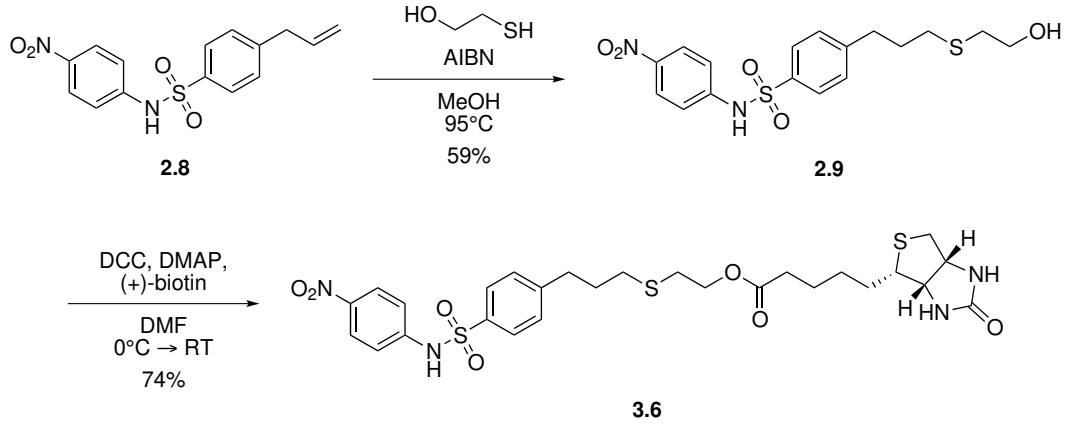

Figure 3.13. – Linker attachment and subsequent biotin labeling

Together with the affinity probe **3.6** we synthesised a negative control probe (**3.7**) which only contained biotin coupled to an empty linker to correct for non–specific interactions (fig. 3.14).

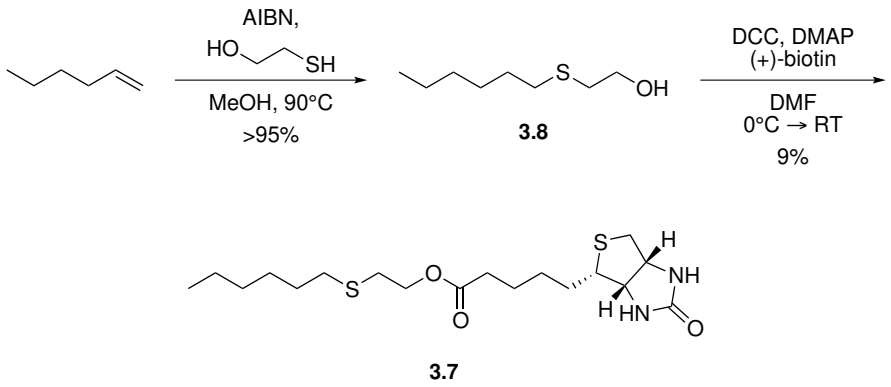

Figure 3.14. – Synthesis of negative–control affinity probe

Both the functional construct as well as the negative control probe were applied in target pull–down experiments. The proteomics approach consisted of treating one batch of cell lysate with streptavidin beads and **3.6** and another batch with beads and **3.7**. The beads were then removed from the supernatant and bound targets were released from the beads and analyzed via gel electrophoresis. Stained bands were cut out and the protein material was digested on gel to obtain a peptide mixture that was subjected to HPLC–MS analysis. Multiple repeats led to a list in which clathrin heavy chain was recurrently isolated and showed the highest number peptide sequence matches. Also, the clear link with the observed phenotype, suggested that clathrin heavy chain could be the primary target. The FM4–64 uptake blocking activity of ES9 might thus originate from impaired CHC function triggered by an ES9 binding event.

3.2.4. Protonophoric uncouplers inhibit endocytosis

CME is an energy dependent process and it has been shown before that ATP depletion severely reduces CME in mammalian systems.[77] Therefore, the effect of ES9 on cellular ATP levels was also assessed in this study.[75,78] Compared to the positive controls, Antimycin A (AA), Oligomycin and carbonyl cyanide m-chlorophenyl hydrazone (CCCP), which interfere with the mitochondrial function, ES9 was shown to induce a 50 % decrease

in cellular ATP, after 2 min of treatment.[75,78] Moreover, TyrA23 was shown to exhibit the same effect.[75]

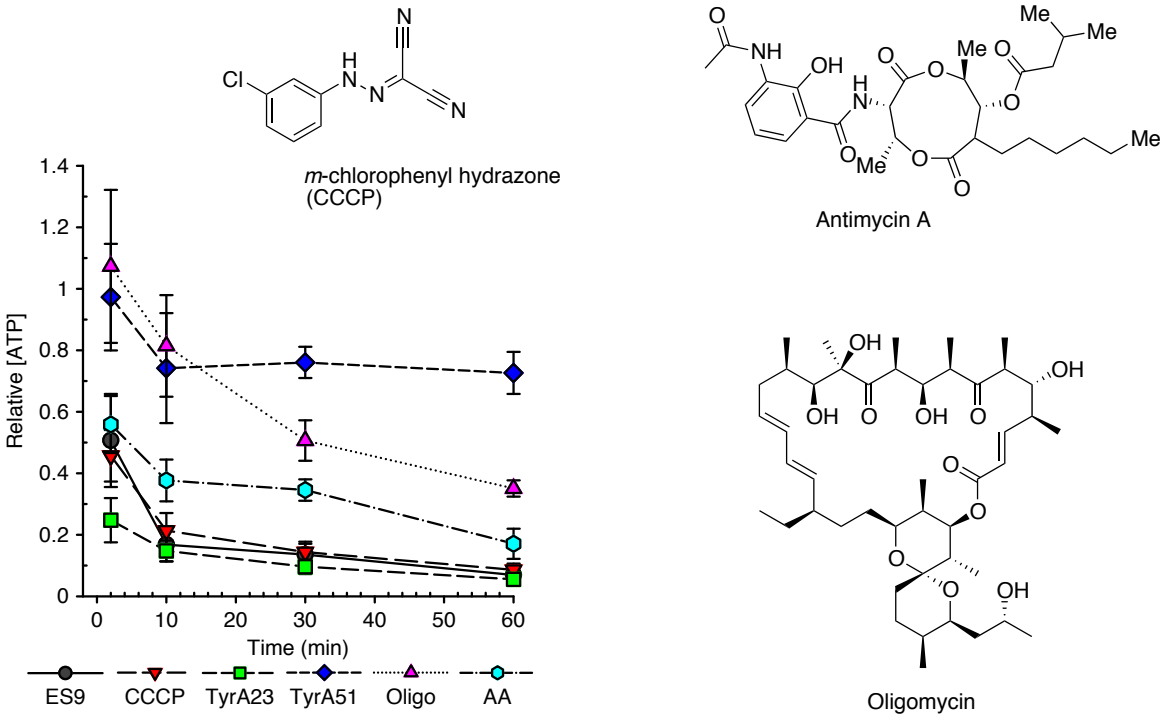

Figure 3.15. – Evolution of ATP–levels after treatment with different small organic molecules

As CME depends on ATP–concentration and both are affected by ES9, we could thus not readily conclude what mode of action ES9 exhibited. Although a CME–related target was found from affinity pull–down, the dramatic decrease of ATP levels could not be ignored as a competitive mechanism. Moreover, measurement of oxidative respiration (mitochondrion) and cellular pH indeed showed that ES9 exhibited protonophoric activity.

Protonophores are organic Brønstedt acids that are in equilibrium with their respective conjugate base. Under physiological conditions, their molecular structure however, allows them to pass through the membranes even as a charged species. The reason for

this is usually the negative charge being distributed over a large area (cf. aromatic structures) as well as the negative charge being flanked by large hydrophobic substructures (figs. 3.16 and 3.17). Indeed, under physiological conditions, nitroaniline sulfonamides are known to be in a spontaneous chemical equilibrium with a resonance stabilised deprotonated form, which is rather lipophilic. This was experimentally verified in this work as the sodium salt of ES9 readily dissolves in organic solvents.

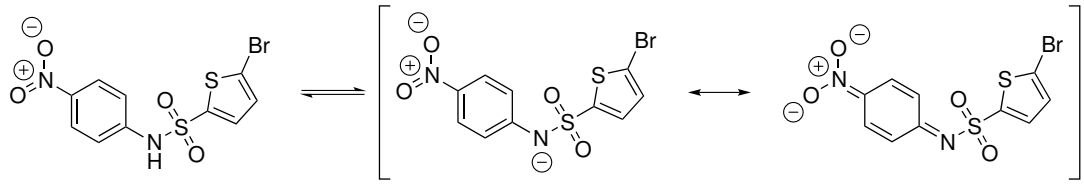

Figure 3.16. – Resonance stabilization of conjugated base of ES9

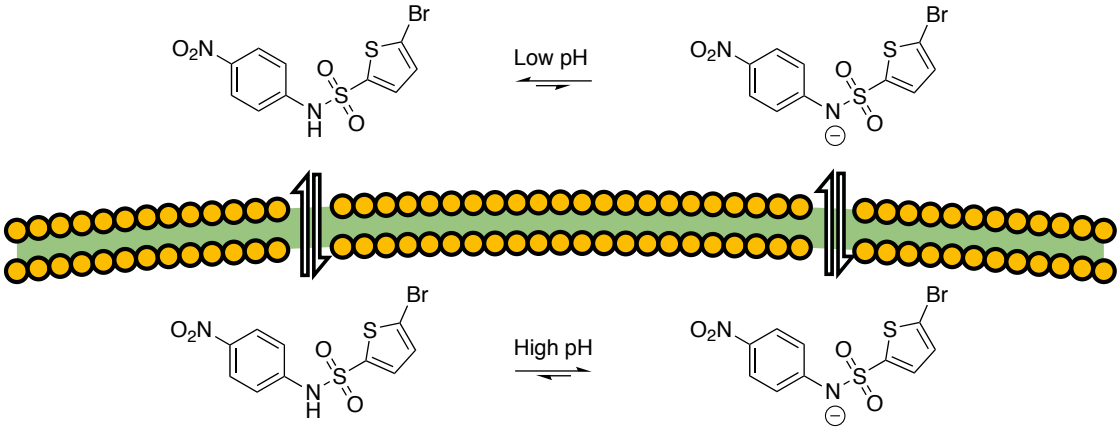

Figure 3.17. – Protonophore mode of action

Following this surprising observation of protonophoric action of ES9, Dejonghe *et al.* have shown that many of the presumed specific inhibitors of CME block endocytosis

through protonophoric activity, among which is also the previously mentioned tyrphostin A23.[78] As the charged molecule passes through the membranes, protons get shuttled back and forth between membrane separated compartments resulting in a disturbance of the acidity balance. The fact that the mitochondria show decreased oxidative phosphorylation activity as well as ATP levels decrease can easily be explained by this effect. The mitochondrial production of ATP goes via the electron transport chain, a biochemical pathway that relies on the energy harvest from NADH,$FADH_2$ and molecular oxygen to pump protons over the mitochondrial inner–membrane to establish an electrical potential that by dissipation through the ATP synthase complex produces ATP. A molecule having protonophoric activity, shuttles the protons back and forth between the matrix and intermembrane space, efficiently depleting the proton gradient and thus decoupling the consumption of oxygen from the production of ATP (fig. 3.18).

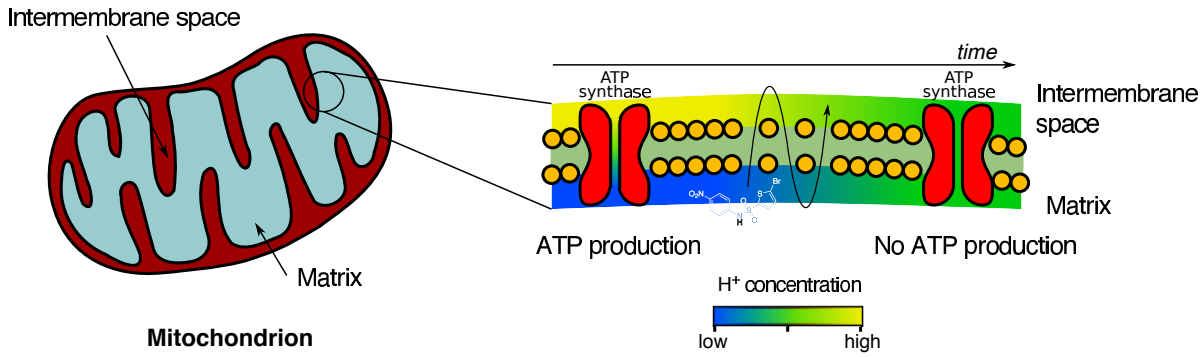

Figure 3.18. – Impaired mitochondrial ATP production through protonophoric action

Monitoring of FM4–64 uptake when applying Antimycin A, oligomycin and CCCP showed that although these molecules also deplete ATP levels, FM4–64 is only slightly affected in the case of Antimycin A and oligomycin, indicating that ATP depletion by itself is not sufficient to block CME.

Measurements of the cytosolic pH showed an increased acidity which can be attributed to the same protonophoric activity, as this disturbs a similar proton gradient across the plasmamembrane, between the apoplast and cytosol. Studies in mammalian systems have shown that acidification interferes with incipient clathrin–coated vesicles.[79] Both the acidification and gradient dissipation might thus, at least partially, be responsible for CME–inhibition.

The increase in acidity was thought to originate mainly from the proton shuttling between the apoplast and cytosol because of the minor pH–disturbance of the vacuole. Interestingly, growing plants in more alkaline medium, which was thought to reduce the influx of protons from the apoplast, does not restore the endocytic activity for ES9 whereas it was restored completely for CCCP and tyrphostin A23 thus indicating that ES9 blocks CME not only by proton shuttling but also by other effects presumably more specific to CME (also suggested by our target pull–down which gave clathrin heavy chain as putative target).[75]

3.2.5. Decoupling protonophoric activity from endocytosis inhibition: second generation SAR

With the aim to decouple the specific and non-specifc endocytosis inhibiting effects of ES9, a further SAR analysis was performed by focusing on analogues that might not show the protonophore activity, but retain specific binding to possible biomolecular targets. In order to decouple protonophoric activity of a molecule from its putative specific effect we could follow three strategies:

1. As the protonophoric activity is dependent on the presence of acidic protons, finding structural analogues that lack those protons is a viable strategy provided that the activity is not impaired,

2. should the presence of the proton–containing functional groups be necessary, one can change the molecular architecture in order to reduce the pK_a, again provided

that the activity is not impaired,

3. a final possibility exists in influencing the solubility of the conjugated base in the lipid bilayer of the membranes. This poses the biggest challenge as making the overall molecular structure more hydrophilic, can also have a profound impact on its binding.

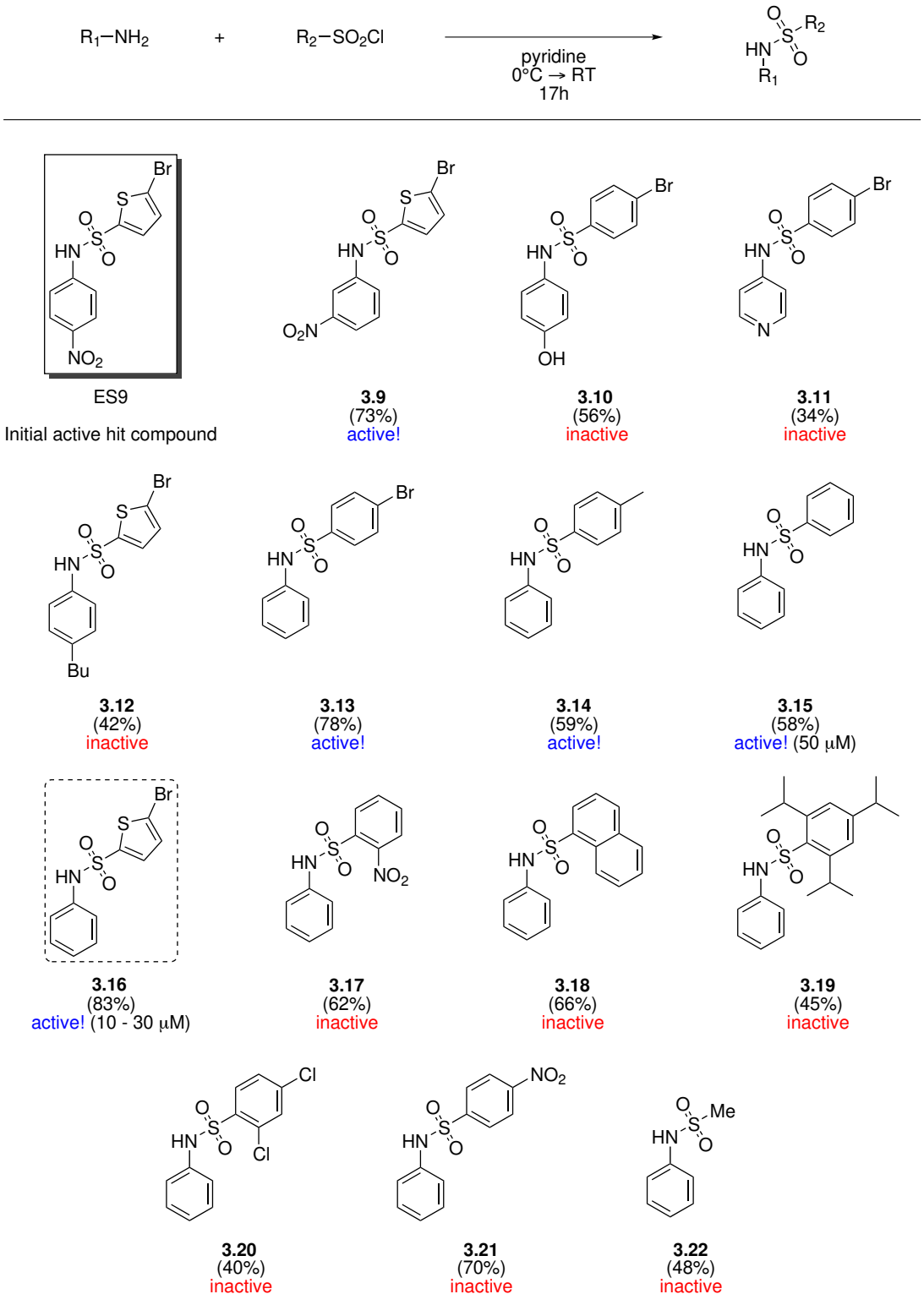

Figure 3.19. – Synthesis and activity in FM4–64 uptake inhibition assay of second generation analogues; isolated yields are in brackets

A logical first step would be replace the acidic proton of the sulfonamide, but we had shown already that replacing the acidic NH by a methyl group was detrimental to the endocytosis activity (see **3.4**, fig. 3.11b).

We then synthesised a second collection of synthetic analogues by using the same synthetic procedure as was described in section 3.2.3 (fig. 3.19). Moving the nitrogroup from the *para* to the *meta* position was expected to make the sulfonamide less acidic (analogue **3.9**), while preserving specific contacts with target biomolecules. This analogue retained activity but it also retained protonophore activity, indicating the sulfonamide is still too acidic. Other variations of the nitro–group on the phenyl ring all led to loss of endocytosis blocking activity (analogues **3.10**, **3.11** and **3.12**).

Removing the nitro group was expected to strongly shift the equilibrium towards the protonated form but could also seriously affect binding affinities for biomolecular targets. Some analogues lacking the nitro–group were shown to retain activity in the FM4–64 uptake inhibition assay (analogues **3.13**, **3.14** and **3.15**).

Interestingly, we found that the still active analogue **3.13** showed no sign of protonophoric activity or of plasma acidification. This result was confirmed by the synthesis of **3.16** (fig. 3.19, dashed frame), a close analogue to ES9 which actually inhibits endocytosis with the same potency as ES9, but completely lacks the protonophore activity (as is also expected from its molecular structure wherein no charge resonance to a nitro–group is possible). Other analogues of **3.13** in which variations of the thiophene–ring were introduced, all resulted in loss of activity (analogues **3.17**, **3.18**, **3.19**, **3.20**, **3.21** and **3.22**).

3.2.6. Target validation and mode of action

By using the biotinylated construct **3.6**, we identified clathrin heavy chain (CHC) as a possible target of ES9. This result was validated by CETSA and DARTS measurements which are shown in fig. 3.20. CETSA shows a thermal shift of 2 °C as compared to dmso treatment and the DARTS measurements showed a stabilization towards pronase digestion, indicating ES9 binding.

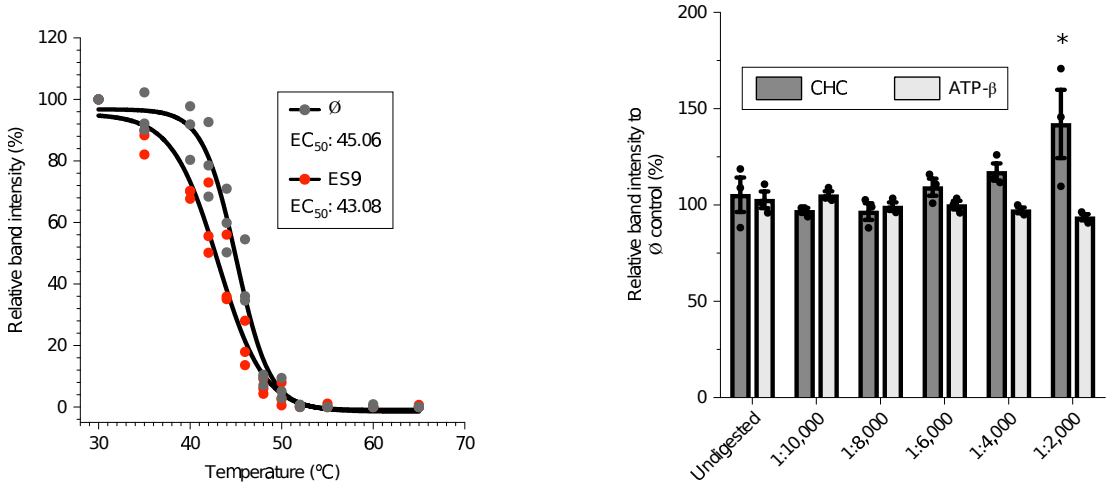

(a) CETSA curves for ES9 **(b)** DARTS measurements for ES9

Figure 3.20. – Validation experiments for ES9

Molecular docking of ES9 suggested that ES9 binds the *N*–terminal domain of human[2] CHC, a site that also accommodates the known human CHC inhibitor Pitstop2 (fig. 3.21), which was however shown to be inactive in *Arabidopsis*.

[2]The reason why human CHC was used is because there are no structures of plant CHC available.

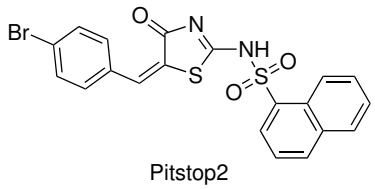

Figure 3.21. – Structure of Pitstop2, a known inhibitor of CHC

X-ray crystallography studies confirmed that ES9 indeed binds the *N*–terminal domain of human CHC at a clathrin box motif–containing recognition site for adaptor proteins. Specific contacts with the nitro–group, bromine and thiophene sulfur of ES9 are shown in fig. 3.22.

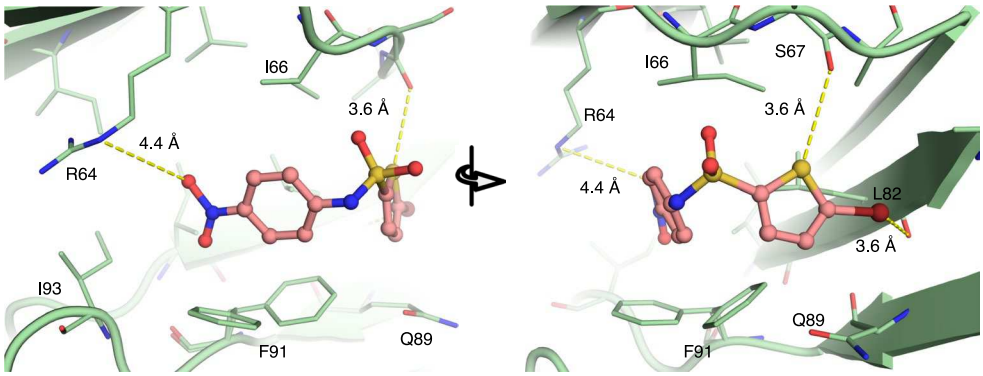

Figure 3.22. – Interaction details of ES9 bound to the *N*–terminal domain of human CHC

The unwanted protonophoric effect of ES9 then led to the identification of analogue **3.16**. As **3.16** shared the same phenotypic profile, it was hypothesized that **3.16** would also bind CHC. This was confirmed as CETSA showed a similar thermal shift as for ES9 and DARTS showed stabilization of CHC towards pronase digestion (fig. 3.23).

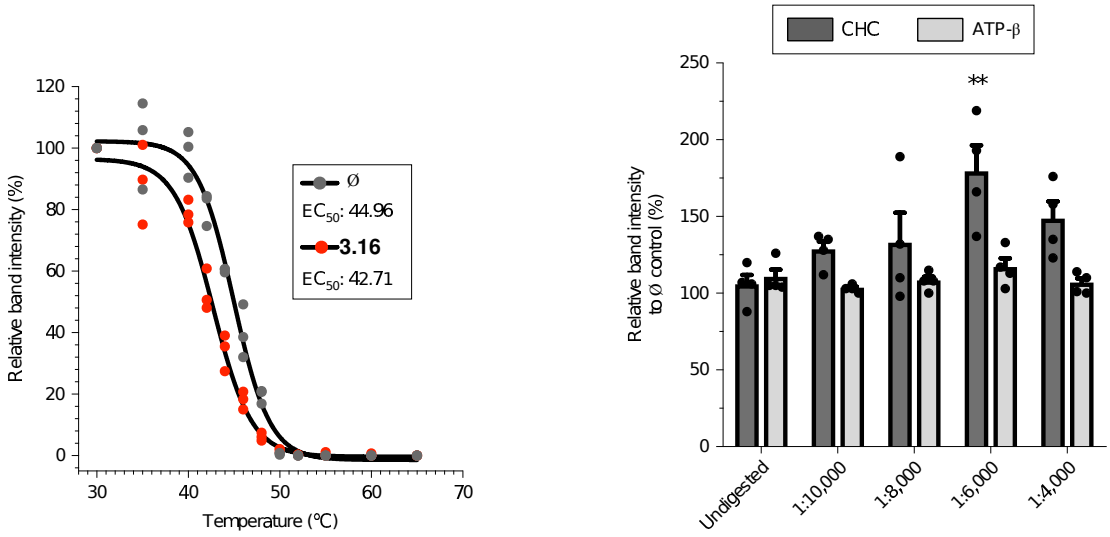

(a) CETSA curves for analogue **3.16** **(b)** DARTS measurements for ES9

Figure 3.23. – Validation experiments for **3.16**

The identification of the non–protonophoric analogue **3.16** is most likely the only example of a specific inhibitor of CME in plants. Future research might thus focus on finding more (improved) analogues related to ES9. We took a first step in this as we re–analysed one of the intermediates from the affinity probe construction (alcohol **2.9**, see fig. 3.13), which showed preservation of activity and no protonophoric properties. The presence of the short hydroxyl–terminated linker will indeed prevent the molecule of passing through the hydrophobic fraction of the membrane.

The three possible tactics to influence protonophoric activity (section 3.2.5) have thus resulted in three different analogues (fig. 3.24). The inactive methylated analogue **3.4** and the two active analogues **2.9** and **3.16**. The further development of **2.9** can surely be of great interest as it could expand the small–molecule toolbox for CME in plants.

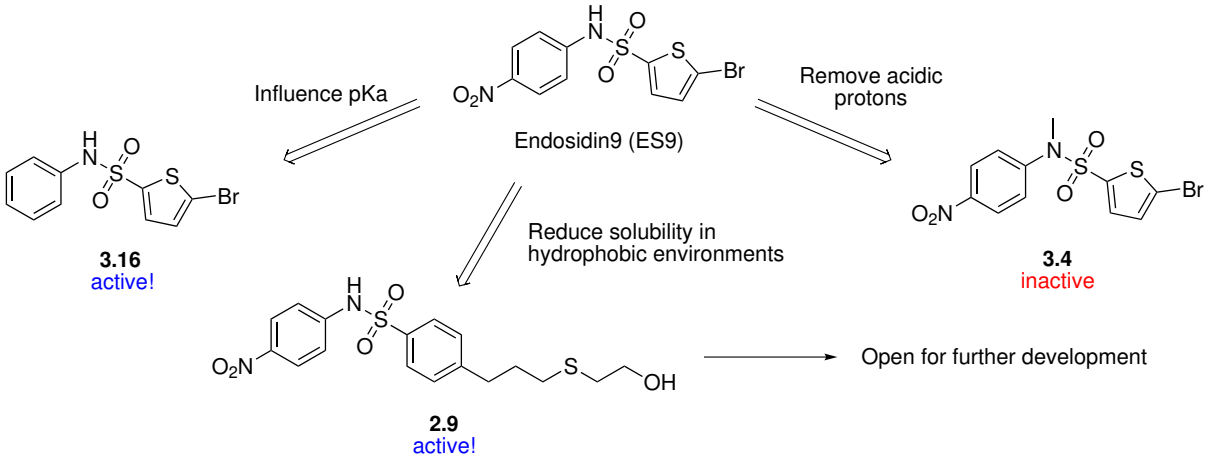

Figure 3.24. – Non-protonophoric analogues of ES9

3.3. Conclusions

We identified the small molecule ES9 as a very potent inhibitor of clathrin mediated endocytosis (CME). Synthesis of different analogues provided a suitable site for derivatisation and subsequent attachment of a biotin molecule. Target identification pull–down experiments pointed at clathrin heavy chain, a very important structural protein involved in CME, as a putative target; an observation which was also confirmed by CETSA and DARTS. The possible binding site of ES9 was assessed in human systems which showed binding to the *N*–terminal domain of clathrin heavy chain at the same site as the known CME inhibitor Pitstop2.

Although ES9 was shown to be a very efficient inhibitor of CME, this was compromised by its protonophoric properties. A directed SAR study led to the identification of the ES9 analogue **3.16**, which showed similar activity but lacked the protonophoric effect. As both compounds shared the same phenotype inducing properties, the hypothesis of binding to CHC was confirmed by using CETSA and DARTS. However, as **3.16** does not contain the nitro–group, specific contacts in the active site might be lost resulting in a different

binding orientation and efficiency.

In this work we have identified **3.16** as a specific inhibitor of CME in plants and as the known inhibitor of CHC, Pitstop2, was shown to be inactive in this system, **3.16** is the only known specific inhibitor of CME in *Arabidopsis*.

Re–analysis of the first generation SAR compounds showed that the intermediate **2.9** also fits the criteria for not being a protonophore as it contains a hydrophilic hydroxyl group by which passing through the membranes becomes impossible. Further research into this analogue would certainly be of interest as it lacks protonophoric properties but retains it CME–blocking activity and could thus serve as an additional small molecule tool for biology research.

4 Finding the target of Secdin

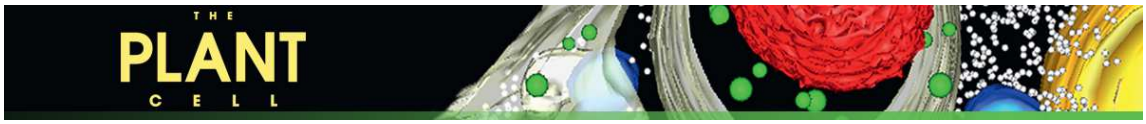

Nonselective Chemical Inhibition of Sec7 Domain-containing ARF GTPase Exchange Factors[80]

Kiril Mishev,[a,b,c,1] Qing Lu,[a,b,1] Bram Denoo,[d] François Peurois,[e] Wim Dejonghe,[a,b,2] Jan Hullaert,[d] Riet De Rycke,[a,b,f] Sjef Boeren,[g] Marine Bretou,[h] Steven De Munck,[i,j] Isha Sharma,[a,b] Kaija Goodman,[k] Kamila Kalinowska,[l,3] Veronique Storme,[a,b] Le Son Long Nguyen,[m,n] Andrzej Drozdzecki,[m,n] Sara Martins,[o] Wim Nerinckx,[i,p] Dominique Audenaert,[m,n] Grégory Vert,[o] Annemieke Madder,[d] Marisa S. Otegui,[k] Erika Isono,[l,q] Savvas N. Savvides,[i,j] Wim Annaert,[h] Sacco De Vries,[g] Jacqueline Cherfils,[e] Johan Winne,[d] and Eugenia Russinova[a,b]

[a]Department of Plant Biotechnology and Bioinformatics, Ghent University, 9052 Ghent, Belgium. [b]Center for Plant Systems Biology, VIB, 9052 Ghent, Belgium. [c]Institute of Plant Physiology and Genetics, Bulgarian Academy of Sciences, 1113 Sofia, Bulgaria. [d]Department of Organic and Macromolecular Chemistry, Ghent University, 9000 Ghent, Belgium. [e]Laboratoire de Biologie et Pharmacologie Appliquée, Centre National de la Recherche Scientifique, Ecole Normale Supérieure Paris-Saclay, 94235 Cachan, France. [f]VIB BioImaging Core, 9052 Ghent, Belgium. [g]Laboratory of Biochemistry, Wageningen University, 6708 Wageningen, The Netherlands. [h]Laboratory for Membrane Trafficking, VIB Center for Brain and Disease Research, KU Leuven, Department of Neurosciences, Leuven, Belgium. [i]Laboratory for Protein Biochemistry and Biomolecular Engineering, Department of Biochemistry and Microbiology, Ghent University, 9000 Ghent, Belgium. [j]Center for Inflammation Research, VIB, 9052, Ghent, Belgium. [k]Laboratory of Cell and Molecular Biology and Departments of Botany and Genetics, University of Wisconsin-Madison, WI 53706, USA. [l]School of Life Sciences Weihenstephan, Technical University of Munich, 85354 Freising, Germany. [m]VIB Screening Core, 9052 Ghent, Belgium. [n]Expertise Centre for Bioassay Development and Screening (C-BIOS), Ghent University, 9052 Ghent, Belgium. [o]Institute for Integrative Biology of the Cell (I2BC), CNRS/CEA/Univ. Paris Sud, Université Paris-Saclay, Gif-sur-Yvette 91198, France. [p]Center for Medical Biotechnology, VIB, 9052 Ghent, Belgium. [q]Department of Biology, University of Konstanz, 78457 Konstanz, Germany. [1]Contributed equally to the work. [2]Current address: Center for Plant Cell Biology and Department of Botany and Plant Sciences, University of California, Riverside, CA 92521, USA. [3]Current address: Cell Biology and Plant Biochemistry, Biochemie-Zentrum Regensburg, University of Regensburg, 93053 Regensburg, Germany.

Author contribution: B.D. did synthesis of non–commercial analogues, development of affinity pull–down probes and SAR

4.1. INTRODUCTION

In the previous chapter we discussed the identification of a specific inhibitor of clathrin heavy chain, a structural coating protein involved in clathrin–mediated endocytosis (CME). The endocytic machinery is however more complex and as was mentioned earlier comprises a lot more interacting proteins. This chapter discusses the identification of another target involved in the broader endocellular trafficking machinery.

4.2. ARF REGULATION IN ENDOMEMBRANE TRAFFICKING

The adenosine-ribosylation factor (ARF) family of GTPases plays an important role in vesicle formation and both endo– and exocytosis.[81] In *Arabidopsis*, 12 different ARF's are found which are reported as highly specialized proteins.[82] ARF's are localised at the membranes such as the plasmamembrane as well as the membranes of the secretory pathways and endosomal/lysosomal pathways.[83] They act as supramolecular switches which are inactive when bound to guanosine diphosphate (GDP) and, by activity of guanine–nucleotide exchange factors (GEF), the bound GDP is transformed in guanine triphosphate (GTP) by which the ARF becomes active (fig. 4.1a).[82,83] The deactivation is regulated by GTPase–activating proteins GAP that mediate the hydrolysis of the bound GTP.

Once activated, the ARF undergoes a conformational change which exposes an amphiphilic α–helical chain critical for the association with membranes.[82] The bound ARF then recruits, among others, coat proteins and other effectors of membrane trafficking and organelle structure (see fig. 4.1b).[83] For instance, Arf1 and Arf3 recruit the cytosolic coatomer complex I (COPI) to the Golgi membranes which are coat proteins for vesicle transport from the *cis*–Golgi side to the endoplasmatic reticulum.[84] Also, ARF–proteins recruit several clathrin adaptor proteins to the *trans*–Golgi network (TGN) and endosomes,[85] and by doing so they regulate trafficking between the endosomes and the TGN.[86]

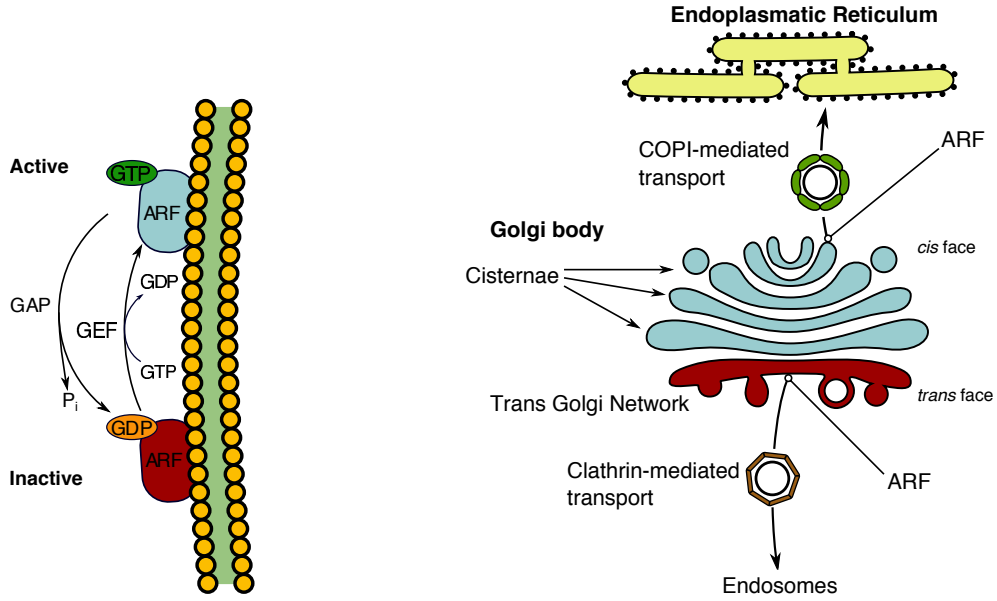

(a) Activation/deactivation cycle of ARF proteins

(b) Relevant sites of ARF mediation around the Golgi body

Figure 4.1. – The role of ARF GTPases

The most well–known example of a small molecule interfering with the ARF dependent machinery is the fungal toxin brefeldin A, which specifically targets the ARF GEF proteins. As these are inhibited by brefeldin A, activation of the GDP bound ARF's is also inhibited. The most radical change within the cell is the partial collapse of the cisternal structure of the Golgi body,[87,88] into clusters of TGN/EE aggregates surrounded by Golgi stacks, called "BFA bodies" (fig. 4.2).

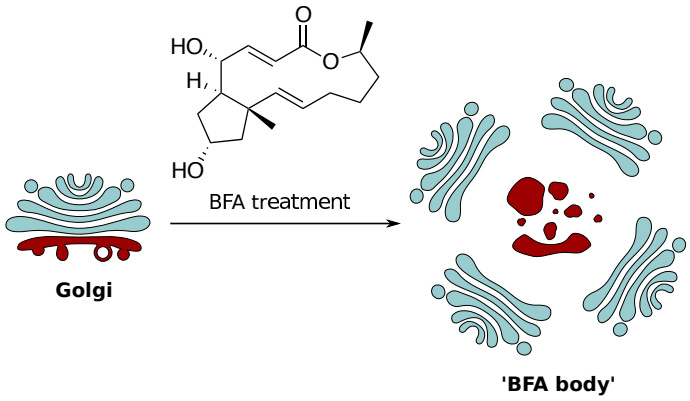

Figure 4.2. – Partial collapse of Golgi cisternal structure upon BFA treatment

4.3. IDENTIFICATION OF A SMALL-MOLECULE INHIBITOR OF ENDOMEMBRANE TRAFFICKING

A library containing 10,000 small molecules (DIVERSet™ ChemBridge library) was screened for hypocotyl growth inhibition as well as localisation of BRI1–GFP and 196 hypocotyl growth–inhibitors were identified, of which 10 caused mislocation of BRI1–GFP. From those 10 compounds, secdin (SCD) was chosen as the most promising compound. Treating *Arabidopsis* seedlings with secdin showed inhibition of hypocotyl growth as well as root growth with an IC_{50} concentration of 4 µM. Also BRI1–GFP accumulated in intracellular compartments ("SCD bodies") showing higher GFP signals. The effects on endomembrane trafficking was not restricted to BRI1, other plasmamembrane bound proteins also showed aberrant trafficking dynamics (e.g. Auxin transporters PIN1 and PIN2).

4.3.1. SAR and synthesis of secdin analogues

Assessment of the ability of SCD–analogs to induce 'SCD bodies', was performed using a set of commercially available compounds related to SCD (figs. 4.3 and 4.4). Substitutions at the piperazine ring are mostly tolerated (apart from **4.1** and **4.2**) but only hydrophobic

moieties allow preservation of the activity (analogues **4.3**, **4.4** and **4.5**), while hydrophilic groups are not tolerated (analogue **4.6**). Alterations at other positions — mainly the phthalazinone structural fragment — all resulted in loss of activity (analogues **4.7**, **4.8**, **4.9**, **4.10**, **4.11**, **4.12** and **4.13**).

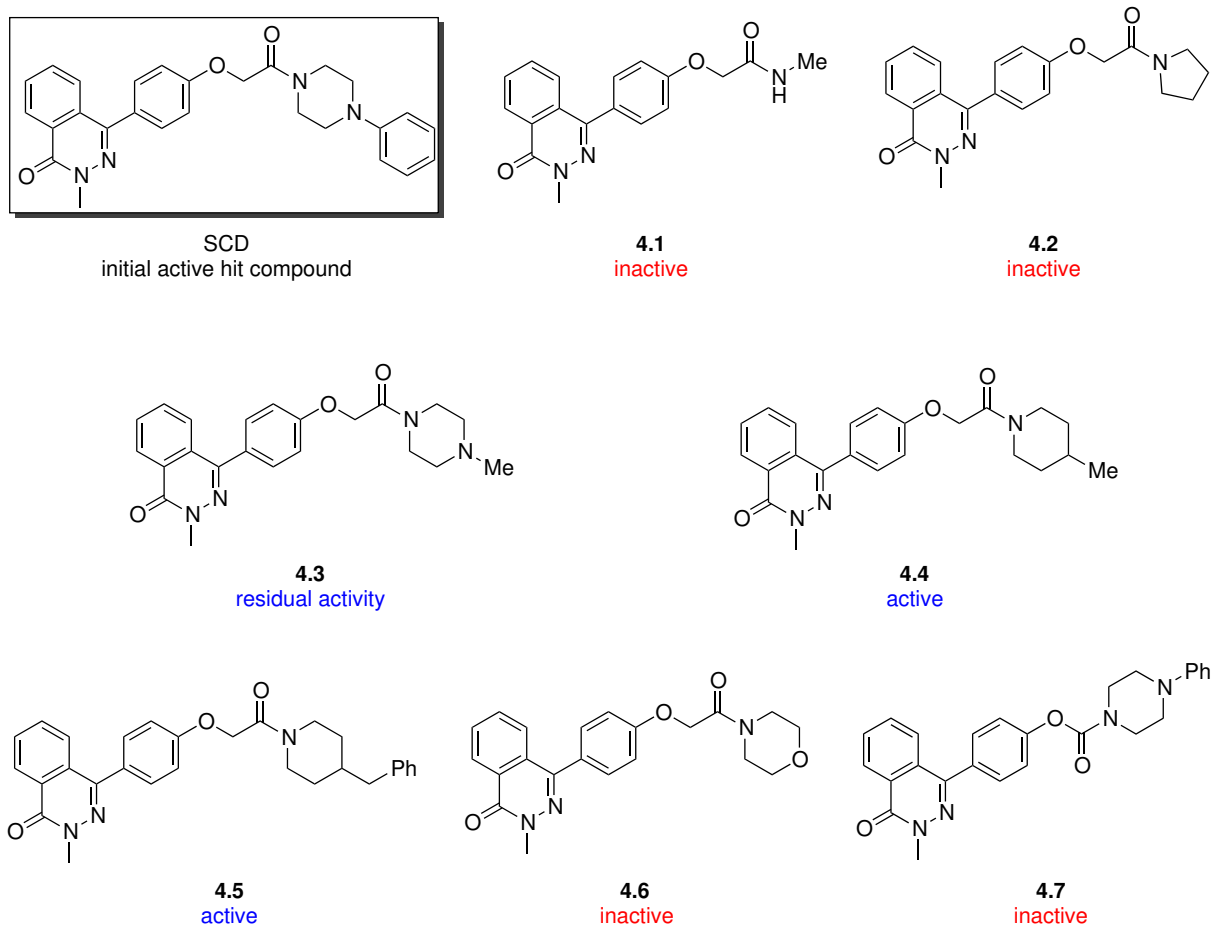

Figure 4.3. – Commercial analogues of SCD

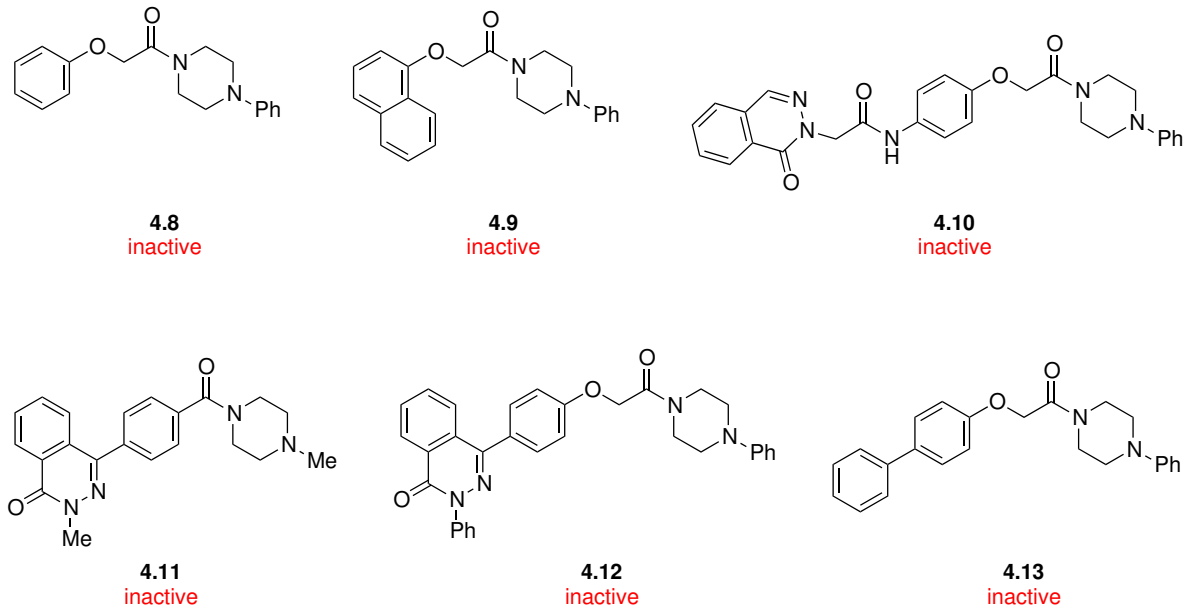

Figure 4.4. – Commercial analogues of SCD *(continued)*

In order to arrive at different synthetic analogues, we had to develop a suitable synthesis route towards the non–commercial phthalazinone part (**2.3**) of the original SCD molecule. A first method, that was developed in our lab, was the thermal fragmentation of SCD, which resulted in only small amounts of the phthalazinone precursor (fig. 4.5). However, the limited scalability as well as the high cost of SCD, made this method rather inefficient and spurred us to look for alternative routes.

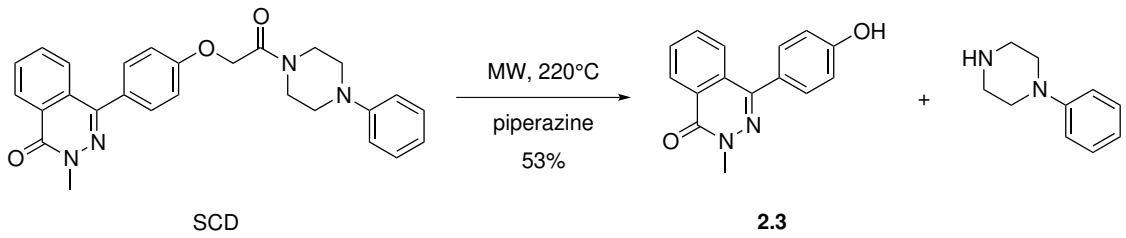

Figure 4.5. – Thermal fragmentation of original SCD–hit for the synthesis of **4.14**

An alternative method, published by Hardcastle,[89] made use of the carboxylic acid **4.14** (fig. 4.6), which can readily be obtained by heating phenolphthalein and hydroxylamine hydrochloride in a concentrated potassium hydroxide–solution, followed by an acid hydrolysis of an intermediate oxime, a method originally developed by Friedländer.[90]

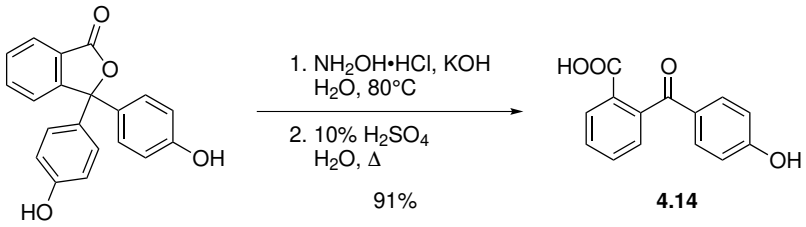

Figure 4.6. – Synthesis of acid **4.14**

The nature of the intermediate oxime has been studied in the first half of the 20th century and assumes a structure (**4.15**) as indicated in fig. 4.7 which is better identified as an N–substituted hydroxamic acid.[91–93] The main argument for this, is the observation of *p*-aminophenol formation upon acid treatment of the hydroxamic acid. The mechanism supposedly goes through an acid–induced Beckmann–type rearrangement into intermediate **4.16**, which after hydrolysis gives the carboxylic acid **4.14**.

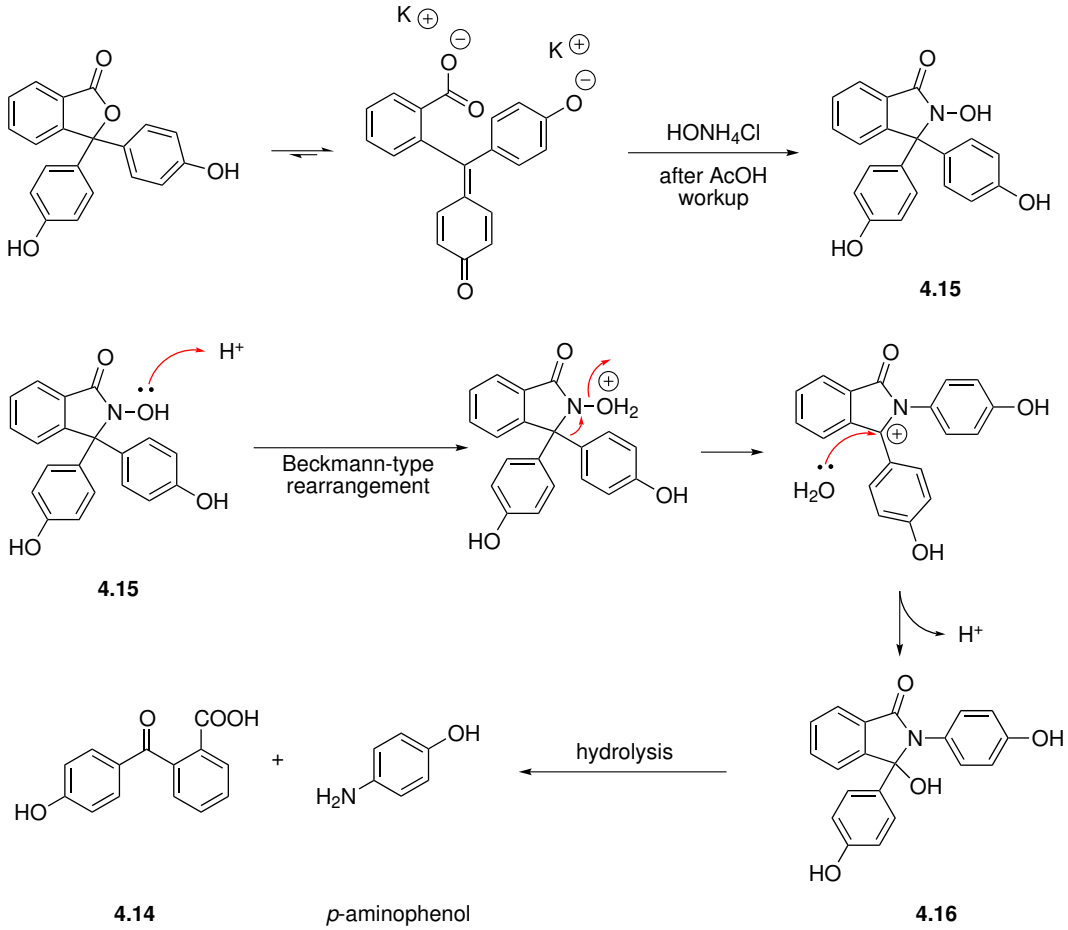

Figure 4.7. – Proposed mechanism for the formation of acid **4.14**, based upon findings of Orndorff and co–workers

Subsequent treatment with dimethyl hydrazine then readily yields the phthalazinone fragment **2.3** as was reported by Hardcastle (fig. 4.8).[89] Treating phthalazinone **2.3** with different building blocks allowed for the diversification of the original piperazine fragment (fig. 4.9).

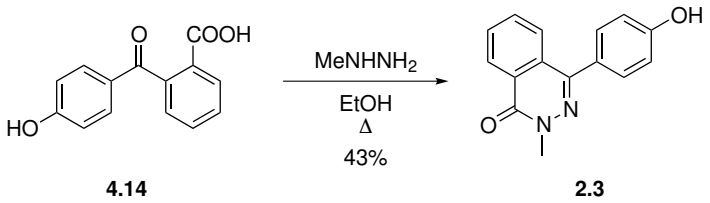

4.14 **2.3**

Figure 4.8. – Synthesis of phthalazinone building block **2.3**

To develop a set of synthetic analogues, we chose to adopt a diversity–oriented approach (fig. 4.9). The analogue **4.17** could readily be obtained by introducing a bromine atom on the phenyl ring present on the piperazine nitrogen. With the building block **2.3** in hand, variations of the piperazine fragment were accessible by reacting the **2.3** with different piperidine building blocks (**4.18** and **4.19**) to give the analogues **2.11** and **4.20**. Surprisingly, replacing the piperazine by a piperidine ring, as in analogue **4.20**, retained activity and was identified as the minimal active scaffold for SCD–activity (see dashed frame) — this in contrast to the commercial analogue **4.2** (fig. 4.3) in which pyrrolidine ring substitution was shown to result in loss of activity. The analogue **2.11** expectedly lost activity as we had found earlier that hydrophilic substitutions at the piperazine ring are not tolerated. However, **2.11** provided a platform for the preparation of several active analogues (**4.21**, **4.22** and **4.23**) which suggested a suitable anchoring place for attachment of a linker and biotin tag. Also, the building block **2.4** — described in chapter 2 — allowed for the synthesis of the active analogue **4.24**, indicating a second possible derivatisation site for the construction of a pull–down probe.

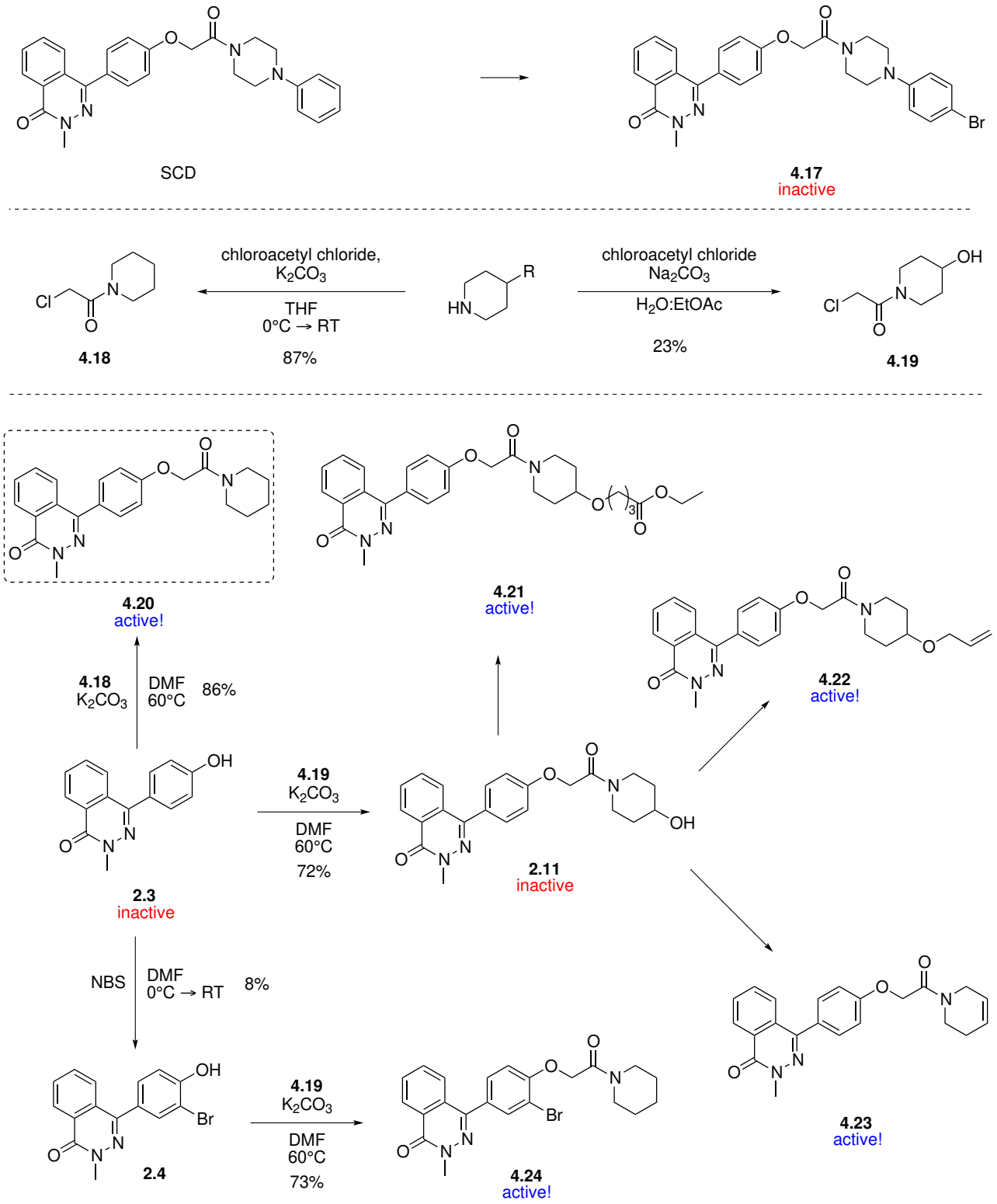

Figure 4.9. – Synthesis and activity of synthetic analogues of SCD; Analogues **4.21**, **4.22** and **4.23**: Bachelorproject Jan Hullaert, Tom De Saedeleer, Bart Vanderstraeten

4.3.2. First generation affinity probe

Starting from analogue **2.11**, our lab developed a first generation affinity probe, containing a photo–crosslinking benzophenone unit and a long linker attached to biotin (**4.25**, fig. 4.10). Pull–down experiments however, showed a rather non–specific binding profile, possibly owing to the reactivity of the benzophenone biradical. Should SCD be a low–affinity ligand, relatively high concentration of the unbound probe can indeed be expected to cross–link to other proteins in the cytosol.

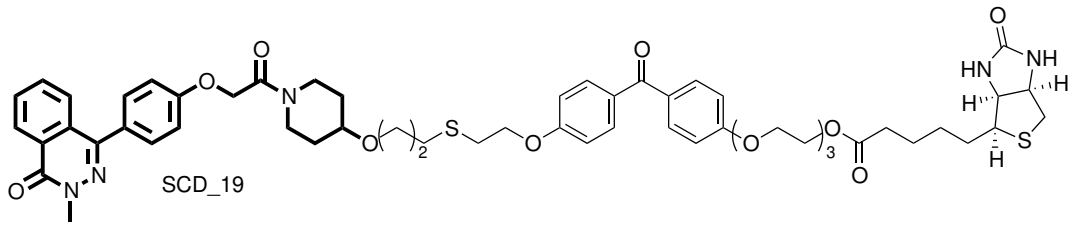

4.25

Figure 4.10. – First generation pull–down probe

4.3.3. Second generation affinity probe

In order to avoid the non–specificity of the benzophenone–containing probe, we chose to develop an affinity probe without a cross–linking unit. Starting from **2.11**, an O–allylation—hydrothiolation tandem provided the alcohol **4.26**. The subsequent coupling of biotin to the resulting alcohol however proved to be rather difficult as neither Steglich esterification, Mitsunobu reaction conditions nor acyl substitution of acid chloride **4.27** could provide the affinity probe (fig. 4.11).

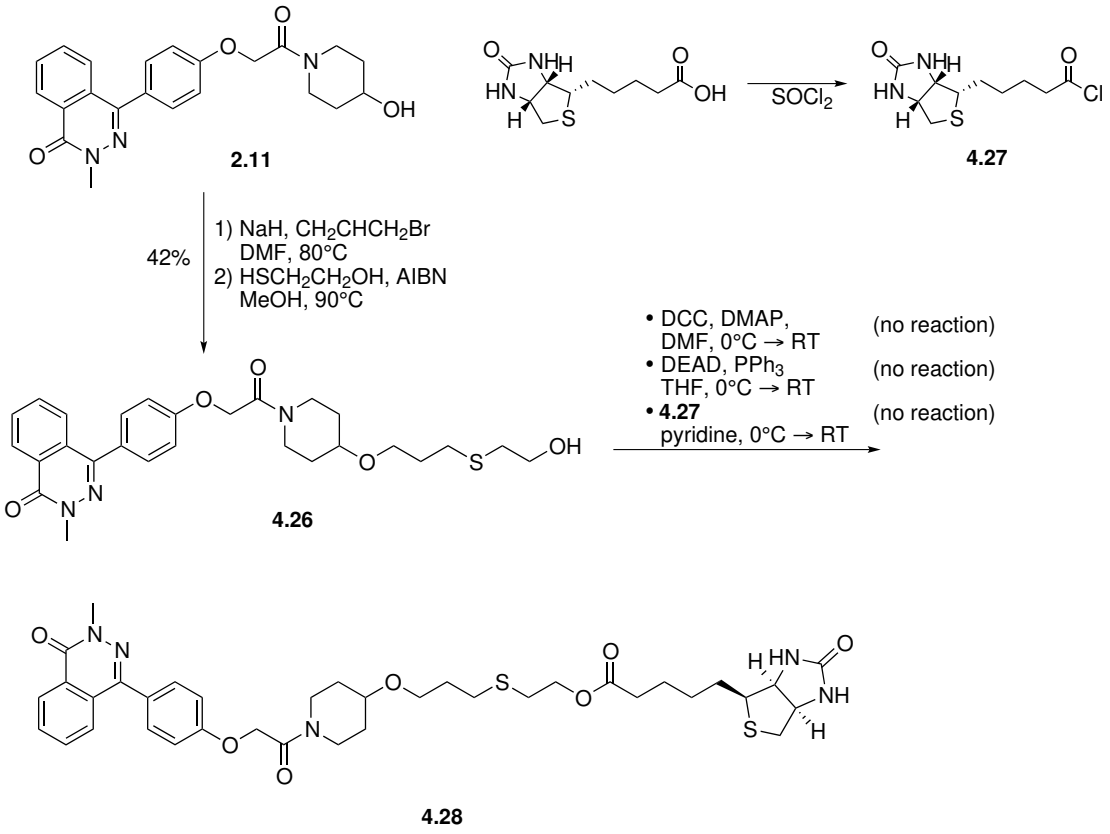

Figure 4.11. – Attempted synthesis of second generation pull–down probe **4.28**

The more convergent approach, involving the O–allylation—hydrothiolation tandem with biotin sulfide **2.10** — which was already discussed in chapter 2 — provided the second generation affinity probe **2.12** (fig. 4.12).

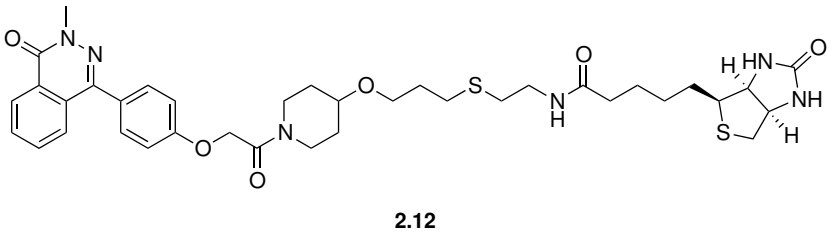

Figure 4.12. – second generation pull–down probe **2.12**

However, pull–down experiments with this probe could not isolate or identify any protein of interest. This led to the hypothesis that the rather bulky affinity matrix (linker and biotin) could possibly interfere with the binding event. We chose to explore an alternative site of derivatisation leading to a third generation affinity probe.

4.3.4. Third generation affinity probe

The bromine–substituent could allow for a direct Stille cross–coupling reaction to introduce the allyl handle. This could enable subsequent introduction of the linker–biotin unit via the tagging agent **2.10**. However, reacting **4.24** under Stille reaction conditions, showed a rather sluggish and difficult transformation (fig. 4.13). Slow conversion resulted in a hard to separate mixture of mainly starting product and small amounts of the allylated product **4.29**.

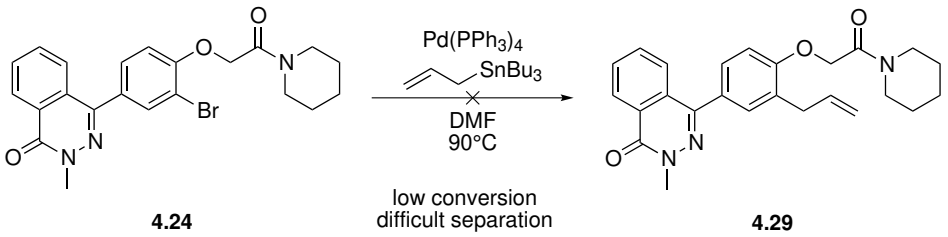

Figure 4.13. – Attempted Stille coupling for allyl group introduction into **4.24**

In chapter 2 (fig. 2.14) we have shown the efficient transformation of phthalazinone **2.3** into the allylated analogue **2.7**. As the allyl group should be introduced on the aromatic ring on the *ortho*–position relative to the oxygen, we thought of using a Claisen rearrangement to shift the allyl group from the oxygen to the aromatic ring, and thereby bypass the difficult bromine substitution on **4.24**. Heating **2.7** under microwave irradiation (250 °C, 15 min) in sulfolane readily gave the alcohol **4.30**. Coupling with the piperidine building

block **4.18** provided the analogue **4.29** which, after radical hydrothiolation with biotin compound **2.10**, gave the affinity probe **4.31** (fig. 4.14).

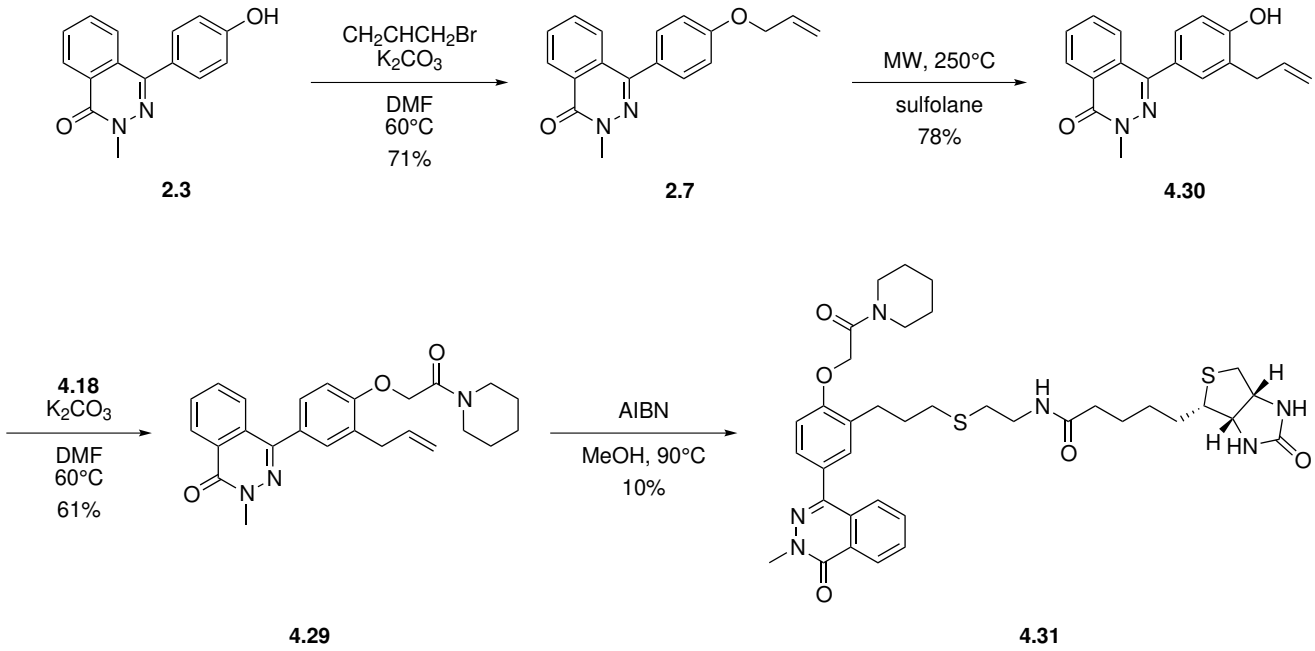

Figure 4.14. – Synthesis of third generation pull–down probe

4.4. Target identification and Secdin mode of action

4.4.1. Target pull–down and validation

As was mentioned before, pull–down experiments with affinity probe **2.12** have been unsuccessful, as specific targets were difficult to identify. Also, similar pull–down experiments with affinity probe **4.31** did not lead to statistically significant enrichment of protein targets. However, in the two repeats of pull–down experiments, a member of the ARF GEF family of proteins, BIG5, was recurrently found which led to the hypothesis that **4.31** might interact with BIG5 *in vivo*.

To validate that ARF GEF's are putative targets of secdin, DARTS was used and indeed showed stabilization of all ARF GEF proteins in *Arabidopsis* (fig. 4.15).

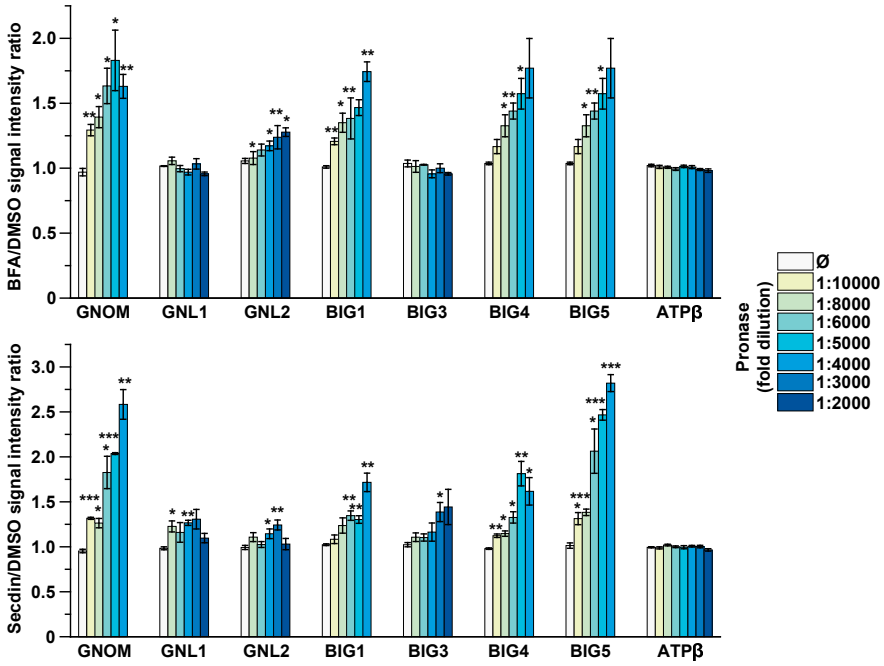

Figure 4.15. – DARTS analysis of brefeldin A and secdin for several ARF GEF proteins, relative to mock dmso treatment. ATPβ is added as a control.

Interestingly, from these data we can conclude that secdin probably targets another active site of the ARF GEF proteins as some brefeldin A–insensitive proteins are still proteolysis–stabilized when treated with secdin; also confirmed by observed stabilization of brefeldin A–insensitive mutants by secdin. Conversely, as brefeldin A is known to target the sec7–domain of ARF GEF proteins, purified sec7 residues showed no affinity for secdin whereas clear responses were measured for brefeldin A treatment.

4.4.2. Secdin mode of action

Secdin possibly targets the ARF GEF family of proteins, but the active site of interaction remains unclear. Secdin seems to interfere with multiple trafficking routes, which ultimately leads to plasmamembrane–bound proteins accumulating in the multivesicular bodies and late endosomes and subsequently enhanced degradation. It has been hypothesized that secdin interferes with the recruitment of ARF GEF to the membrane, a necessary step for the local activation of ARF's. If this is the case, for the time being, remains a matter of further research.

4.5. Conclusions

In this chapter we discussed the identification of the endocytosis inhibitor Secdin (SCD). An extensive SAR analysis was performed by using commercial as well as synthetic analogues of this small molecule. We developed a reliable synthesis route towards the main core of SCD from which several analogues could be prepared. From the information obtained from the SAR analysis, we could identify several structural fragments of SCD that tolerate modification for the introduction of a linker and biotin tag, which resulted in three generations of pull–down probes.

The first generation contained a cross–linking benzophenone but was rapidly discarded as the signal to noise ratio in the pull–down experiments was shown to be very low, possibly owing to the non–specific cross–linking of the benzophenone. From there we designed the second generation probe which is very similar to the first except for the shorter linker and the absence of the cross–linking unit; the third generation introduced the linker at an alternative position.

Neither one of the affinity probes led to the significant detection of a putative target, however, a member of the ARF GEF family of proteins was found in multiple repeats of the pull–down experiments. ARF GEF proteins are involved in the activation cycle of ARF GTPases which are macromolecular switches especially important in endocytic processes

and organelle structure. This putative target was validated by using DARTS and showed proteolytic stabilization of all members of the ARF GEF family.

The exact mode of action of SCD remains unclear; the known ligand of the GEF family, brefeldin A, targets the sec7 domain of its target whereas SCD was found not doing so. The current hypothesis would be that SCD inhibits the recruitment of ARF GEF proteins to the membranes and thereby effectively disturbs the ARF GTPtase activation cycle; if this is the case remains subject of further research.

5 Conclusions for the first part

In spite of detailed characterization of genomes, trying to make sense of the basic manual of living organisms and biocellular processes is an outstanding challenge, attracting the attention of many scientists within the natural sciences community. Over the years, not only the ever increasing plethora of techniques allowing for the biochemical dissection of living systems has allowed for the description of biochemical processes, but also joining forces with chemistry has greatly facilitated the advance of biology research. Chemical biology as it is now called, relies upon the interchange of knowledge, back and forth, between chemistry and biology. More specifically, chemical genetics is aimed at chemically influencing the biological system by means of small molecules in order to gain understanding of some of the most vital functions that operate within the cell.

In chapter 1 we discussed some of the affinity–based techniques that are used today to find relevant targets that are part of biochemical processes. It soon became clear that chemical modification of small organic molecules is paramount in order to complete a successful target identification trajectory and that one can adopt different strategies in order to achieve this.

Chapter 2 discussed our first attempts to develop a suitable generic strategy for the derivatisation of small organic molecules. Guided by some of the recent literature reports, we explored different chemical transformation classes to end up with a solution that lies in between the more efficient CH–transformations and the less desirable resynthesis of organic ligands. To our judgement, introduction of an allyl group seemed the

most suitable route given the class of aromatic ring–containing organic ligands which were the focus of ongoing biology research at the time. As palladium–catalysed cross–couplings allow for the easy introduction of such a group, direct derivatisation should be possible by employing aromatic substitution reactions.

These strategies were subsequently employed in the target identification research into the dynamic interplay between brassinosteroid signaling and clathrin mediated endocytosis in *Arabidopsis thaliana*. Successful target pulldown led to the development of one of only few specific inhibitors of clathrin mediated endocytosis, illustrating the shear complexity of target identification research. Indeed the main initial focus was defined around the brassinosteroid pathway together with clathrin mediated endocytosis (CME) but diverged into specific interactions with the endocytic machinery rather than the interplay between both pathways.

A second biological system in which we employed our envisaged strategy, was the target identification of the small molecule Secdin. The importance of dedicated organic chemistry research was nicely illustrated as we had to go through three generations of pulldown probes to achieve successful target identification along with target validation. Secdin was found to induce phenotypes comparable to the fungal toxin brefeldin A.

These two cases show that this kind of research can be very rewarding, provide new insights primordial for the deeper understanding of biology as well as development of engineered organisms. Although both projects successfully identified relevant targets, they are very time consuming and require an extended collaboration between biologists and chemists.

For the future, further research might focus on the direct CH–activation techniques as these are the most generally incorporated in target identification research. Our group is currently involved in the development and integration of these strategies in ongoing biology research. Also, the remaining open questions with regard to the identified targets in this part, can surely be the subject of further research. The possibility of developing

the ES9–analogue **2.9** or analogues thereof as a useful probe in dissecting the CME may be of interest. Also, further research on the target of SCD to identify the active site, may provide new insights in the near future.

The chemists are a strange class of mortals, impelled by an almost insane impulse to seek their pleasures amid smoke and vapour, soot and flame, poisons and poverty; yet among all these evils I seem to live so sweetly that may I die if I were to change places with the Persian king.

(J. J. Becher)

II

Cationic Cycloadditions

Mechanistic Rationale of Their Selectivity and Applications in the Generation of Complex Carbocyclic Scaffolds

6 Introduction: mechanistic considerations on cycloadditions

6.1. Cycloadditions: two reactants, two new bonds

Cycloaddition reactions are amongst the most valuable transformations in the organic chemist's toolbox. They are very efficient processes in which two bonds are formed in a single step by joining two unsaturated reaction partners at the ends of their π-systems. The formation of two strong σ–bonds in exchange for relatively weak π–bonds is a major driving force that can even overcome high ring strain barriers and yield very interesting (poly)cyclic systems (for example see fig. 6.1).

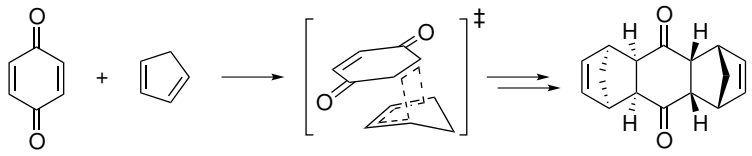

Figure 6.1. – The Diels–Alder reaction as reported by Diels and Alder[94]

Most of the well studied cycloadditions, like the Diels–Alder reaction or 1,3–dipolar cycloadditions,[95] obey laws and rules which makes their mechanistic paths predictable and their reaction products rationalizable. In general, cycloaddition reactions can proceed via

either a concerted or stepwise reaction mechanism. We should make a clear distinction between the terms *concerted* and *pericyclic*. IUPAC defines a pericyclic reaction as:

> "A chemical reaction in which concerted reorganization of bonding takes place throughout a cyclic array of continuously bonded atoms."

While a pericyclic reaction, by definition, proceeds in a concerted fashion, a concerted transformation does not necessarily have to go through a pericyclic reaction step. A pericyclic process means that the formation and breaking of bonds occurs at the same time, by which electrons flow in a closed circuit along all atoms involved. As these are highly ordered transition states, these reactions can show a high degree of stereo– and regioselectivity as well as stereospecifity. The works of Woodward and Hoffmann,[96] and also of Zimmerman and Dewar,[97] on the conservation of orbital symmetries in cycloadditions, have provided a set of rules that enabled chemists to gain an understanding in the nature of these transformations.

It must be noted that the term cycloaddition is most often associated with those processes that proceed via concerted reaction paths. There is however no basis to limit the term 'cyclocloaddition' as such since IUPAC defines it as:

> "A reaction in which two or more unsaturated molecules (or parts of the same molecule) combine with the formation of a cyclic adduct in which there is a net reduction of the bond multiplicity."

Despite the ease of predicting reaction outcomes for concerted processes, their stepwise counterparts introduce some difficulties when it comes to predictability as these do not go through the same kind of ordered transition state like pericyclic reactions (fig. 6.2). As the two forming bonds each have to go through a separate reaction barrier, the intermediates that are inevitably formed during the reaction are most often highly charged or radical in nature. The high reactivity of these transient intermediate species makes them highly susceptible to a large array of possible side reactions such as premature termination or competing ring closures that are hard to control and even much harder to predict. Apart

from that, the absence of compact and well–defined transition states often leads to a lower degree of stereo– and regioselectivity.

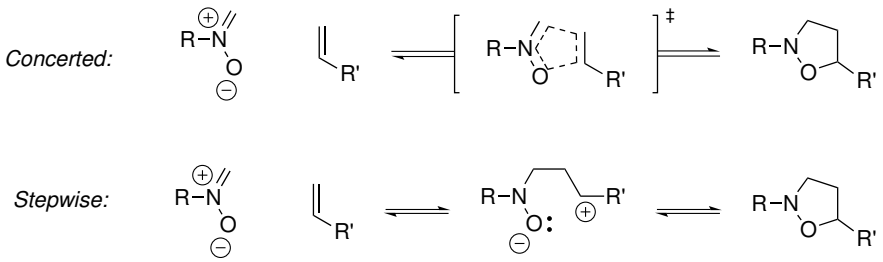

Figure 6.2. – Concerted and stepwise cycloaddition between nitrones and olefins

6.2. The Woodward–Hoffmann rules: predicting transition state geometries

6.2.1. Terminology and notation

To indicate types of cycloadditions we use a specific set of notation conventions as defined by IUPAC. If we mention the type of cycloaddition between round braces (eg. (4+3)) this indicates the number of atoms that is involved; the notation between brackets (e.g. $[_{\pi}2_s +_{\pi} 4_s]$) indicates the number of electrons that are part of the cycloaddition. The greek letters indicate the type of electrons: π: π–electrons, σ: electrons in σ bonds and ω: free electron pairs in hybridised or p–orbitals. The subscript a or s stands for antarafacial or suprafacial respectively.

6.2.2. Symmetry and orbital correlation

The Woodward–Hoffmann rules (WH-rules) were established from the need to explain the stereoselectivity of electrocyclic reactions.[96] The essence was to correlate electronic

states of the reactants with those of the products, which could be done by imposing orbital symmetry limitations onto the process, meaning that orbital symmetry should be conserved along the reaction coordinate. It became possible to predict under which conditions, thermal or photochemical, the molecular mechanism by which a cycloaddition can occur, including the TS–geometry. Although the WH–rules can predict how a reaction can occur, they do not predict the relevant kinetics or thermodynamics (*vide infra*).[98] Therefore not only the symmetry of the reacting orbitals are important to consider, but also the energy levels of different intermediates and transition states are of vital importance to gain a thorough understanding of cycloaddition reactions.

Imposing symmetry to a concerted reaction pathway, starts from the prerequisite that orbitals from the reactants should transform into orbitals for which symmetry (**S**ymmetric or **A**symmetric), relative to certain symmetry elements, is conserved. When the molecular states (ground state, singly excited state, ...) before and after reaction are analysed, one can see which reactant and product states correlate with each other. Also, taking into account that states with the same symmetry cannot cross, what is obtained is actually a qualitative diagram representing a one–dimensional cross–section of the potential energy surface in which multiple excited surfaces are also included.

In fig. 6.3 the example of the Diels–Alder reaction (fig. 6.3b) is depicted. The conserved symmetry element in this case is a bisecting mirror plane (see dashed verticalline). The molecular ground states of reactants and product correlate with each other, meaning that the proces can take place under thermal conditions. For the case of a (2+2)– or $[_{\pi}2+_{\pi}2]$–cycloaddition, shown in fig. 6.3a, we have to take into account two planes of symmetry (dashed lines). Full analysis reveals that the ground states are separated by a symmetry imposed energy barrier. However, the first excited state of the reactants correlates nicely with the first excited state of the products meaning that the concerted proces is possible under photochemical conditions.

It should be stressed that, although correlating states are in this case seemingly connected with no barrier separating them, this can be rather misleading. These diagrams

are merely aimed at showing the barrier originating from symmetry arguments which are in the order of energy differences between electronic states. Activation energies are determined by the topology of the potential energy surface where the two correlating states are located.

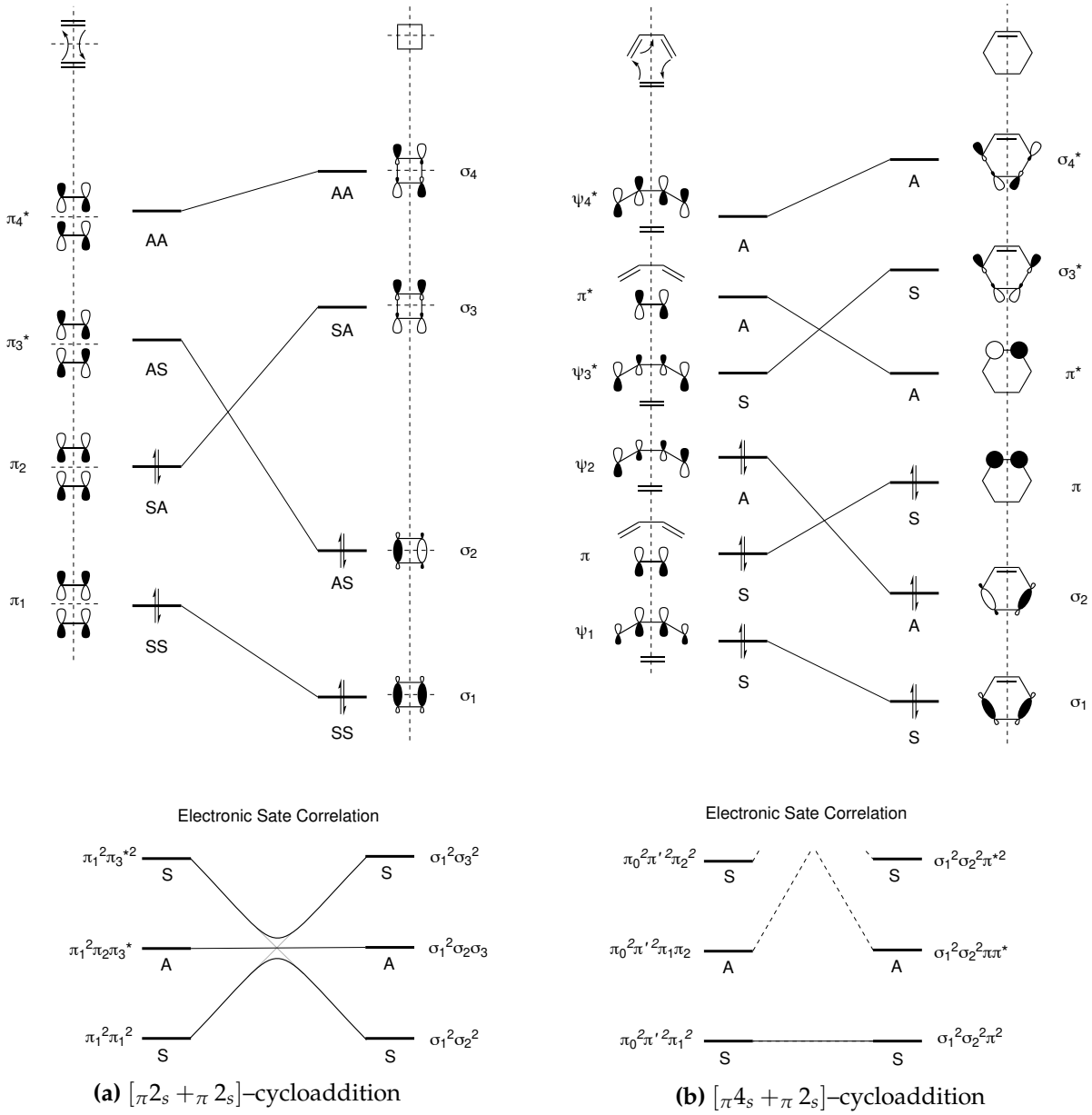

(a) $[\pi 2_s + \pi 2_s]$–cycloaddition **(b)** $[\pi 4_s + \pi 2_s]$–cycloaddition

Figure 6.3. – Orbital correlation diagrams of $[\pi 4_s + \pi 2_s]$–cycloaddition and $[\pi 2_s + \pi 2_s]$–cycloaddition (adapted from Fleming[99])

As the analysis of orbital correlation diagrams is in general not straightforward, Woodward and Hoffmann summarised these findings into a general set of rules which can be applied to determine whether a transformation is allowed or not. For a π–system with q electrons reacting with a π–system with p electrons applies that:

> the process is thermally allowed when the total number of $(4q + 2)$ components reacting suprafacially and $(4r)$ components reacting antarafacially is odd.

In fig. 6.4 some examples of cycloadditions are given together with the application of the WH-rules. The examples in which there is an antarafacial component are thermally allowed but geometrically unfeasible.

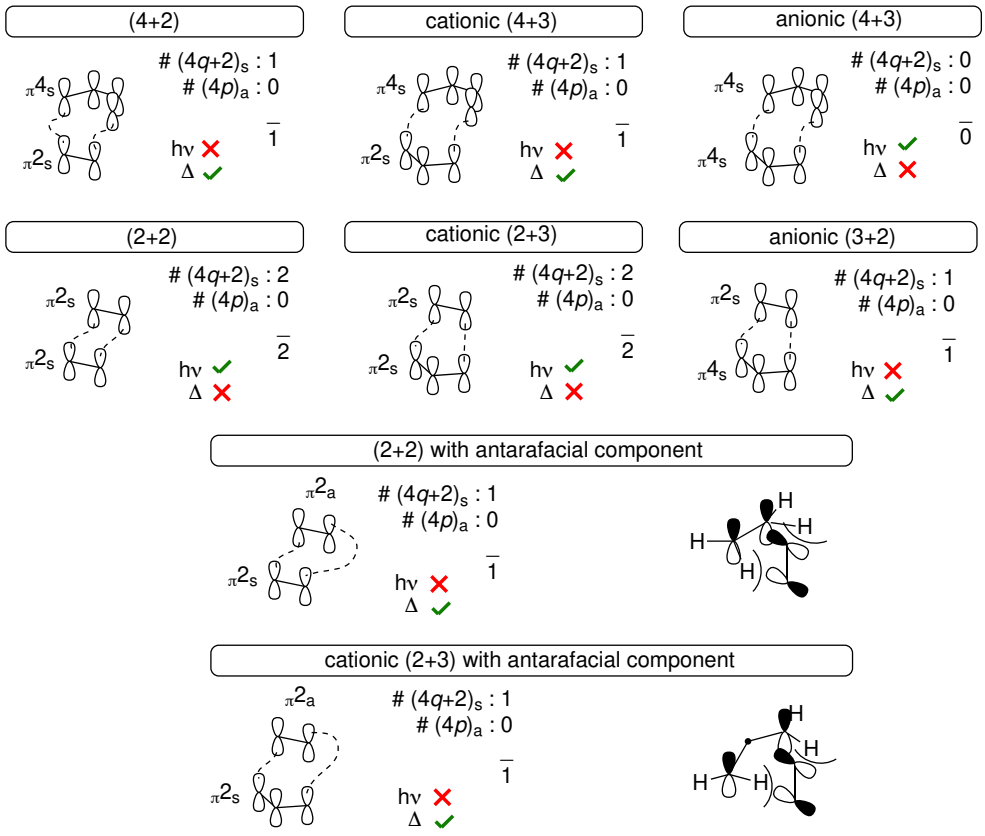

Figure 6.4. – Application of the WH–rules to selected examples of cycloadditions

6.3. THE PERTURBATION MOLECULAR ORBITAL MODEL (PMO): PREDICTING TRANSITION STATE ENERGIES

As a refinement of the intuitively satisfying WH–rule, Sustmann has set up a model by which reaction rates for concerted cycloadditions in particular could be estimated based on substitution patterns of the reactants.[98,100] This model can rationalise the classical Diels–Alder reaction of electron–poor dienophiles and electron–rich dienes. Perturbation theory states that the HOMO of one of the reactants interacts with the LUMO of the other and *vice versa*, in which the strength of each of those interactions is proportional to the energy difference between them. Other orbital interactions (e.g. between filled orbitals) are in these not considered within the framework of the frontier orbital theory as described by Fukui.[101]

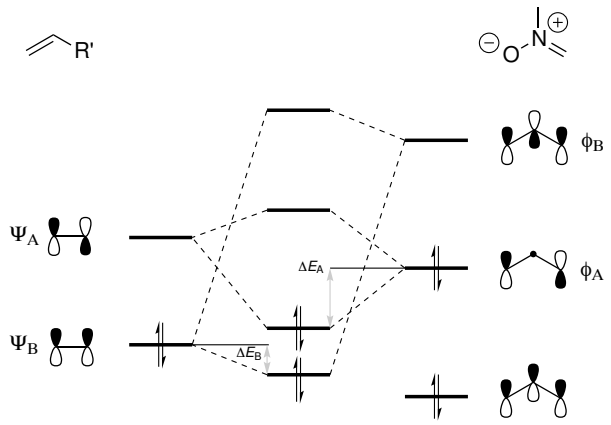

Figure 6.5. – PMO model for a (2+3)/$[_\pi 2 +_\pi 4]$–cycloaddition of a nitrone and an olefin

This model can also be used to predict or at least rationalise the relative ease of concerted and stepwise cycloaddition pathways. As an example we will consider the addition of a olefin and nitrogen 1,3-dipole (fig. 6.5, see also fig. 6.2). When the $\text{HOMO}_{\text{dipole}}$–$\text{LUMO}_{\text{dipolarophile}}$ gap ($\Psi_A - \phi_A$) becomes very large as compared to the $\text{HOMO}_{\text{dipolarophile}}$–

$\text{LUMO}_{\text{dipole}}$ gap ($\Psi_B - \phi_B$), the former becomes the dominant interaction and the contribution of the second will become negligible ($\Delta E_A > \Delta E_B$). At a given point, when the enthalpic contribution of the mutual HOMO–LUMO interactions no longer outweighs the entropic penalty for a highly organized concerted transition state, a stepwise process will gain a competitive advantage.[102] Changing substituents on either one of the reactants is known to influence the relative positions of HOMO and LUMO and changes may indeed make the reaction more or rather less likely to follow a concerted path.

6.4. Cycloadditions that give odd–membered rings

(2+2)– and (4+2)–cycloadditions (Diels–alder reaction) are widely known processes. Therefore, we will omit a detailed discussion on the factors that govern their stereoselectivity and –specificity in this disertation. Instead, we will focus on the less frequently encountered cycloadditions in the sections to follow. The orbital symmetric arguments governing the mechanism of the (2+2)– and (4+2)–cycloaddition reactions can be found in the introduction (section 6.2.2, fig. 6.3) and for accounts of their applications we refer to the literature.[103–107]

6.4.1. (2+1)–cycloadditions

(2+1)–cycloadditions can be classed as cheletropic reactions, meaning that both σ–bonds are formed from a conjugated π–system's ends onto a single atom of a monocentric reagent. This type of reaction can be exemplified by the addition of carbenes to alkenes. Many methods have been developed to use these very reactive species in syntheses (eg. Simmons–Smith) but a complete overview of the different methods of generating carbenes is beyond the scope of this dissertation, instead we refer to the literature.[108,109] These reactions can however offer a fine example of the selectivity differences encountered with stepwise or concerted reaction paths.

Carbenes can for instance be generated from diazo compounds by either thermal ex-

trusion of nitrogen gas or by photo-irradiation which also releases nitrogen gas upon electronic excitation. Carbenes can either exist in an electronic triplet or singlet state which largely depends on the substituents of the carbene carbon. In a triplet carbene, both electrons have aligned spins and one is found in what is called the p_π–orbital and the other one in the carbene σ–orbital. The singlet carbene has both electrons paired in the σ–orbital.

Singlet carbenes can add to alkenes in a concerted way which is a rather strange feature when looking at the orbital correlation diagram from which we can learn that the ground states are not correlated and thus such a transformation should formally be forbidden (fig. 6.6).

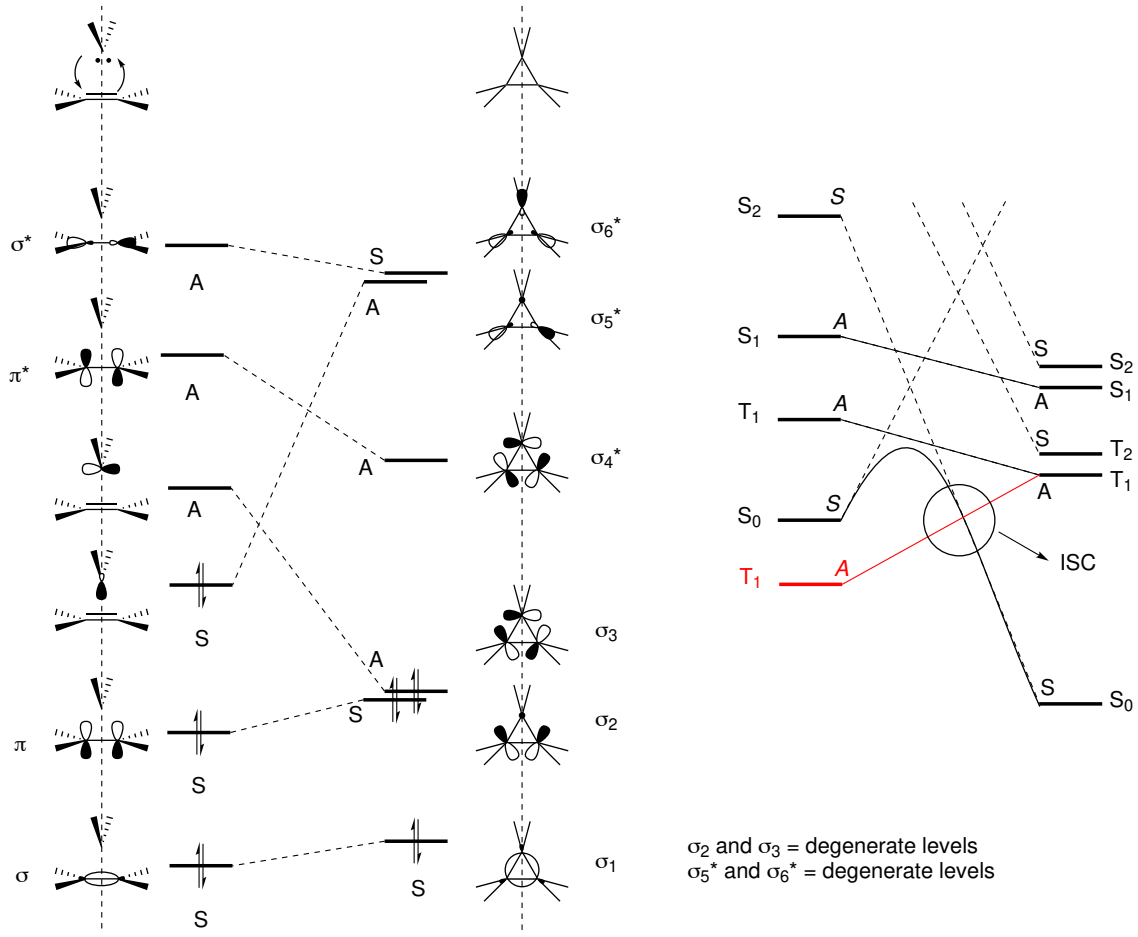

Figure 6.6. – Orbital correlation for a $[_\omega 2_s +_\pi 2_s]$ cycloaddition (adapted from Rauk[110])

However, this diagram assumes a complete symmetrical approach from the carbene to the olefin which also called a linear cheletropic addition and is written as $[_\omega 2_s +_\pi 2_s]$ in which both react suprafacially; an approach that is indeed forbidden according to the WH–rules (fig. 6.7a). Adding the carbene with a skew angle, and thereby allowing the empty p_π–orbital to participate, adds a $_\omega 0$–component to the reaction that reacts in an antarafacial way, making it a $[_\omega 2_s +_\pi 2_s +_\omega 0_a]$ addition.[111] Applying the general WH–rule learns that this approach is thermally allowed (fig. 6.7a). The resulting pathway is actually no longer a pericyclic reaction, but a concerted reaction in a non–cyclic electronic array between three components.

A triplet carbene only correlates with a higher triplet energy level of the cyclopropane and is expected to react as a biradical. One carbene up-electron pairs up with a down-electron from the alkene leaving an up-electron to pair up with the remaining down-electron in the carbene. One can see this spin flip as the molecular system crossing from the triplet potential energy surface (PES) to the singlet PES by an intersystem crossing (ISC). This ISC can be located on the correlation diagram (fig. 6.6) and is considered much slower than any other molecular process. Rotation around carbon–carbon bonds will thus be possible and the biradical intermediate will equilibrate between two rotamers, scrambling the stereochemistry of the final product (fig. 6.7b).

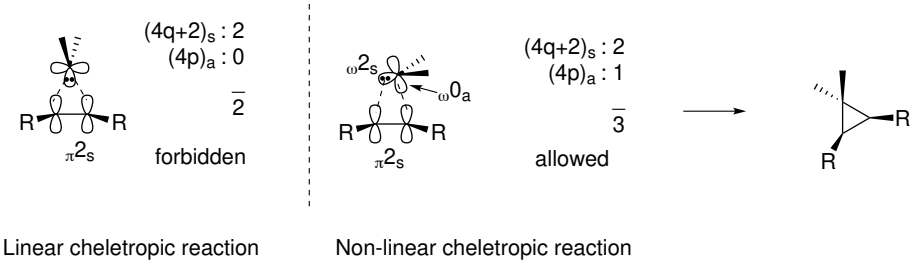

(a) Singlet carbene addition to olefin

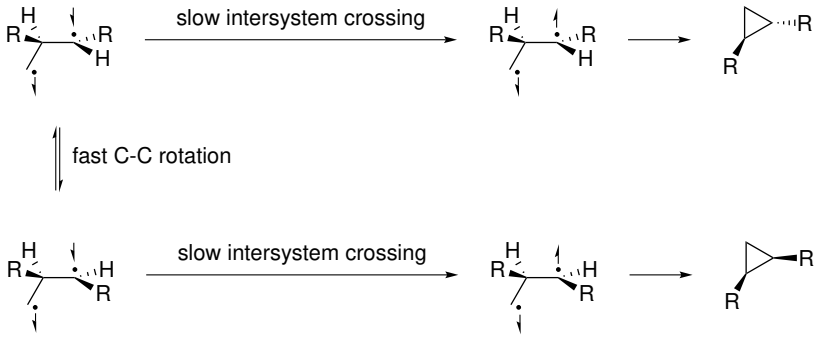

(b) Triplet carbene addition to olefin

Figure 6.7. – Differential stereoselectivities for (2+1)–cycloadditions [111]

6.4.2. (3+2)–cycloadditions

The most well–known (3+2)–cycloaddition is arguably the 1,3–dipolar cycloaddition between an azide and an alkyne, first described by Dimroth and Fester but popularized by Huisgen.[112] This cycloaddition is a $[_\pi 2 +_\pi 4]$–transformation, and is mostly found to proceed in a concerted fashion (fig. 6.8).[102]

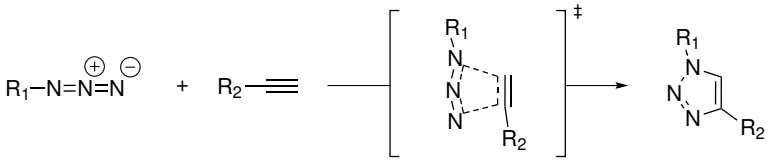

Figure 6.8. – (3+2)–cycloaddition between an azide and an alkyne

Allyl anions are mostly associated with metal cations and can theoretically undergo (3+2)–cycloadditions with alkenes via a 6–electron TS (fig. 6.9).[113] However, the initial cycloadduct that is formed is a highly unlikely localized "naked" carbanion. This results in a very high energy barrier for these thermally allowed $[_\pi 4_s +_\pi 2_s]$–cycloadditions.

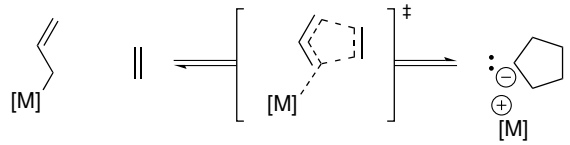

Figure 6.9. – (3+2)–cycloaddition between an allyl anion and an olefin

Next to that, although less commonly found, there is the more classical (3+2)–cycloaddition of oxyallyl cations to alkenes in general, a $[_\pi 2 +_\pi 2]$–transformation. Analysis

of the molecular orbitals learns that these cycloadditions have to go through a stepwise mechanism under thermal conditions, as the ground states of reactants and products do not correlate (cf. WH–rules). Concerted pericyclic addition is however also possible under photochemical conditions like in the synthesis of methyl rocoglate **6.1**, in which the hydroxyflavone **6.2** is photochemically converted into oxyallyl cation **6.3** and reacted with methyl-*trans*-cinnamate to yield bridged bicycle **6.4** (fig. 6.10).[114] Mark the retention of geometry of the alkene as the ester functionality and the phenyl group are found to be *trans* oriented relative to each other.

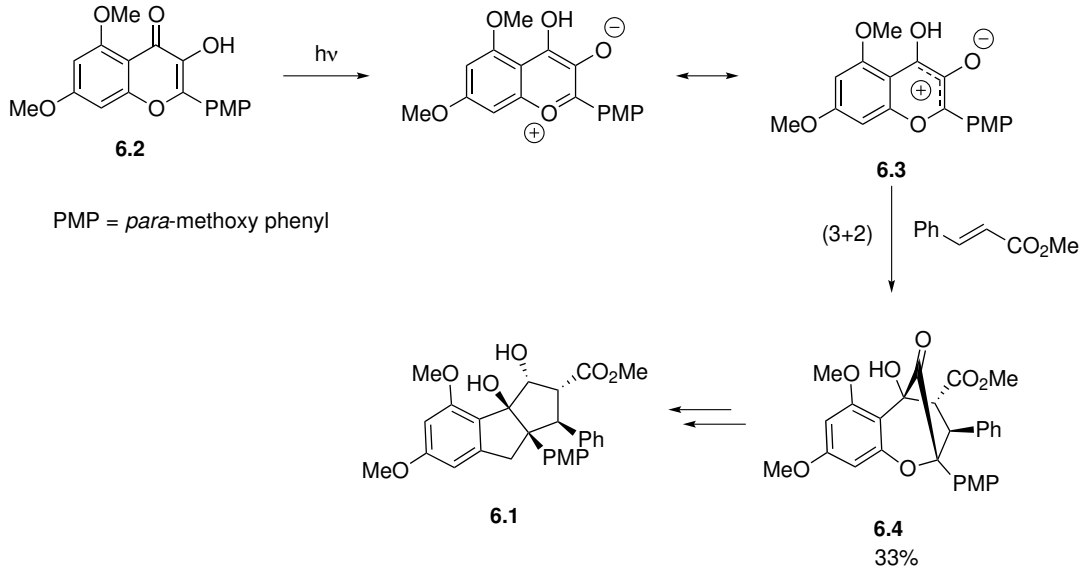

Figure 6.10. – Synthesis of methyl rocoglate by using a photochemical (3+2)–cycloaddition as a key–step

An interesting case of a stepwise (3+2)–cycloaddition of an allyl cation is found in the work of Kuwajima and co-workers.[115,116] The reaction of a 3-(alkylthio)-2-siloxyallyl cation with vinyl sulfides have proven to be a reliable and efficient method for the generation of substituted cyclopentane cores. Moreover, the observed diastereoselectivities were quite remarkable as this transformation is assumed to go via a stepwise mechanism.

The example of **6.5** and **6.6** is shown in fig. 6.11 and includes a fast equilibrating geometry between the olefins under the given conditions, as any of the two vinyl sulfide isomers (**6.5** and **6.6**) yields the same major diastereoisomer. Kuwajima and co–workers proposed a six–membered transition state for the first addition step in which the sulfur atom of the vinyl sulfide partcipates (fig. 6.11). They assume a chair geometry to be the most favoured, meaning that in this case **TS1** would be the preferred reaction path as it lacks 1,3-diaxial interaction of the bulky silyloxy group and the methyl group of the vinyl sulfide. Because of the fast equilibrium between the two vinyl sulfide isomers, the diastereomeric ratio is expected to depend completely on the energy difference between **TS1** and **TS2** as the second ring–closure of the intermediates (**Int1** and **Int2**) can readily occur without bond rotation. A similar model has also been proposed earlier for the (2+2)–cycloaddition of vinyl selenides and enones, a similarly forbidden ground state transformation.[117,118]

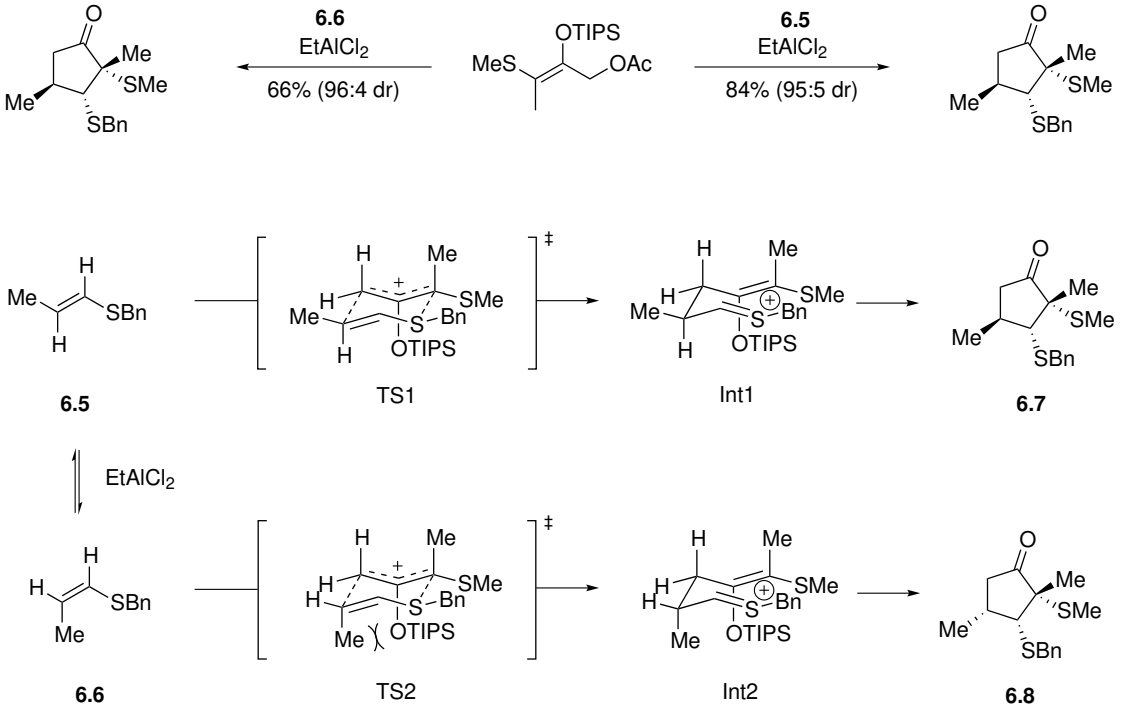

Figure 6.11. – Diastereoselective (3+2)–cycloaddition of vinyl sulfide and a 3-(alkylthio)-2-siloxyallyl cation

We could however explain these results by a different model. If we assume the addition of the olefin to vinyl sulfide **6.6**, not going through a pre–organised transition state, rotational freedom of the intermediate can also lead to the same major diastereoisomer as was reported by Kuwajima. In this case, the diastereomeric ratio might be determined by thermodynamics rather than kinetics.

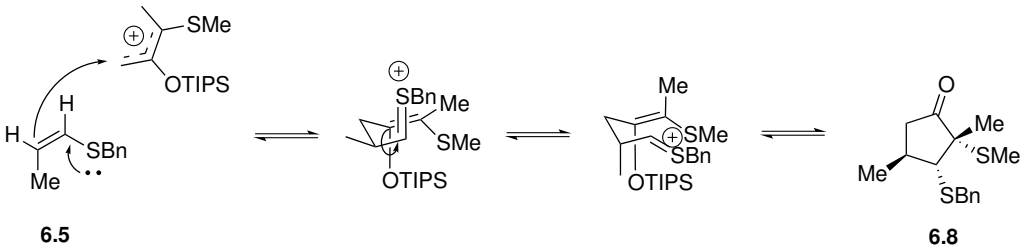

Figure 6.12. – Alternative mechanism for the (3+2)–cycloaddition as reported by Kuwajima

6.4.3. (4+3)–cycloadditions

The first example of a (4+3)-cycloaddition, more specifically a $[_\pi 2 +_\pi 4]$–cycloaddition, came from the work of Fort in which α-chloroketone **6.9** was treated with 2,6-lutidine in the presence of furan, generating the bicyclic ketone **6.10** as a mixture of different diastereoisomers (fig. 6.13).[119]

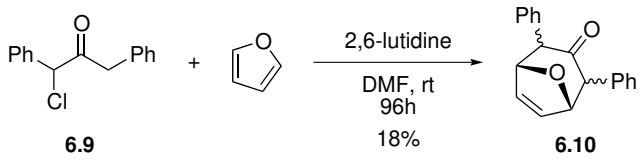

Figure 6.13. – First reported (4+3)–cycloaddition

The action of 2,6-lutidine onto α-chloroketone **6.9** yields the enolate **6.11** that, upon losing the chlorine atom, forms an intermediate which is also found in the Favorskii rearrangement (fig. 6.14). The open form **6.12** is called an oxyallyl cation or propenylium-2-olate, and serves as the three–center allyl cation for the cycloaddition.

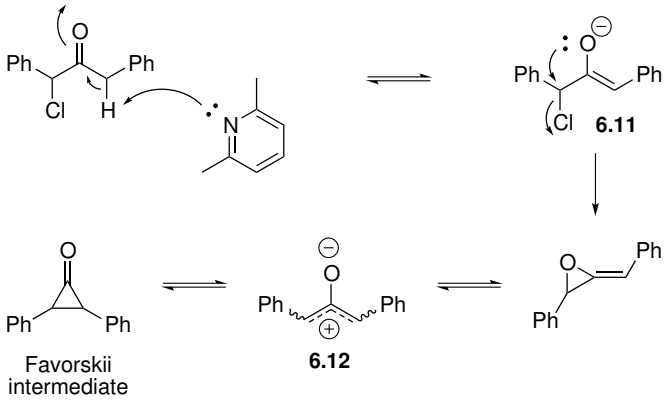

Figure 6.14. – Formation of the oxyallyl cation

From the molecular orbitals of an allyl cation and butadiene we see that the overlap of HOMO and LUMO is symmetry–allowed, meaning that a concerted reaction path is possible under thermal conditions (fig. 6.15). However, (4+3)–cycloadditions are most likely to proceed via a stepwise mechanism because of the relative energy levels of the involved π–systems.[120–122]

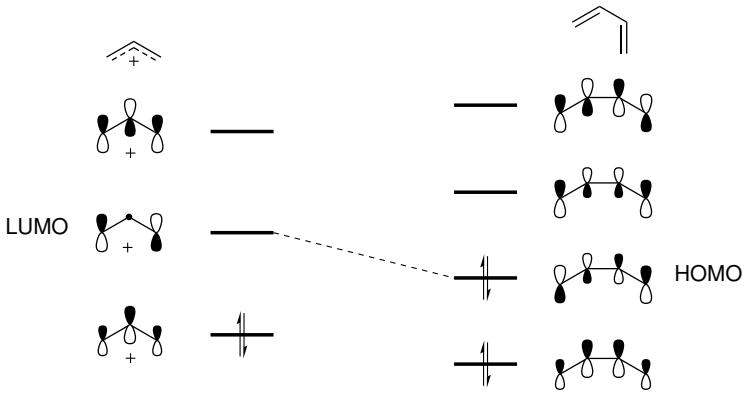

Figure 6.15. – Molecular orbitals of a generic allyl cation and butadiene

Although a concerted path is thermally allowed, the low–barrier stepwise pathways give rise to several possible reaction outcomes that can be classified into different types (fig. 6.16).

Class A: Concerted cycloaddition As was mentioned in the introduction, this mode of addition will proceed with high degrees of stereoselectivity and stereospecificity. The resulting product will be a 7–membered bicyclic molecule.

Class B: Stepwise cycloaddition The second mode is that in which the allylic cation attacks one side of the diene π–system and then in a second step annulates into the same bridged bicycle as in class B. Depending on the substitution pattern of the allylic cation and the lifetime of intermediate **6.13**, the stereoinformation can either be retained or lost.

Class C: Alternative termination As the intermediate cation **6.13** in its own is a very reactive species, several side reactions can occur to yield other products than the expected cycloadduct **6.14** (*vide supra*). (a) Based on geometric constraints, the annulation into the 7–membered ring might be slower compared to ring–closure to the 5–membered ring. If Y is nucleophilic enough, heterocyclic products might be formed as well. (b) The presence

of nucleophiles in the reaction mixture (e.g. anionic counter ions, water, ...) can capture intermediate **6.13**. (c) Loss of a proton, by which in some cases a very stable conjugated system is formed.

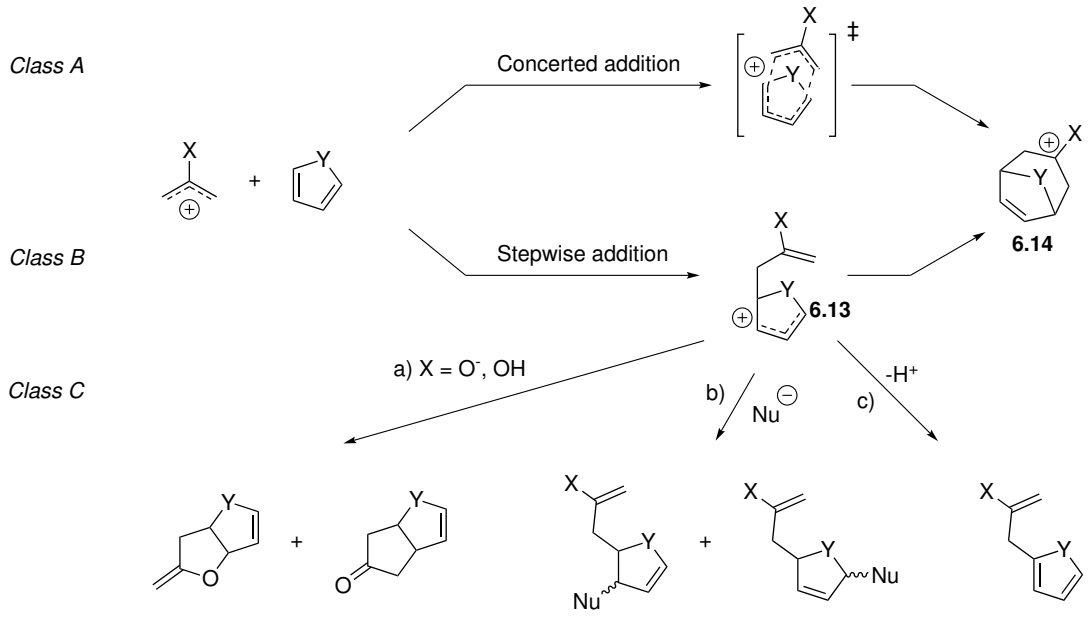

Figure 6.16. – Different classes of reaction paths in (4+3)–cycloaddition

These alternative termination pathways (e.g. Class C) strongly depend on the longevity of the intermediate cation, which is a delicate balanced situation. Should the cation be to stable, postponing any further reaction, problems might indeed arise as competing (intramolecular) pathways can become imminent. On the other hand, a too reactive cation can induce problems as it will react indiscriminately along the possible intramolecular pathways.

Apart from the reactivity of the cationic intermediate and possible side reactions, another important factor to consider in these type of reactions is the stereoselectivity and stereospecificity. It was mentioned before that the class A cycloaddition would indeed

proceed with a high degree of stereoselectivity and -specificity owing to the highly ordered transition state. There are a number of important factors that influence the stereochemical outcome of a (4+3)–cycloaddition or any cycloaddition in general: the geometry of the starting materials, the regioselectivity and the manner in which both reactants approach each other.

When the oxyallyl cation is considered, one can see that there are three possible geometries which it can adopt: ”U”–shaped, ”W”–shaped and ”sickle”–shaped (fig. 6.17). The ”W”-shaped oxyallyl cation is the most stable of the three since steric interactions between both substituents are minimised. This in contrast to the ”U”–shaped geometry which has the highest energy, leaving the ”sickle”-geometry somewhere in between. For pericyclic concerted additions, each of those geometries will give rise to a specific stereochemical outcome related to the original oxyallyl cation stereochemistry, illustrating the stereospecific nature of a concerted reaction path.

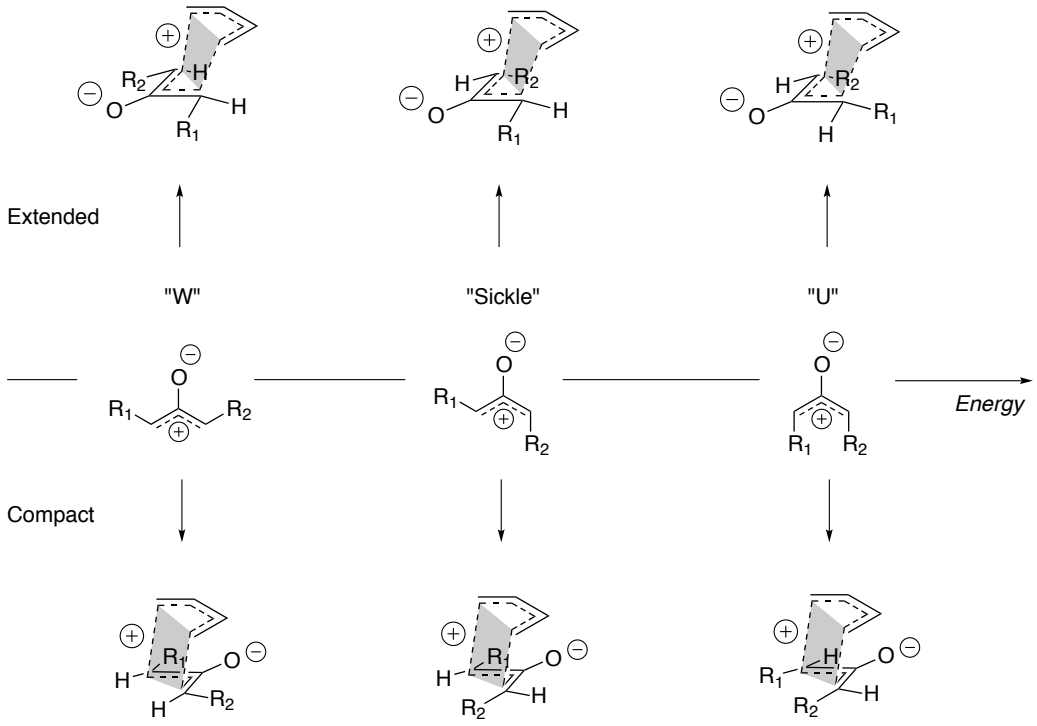

Figure 6.17. – Different geometries of the oxyallyl cation

As was briefly mentioned before, for class B transformations, stereoinformation might be lost due to rotational freedom of the intermediate. Attack at either side of the enolate is possible, generating different epimers, which is certainly true for long–living cationic intermediates.

As the oxyallyl cations are in most cases non–symmetric, regioselectivity will have a profound impact on the reaction's outcome. Frontier orbital coefficients, charge distribution and steric effects are the determining factors for the observed regioisomers.

The relative orientation of diene and allyl cation is also of importance. Approach of both reactants can occur via an extended "chair–like" transition state in which both π–systems are on opposite sides of the incipient σ–bonds or via a transition state having a more compact "boat–like" geometry in which both π–systems are superimposed on each other (fig. 6.17). This is analogous with the more common *exo* and *endo* nomenclature associated with the Diels–Alder reaction, but as IUPAC reserves this for designating the relative substituent positions in bicyclic bridged systems, the terms *extended* and *compact* are preferred. For cationic reactions like these, the *extended* approach is in general found to be more favoured as a compact transition state brings both partial positive charges, smeared out along the entire π–system, closer together resulting in a Coulombic repulsion and thus a higher energy. For zwitterionic (neutral) oxyallyl cations, the compact approach is favoured as the negatively charged oxygen is then in closer proximity to the partially positively charged π–system.

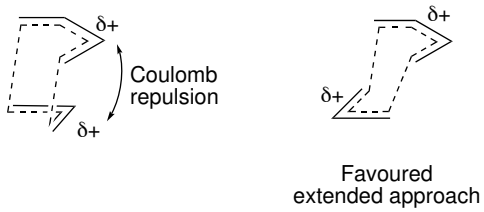

(a) Allyl cation prefers extended approach

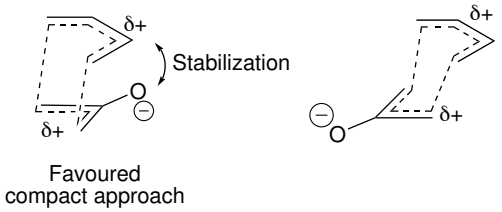

(b) Zwitterion prefers compact addition

Figure 6.18. – Difference between zwitterion and allyl cation approach

A fine example of a (4+3)–cycloaddition comes from the work of Harmata concerning synthetic studies into tricycloclavulone.[123] The key intermediate is accessed through a (4+3)–cycloaddition between cyclopentanone **6.15**–derived oxyallyl cation and cyclopentadiene. From the resulting compact reaction product (**6.16a**), the tricyclic core of tricycloclavulone (**6.17**) was synthesised (fig. 6.19). A fine overview of this transformation is also found in the literature.[124]

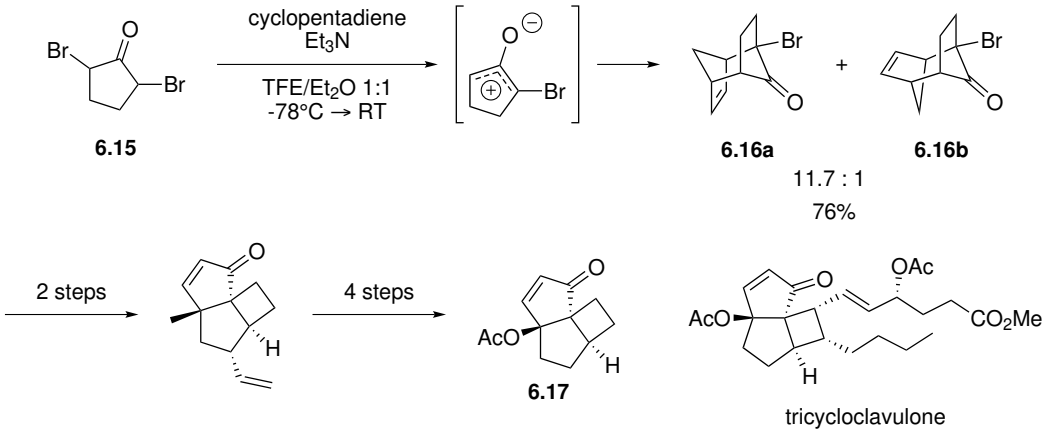

Figure 6.19. – Synthesis of the cyclic core of tricycloclavulone by using a (4+3)–cycloaddition

6.5. Conclusions

Cycloadditions can proceed through various mechanistic pathways. The most distinct difference can be made between stepwise and concerted mechanisms, which was described in detail by Woodward and Hoffmann and culminated in the widely accepted Woodward–Hoffmann (WH) rules. This geometric considerations on transition states were then complemented by the perturbation molecular orbital (PMO) model which allowed for rationalization of transition state energies. Both of these concepts provided the theoretical framework for estimates of the nature of the transition states through which cycloadditions have to go.

There are numerous examples of cycloaddition reactions in which cyclic molecules are formed but the most well known are arguably the (2+2)– and (4+2)–cycloaddition (Diels–Alder), providing four– and six–membered rings respectively. However, in this chapter we focussed on the lesser known cycloaddition reactions that produce odd–membered rings ((2+1), (2+3), (3+4)). As these are in general found to involve radical, charged or zwitterionic reaction partners, the analysis of possible outcomes can become increasingly complex depending on concerted or stepwise mechanisms.

The concepts that were introduced in this chapter will now be applied in the following chapters in specific cases of cycloadditions that were developed in our lab.

7 Stereoselectivity in stepwise (4+3)-cycloadditions of furfuryl cations

Selectivity in stepwise (4+3) cycloadditions of furfuryl cations: stereocontrol by highly organized transition states in a nonstop cycloaddition mechanism (*in revision*)

Dietmar Hertsen,[a,†] Bram Denoo,[b,†] Oykum Naz Avci,[c] Veronique Van Speybroeck,[a] Johan M. Winne,[b] Saron Catak[a,c]

[a] Center for Molecular Modeling, Ghent University, Tech Lane Ghent Science Park Campus A, Technologiepark 903, 9052 Zwijnaarde, Belgium. E-mail: [b] Organic Synthesis Research Group, Department of Organic and Macromolecular Chemistry, Ghent University, Krijgslaan 281(S4), 9000 Gent, Belgium. [c] Bogazici University, Department of Chemistry, Bebek, Istanbul, 34342, Turkey. † These authors contributed equally to this manuscript.

Author contribution: B.D. did the experimental work

7.1. INTRODUCTION: (4+3)–CYCLOADDITIONS OF FURFURYL CATIONS

In 2009 Winne and Pattenden reported a novel dehydrative [4+3] cycloheptannulation between a 1,3-diene and a furfuryl alcohol during synthetic studies into the polycyclic diterpene rameswaralide (**7.1**).[125] Treating **7.2** with trifluoroacetic acid (TFA) unexpectedly yielded **7.3** (fig. 7.1).

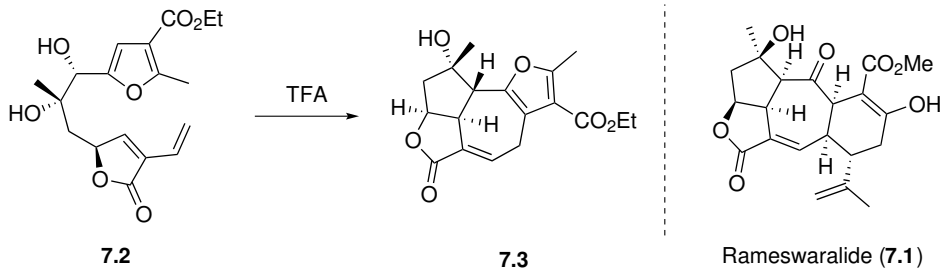

Figure 7.1. – Unexpected dehydrative (4+3)–cycloaddition in the total synthesis of Rameswaralide

The reaction can be rationalized by assuming that the Brønsted acid TFA protonates the furfuryl alcohol after which, by releasing water, a fairly stable oxyallyl–type furfuryl cation is formed (see chapter 5). The cationic three–center reacts with the 1,3-diene yielding a oxonium intermediate, which, after elimination of a proton, restores the aromatic furan ring yielding a furan–fused 7–membered ring (fig. 7.2).

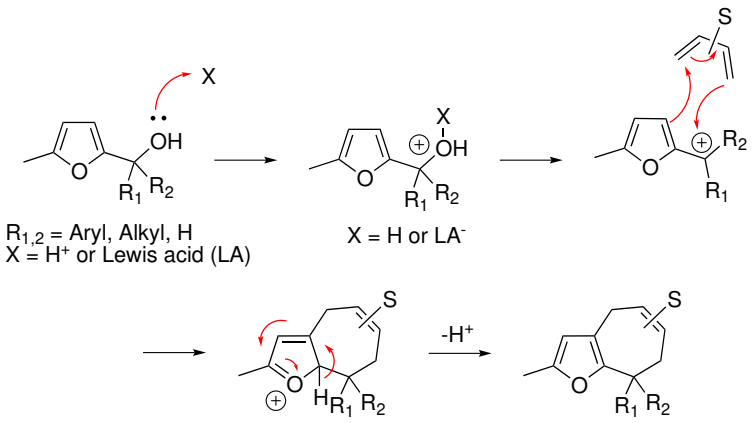

Figure 7.2. – General scheme of (4+3)–cycloaddition between a furfuryl cation and a 1,3–diene

In 2011, Winne *et al.* published follow–up research in which they showed that this remarkable transformation is very well suited for the generation of a family of complex carbocyclic structures. A thorough investigation on the scope of this reaction, indicated that titanium(IV)chloride–generated furfuryl cations are very reliable reaction partners in intermolecular (4+3)–cycloadditions with a lot of different 1,3–dienes. This is in contrast to the more classical (4+3)–cycloadditions with oxyallyl cations, which are in general limited to intermolecular reactions with furan and cyclopentadiene or intramolecular cycloadditions.[124] The furfuryl cation requires the presence of a substituent on the nucleophilic 5–position in order to avoid furan oligomerisation.[126] Interestingly, different substitution patterns at the carbinol carbon of the furfuryl alcohol give mixtures of diastereoisomers which mainly arise through relative addition geometries.

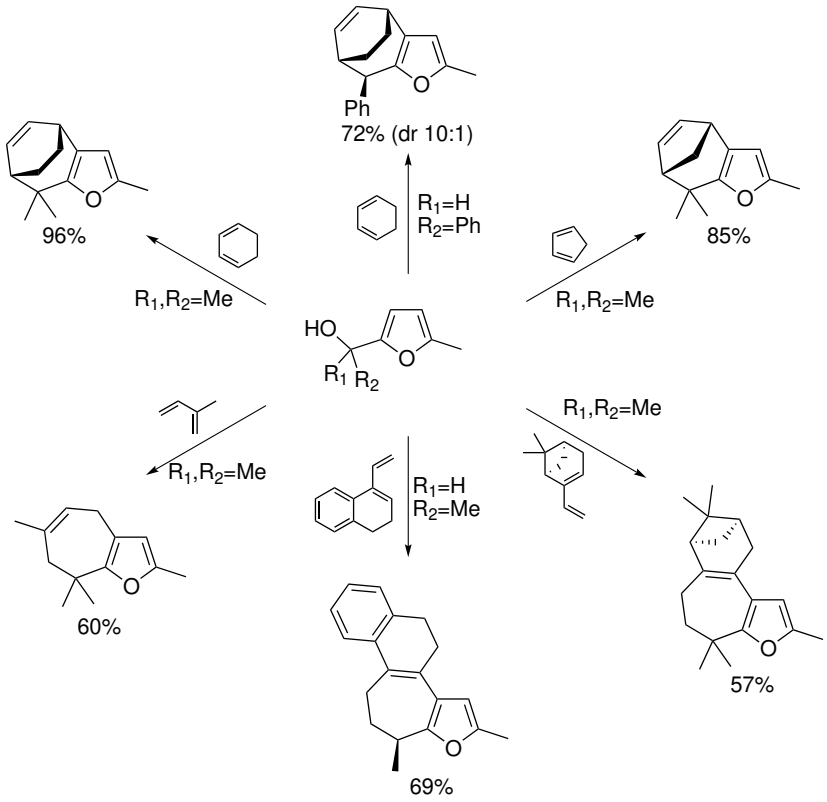

Figure 7.3. – Selected examples of different dienes reacting with furfuryl cations in a (4+3)–cycloaddition

The secondary furfuryl alcohols can give two different (*E*)and (*Z*) isomers when dehydrated with titanium(IV)chloride (fig. 7.4). In chapter 6 we discussed the *compact* and *extended* approaches for concerted reactions but these terms are equally well–suited for designating different stereochemical outcomes of the reaction of 1,3–cyclohexadiene and a secondary furfuryl cation (fig. 7.4.

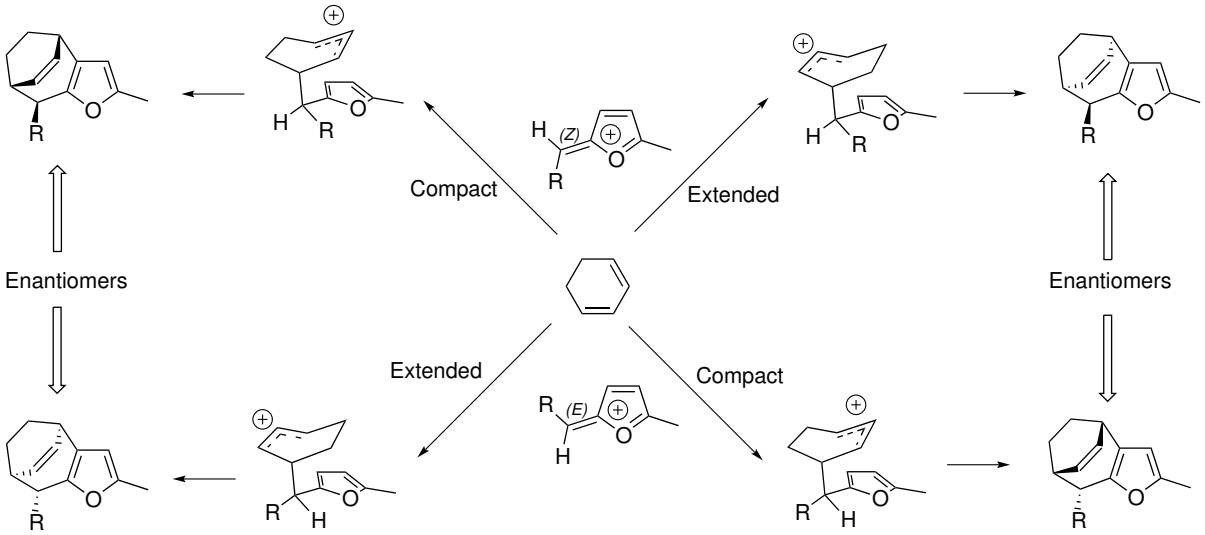

Figure 7.4. – Different addition approaches of 1,3–cyclohexadiene onto (*E*)and (*Z*) furfuryl cations

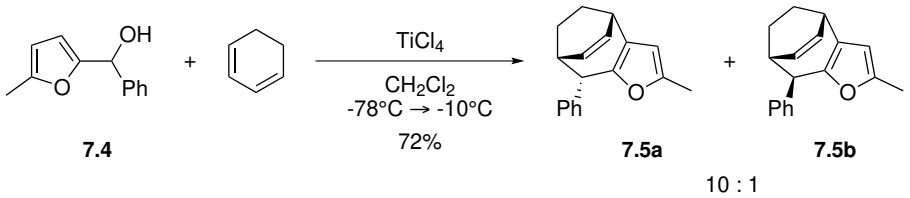

7.4 **7.5a** **7.5b**

Figure 7.5. – Cycloaddition reaction between alcohol **7.4** and cyclohexadiene as reported by Winne and co–workers

A rationalization of the putative mechanism of this cycloaddition was done with the help of DFT calculations. Stationary points for the model reaction between the cation from alcohol **7.4** and 1,3-cyclohexadiene (fig. 7.6) considered competing stepwise and concerted mechanisms (**TSc**), showing the concerted pathway being favoured by at least 10 kJ/mol for both a compact (*C*) and extended (*Ex*) approach. The stepwise reaction goes through two distinct steps in which the first electrophilic addition step was shown to be rate–limiting. This study did not show a clear preference for *compact* or *extended* reaction approaches.

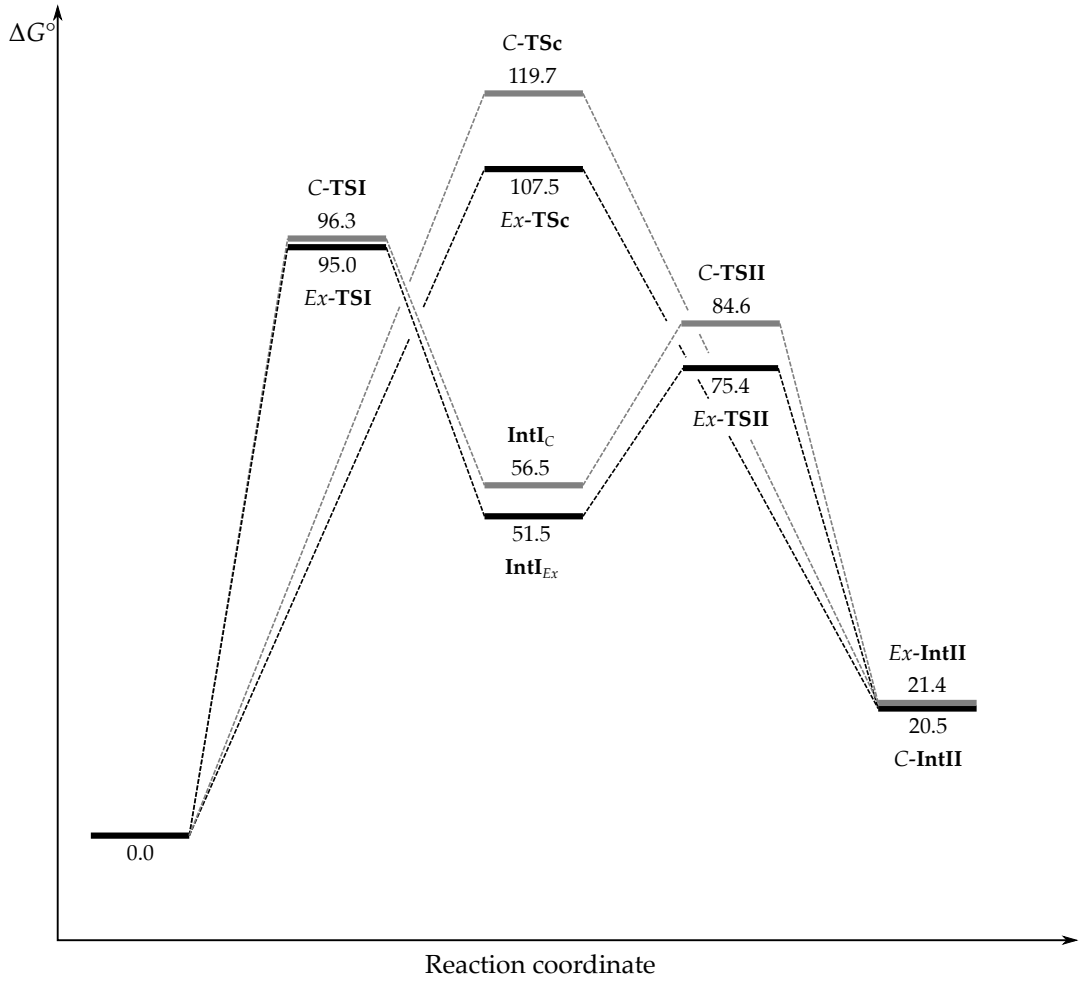

Figure 7.6. – Free–energy profile for the reaction between alcohol **7.4** and cyclohexadiene. Free energies in kJ/mol at the BMK/6-311+G(d,p)//B3LYP/6-31+G(d,p) level of theory, CPCM (ϵ=8.93, dichloromethane)

7.2. Stereoselective intermolecular (4+3)–cycloadditions with α-phellandrene

Previous studies have shown that intermolecular (4+3)–cycloadditions with furfuryl cations can be applied with a lot of different dienes. This spurred us to investigate the use of asymmetric/chiral dienes to see whether stereo–induction directs the stereochemical out-

come of the cycloaddition reaction. We chose to use the natural sesquiterpene (*R*)-*α*-phellandrene as an initial testsubstrate for this purpose.

Interestingly, the reaction between dimethyl furfuryl alcohol **7.6** and the monoterpene (*R*)-*α*-phellandrene under standard conditions, gave a mixture of the expected cycloadduct **7.7** and the alkylated adduct **7.8**, which came from a Friedel–Crafts alkylation reaction of cycloadduct **7.7** and a phellandrene–derived cation.

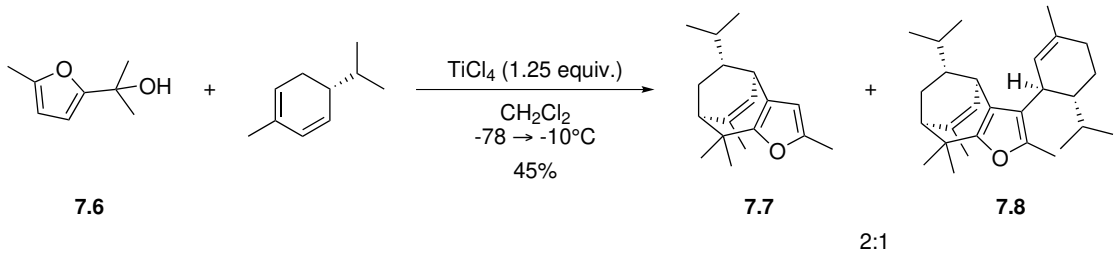

Figure 7.7. – Cycloheptannulation between furfuryl alcohol **7.6** and phellandrene

Both adducts were shown to be formed as single diastereoisomers in which distinct nOe contacts between isopropyl hydrogens and the hydrogen on the double bond showed that the isopropyl group on the ethylene bridge was *exo*–orientation. Moreover, the Friedel–crafts alkylation was also shown to proceed with a high degree of stereoinduction from the phellandrene isopropyl group. The relative stereochemistry could be attributed by distinct 1,3–diaxial nOe contacts on the phellandrene ring.

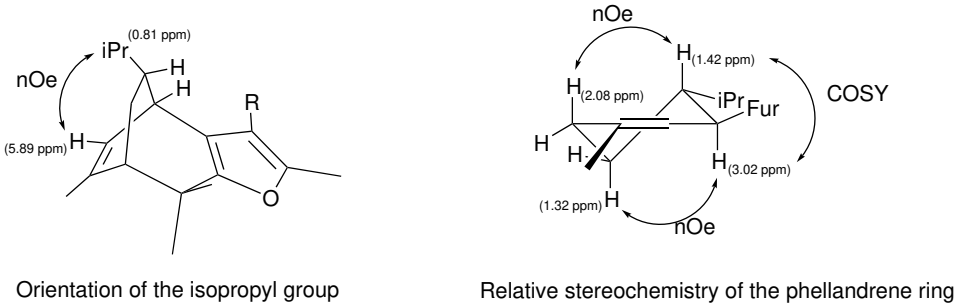

Figure 7.8. – Charactareistic nOe and COSY correlations for **7.7** and **7.9**

Although promising, this transformation was compromised by the presence of the alkylated product **7.8**. Optimisation experiments in order to suppress the Friedel–Crafts alkylation pathway led to the establishment of an alternative set of conditions which included the addition of water to the reaction mixture,[127] giving cycloadduct **7.7** with a yield of 87 %.

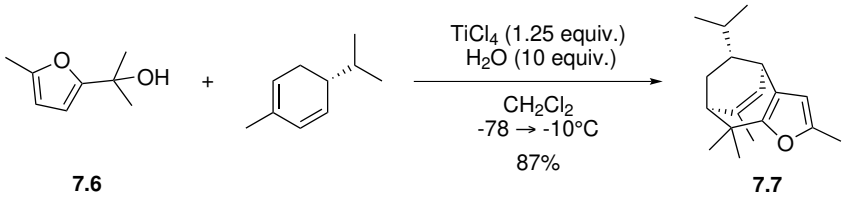

Figure 7.9. – Optimized conditions for the synthesis of **7.10**

Further studies into the stereocontrol of this transformation were done by changing the substituents on the carbinol position of the furfuryl alcohol (fig. 7.10). Different furfuryl alcohols were easily accessible starting from commercially available furan precursors. Sodium borohydride reduction of 1-(5-methylfuran-2-yl)ethanone and 5-methylfuran-2-carbaldehyde readily gave the alcohols **7.11** and **7.12** respectively. Alcohols **7.4** and **7.13**

could easily be prepared by reacting 5-methylfuran-2-carbaldehyde with the appropriate Grignard reagent. Reacting benzofuran with butyllithium and acetone gave the alcohol **7.14**.

Reaction of phellandrene with the prepared alcohols gave the cycloadducts **7.15**, **7.16**, **7.17**, **7.18** and **7.19**. The isolated yields can be correlated with the substitution at the carbinol position. The relative stability of the cation will be determining for the efficiency of the cycloaddition, as furfuryl cations are prone to react with themselves. In general, secondary furfuryl alcohols will be more sensitive to undergo side reactions. A notable exception is the phenyl–substituted alcohol (**7.4**), a feature that can be attributed to the cation stabilizing effect of the aromatic ring. The primary furfuryl alcohol **7.12** shows the least optimal performance as primary cations will most likely be too reactive.

Interestingly, in each case, we observed complete stereoselectivity on the newly formed bonds resulting in the exclusive *exo*–orientation of the isopropyl group. The stereocenter that was introduced by the asymmetrically substituted furfuryl alcohol completely determines the diasteromeric ratios that are observed. Moreover, these ratios seem to correlate with the bulkiness of the substituent.

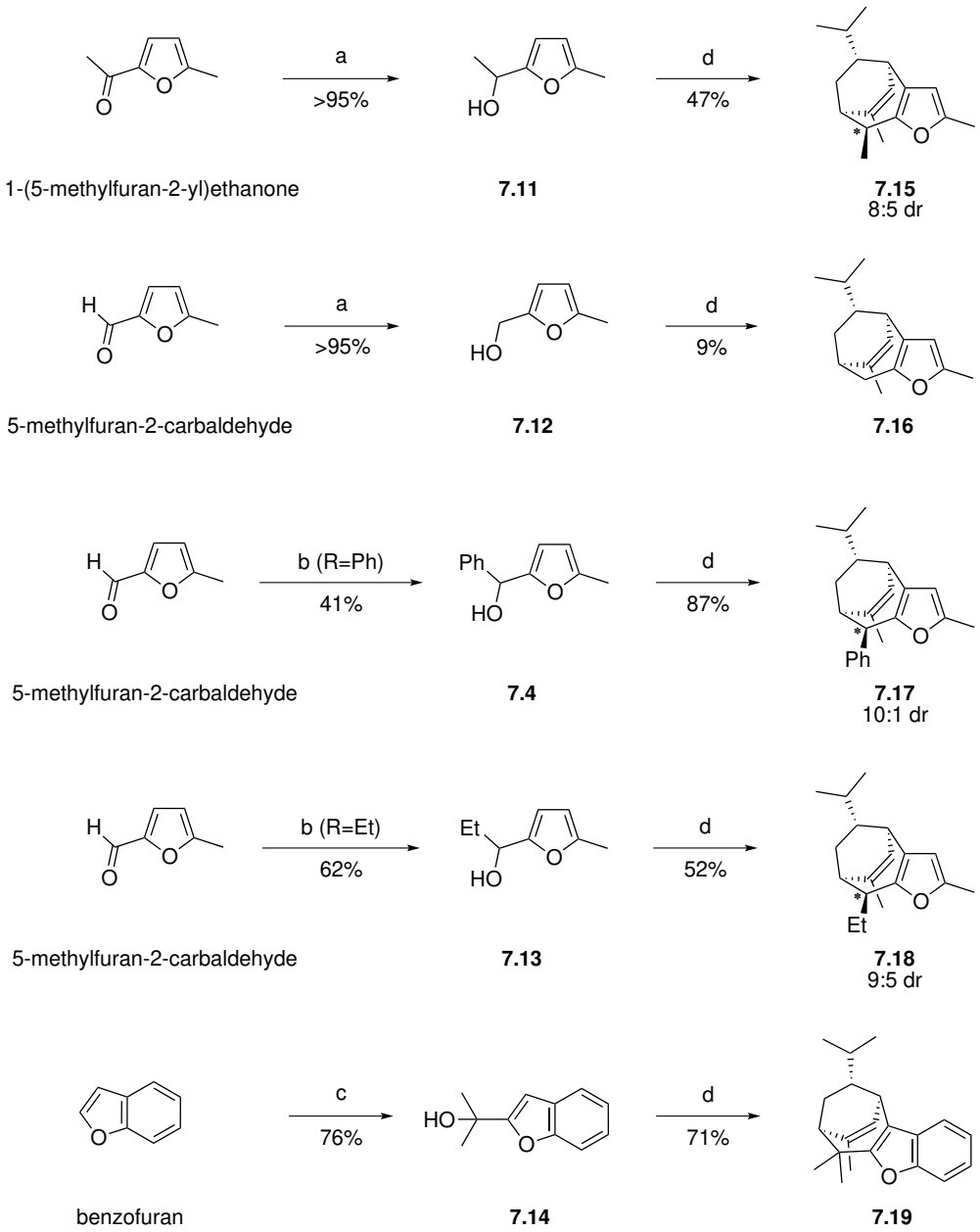

a) $NaBH_4$, MeOH, -20°C to RT; b) RMgCl, THF, 0°C to RT; c) 1. BuLi, THF, -78°C 2. acetone, THF
d) $TiCl_4$, H_2O, CH_2Cl_2, -78°C to -10°C

Figure 7.10. – Different furfuryl alcohols and corresponding cycloadducts. In case of mixtures of diastereoisomers, the major isomer is shown

The orientation of the isopropyl group could again be determined by the characteristic nOe contacts of the isopropyl hydrogens and the hydrogen present on the double bond. The relative orientation of the carbinol substituents could then be designated by specific nOe contacts with the *endo*–hydrogen on the ethylene bridge. The H–NMR spectrum of cycloadduct **7.17** showed a remarkably low chemical shift for the methyl group on the double bond of the minor isomer, which could be explained by a diamagnetic anisotropy effect of the proximal phenyl group.

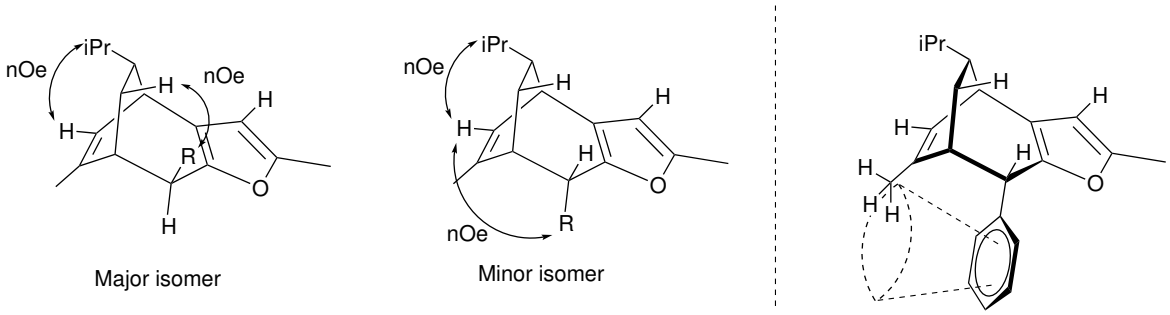

Figure 7.11. – Characteristic nOe contacts for cycloadducts from asymmetric cycloaddition reactions

The exclusive *exo*–orientation of the isopropyl group can be explained as follows. Either the reaction goes via a compact concerted transition state which is completely stereoinduced by the isopropyl group (fig. 7.12a), or via a stepwise process in which the first electrophilic attack goes via a 'boat'–type transition state in which maximum staggering of substituents is pursued,[128] and again the orientation of the isopropyl group directs the attack to the opposite face (fig. 7.12b).

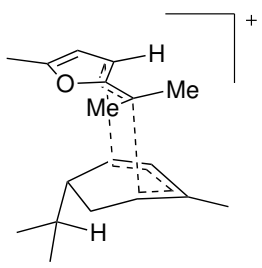

(a) Concerted transition state

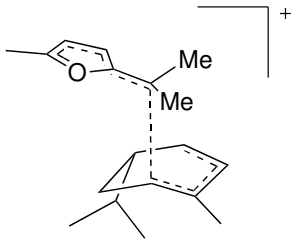

(b) Staggered 'boat'–like transition state for first electrophilic addition step

Figure 7.12. – Possible transition states for (a) concerted mechanism (b) stepwise mechanism

We discussed earlier that this (4+3)–cycloaddition reaction probably goes via a stepwise process, but the question then remains if this can account for the observed high stereoselectivities. The literature holds multiple accounts in which a similar degree of stereoselectivity is observed in cycloadditions with phellandrene.

Thermal (2+2)–cycloadditions of phellandrene with ketenes yield bicyclic adducts in which the isopropyl group and cyclobutane are found primarily at opposite faces.[129,130] Also, an oxidative (3+2) cycloaddition shows a product distribution of two regioisomers of which both isomers again show the same *trans*–relation of the five membered ring relative to the isopropyl group.[131] This can be seen for the cerium ammonium nitrate–induced reaction of phellandrene with **7.20**, which is a key step in the total synthesis of the natural products callistrone A–E (fig. 7.13). Similarly, Diels–Alder reactions with phellandrene have been reported to give high stereoselectivities. An illustrative example is given by the reaction between phellandrene and protoanemonin giving a mixture of extended and compact addition products (**7.21a** and **7.21b**) both showing an *exo*–oriented isopropyl group.[132] Also, the synthesis of the chiral catalyst ligand **7.22** gives a single *exo*–diastereoisomer.[133]

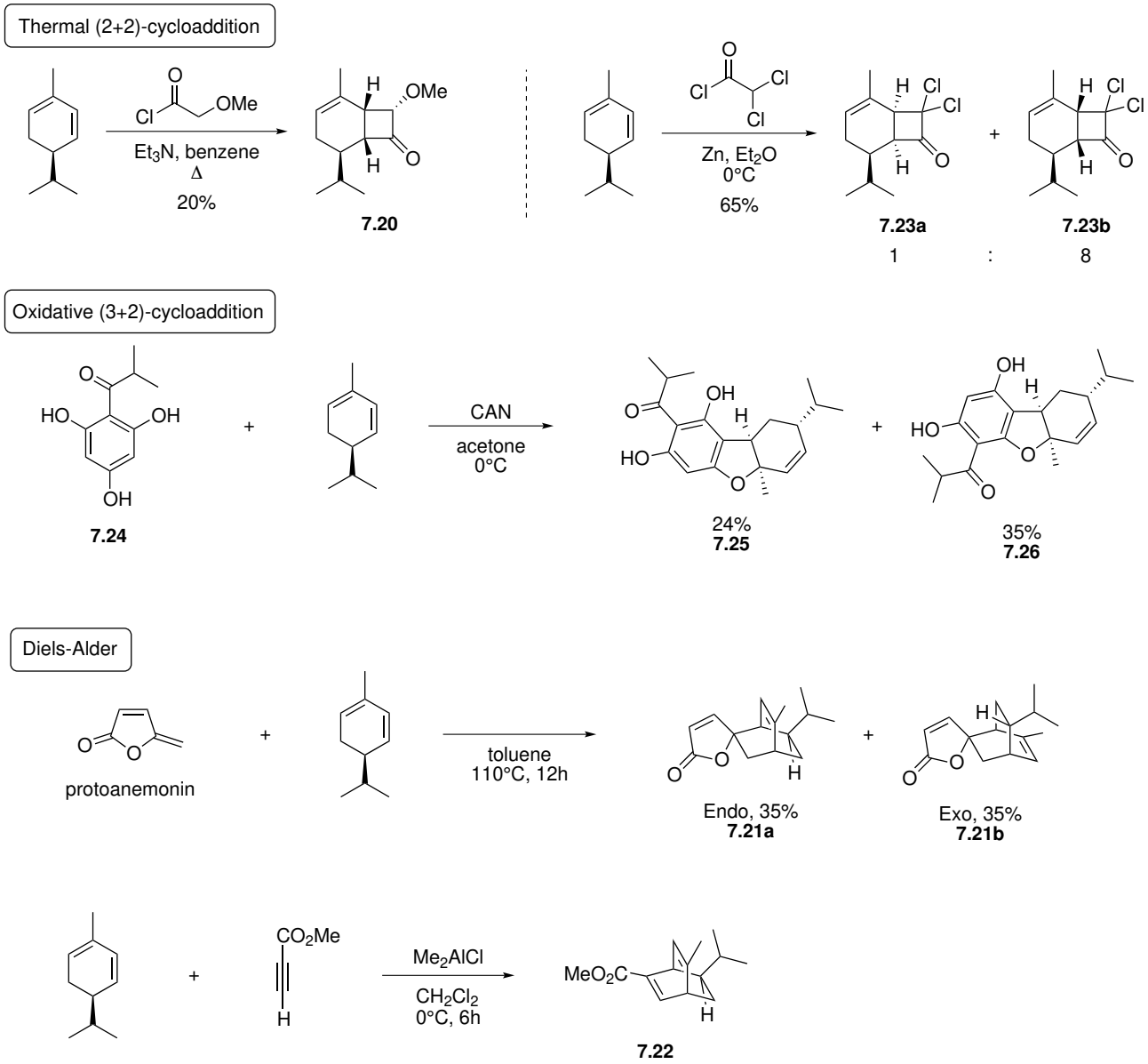

Figure 7.13. – Illustrative examples of stereoselective cycloaddition reactions with phellandrene

A number of electrophilic addition reactions of phellandrene are also reported to give high stereoselectivities (fig. 7.14). A hydroboration–carboxylation tandem of phellandrene yields two regiosomers (**7.27**) of the resulting carboxylic acid, which is oriented *trans* relative to the isopropyl group. Also, an electrophilic aromatic substitution of **7.28**

with a phellandrene–derived cation is shown to give **7.29** yield in a stereoselective way.

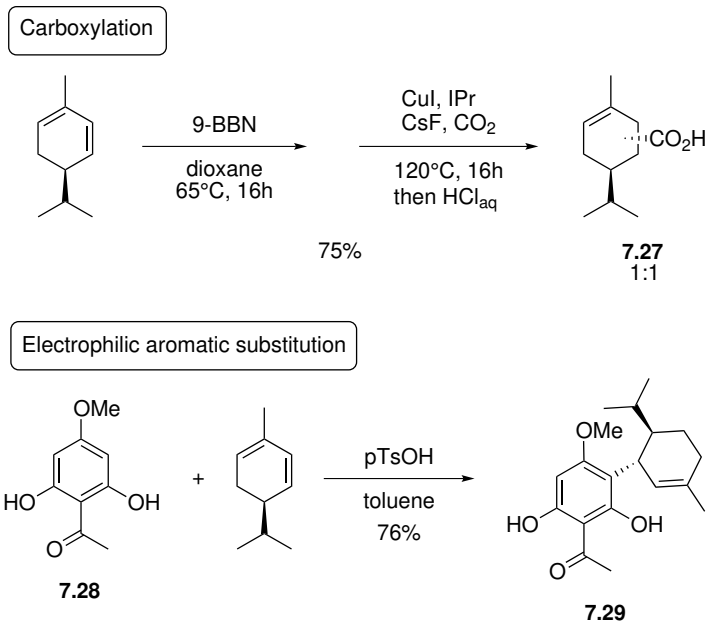

Figure 7.14. – Illustrative examples of stereoselective electrophilic addition reactions with phellandrene

These examples suggest that even if a stepwise addition onto phellandrene is the prevalent pathway, high stereoselectivities can be expected. Nevertheless, in order to get a complete picture of the factors that govern the stereoselectivity in the particular case of the (4+3)–cycloaddition of furfuryl cations with pellandrene, we decided to perform an elaborate computational study on this transformation.

7.3. Theoretical study of the reaction between furfuryl cations and (*R*)-α-phellandrene

7.3.1. Transition state theory: an introduction

In 1935, Eyring proposed the concept of the transition state theory as a means to describe kinetics of molecular reactions. Before that, reaction rates were calculated by estimating the number of collisions between reacting molecules.[134] Central in the kinetics treatment according to Eyring is the potential energy surface on which a specific temporary state is singled out called the transition state (‡). The trajectory of any molecular system from starting material through the transition state to the final products is called the reaction coordinate and plotting the energy along this coordinate gives us a curve like the one in fig. 7.15, which is called the potential energy profile.

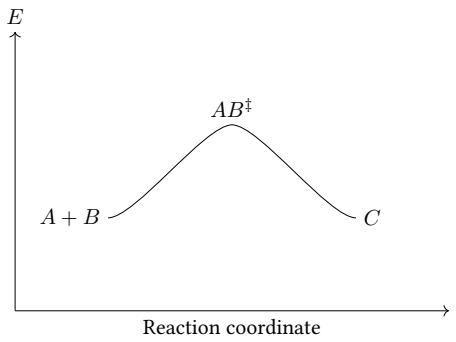

Figure 7.15. – The reaction coordinate

The hypothesis on which Eyring built his theory was based on the assumption that the starting materials are in thermodynamic equilibrium with the transition state. Hence, a reaction like:

$$A + B \rightarrow C \tag{7.1}$$

Becomes:

$$A + B \rightleftharpoons AB^{\ddagger} \rightarrow C \tag{7.2}$$

Which implies:

$$K^{\ddagger} = \frac{[AB^{\ddagger}]}{[A][B]} \tag{7.3}$$

Eyring derived an equation (which is not given here) that could relate the rate constant of such a reaction (cf. eq. (7.1)) with the equilibrium constant $K^{\ddagger}$. Provided that the reactive trajectory is plotted in free energies (then called the free energy profile), the rate constant becomes:

$$k = \frac{k_B T}{h} K^{\ddagger} = \frac{k_B T}{h} \exp(-\frac{\Delta G^{\circ,\ddagger}}{RT}) \tag{7.4}$$

This is particularly suitable for comparing reaction rates between two competing reaction paths (see fig. 7.16) for which the relative rate becomes:

$$\frac{k_1}{k_2} = \exp(-\frac{\Delta G_1^{\circ,\ddagger} - \Delta G_2^{\circ,\ddagger}}{RT}) \tag{7.5}$$

This means that for an energy difference of 10 kJ/mol between two transition states at $-78\,^{\circ}\mathrm{C}$, the lowest energy reaction path will be 477 times faster.

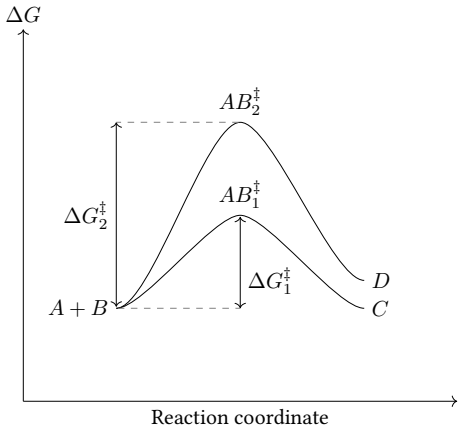

Figure 7.16. – Relative rates for competing reaction paths

7.3.2. (*R*)-α-phellandrene and furfuryl alcohol 7.6

In the previous section we discussed the experimental observations found in several (4+3)–cycloadditions between furfuryl cations and several dienes. In particular, the case of furfuryl alcohol **7.6** and (*R*)-α-phellandrene caught our attention as this reaction proceeds with a very high degree of stereoselectivity (see fig. 7.9). Therefore we chose this transformation as a case study for a detailed computational survey in order to elucidate the stereocontrolling factors that induce the remarkably high selectivity.

In fig. 7.18 we have given an overview of the possible addition modes between phellandrene and furfuryl cation $\mathbf{I}_{Me_2}$. Electrophilic addition of the furfuryl cation onto phellandrene gives intermediate $\mathbf{II}_{Me_2}$. There are two distinct modes of attack depending on the relative orientation of the isopropyl group and the forming bond which will lead to two different allyl cation intermediates, *cis*–$\mathbf{II}_{Me_2}$ and *trans*–$\mathbf{II}_{Me_2}$. In both cases, however there are multiple possible geometries for $\mathbf{TSI}_{Me_2}$ determined by the dihedral angle around the incipient bond.

Initially we selected four preorganised transition state geometries resembling those of concerted transitions states. These transition states will be indicated with the *Compact* (*C*) and *Extended* (*Ex*) which is normally used for concerted transition states, thus giving: *cis*, *Ex*–$\mathbf{TSI}_{Me_2}$; *cis*, *C*–$\mathbf{TSI}_{Me_2}$; *trans*, *Ex*–$\mathbf{TSI}_{Me_2}$ and *trans*, *C*–$\mathbf{TSI}_{Me_2}$. The optimized geometries of the different possibilities for $\mathbf{TSI}_{Me_2}$ are given in fig. 7.19 and were obtained by cleavage of the cycloadduct. At this point there is no reason to assume these geometries to be privileged over any other possible geometry of $\mathbf{TSI}_{Me_2}$.

The second ring closing step of intermediate can give four distinct oxonium intermediates ($\mathbf{III}_{Me_2}$) through four distinct transition states ($\mathbf{TSII}_{Me_2}$). As these are geometrically comparable to concerted transition states we also adopt the *Compact* (*C*) and *Extended* (*Ex*) nomenclature as for $\mathbf{TSI}_{Me_2}$. From the oxonium intermediates $\mathbf{III}_{Me_2}$, follows an exothermic protonation step, restoring the furan aromaticity and giving the final products *iso*–**7.7** and **7.7**. From all these possibilities only the *trans*–pathway can give the observed

cycloadduct **7.7**.

It should be mentioned that concerted geometries were also located for the *trans*, *C* and *trans*, *Ex* pathways (fig. 7.17). These were however found to be consistently higher in energy then the corresponding $\mathbf{TSI}_{Me_2}$ energies (at the M06-2X/6-31+G(d,p)//B3LYP/6-31+G(d,p) level of theory, IEFPCM (ϵ=8.93, dichloromethane)).

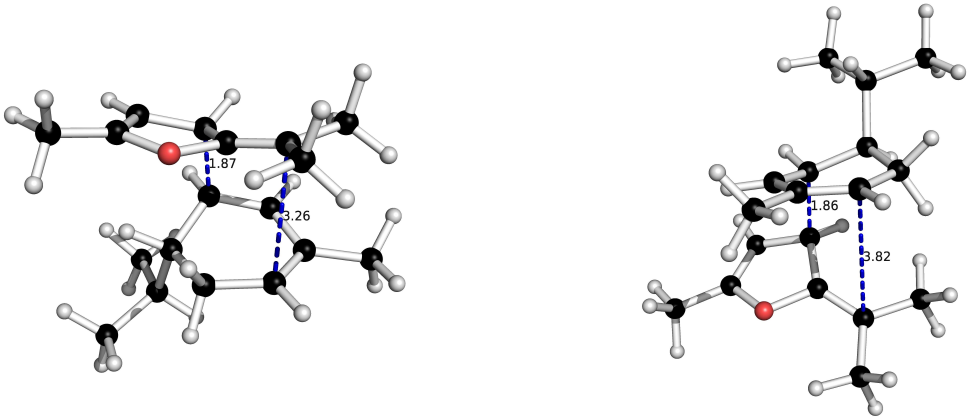

(a) *trans*, *Ex*–$\mathbf{TSc}_{Me_2}$ **(b)** *trans*, *C*–$\mathbf{TSc}_{Me_2}$

Figure 7.17. – Geometries of concerted transition states for the reaction between the cation from **7.6** and phellandrene. M06-2X/6-31+G(d,p)//B3LYP/6-31+G(d,p) level of theory, IEFPCM (ϵ=8.93, dichloromethane), distances in Å

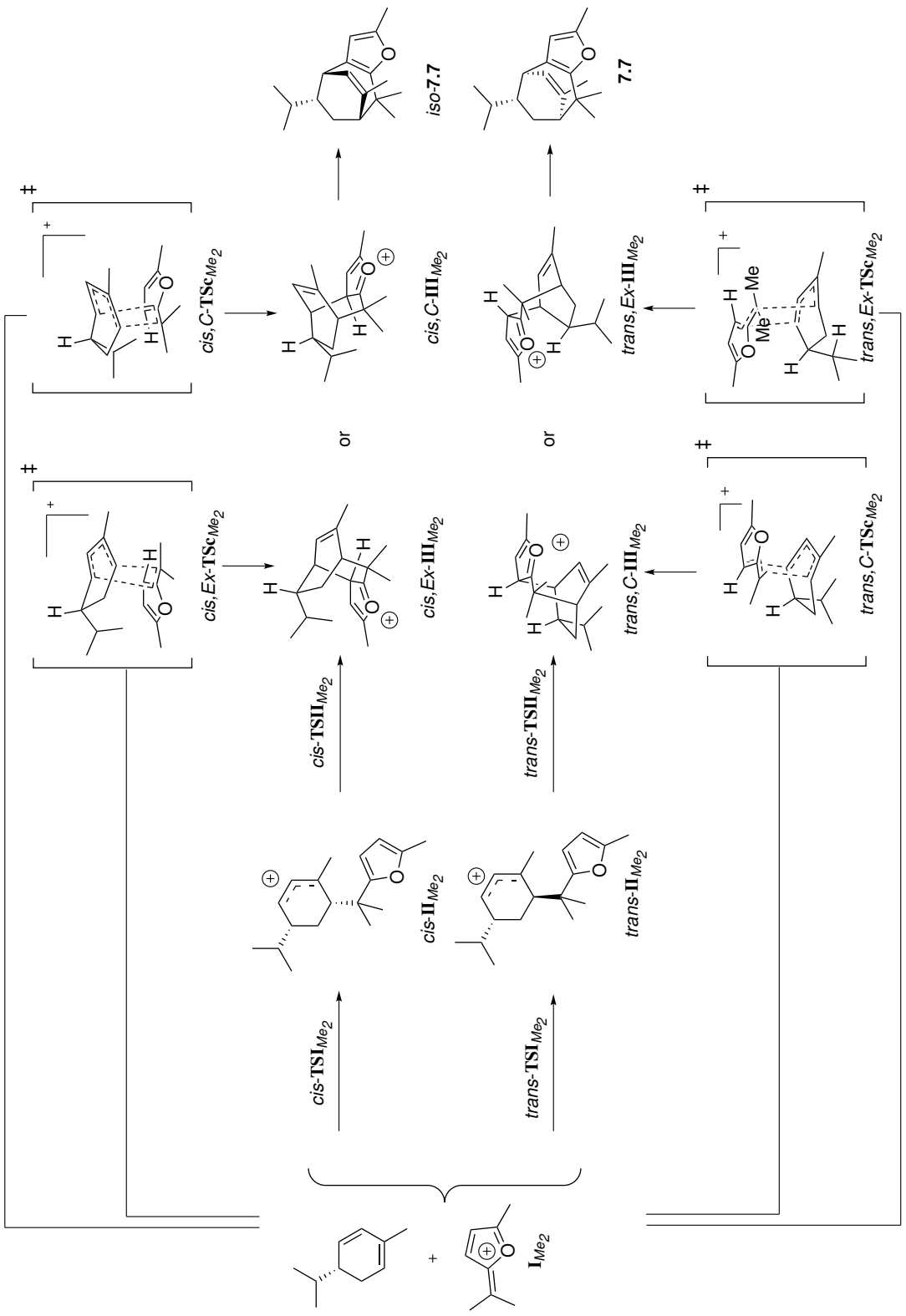

Figure 7.18. – Possibilities for the reaction between furfuryl cation $\mathbf{II}_{Me_2}$ and (*R*)-α-phellandrene

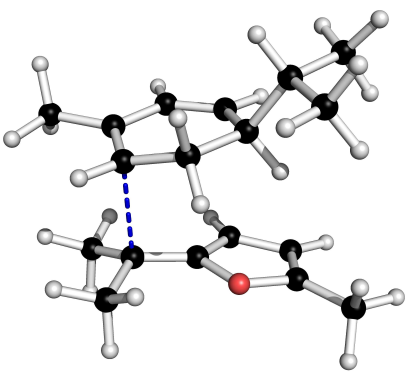

(a) *trans*, *Ex*–**TSI**$_{Me_2}$

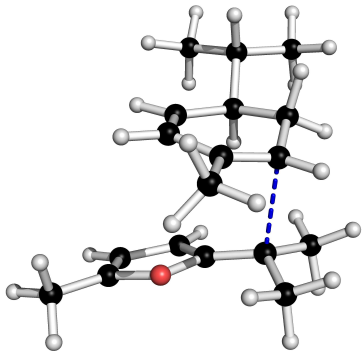

(b) *trans*, *C*–**TSI**$_{Me_2}$

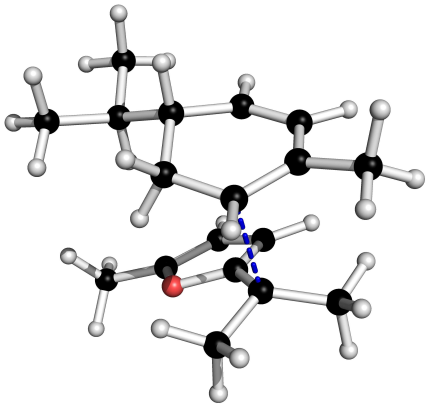

(c) *cis*, *Ex*–**TSI**$_{Me_2}$

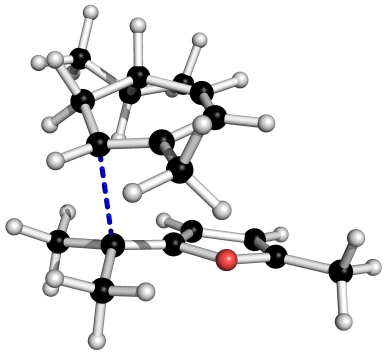

(d) *cis*, *C*–**TSI**$_{Me_2}$

Figure 7.19. – Selected transition states for the first electrophilic addition step (M06-2X/6-31+G(d,p), 298 K, 1 atm, IEF-PCM (CH_2Cl_2, $\epsilon = 8.93$)

From the obtained geometries and corresponding energies, we can now construct a complete potential energy diagram which is given in fig. 7.20. From these diagrams it immediately becomes clear that the *trans*–pathway is kinetically favoured regardless of a *compact* or *extended* approach; the barriers for the *cis*–pathways are consistently higher with approximately 10 kJ/mol for each step.

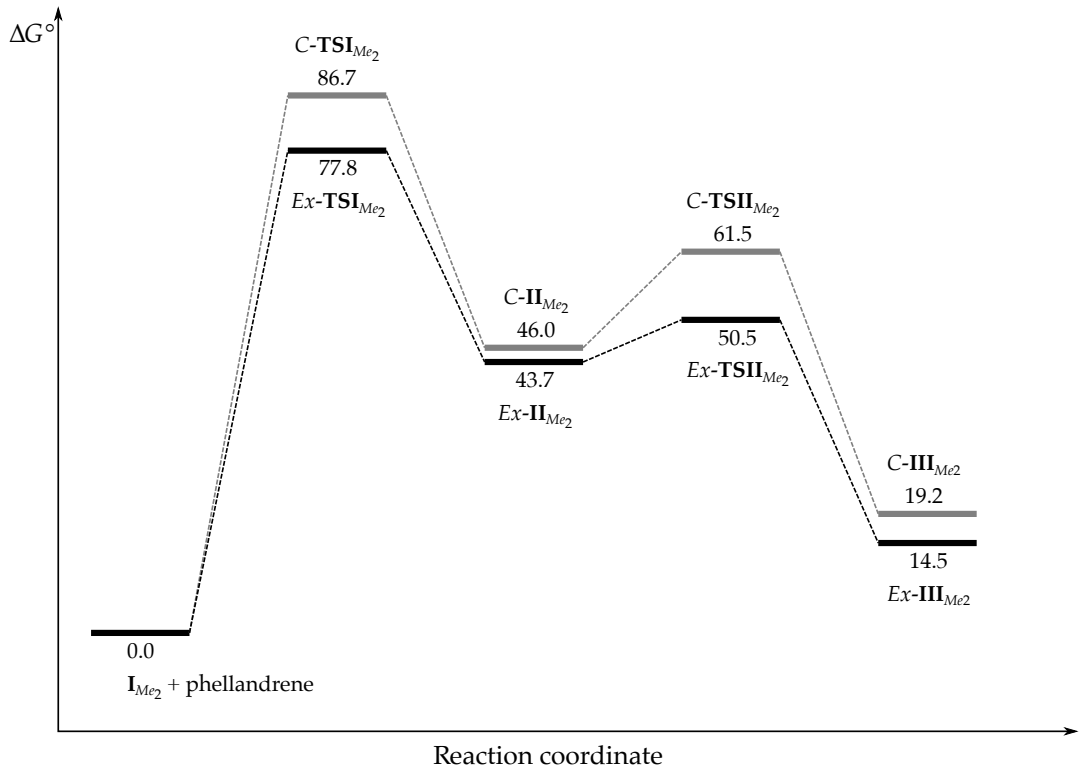

(a) *cis*–pathway

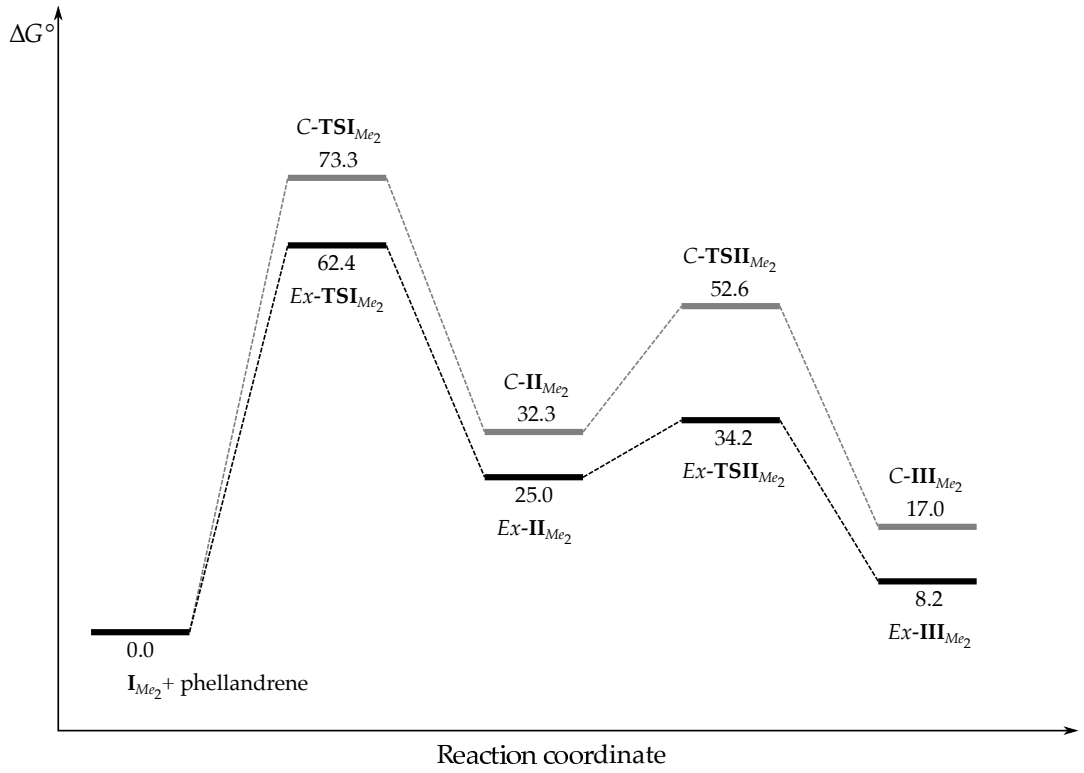

(b) *trans*–pathway

Figure 7.20. – Free–energy profiles for the cycloaddition between phellandrene and cation $\mathbf{I}_{Me_2}$; energies are given in kJ/mol relative to separate reactants (M06-2X/6-31+G(d,p), 298 K, 1 atm, IEF-PCM (CH_2Cl_2, $\epsilon = 8.93$))

The lowest energy *trans,Ex* addition goes through a rate–limiting electrophilic addition step and is in line with the experimental observation of **7.7** as a single isomer. However, the pre-organized nature of the selected transition states could introduce a certain bias in the conclusions that are drawn from the constructed potential energy diagram. To remove this bias, a rotational profile scan around the forming bond in $\mathbf{TSI}_{Me_2}$ was performed to to take into account other possible geometries.

The practical implementation of this rotational scan consists of fixing the distance between the reacting carbons, increasing the dihedral angle in discrete steps and optimising the geometry at each increment. From that we find a rotational profile of relaxed geometries, based on the original transition state geometry, in which the length of the forming bond is fixed. To compare the different dihedral angles in the electrophilic addition step, all minima on the rotational profile are then reoptimized to a transition state (fig. 7.21). Interestingly, these conformational scans showed that the pre–organized *trans*, Ex–$\mathbf{TSI}_{Me_2}$ is consistently the lowest in energy when compared to the other $\mathbf{TSI}_{Me_2}$ barriers (fig. 7.21).

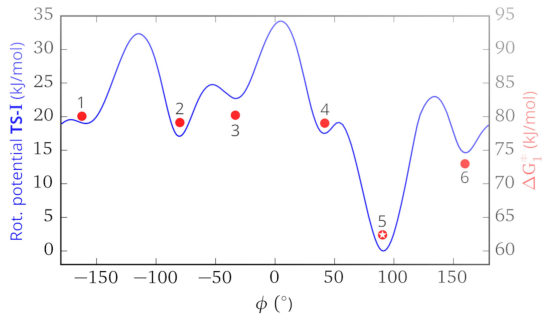

(a) *trans*, *Ex*–**TSI**$_{Me_2}$

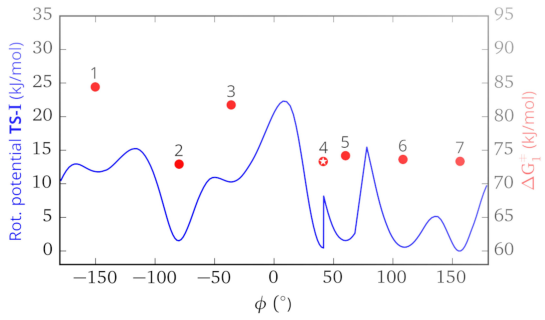

(b) *trans*, *C*–**TSI**$_{Me_2}$

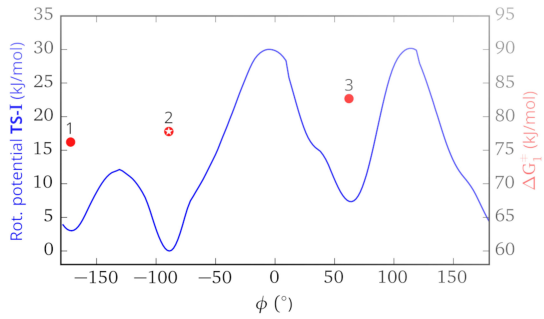

(c) *cis*, *Ex*–**TSI**$_{Me_2}$

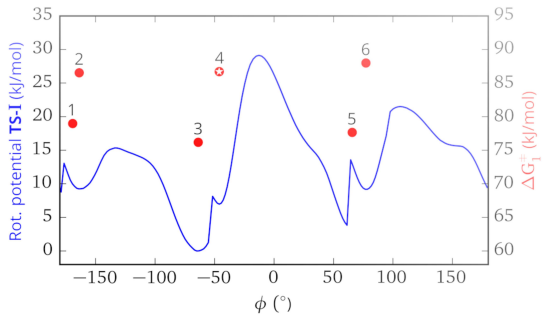

(d) *cis*, *C*–**TSI**$_{Me_2}$

Figure 7.21. – Relaxed rotational scans around the forming bond (blue curve), reoptimised transition state energies (red dots), ✪ pre–organised transition states

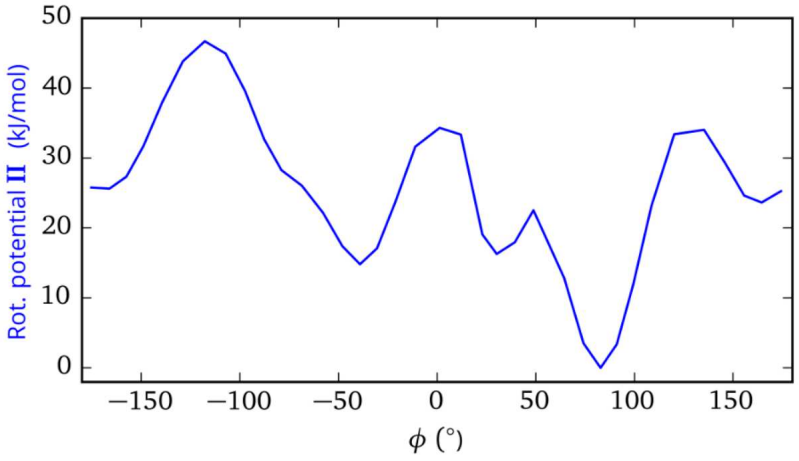

Figure 7.22. – Rotational scan of intermediate *trans*, *Ex*–**II**$_{Me_2}$

The highly organized transition state *trans*, *Ex*–$\mathbf{TSI}_{Me_2}$ of the rate–determining first step results in the intermediate *trans*, *Ex*–$\mathbf{II}_{Me_2}$ which has the involved atomic centers in the second ring–closing step already properly aligned. Because of this, almost no conformational change has to occur for the ring–closing step of the intermediate, as high rotational barriers conformationally confine the geometry (as in the rotational profile for *trans*, *Ex*–$\mathbf{II}_{Me_2}$ in fig. 7.22), just like for *trans*, *Ex*–$\mathbf{TSI}_{Me_2}$. The highly organized nature of this stepwise reaction, can be compared to a so-called 'nonstop reaction' as was first introduced by Albert Eschenmoser.[135,136] It was referred to as:

> "A process in which no stable compounds that could arise through saturation (hydration, H-elimination) of the cyclizing molecule's positive charge should be formed as intermediate"

The confined geometry dynamically forces the reaction into one direction along the reaction coordinate without eliminating a proton or inducing any other side reaction. Eschenmoser wanted to make a clear distinction between the dynamics of the polycyclisation mechanisms of squalene and those of already known concerted processes which, as he stated, were not at all applicable in that case. To our judgement, this concept is in line with the pre–organized transition state we propose since the geometry of the first TS is clearly pre–organised but it cannot be designated as a strictly stepwise or concerted reaction step.

As the geometry of the first addition step gets closer to the transition state, the positive charge from the original furfuryl cation is partially transferred to the diene giving a smeared out positive charge over both the furan ring and the diene, an argument that also explains the tendency to prefer the *extended* over the *compact* approach (section 6.4.3).

Since this first step is endothermic, Hammond's postulate applies and any factor stabilising the intermediate should also stabilise the transition state. At the intermediate stage, the positive charge from the furfuryl cation is completely transferred into the intermediate allylic cation. The electron–rich furan ring can now stabilize the positive charge (e.g.

π–cation interaction) provided that both are properly aligned to do so, hence the pre–organisation, an effect we can expect to also contribute to the lowering of the TS energy (fig. 7.23).

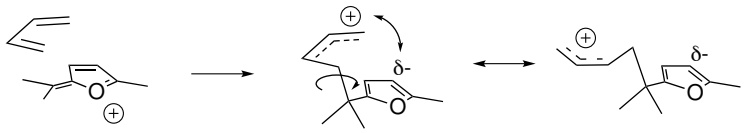

Figure 7.23. – Pre–organisation stabilizes the transition state and intermediate

This kind of preorganized transition states in stepwise cationic (4+3)–cycloadditions, observed in DFT studies, have been reported before by Harmata *et al.* and were termed 'closed arrangement' transition states. They were also rationalized by electrostatic stabilization of developing charges in the diene system.[137,138]

7.3.3. (*R*)-α-phellandrene and furfuryl alcohol 7.4

The model of a pre–organized rate–determining electrophilic addition step explains the experimental observations in the reaction between phellandrene and the symmetric alcohol **7.6** quite well. Intrigued by these results we chose to apply the same theoretical analysis for the cycloaddition between furfuryl alcohol **7.4** and (*R*)-α-phellandrene (fig. 7.10) leading to cycloadduct **7.15**. As the cation that is formed from the alcohol **7.4** can exist in two isomers, an extra stereocenter is introduced during cycloaddition, resulting in the analysis of no less than eight possible transition states (**TSI**$_{Me}$, figs. 7.24 and 7.25) for the rate–limiting first electrophilic addition step. These eight possible pre–organized geometries for **TSI**$_{Me}$ were thus located, corresponding to eight different cationic intermediates **II**$_{Me}$ (fig. 7.25).

The minor isomer (*R*),*trans*–**7.15** and the major isomer (*S*),*trans*–**7.15** are each accessible via two pathways. The major isomer can be formed through a (*Z*),*trans*,*Ex*–pathway (fig. 7.24) or an (*E*),*trans*,*C*–pathway (fig. 7.25). The minor isomer can be formed through

a (*Z*),*trans*,*C*–pathway (fig. 7.24) or an (*E*),*trans*,*Ex*–pathway (fig. 7.25). The complete potential energy diagrams (figs. 7.26 and 7.27) show that the reaction with the secondary cation (*E*)/(*Z*)–$\mathbf{I}_{Me}$ is more exergonic as compared to the tertiary cation $\mathbf{I}_{Me_2}$, which can be expected as secondary cations are less stable than tertiary cations.

Interestingly, for both cation isomers, the *trans*,*Ex*–pathway is the most favoured, showing a larger difference between *compact* and *extended* approach for the (*Z*)–$\mathbf{TSI}_{Me}$ as compared to (*E*)–$\mathbf{TSI}_{Me}$. The geometries for the lowest energy transition states *trans*,*Ex*–$\mathbf{TSI}_{Me}$ are given in fig. 7.28.

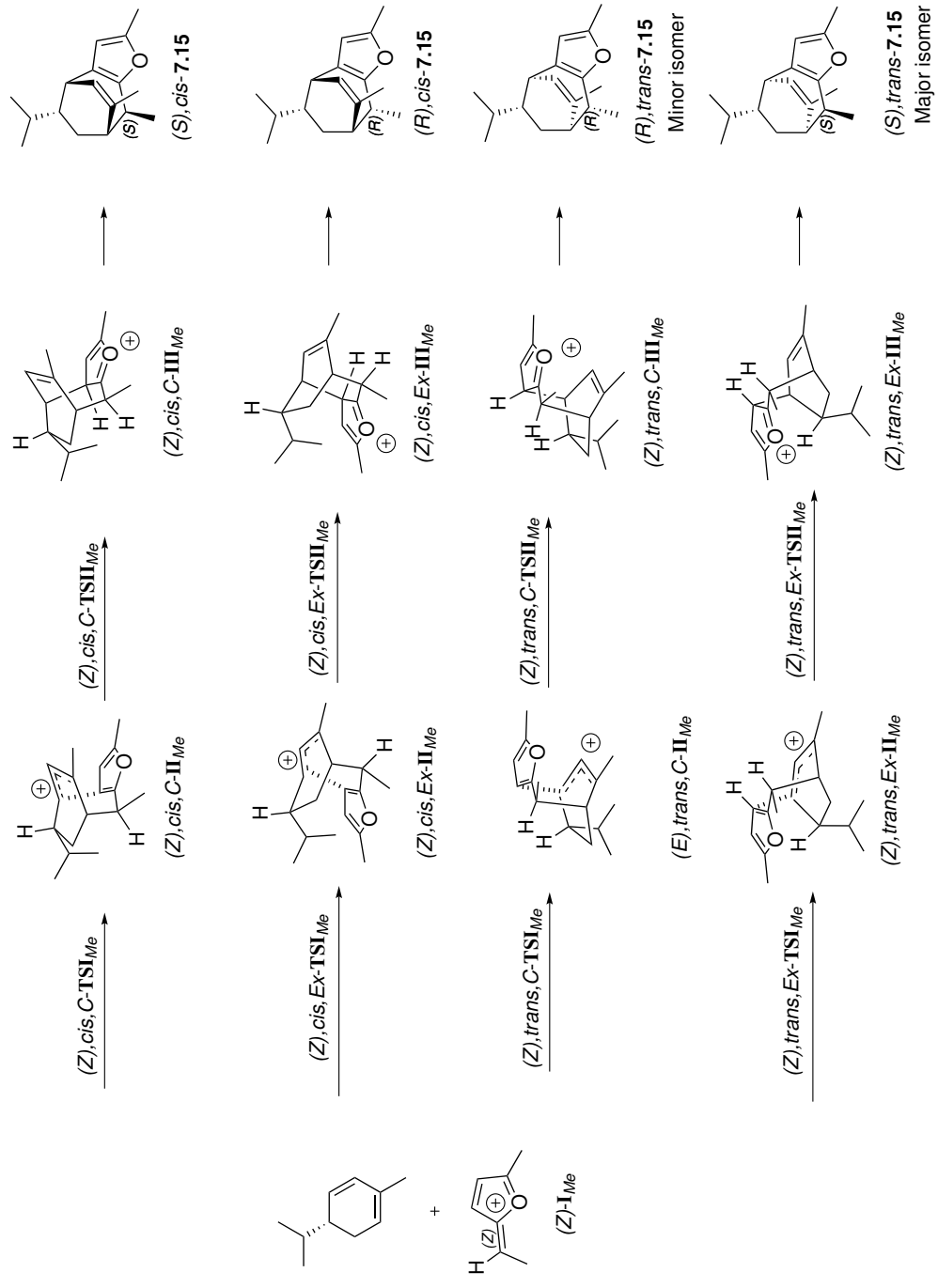

Figure 7.24. – Possibilities for the reaction between (Z)–furfuryl cation and (*R*)-α-phellandrene

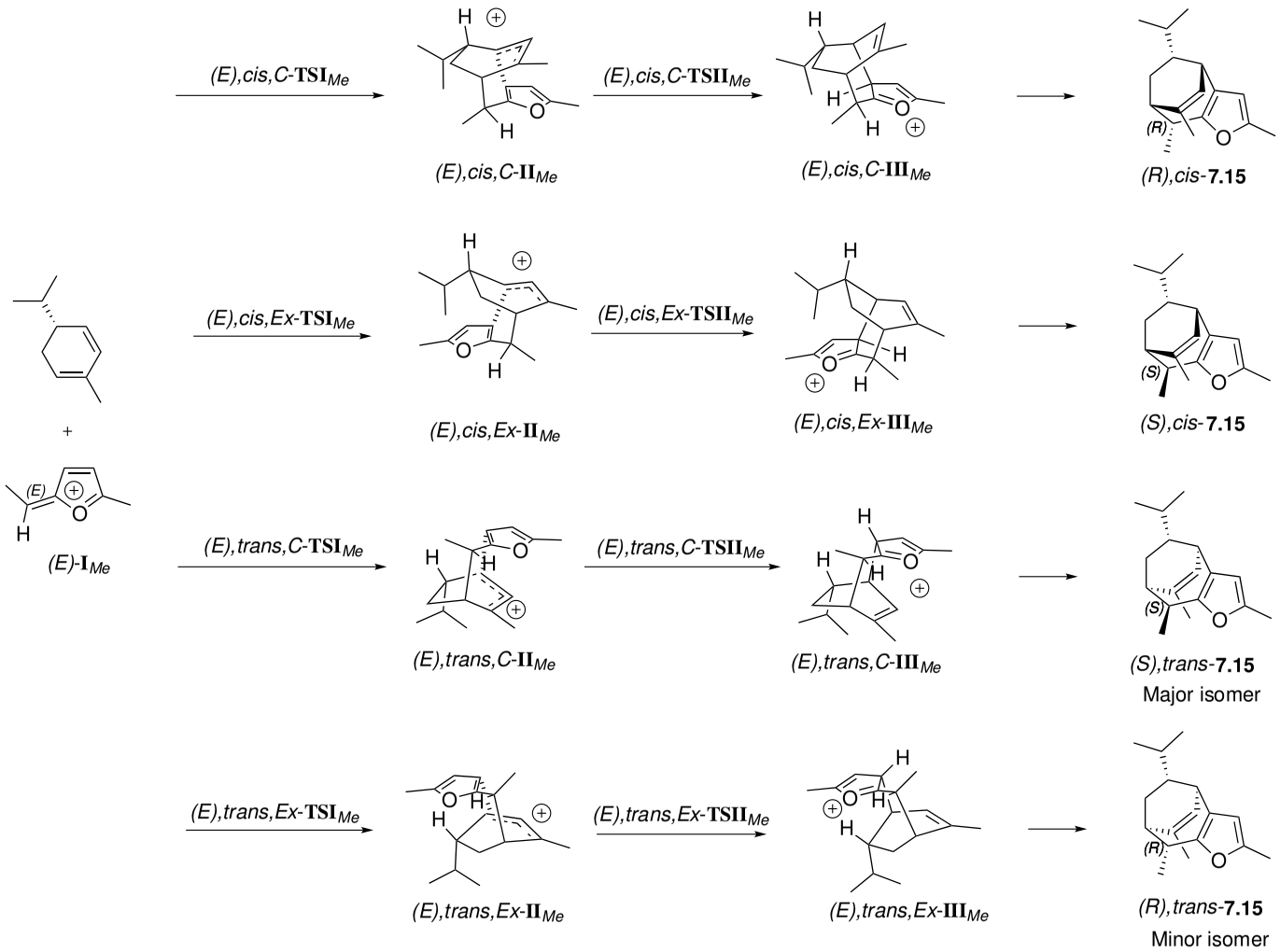

Figure 7.25. – Possibilities for the reaction between (*E*)–furfuryl cation and (*R*)-α-phellandrene

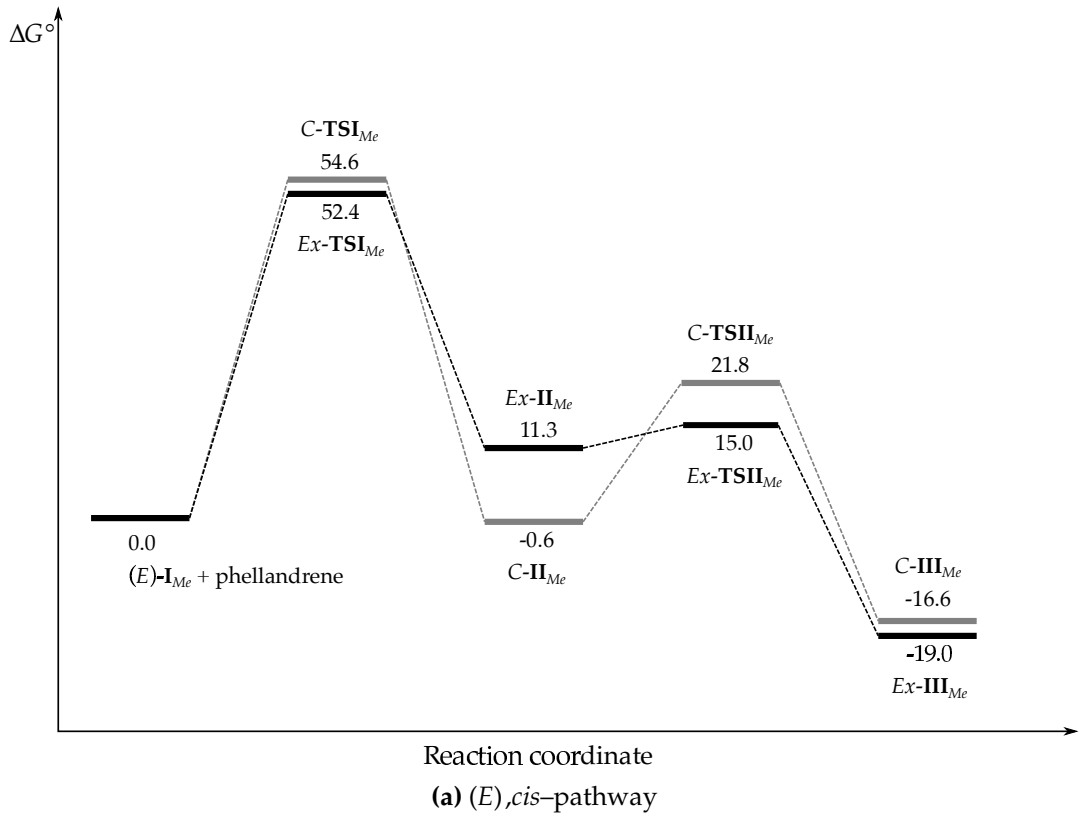

(a) (*E*),*cis*–pathway

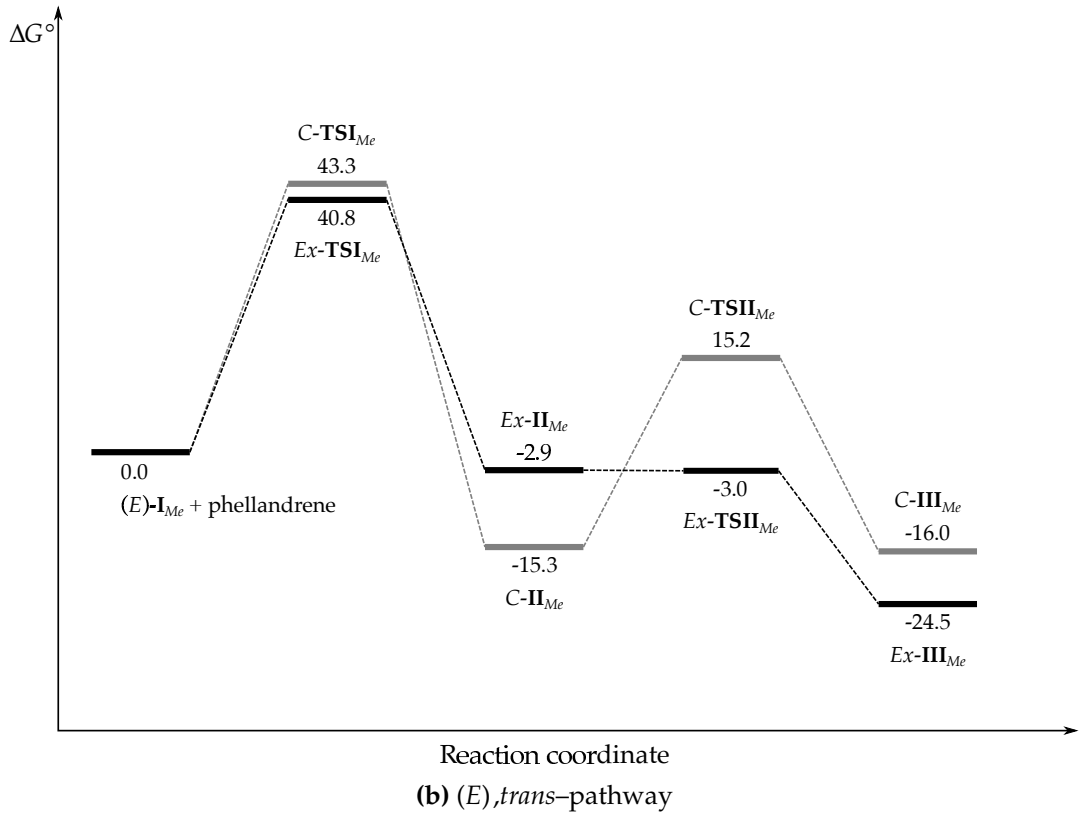

(b) (*E*),*trans*–pathway

Figure 7.26. – Free–energy profiles for the cycloaddition between phellandrene and cation (*E*)–$\mathbf{I}_{Me}$; energies are given in kJ/mol relative to separate reactants (M06-2X/6-31+G(d,p), 298 K, 1 atm, IEF-PCM (CH_2Cl_2, $\epsilon = 8.93$))

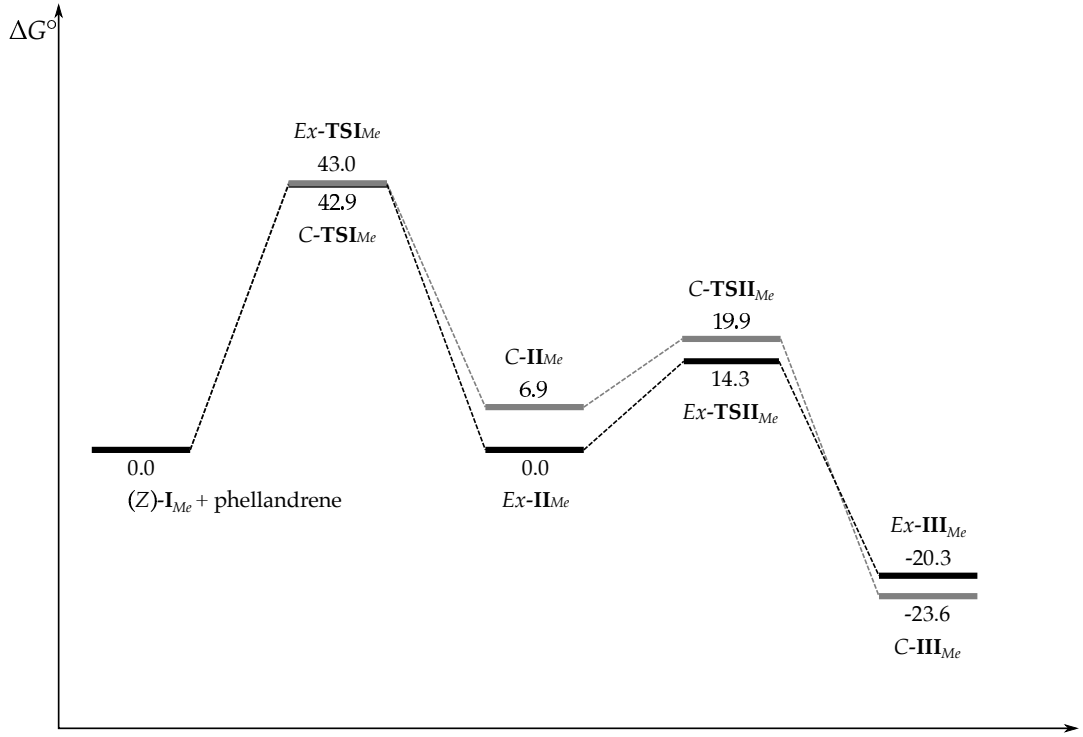

(a) (Z),*cis*–pathway

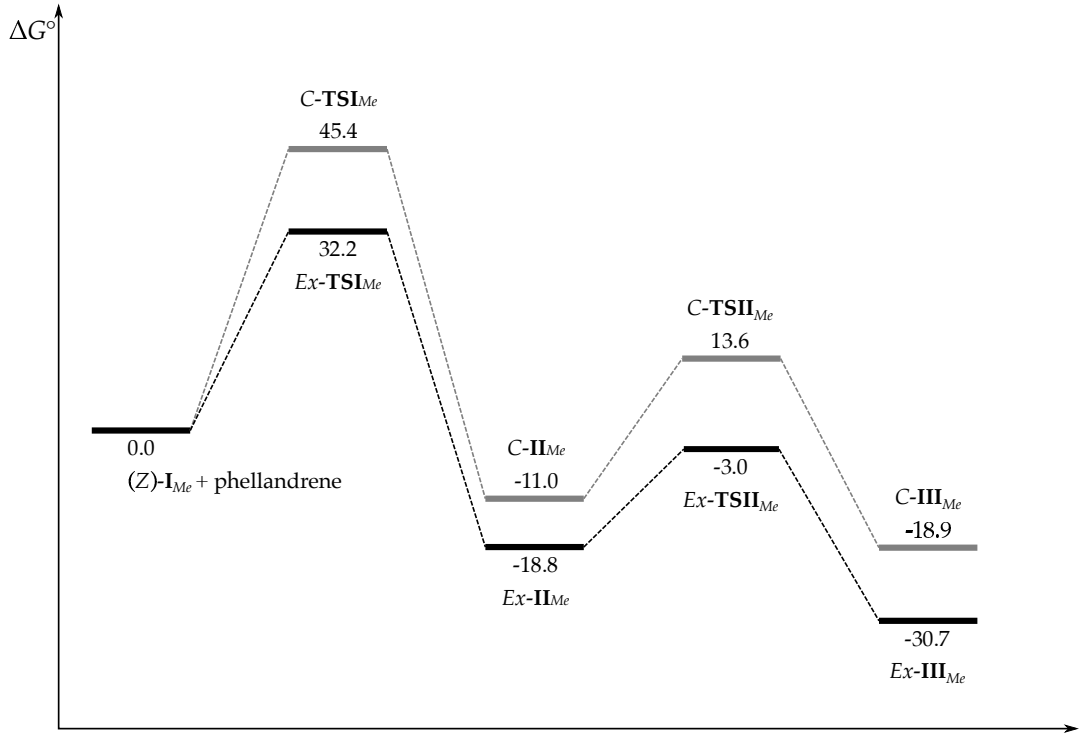

(b) (Z),*trans*–pathway

Figure 7.27. – Free–energy profiles for the cycloaddition between phellandrene and cation (Z)–$\mathbf{I}_{Me}$; energies are given in kJ/mol relative to separate reactants (M06-2X/6-31+G(d,p), 298 K, 1 atm, IEF-PCM (CH_2Cl_2, $\epsilon = 8.93$))

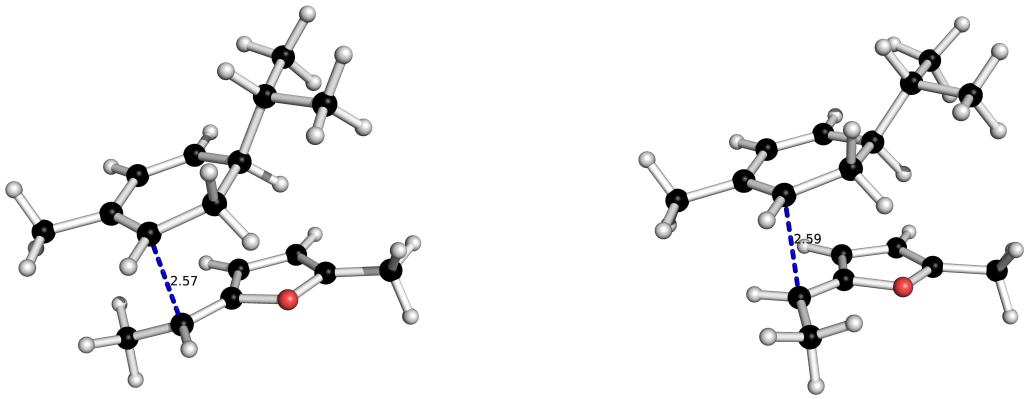

(a) (*E*),*trans*, *Ex*–**TSI**$_{Me}$ **(b)** (*Z*),*trans*, *Ex*–**TSI**$_{Me}$

Figure 7.28. – Selected transition states for the first electrophilic addition step (M06-2X/6-31+G(d,p), IEF-PCM (CH_2Cl_2, $\epsilon = 8.93$), distances in Å

Again, in order to check for other possible geometries of all the preorganized transition states **TSI**$_{Me}$, full rotational scans around the forming bond were performed, which showed that (*E*),*trans*, *Ex*–**TSI**$_{Me}$ and (*Z*),*trans*, *Ex*–**TSI**$_{Me}$ are clearly preorganized.

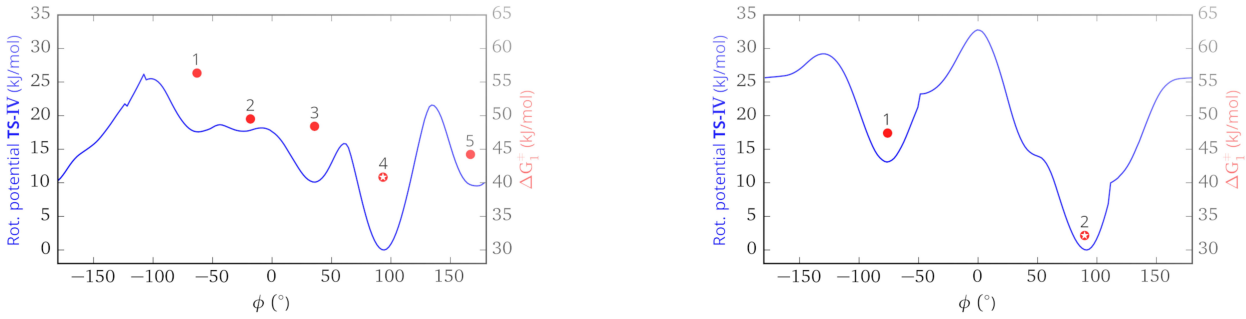

(a) (*E*),*trans*, *Ex*–**TSI**$_{Me}$ **(b)** (*Z*),*trans*, *Ex*–**TSI**$_{Me}$

Figure 7.29. – Relaxed rotational scans around the forming bond (blue curve), reoptimised transition state energies (red dots), ✪ pre–organised transition states

Interestingly, the (*Z*),*cis*–pathway is at least 2 kJ/mol lower in energy than the (*Z*),*trans*, *C*–pathway which leads to the minor isomer. The experiment shows however that no *cis* products were formed, suggesting that (*E*)–$\mathbf{I}_{Me}$ exclusively reacts via the *trans*, *Ex*–pathway. We can then rationalize the observed diastereomeric ratio by considering two different possibilities. When the secondary alcohol is treated with titanium(IV)chloride, they give two different isomers ((*E*)–$\mathbf{I}_{Me}$ and (*Z*)–$\mathbf{I}_{Me}$). Either both cation isomers are in equilibrium with each other, implying a Curtin–Hammett scenario. The ratio of cycloadduct isomers will in this case depend on the the relative barrier heights of the rate–determining electrophilic addition step through which each of the cation isomers has to go ($\frac{\Delta G^{\ddagger}_{(Z)}}{\Delta G^{\ddagger}_{(E)}}$, fig. 7.30a). As we can assume that the formation of the cations under titanium(IV)chloride conditions will be irreversible, a non Curtin–Hammett scenario in which the interconversion between the (*E*) and (*Z*) cation is insignificantly slow, would be more appropriate ($\Delta G_{(Z)-(E)}$, fig. 7.30b). Therefore, the diasteromeric ratio will rather be a reflection of the initial ratio of cation isomers (*Z*)–$\mathbf{I}_{Me}$ and (*E*)–$\mathbf{I}_{Me}$, which is 3.8 kJ/mol higher in energy. This argument can also explain the trend in observed diastereomeric ratios as this energy difference will be more pronounced for sterically more demanding substituents.

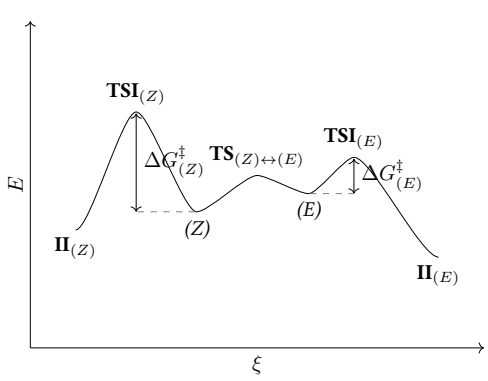

(a) Curtin–Hammett scenario

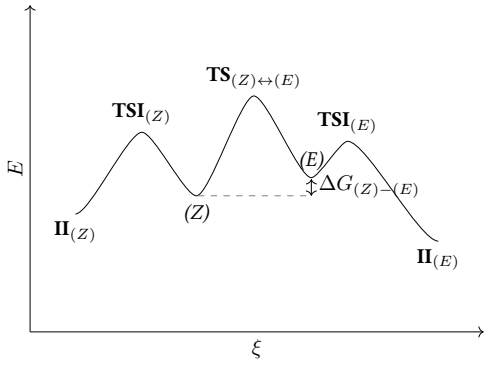

(b) Non Curtin–Hammett scenario ("kinetic quench")

Figure 7.30. – Different scenarios for the diastereomeric ratio of cycloadditions with asymmetrically substituted furfuryl alcohols

7.3.4. Revisiting the cycloaddition with 1,3-cyclohexadiene and isoprene

In order to consolidate the idea of a pre–organised process, two reactions that were reported in the 2011 paper of Winne *et al.* were also analysed in view of the insights obtained in the discussions above.

7.3.4.1. 1,3-cyclohexadiene

The reaction between 1,3-cyclohexadiene and the alcohol **7.4** had been subject to computational studies as was mentioned in the introductory sections, however not considering pre–organized geometries; the first electrophilic addition step was then found to be non–organised. A reanalysis has located another reaction path which is lower in energy and goes through the same pre–organised stationary points like in the case of (*R*)-*α*-phellandrene.

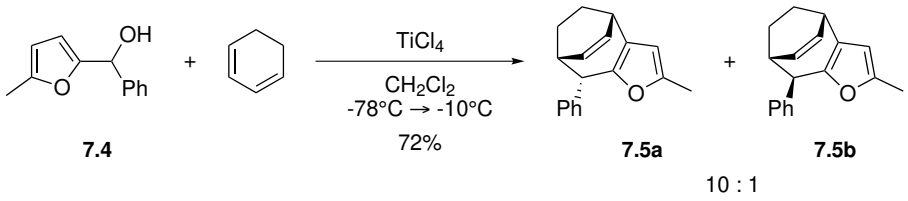

Figure 7.31. – Cycloaddition reaction between alcohol **7.4** and cyclohexadiene as reported by Winne and co–workers

7.3.4.2. Isoprene

Isoprene has been proven to be a reliable reaction partner in the (4+3)–cycloaddition. The reaction with the cation from alcohol **7.6** requires a larger excess than normal to compensate for the loss of diene in oligomerisation reactions. Computational studies have now

located a pre–organised transition state which is again found to be the lowest in energy, endorsing the model we established earlier on.

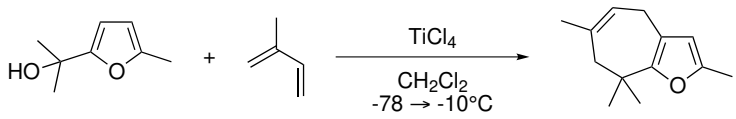

Figure 7.32. – Cycloaddition reaction between alcohol **7.6** and cyclohexadiene as reported by Winne and co–workers

7.3.5. From theory to experiment: comparing the pre–organised path with a truly stepwise mechanism

The tendency of (4+3)–cycloadditions to proceed via a stepwise pre–organised pathway found in multiple cases suggests a rather general feature of these types of reactions and not just a substrate–dependent steric effect. To check whether the model we propose has any predictive power, a reaction between diene **7.30** and alcohol **7.6** was designed. The diene was easily synthesized from 4-*tert*-butyl-cyclohexanone and the phosphonium salt **7.31** by a Wittig olefination. The phosphonium salt was prepared by heating a solution of methallyl chloride and triphenylphosphine in toluene to 100 °C in a pressure tube for 14 hours. The diene **7.30** was then reacted with alcohol **7.6** under the standard conditions for cycloaddition.

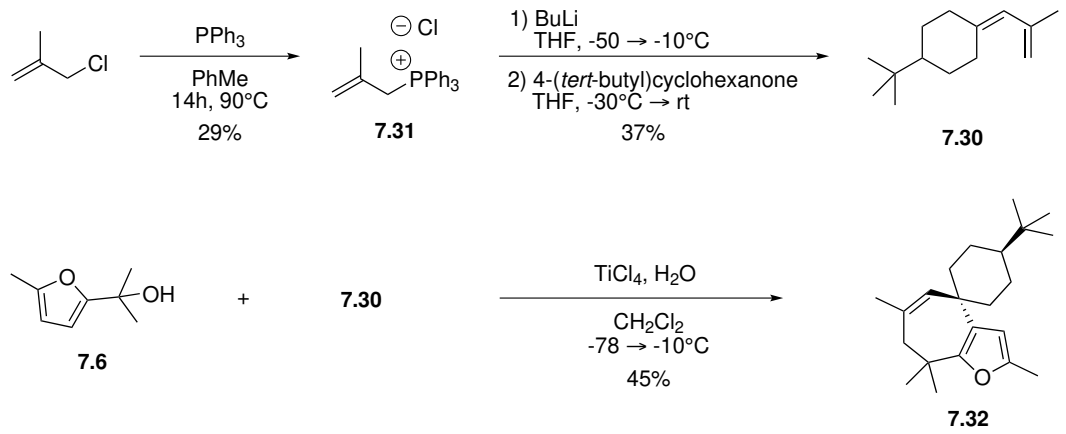

Figure 7.33. – Model reaction for probing of pre–organised reaction mechanism

Possible reaction outcomes are determined by the geometry of the cyclohexane unit of the diene. The *tert*-butyl group confines the geometry of the chair in such a way that pre–organised approach is only feasible *trans* relative to the *tert*-butyl group (fig. 7.34), whereas non–preorganized transition states will probably have no such stereo–induction.

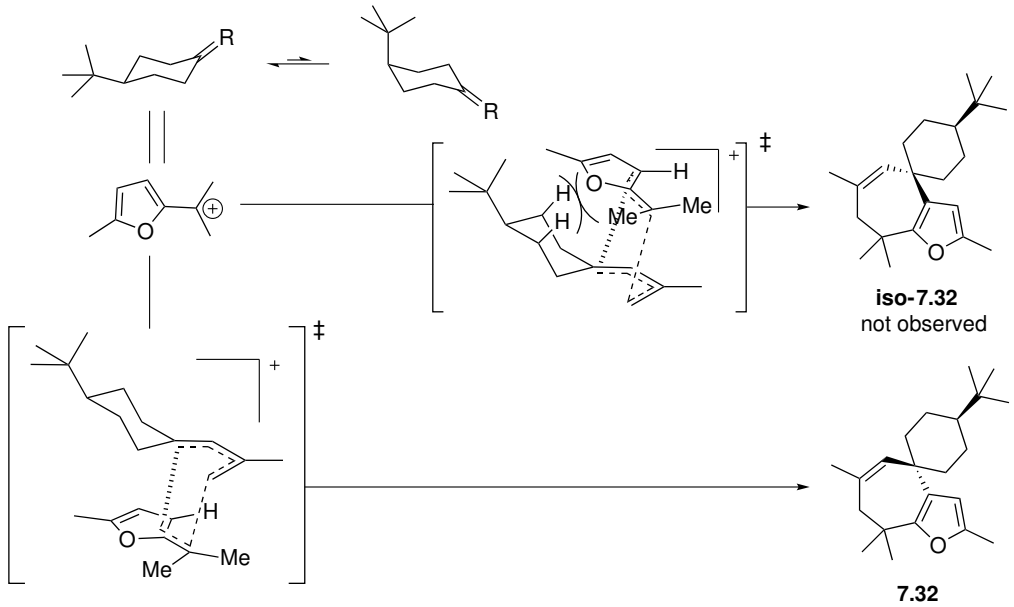

Figure 7.34. – Different approaches for the formation of **7.32**

From the experiment we found indeed the cycloadduct **7.32** as a single diastereoisomer, coinciding with the predicted isomer. NMR-spectroscopy enabled the unambiguous identification of the formed diastereoisomer (fig. 7.35).

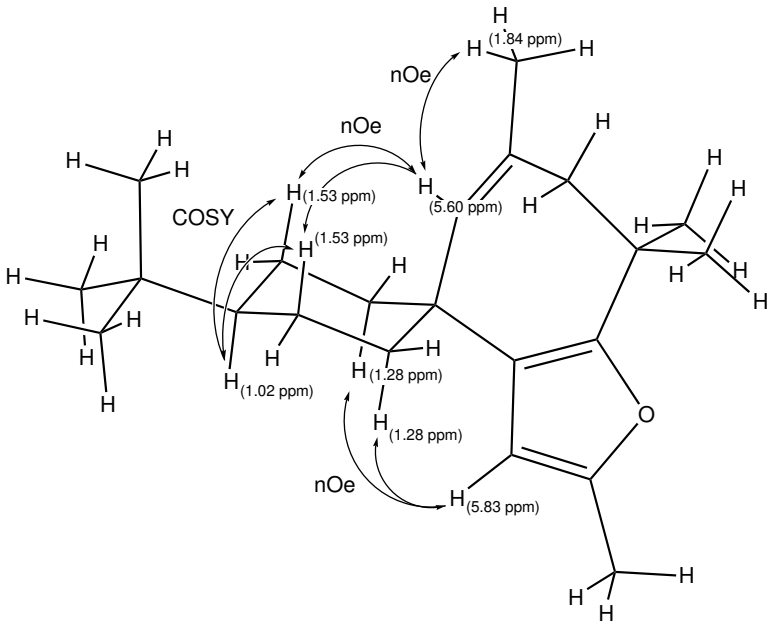

Figure 7.35. – Characteristic nOe and COSY correlations in cycloadduct **7.32**

The reaction also produced some diene related sideproducts — determined by GC/MS — which were difficult to remove by classical chromatographic methods. Instead purification was done by treating the impure mixture with mercaptoethanol and AIBN in methanol in a pressure tube at 95 °C. Keeping reaction times short this allowed for the selective removal of the side products with only a minimal loss of major product. The cycloadduct was then obtained in 45 % overall yield.

Although, at first sight this seems to confirm the pre–organisation model we suggested, caution should be taken as we cannot estimate the dynamics of the reaction should it proceed in a non–organised fashion. In order to get an idea of what the reaction outcome

could be in the non–organised case, we designed an experiment in which a linear precursor is transformed into the putative intermediate cation. Further ring closure should then either yield the same isomer **7.32**, a mixture of isomers and/or class C sideproducts.

The linear precursor was synthesised from methylfuran and mesityl oxide by applying conditions that were established for methyl vinyl ketone by Kouridaki.[139], which did not yield the desired product in our case. Treating a mixture of methylfuran and mesityl oxide with boron trifluoride in dichloromethane gave ketone **7.33** in good yield. For the diene part we transformed 4-*tert*-butyl-cyclohexanone into olefin **7.34** by a Takai–Ushimoto olefination. Ketone **7.33** and olefin **7.34** were then coupled by treating a mixture of both with *n*-butyllithium at 0 °C to yield the alcohol **7.35**.

The linear precursor was treated under the same conditions as would be the case in a regular cycloaddition and yielded the same diastereoisomer. It has thus been impossible to draw any conclusions from this experiment as the steric forcing of the *tert*-butyl group seems to dominate the non–organised stepwise addition as well. In conclusion, the substrate proved to be a poor choice as also the fully stepwise reaction is here a completely stereoselective process, related to the steric induction around the receiving cation.

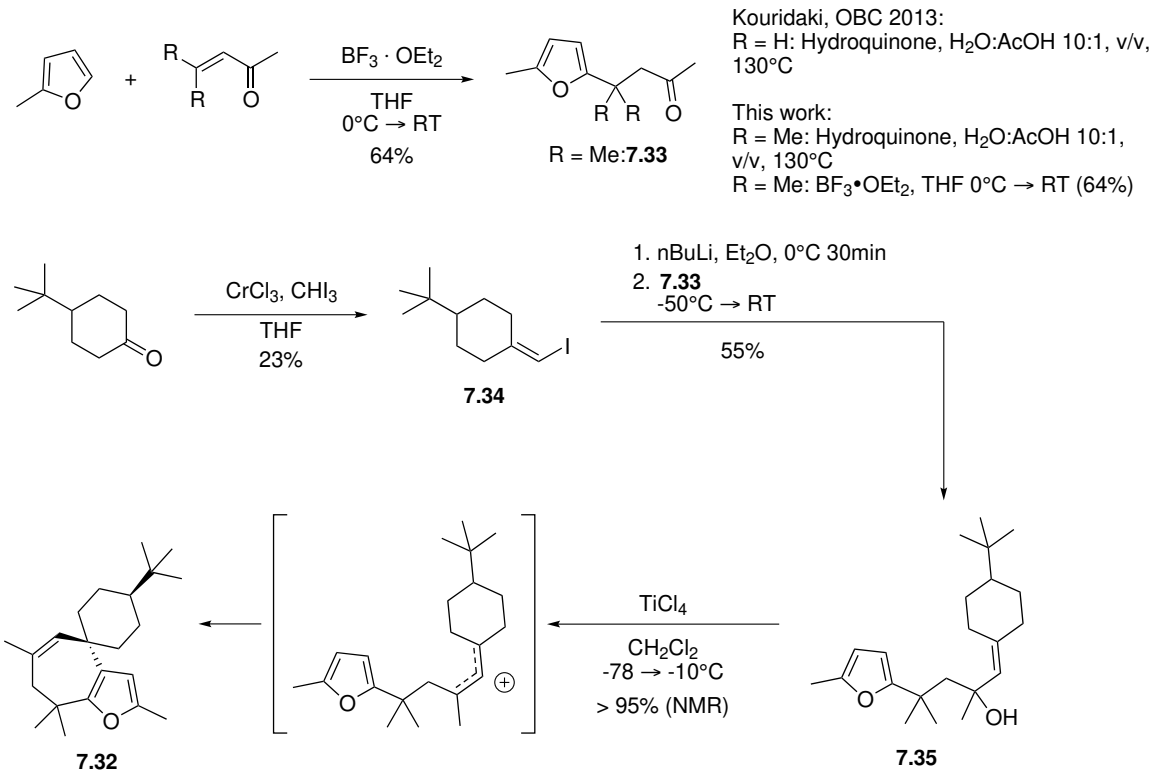

Figure 7.36. – Synthesis of linear precursor and subsequent non–organised cyclisation

7.3.6. Studies into the stereospecificity of the (4+3)–cycloaddition

(*R*)-*α*-phellandrene as a diene is shown to add in a completely stereo– and regioselective fashion to a furfuryl cation. The addition is also stereospecific, since even if the addition would not be pre–organised, geometric constraints of this endocyclic diene would not allow a scrambling of the stereocenter that is formed in the second ring–closing step. The case of 1,3-cyclohexadiene follows the same reasoning as for phellandrene, whereas isoprene does not lead to the formation of diastereoisomers.

As we are interested in the general stereospecificity of this cycloaddition, a set of linear dienes was synthesised with asymmetrically substituted double bonds which were then reacted with the alcohol **7.6**.

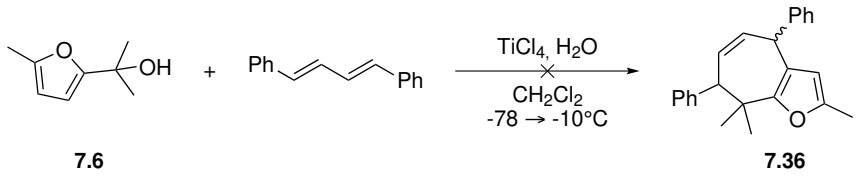

Figure 7.37. – Attempted cycloaddition between alcohol **7.6** and (1(*E*),3(*E*))-1,4-diphenylbuta-1,3-diene

As a first test we chose the commercially available (1(*E*),3(*E*))-1,4-diphenylbuta-1,3-diene (fig. 7.37). Standard conditions for cycloaddition were used but surprisingly, only the intact diene was isolated from the crude mixture. A possible explanation would be that the ground state of this system is too stabilised by the two phenyl groups on the diene. This would mean that the diene is probably less nucleophilic than the furan itself, and only furan oligomerisation occurs here.

As an alternative, a Shlosser modified Wittig olefination gave diene **7.37** with a yield of 36 % and a reasonably good (*E*):(*Z*)–ratio of 86:14. Also, diene **7.38** was prepared from hex-2-enal under standard Wittig conditions (fig. 7.38). Both dienes did not lead to a cycloaddition product but a rather complex mixture of oligomers and homocoupled furan compounds (fig. 7.39). From β-cyclocitral we then prepared diene **7.39** under Schlosser modified Wittig conditions as an 83 % solution in pentane and a (*E*):(*Z*)–ratio of 7:93 (fig. 7.38). Again cycloaddition led to the formation of the homocoupled furan products and not the expected cycloadducts.

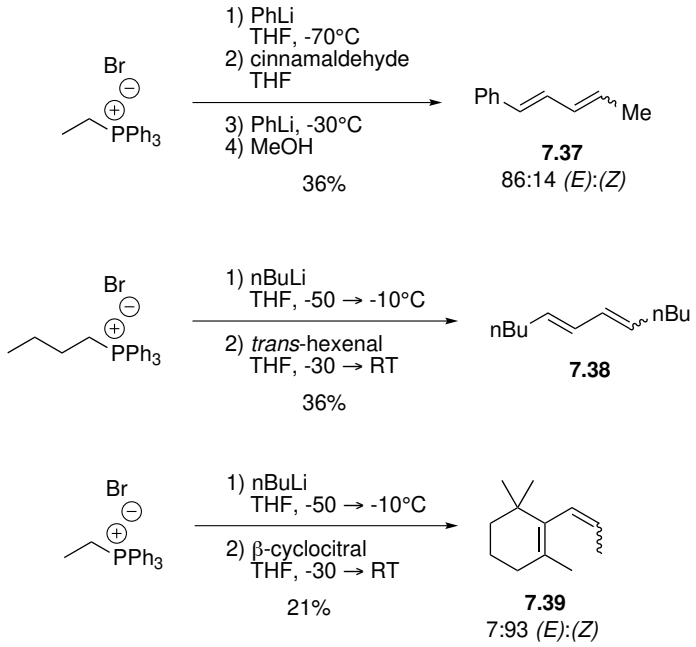

Figure 7.38. – Synthesis of linear dienes

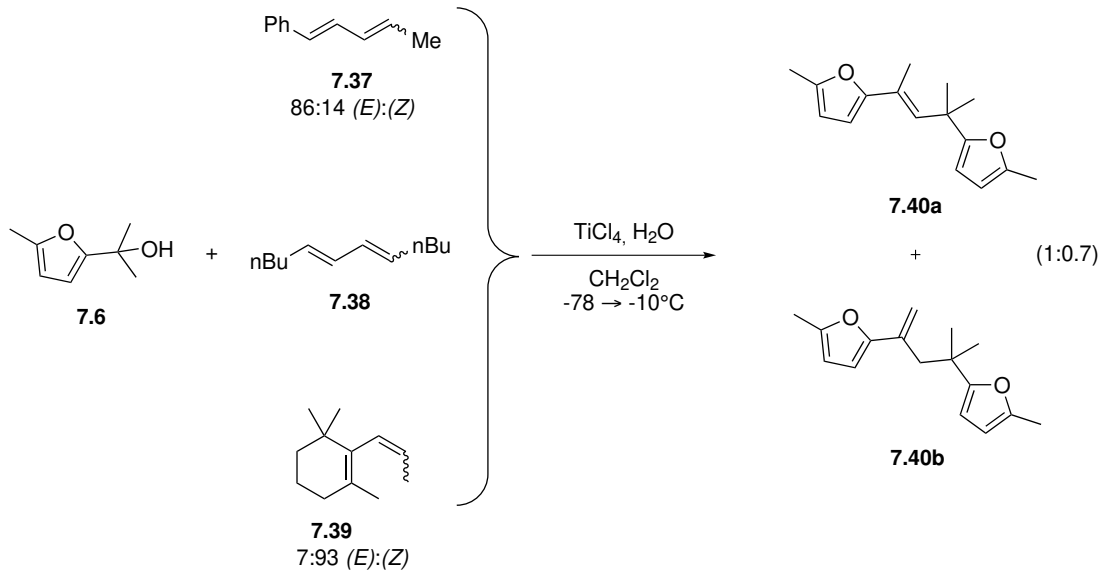

Figure 7.39. – Furan homocoupled products

As these dienes probably react very slowly, the furfuryl cation can react with itself by

first eliminating a proton to form olefin **7.41** which can then serve as an electrophile to trap a second cation. Final elimination might then lead to two different products (**7.40a** and **7.40b**) which were confirmed by NMR–spectroscopy.

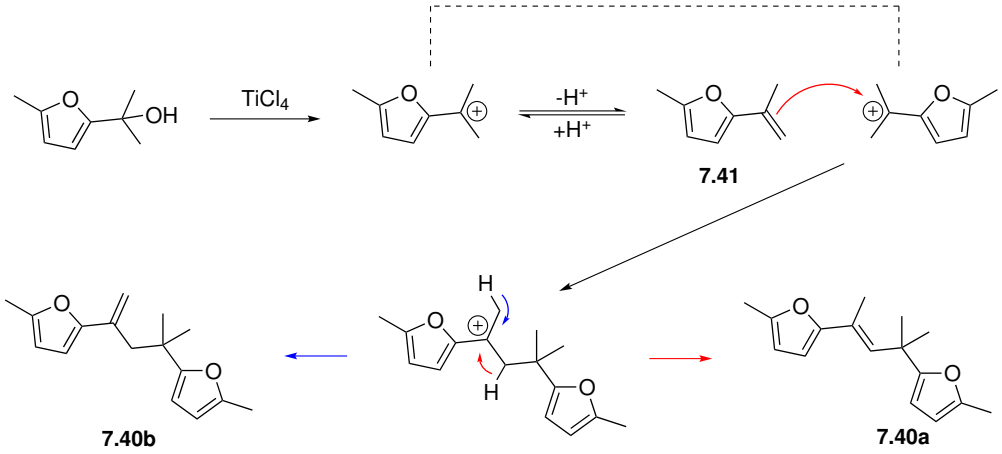

Figure 7.40. – Proposed mechanism for the formation of **7.40a** and **7.40b**

We can conclude that the steric requirements at the electrophilic center of the furfuryl cation is determining in the reactions described above. This is also observed in the syntheses of frondosin B and liphagal. The regioselectivity is determined not by the most nucleophilic centre on the diene, but the steric requirements of the centre involved in the first electrophilic addition step. As it takes too long for the dienes to react, side reactions involving the furfuryl cations prevail over the expected electrophilic addition of the dienes. A possibility to tackle this issue would be to use a less hindered furan as this would diminish the steric requirement of the electrophilic attack of the cation.

Interestingly, Jimmy Wu and co–workers have developed a (4+3)–cycloaddition between indolyl cations and 1,3–dienes in which they show the stereospecific addition to the indole–derived $_{\pi}2$–component.[140]

7.4. Conclusions

The (4+3)–cycloaddition between a 1,3–diene and a furfuryl cation is proven to be a very reliable reaction in the synthesis of complex polycyclic molecules. We have shown that it proceeds with a high degree of regio– and stereoselectivity and reasonable yields in general. Thorough computational studies have revealed a mechanistic pathway in which the stepwise addition is favoured instead of the concerted mechanism. The mechanism involves a rate determining electrophilic addition as a first step followed by an electrophilic aromatic substitution ring closure. A proton is then eliminated from the oxonium ion to give the cycloaddition product with restored furan aromaticity.

Detailed rotational scans around the forming bond in the first step have shown that a pre–organized rate determining step has a substantially lower energy then the non–organized ones. Pre–organisation means that the reacting centers are already aligned even though they only react further up the reaction coordinate. The best situation by which this can be compared was the idea of a nonstop reaction as described by Albert Eschenmoser. The positive charge exists on an extended π–system without eliminating a proton or inducing any other side reaction before cyclisation has ocurred. The substitution pattern of the furfuryl alcohol was shown not to influence the stereoselectivity of the addition. However, asymmetrically substituted alcohols do give different diastereomisomers of which the ratio is largely determined by the steric bulk of the substituent. The non Curtin–Hammett situation in which the isomer ratio of the cation is fixed, then determines the final ratio of diastereomisomers, at least in the case of (*R*)-α-phellandrene, as the steric forcing of the diene can of course make a large difference in the relative addition modes onto different cation isomers. Revisiting earlier reactions confirmed the idea of a pre–organised electrophilic addition step.

When investigating the stereospecificity of the reaction in the case of linear dienes, a number of important issues were encountered: (a) A low energy ground state of the diene leads to a very slow first addition step and consequently furan degradation prevails.

Intact diene is isolated from the reaction mixture. (b) Large steric requirements of the carbon center involved in the first addition step, slow down the reaction to an extent that furan homocoupled products are formed faster.

Wu *et al.* have shown that for the case of (4+3)–cycloadditions with indolyl cations, the reactions indeed proceed stereoselectively and we can assume that this will also be the case for cycloadditions with furfuryl cations. We could not show whether cycloadditions with asymmetrically substituted linear dienes proceeded in a stereospecific fashion. In order to be able to experimentally observe this we could, in the future, use less–hindered dienes or different reaction conditions. Other (4+3)–cycloadditions between indoxyl cations and 1,3–dienes, reported in the literature, showed stereospecific addition and we can assume the cycloadditions between furfuryl cations and 1,3–dienes to also be stereospecific.

8 Applications of allyl cation cycloadditions and further mechanistic investigations

8.1. Application of (4+3)–cycloaddition of furfuryl cations in natural product synthesis

The (4+3)–cycloaddition between a furfuryl cation and a 1,3-diene has already been employed in our group to synthesize a collection of natural products or natural product scaffolds (fig. 8.1). The stereoselectivities in each of those cases is quite remarkable, which can largely be attributed to the intramolecular nature of the cyclisations.

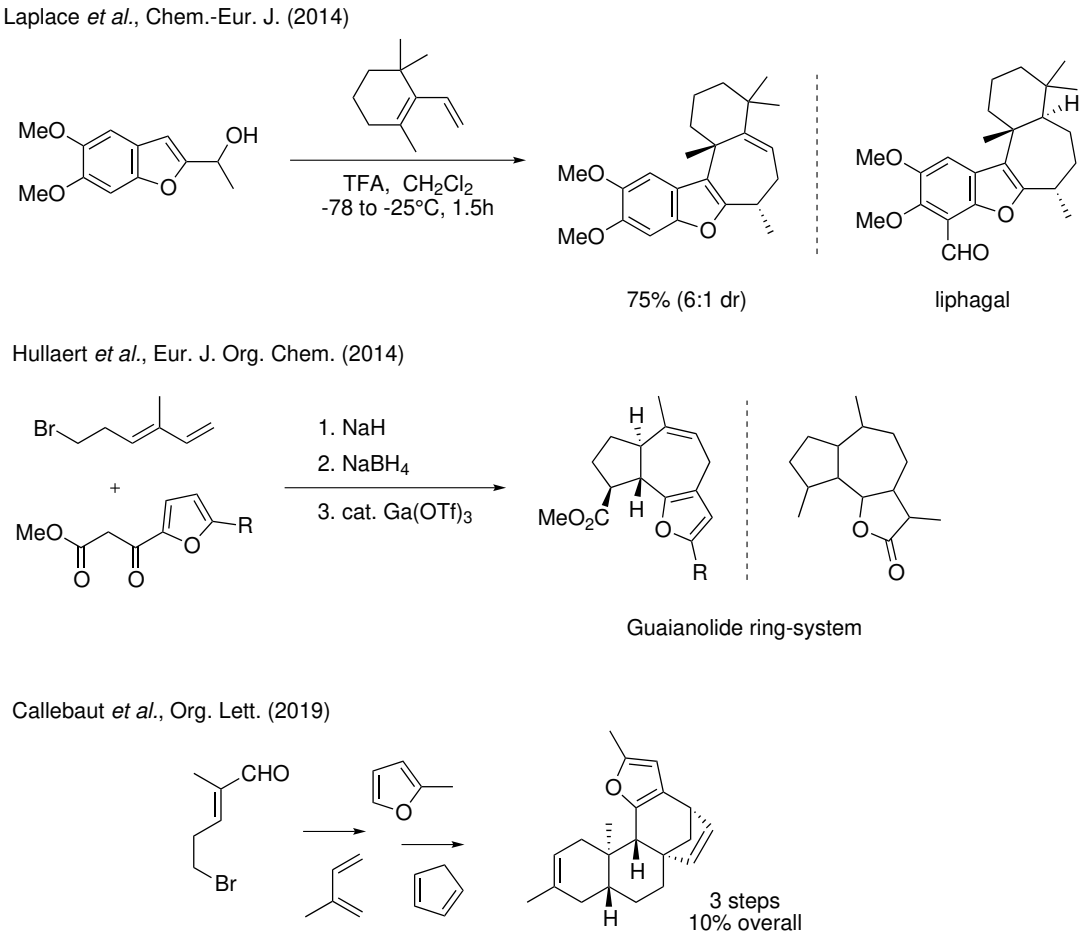

Figure 8.1. – Selected examples of natural product cores synthesised in our lab.[141–143]

As was reported by Laplace *et al.*:[143]

> "It has been argued that the true test of any novel synthetic methodology is its successful application in the total synthesis of a complex natural product."

We explored the possibilities of constructing the carbocyclic core of the natural product family of the scopariusins.

Isodon scoparius is a rare herb that is found on the high planes of the south of China (Yunnan province). It was found that the plants were used for their antipyretic activity by the local inhabitants. From the *Isodon scoparius*, three new natural products (Scopar-

iusin A, B and C (**8.1**, **8.2** and **8.3**)) were isolated which are related to the *ent*–halimane skeleton.[144]

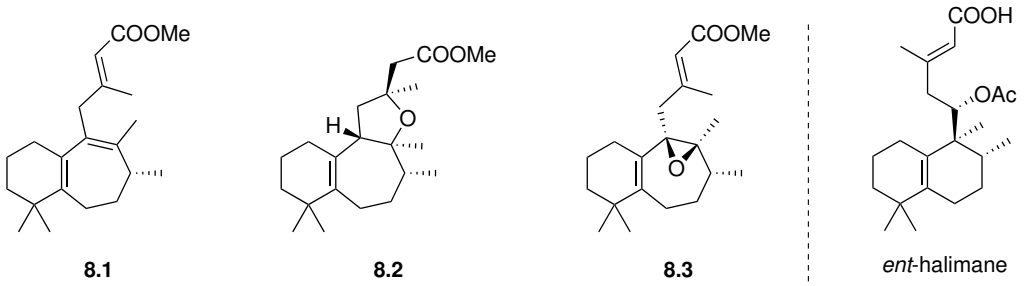

Figure 8.2. – Scopariusin A, B and C (**8.1**, **8.2** and **8.3**) and *ent*-halimane

Careful analysis of the scopariusin A and B structure, reveals that the main skeleton is accessible through a (4+3)–cycloaddition. The diene that is required for the buildup of the natural product core, was also used in the total synthesis of liphagal in our group (**8.4**). Indeed, again using the standard conditions for cycloaddition, and in this case furfuryl alcohol **7.4**, gave the scopariusin core **8.5**.

Interestingly when using trifluoroacetic acid as a dehydration agent, yields were rather low and we isolated the homocoupled furan compound **8.6** (fig. 8.3). The oxidation of the furan ring, which was tried multiple times, proved to be a difficult thing to achieve. Singlet oxygen oxidation gave a complex mixture of products whereas mCPBA only gave very small amounts of ene-dione. Small scale hydrogenation of **8.7** gave an impure sample of **8.8**. As scaling up proved to be difficult and since total synthesis was beyond the broader scope of this work, further investigation into the total synthesis of scopariusins was abandoned.

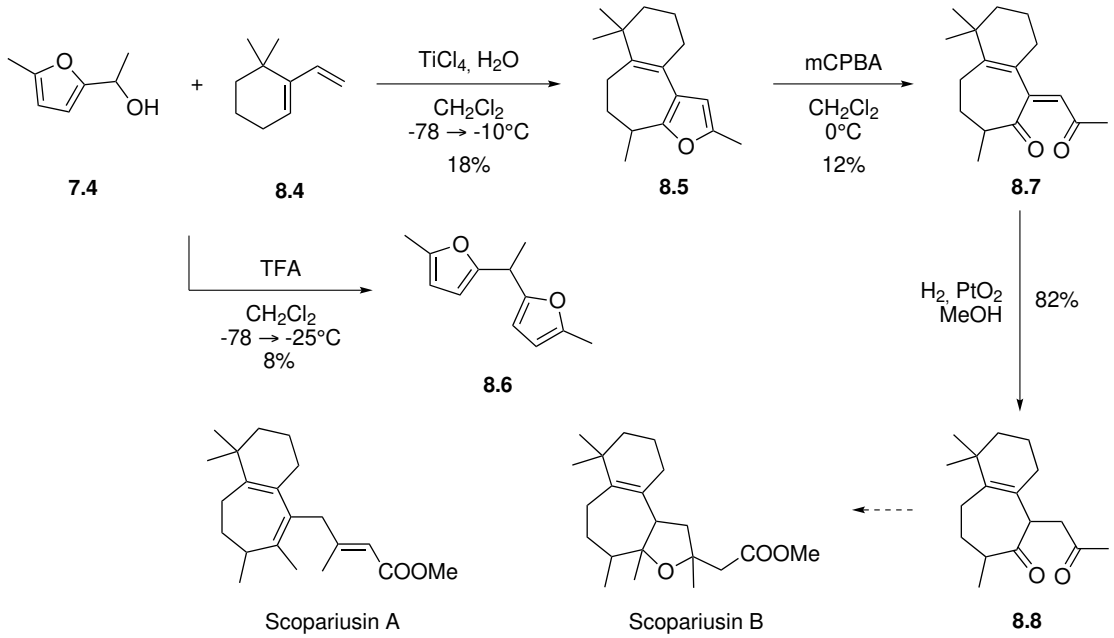

Figure 8.3. – Synthesis of scopariusin A and B precursor

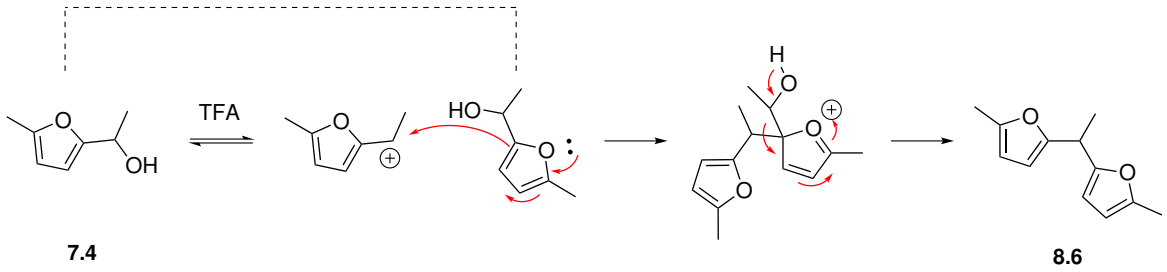

Figure 8.4. – Proposed mechanism for the formation of **8.6**

Some final remarks concerning homocoupled furan compound **8.6** should be discussed. The reader might have noticed the markedly different nature of the bis–furan side products (**7.40a** and **7.40b**) we found in section 7.3.6 compared to homocoupled furan compound **8.6**; the latter being the result of an electrophilic aromatic substitution reaction of the cation on the furfuryl alcohol itself, indicating the two exist at the same time. This should rely on either an equilibrium between the alcohol and the cation or a slow cation

formation by which the cation has time to react with the alcohol. Similarly, **7.40a** and **7.40b** should be the result of either an equilibrium between the cation and olefin **7.41** (fig. 7.40) or a slow elimination proces.

8.2. From seven to five: recruiting heterocyclic cations for (3+2)–cycloadditions

In the previous chapter we have shown that the (4+3)–cycloaddition is a reliable method for the generation of seven membered rings. As the natural product plethora contains quite some examples of seven–membered ring natural products, especially within the family of terpenoids, their synthesis is interesting to investigate.

Of course, other ring sizes like six– and five–membered rings are equally as important, not to say more important as they are found more frequently than cycloheptanoids. Because of this, we set out to investigate the possibility of using the conditions that were established for the (4+3)–cycloaddition between 1,3–dienes and furfuryl cations, as a starting point for the synthesis of five membered rings. An isolated alkene (or at least a stabilised one) or diene would then react with the cation in a strictly stepwise fashion to give a fused cyclopentane unit.

8.2.1. Furfuryl and thienyl alcohols

The reaction between 1,3–dienes and furfuryl and thienyl alcohols respectively was established in the previous chapter. In order to minimise the interference between competing cycloheptannulation and cyclopentannulation pathways we chose to employ ethylvinyl sulfide as an alkene. The sulfur atom was thought to assure sufficient stabilisation for the forming cation as in the work reported by Kuwajima (see fig. 6.11,chapter 6). In table 8.1 an overview is given of the different conditions that were attempted for the (3+2)–cycloaddition.

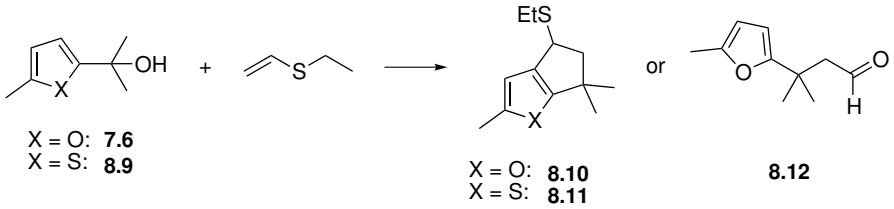

Entry		conditions	equiv. vinyl sulfide	Product	Yield
1	**7.6**	$TiCl_4$,H_2O,CH_2Cl_2, −78 °C to −15 °C	2.0	complex mixture	-
2	**7.6**	TFA,CH_2Cl_2, −78 °C to −10 °C	2.0	polymers	-
3	**7.6**	$TiCl_4$,CH_2Cl_2, −78 °C to −15 °C	2.0	complex mixture	-
4	**7.6**	$Ga(OTf)_3$,$CDCl_3$, RT	2.0	complex mixture	-
5	**7.6**	$Dy(OTf)_3$,CH_3CN, Δ	2.0	complex mixture	-
6	**7.6**	$Ti(OiPr)Cl_3$,CH_2Cl_2, −78 °C to −10 °C	1.2	**8.12** (+polymers)	7 %
7	**8.9**	$Ti(OiPr)Cl_3$,CH_2Cl_2, −78 °C to −10 °C	1.2	**8.11**	9 %
8	**8.9**	$Ti(OiPr)Cl_3$,CH_2Cl_2, −78 °C to −10 °C	2.0	complex mixture	-

Table 8.1. – Tested conditions for the (3+2)–cycloaddition with ethylvinyl sulfide

The reaction between the alcohol **7.6** and ethylvinyl sulfide was first tried by using the standard titanium(IV)chloride–water tandem (entry 1) and trifluoroacetic acid (entry 2) in dichloromethane. Both conditions led to a complex mixture of degraded furan products and polymeric material. Also, omitting the addition of water was no improvement (entry 3). A milder alternative like $Ga(OTf)_3$ and $Dy(OTf)_3$ – conditions that were at that moment developed only recently in our lab – also gave complex mixtures of mainly polymeric material (entry 4 & 5). It was observed before that titanium(IV)isopropoxide was insufficiently strong to promote the cation formation. We thought however, that changing the Lewis acid to trichlorotitanium(IV)isopropoxide, prepared from titanium(IV)chloride and titanium(IV)isopropoxide, could be an interesting possibility to investigate. Under these conditions, furfuryl alcohol **7.6** indeed reacted with the alkene (entry 6) but we only isolated 7 % of the monoaddition product **8.12** along with polymeric material.

We concluded that a fused cyclopentane to a furan ring is hard to accomplish as we can expect this system to be highly strained. Consequently, the second ring closing step should be very slow which explains the isolation of **8.12**. In our lab we had observed the (4+3)–cycloaddition onto thienyl cations as well,[127] so some conditions were also tried with alcohol **8.9**. The thiophene ring is a larger heterocycle so we can expect the strain in the final product as well as the final ring closing step to be less than in the case of a furan ring. Synthesis of five–membered rings with thiophenes was reported earlier by Katritzky et al.[145] (fig. 8.5), in which the cation was prepared from a benzotriazole–substituted thiophene precursor.

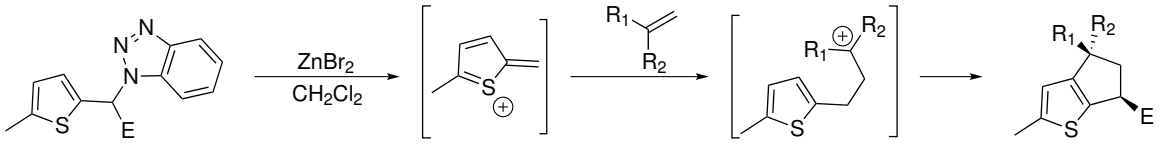

E	R_1	R_2			
H	Ph	Ph	**8.14**		52%
nPr	p-MeC6H4	H	**8.15a**: **8.15b**	1:1	83%
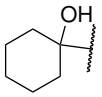	Ph	Me	**8.16a**: **8.16b**	1:2	85%

Figure 8.5. – Preparation of cyclopentanoids as reported by Katritzky et al.

Indeed, by using the trichlorotitanium(IV)isopropoxide we could isolate 9 % of the cyclopentannulated product **8.11** with some minor impurities.

Since yields were rather low, and no substantial synthetic advantage was gained as compared to the method by Katzinsky, we chose to focus on other synthesis methods that were being developed in our lab and stemmed from follow–up research into the (4+3)–cycloaddition described in the previous chapter. We had shown however that we could prepare the cation from thienyl alcohols and obtain cyclopentannulated products which were deemed much more difficult with furfuryl alcohols.

8.3. (5,6-DIHYDRO-1,4-DITHIIN-2-YL)METHANOL (DHDT–METHANOL) AS A VERSATILE ALLYL-CATION EQUIVALENT

8.3.1. In search for a removable heterocycle for (4+3)–cycloaddition with 1,3–dienes

The presence of the furan unit limits the synthetic possibilities of the (4+3)–cycloaddition (chapter 6) to the extent that synthetic targets should contain a furan ring or at least a derivative thereof (e.g. enedione).[127] It would however be of great interest to find a heterocyclic alcohol exhibiting similar properties in the cycloaddition reaction, as this would expand the scope. Especially sulfur–heterocycles are interesting because these can be "removed" by Raney nickel.

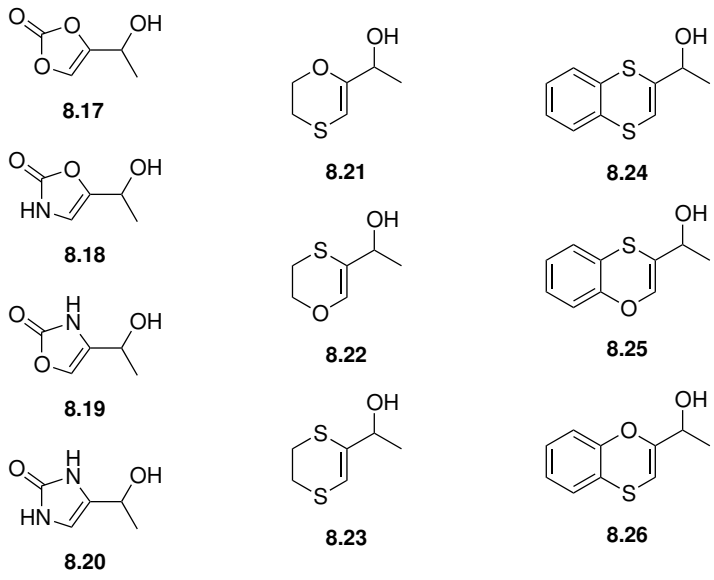

Figure 8.6. – Alternative possibilities for heterocyclic alcohols

From a small collection of possible candidates (fig. 8.6) we chose to focus on alcohol **8.23**.

A literature search suggested that this heterocyclic alcohol could be synthesised in only a few steps starting from diacetyl. An asymmetric transformation of one carbonyl group into 1,3–dithiolane **8.27** by treating diacetyl with ethanedithiol and borontrifluoride was followed by a bromine induced ring expansion to give the dihydrodithiin (DHDT) ketone **8.28**. This gave access to the symmetrically substituted DHDT alcohol **8.29** by reaction with methyllithium.

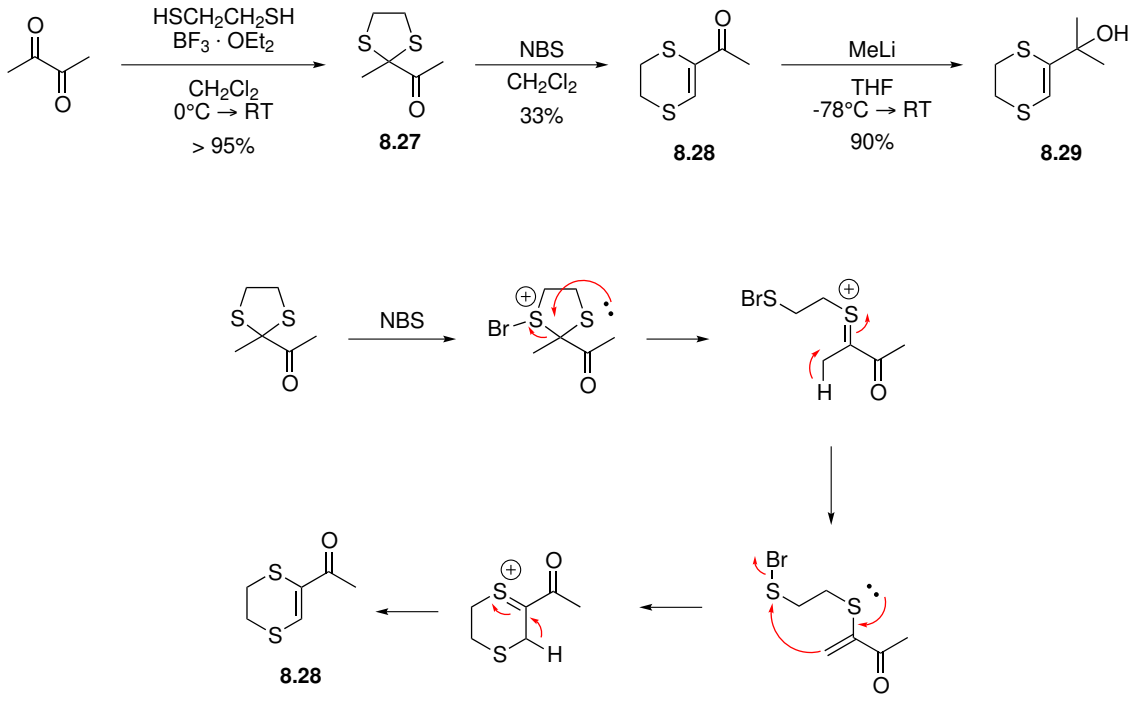

Figure 8.7. – Synthesis of alcohol **8.29** and mechanism of the bromine induced ring expansion of **8.27**

First attempts for cycloadditions with DHDT–methanol **8.30** with titanium(IV)chloride and 1,3-cyclohexadiene resulted in complex mixtures of polymeric materials and no cycloadduct. Also, $Ga(OTf)_3$ nor trifluoroacetic acid gave the expected cycloadducts. In the meantime, a similar test was done by J. Hullaert with the alcohol **8.31**, trifluoracetic acid and diene **8.4** (used in the synthesis of *epi*–liphagal)[143] and gave the cyclopentannulated

product **8.32**; the potential of this promising transformation was developed further in our lab.[146]

8.3.2. A new synthetic method for cyclopentanoid synthesis

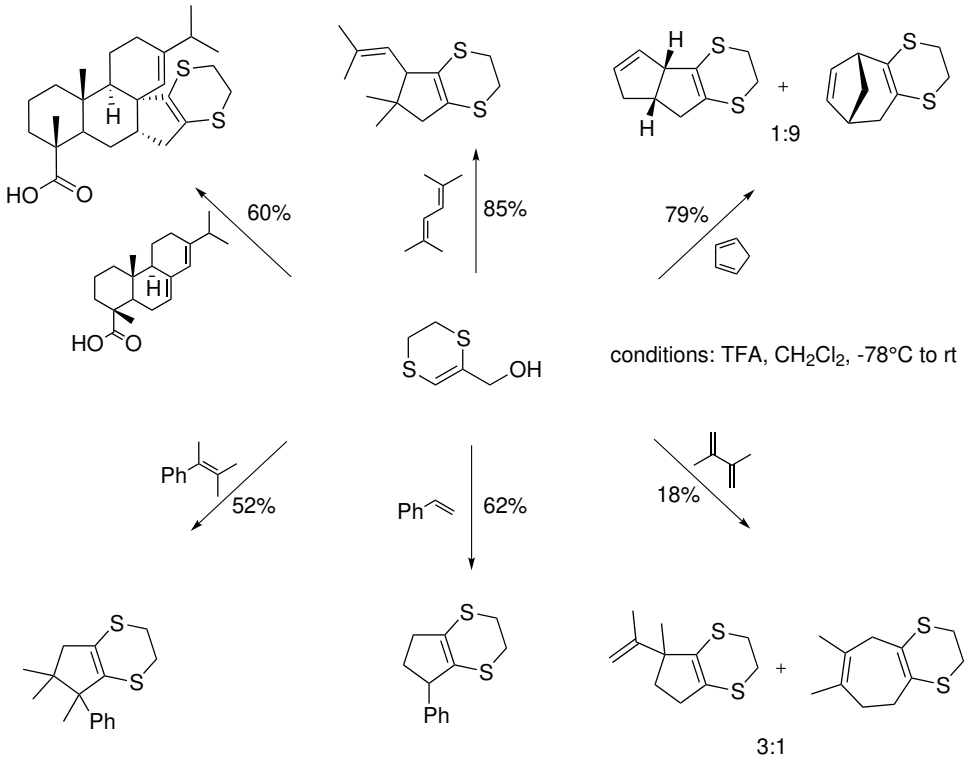

Figure 8.8. – Selected examples of (3+2)–cycloaddition between DHDT–methanol and different dienes[146]

The possibilities of this new (3+2)–cycloaddition is nicely illustrated by the myriad of polycyclic structures that are accessible (fig. 8.8. As was mentioned before, a (3+2)/[$_\pi$2 +$_\pi$ 2]–cycloaddition should go via a stepwise pathway based on orbital symmetry arguments (chapter 6). In this case, as was postulated by Hullaert, one would expect a first electrophilic attack from the DHDT–cation onto the diene (fig. 8.9).[146] From the resulting intermediate, different possibilities for class B side reactions are possible. Kinetically one

would expect the formation of the 5–membered ring to be the prevalent reaction pathway. However, some examples show competing formation of a 7–membered ring (e.g. cyclopentadiene, fig. 8.8).[146] It is worth noting that, as we observed the formation of a cyclopentane ring to be difficult in the case of furfuryl or thienyl cations, cyclopentannulation in the case of the DHDT–cation is quite easy probably owing to the less strained fusion with a dihydrodithiin ring.

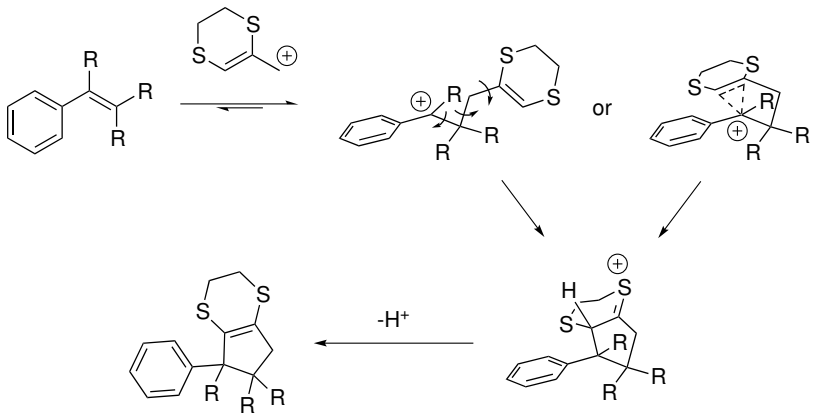

Figure 8.9. – Possible mechanisms for the (3+2)–cycloaddition between a DHDT cation and a diene[146]

8.4. Cycloaddition reactions with methylidene cyclohexenes

Our attention was drawn to dienes which had the general methylidene cyclohexene structure as we supposed that these would react selectively in a (3+2)–cycloaddition with a dihydrodithiin cation. The work of Hullaert indicated that single–*cis* dienes, such as 1,3–cyclohexadiene, are prone to give mixtures of (3+2)– and (4+3)–cycloaddition products. As methylidene cyclohexenes are *trans*–locked dienes, we should expect no competing (4+3)–addition pathways.

In order to gain understanding in the general selectivity aspects, some studies were performed into reactions with rather simple diene partners. Our lab developed a new method for the generation of the dihydrodithiin (DHDT) heterocycle (**8.33**) which allowed for a scale–up synthesis of the alcohol **8.31**. *In situ* prepared dithiinyl lithium, from **8.33** and *n*-butyllithium, is reacted with an aldehyde, ketone or ester to synthesise DHDT–alcohols in a straightforward way. Treating the dithiinyl lithium with dimethylformamide readily gave the aldehyde **8.34** which after a reduction step with sodium borohydride gave alcohol **8.31**.

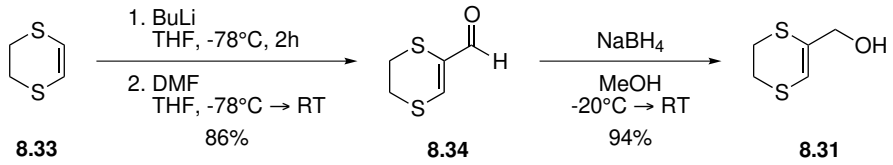

Figure 8.10. – Synthesis of DHDT alcohol **8.31**

8.4.1. Preliminary studies and synthesis of vetivane core

As a start we synthesised diene **8.35** by using Wittig reaction conditions. Standard conditions as were established by Hullaert were applied in the reaction with the diene and alcohol **8.31**. However, diene **8.35** polymerised rapidly under trifluoroacetatic acid conditions (fig. 8.11a). Other dienes **8.36**, **8.37** and **8.38** were again prepared by using standard Wittig conditions (fig. 8.11a). For diene **8.38** we first prepared literature compound **8.39** from (*S*)-carvone by solvent–free hydrogenation with platinum(II)oxide as a catalyst. Removal of the double bond was deemed necessary as to avoid interfering reactions onto the isopropylene group. Neither one of them yielded the expected cycloadduct but rather complex polymerisation products (fig. 8.11b).

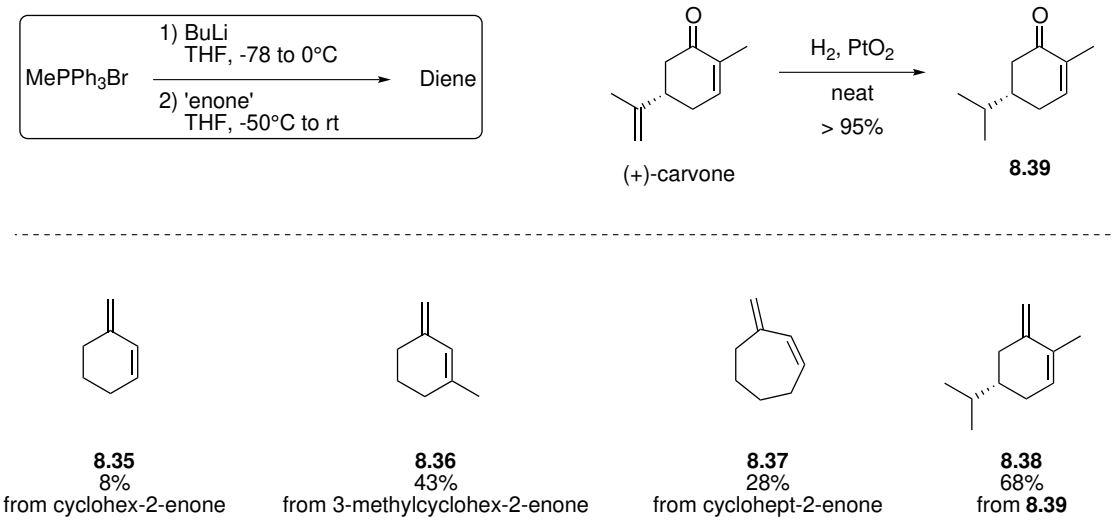

(a) Synthesis of methylidene cyclohexane–based dienes

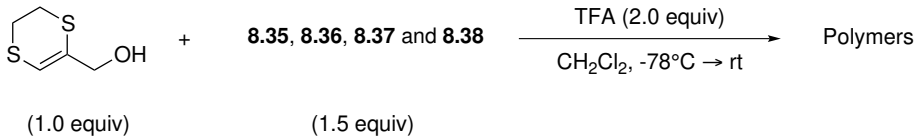

(b) Attempted (3+2)–cycloaddition reactions

Figure 8.11. – Initial test reactions for (3+2)–cycloaddition between methylidene dienes and DHDT cations

A possible explanation can be found in the reactivity of protonated dienes that are in equilibrium with the neutral diene. The involved carbocation is more reactive than the DHDT cation and thus the methylidene carbon can readily attack the cation.

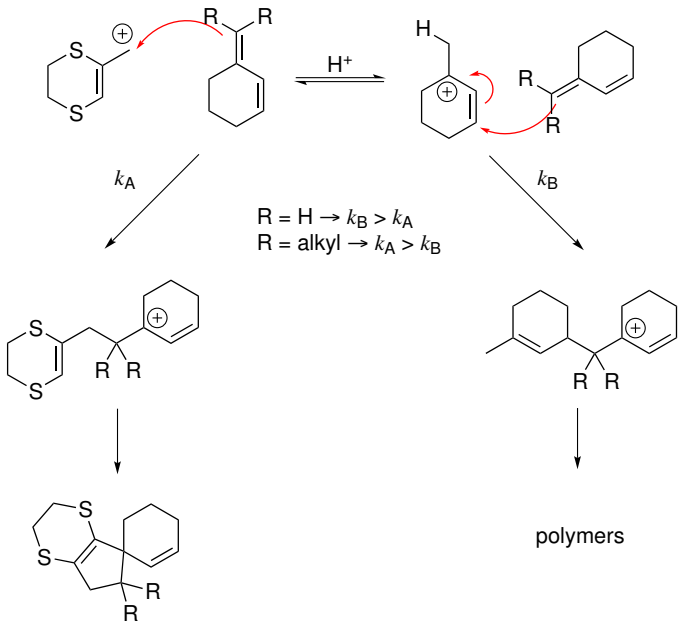

Figure 8.12. – Polymerisation tendency difference for different substitution patterns on the methylidene carbon

As the propagation relies on the reactivity of the methylidene carbon relative to the carbocation, we thought of substituting the methylidene carbon in order to sterically reduce its nucleophilicity (fig. 8.13). Synthesis of diene **8.40** could be achieved by using a Ramirez olefination. The dimethyl susbtitution of the 4–position was found to be necessary as cyclohexenone only gave tarry residues owing to the reactivity of the hydrogens at the 4-position the carbene intermediates in the Ramirez olefination.

Surprisingly, reaction of diene **8.40** with alcohol **8.31** only gave intact diene and degraded alcohol pointing to a very slow first electrophilic addition step. Synthesis of the diene **8.41** was done under standard Wittig conditions from 4,4-dimethyl-cyclohexenone.

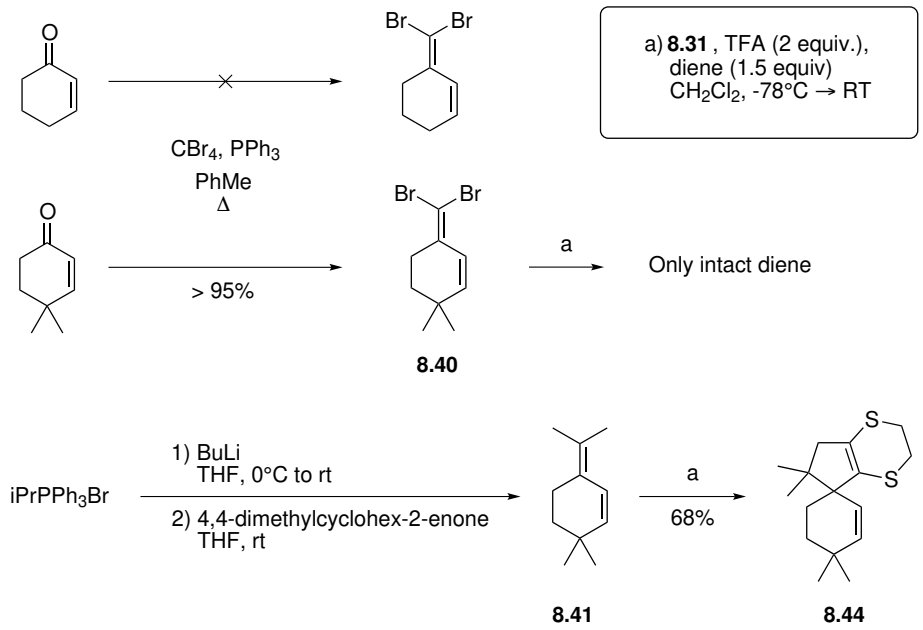

Figure 8.13. – Synthesis of alternative methylidene dienes and subsequent attempts for cycloaddition

Cycloaddition reactions with dienes **8.41** gave the expected adduct **8.44** in good yields and showed exclusive selectivity for the *exo*cyclic double bond. Interestingly, cycloadduct **8.44** closely resembles the carbon core of the natural product β-vetivone. The regioselectivity of the cycloaddition between diene **8.41** and a DHDT–cation could be identified by clear HMBC correlation, which would not be possible for the alternative regiosisomer (fig. 8.14).

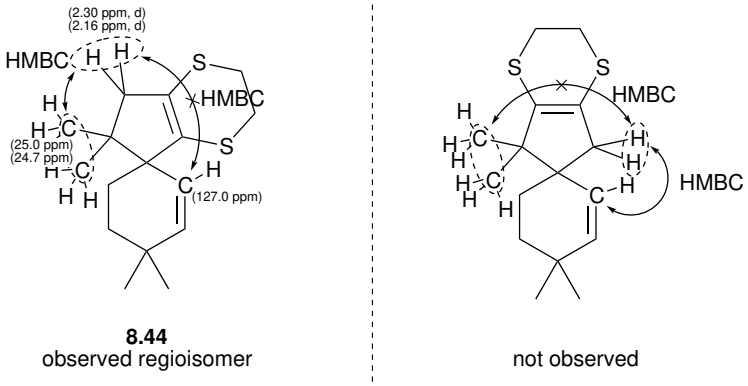

Figure 8.14. – Characteristic HMBC correlation for cycloadduct **8.44**

In conclusion, the substitution pattern of the *trans*–locked dienes we described, seems to be very important for the success of (3+2)–cycloadditions.

8.4.2. Methylidene blocking by latent functionalities

We found that blocking the methylidene position with two methyl groups improved the reaction tremendously. Intrigued by this result, we explored alternative substitutions as the methyl groups narrow down the synthetic possibilities since it would require two alkyl groups as an integral part of the final structure. It would thus be interesting to substitute the dienes with latent functionalities that can be removed/transformed after cycloaddition. Diene **8.40** which was described above would fit this criterion as the two bromine atoms could be reduced afterwards. We have found however that it is unreactive under the standard conditions for cycloaddition.

As the dihydrodithiin heterocycle in its own is a latent functionality that can be reductively removed with Raney nickel, as was shown by Hullaert, blocking the methylidene with a sulfur based substituent would allow for an efficient method of transforming the cycloadduct into a naked carbocycle.

8.4.2.1. Thiophenyl substituted methylidene cyclohexenes

It was shown before that substituting a diene with an ethyl sulfide substituent raised the issue of sulfur alkylation.[146] The DHDT cation is attacked by the sulfur atom which is followed by subsequent elimination steps leading to the thioether **8.45** and no cycloadduct. In order to overcome this problem we thought of using a thiophenyl substituent, as the sulfur atom can be expected to be less nucleophilic because of the phenyl ring that stabilises the sulfur lone pairs.

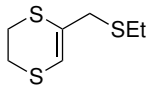

8.45

Figure 8.15. – Thioether **8.45** as reported by Hullaert[146]

The synthesis of diene **8.46** was attempted by treating cyclohexenone with the phosphonium salt **8.47** – prepared from (chloromethyl)(phenyl)sulfane – under normal Wittig conditions. The phosphorus ylid however, quickly decomposed even before addition of the ketone (fig. 8.16). A Peterson olefination with cyclohexenone and the commercial thiophenyl compound **8.48** – prepared from thioanisole – did yield the expected diene **8.46** as well as diene **8.49** from 4,4-dimethyl cyclohexenone (fig. 8.16). A Peterson olefination in general yields a β-hydroxy silane which upon treating with acid or base eliminates to the olefin. In this case however, because of the formation of a conjugated diene, aqueous workup allows for the spontaneous formation of the expected diene albeit as a an inseparable equimolar mixture of both (E) and (Z) isomers ((fig. 8.16)).

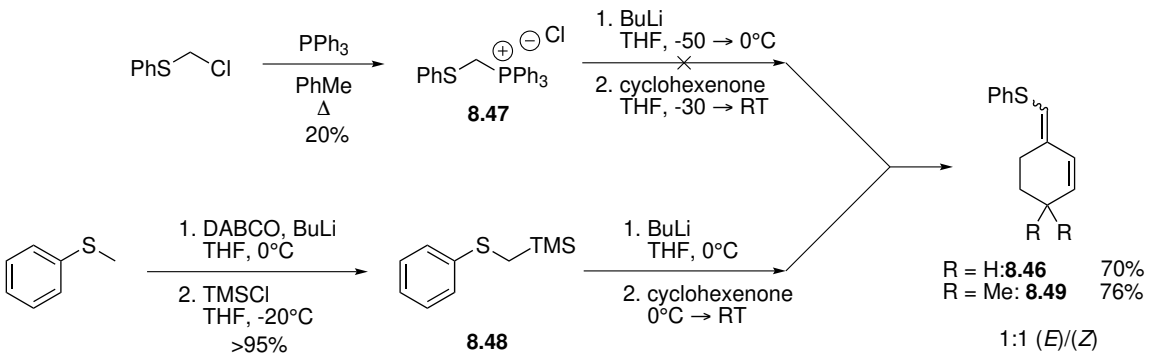

Figure 8.16. – Synthesis of phenylthio–substituted methylidene dienes

Interestingly, the reaction between DHDT–methanol **8.31** and diene **8.46** gave a mixture of different products (fig. 8.17). The cycloaddition products were identified as being **8.51a** and **8.51b** each resulting from reaction with the *exo*– and *endo*–cyclic double bond of **8.46**. We also found the thiophenyl substituted DHDT product **8.51c** resulting from a presumed attack of the DHDT cation onto the diene sulfur atom. The regioselectivity of cycloadduct **8.51a** could unambiguously be identified by a distinct scalar coupling between the hydrogen *geminal* to the thiophenyl group and the CH_2 hydrogens on the cyclopentane (fig. 8.18). The ratio between the cycloaddition on the *exo*– and *endo*–cyclic double bond shows a slight preference for the *endo*–cyclic double bond. Surprisingly, only one isomer of diene **8.46** seems to participate in this addition (fig. 8.18).

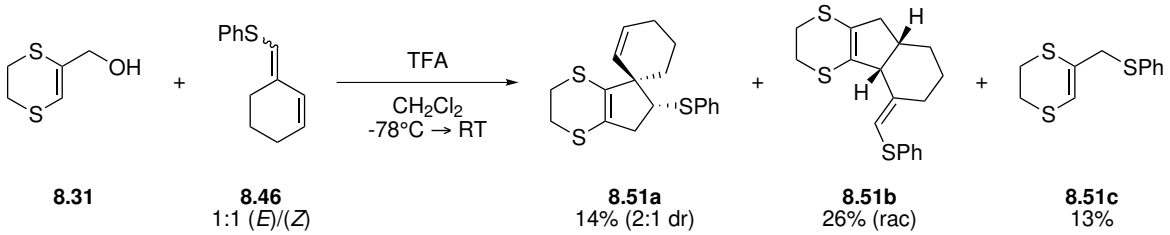

Figure 8.17. – Cycloadditions between DHDT methanol and diene **8.46** (yields are determined by ^{1}H–NMR spectroscopy)

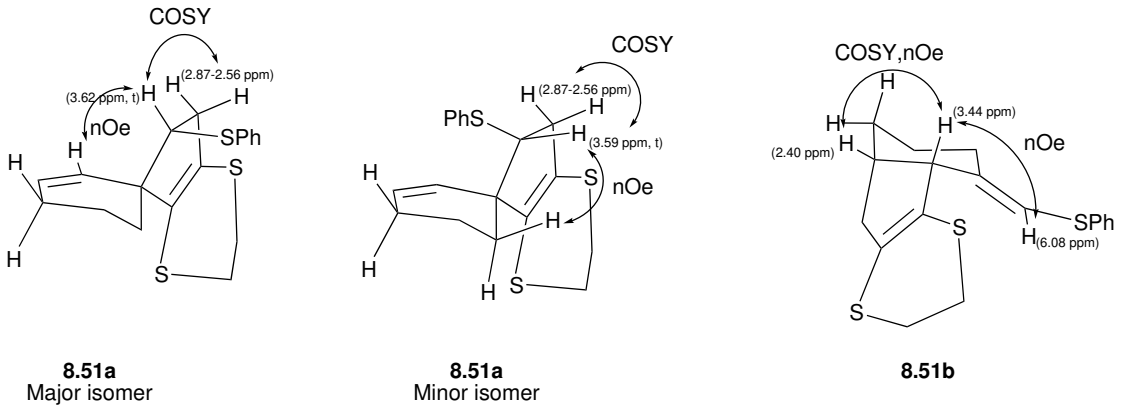

Figure 8.18. – Characteristic nOe and COSY correlation for **8.51a** and **8.51b**

A second cycloaddition between DHDT–methanol **8.31** and diene **8.46** resulted in similar observations. However, the cycloaddition was found to be completely selective for the *exo*–cyclic double bond again showing the same regioselectivity (fig. 8.20).

A remarkable feature of these reactions is the observation that cycloaddition formation is only observed at relatively high temperatures (starting at approximately $-10\,^{\circ}\mathrm{C}$). This could point to low reactivity, and thus slow reaction, of these dienes which might also explain the relatively low yields that are obtained as the dienes will become more susceptible to side reactions.

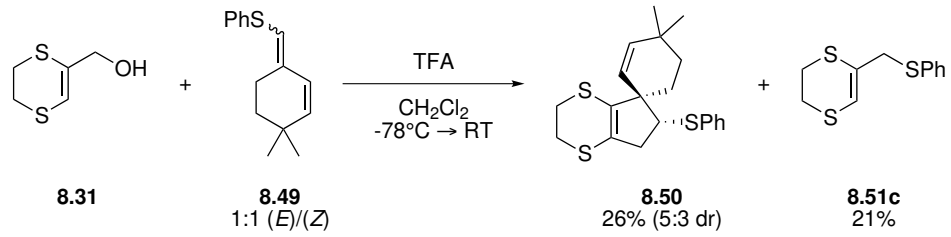

8.31 **8.49** 1:1 (*E*)/(*Z*) **8.50** 26% (5:3 dr) **8.51c** 21%

Figure 8.19. – Cycloadditions between DHDT methanol and diene **8.49** (yields are determined by ^{1}H–NMR spectroscopy)

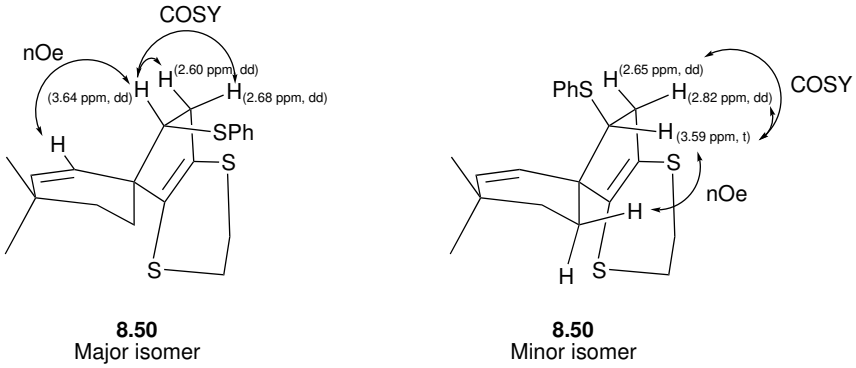

Figure 8.20. – Characteristic nOe and COSY correlation for **8.50**

8.4.2.2. 1,3-dithiane substituted methylidene cyclohexenes

An alternative substitution of the methylidene carbon was done via a Peterson olefination reaction between cyclohexenone and (1,3-dithian-2-yl)trimethylsilane. The reaction of alcohol **8.31** and diene **8.52** did not lead to the expected cycloadduct, but again slow consumption of the alcohol was observed leading to polymeric material and degraded diene.

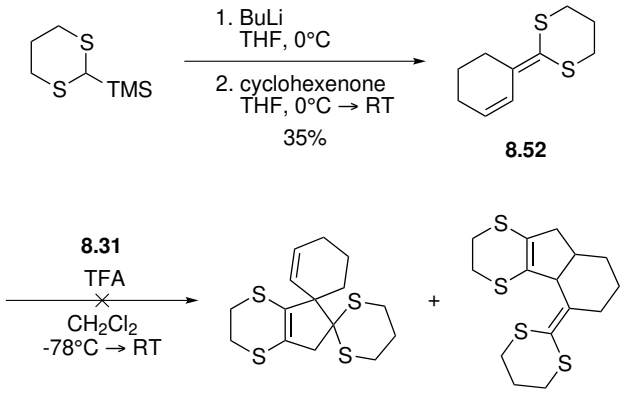

Figure 8.21. – Attempted ycloaddition with diene **8.52**

8.4.3. Selectivity aspects of (3+2)–cycloaddition of substituted methylidene cyclohexene and DHDT–cations

The assumption of a rate–limiting first electrophilic addition step is somewhat hard to reconcile with the results from the previous sections. A sulfur atom and a methyl group are about equally as potent in stabilizing positive charges and double bonds. Hence, we can expect both dienes **8.41** and **8.52** to show the same nucleophilic properties. Yet, the 1,3–dithiane substituted diene does not yield cycloaddition products whereas substitution with two methyl groups does. This raises the question whether these cycloadditions are controlled by ground–state effects on the HOMO of the diene.

Our current hypothesis involves the formation of a pre–reactive complex, and the success of further reaction depends on the equilibrium between this complex and the separate reactants. If we consider the case of the 1,3–dithiane substituted diene, the influence of the substituents on the HOMO are shown in fig. 8.23. The sulfur lone pairs are much higher in energy than the π–bond electrons resulting in a molecular orbital in which the contribution of the π–bond is very small as compared to the contribution of the sulfur. The other double bond shows an interaction with an adjacent σ_{CH} orbital which is much lower in energy. The highest MO for that subsystem has a relatively large contribution of the double bond as compared to the σ–bond. The combination of these two systems results in an overall HOMO which has a very small contribution of the diene π–system and a large one of the sulfur atoms.

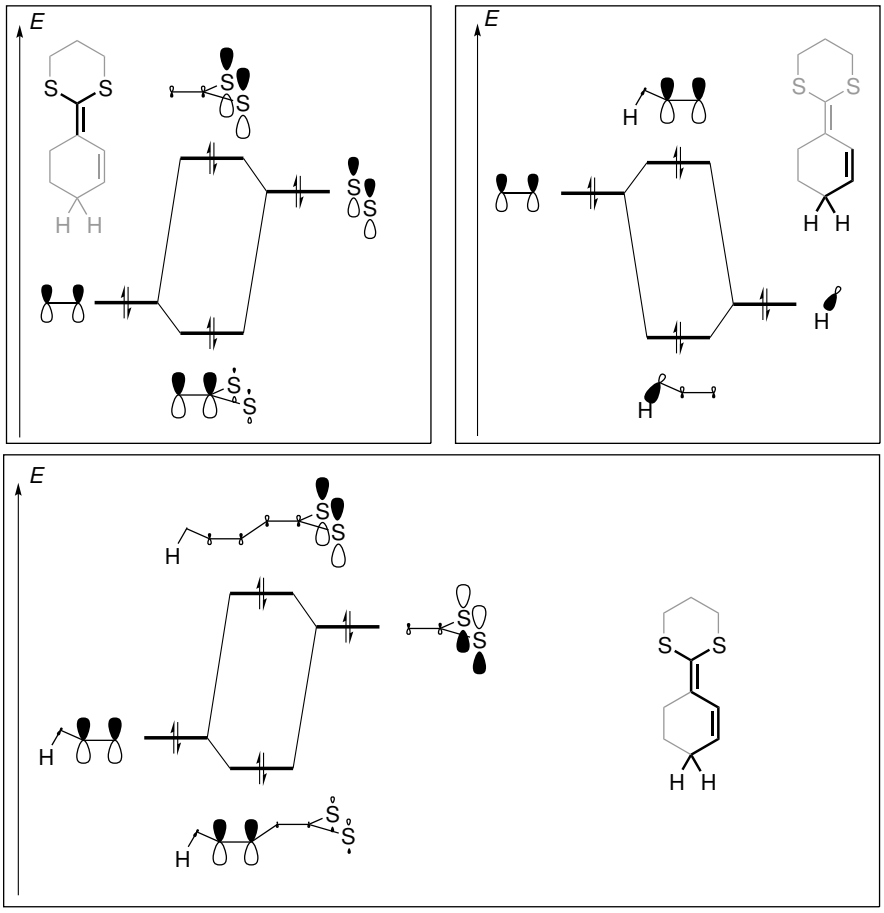

Figure 8.22. – Substituent effect on the HOMO of **8.52**

We can expect the formation of a pre–reactive complex – depending on the interaction of the entire HOMO of the diene and the LUMO of the DHDT–cation – to be unfavorable as there is no orbital contribution from the double bonds. Hence, the equilibrium will shift to the side of the separate reactants. We should that that this discussion also applies to the example of diene **8.53** as this also involves interaction with higher energy lone pairs (on the bromine atoms) that will also result in a similar π–bond contribution.

Interestingly, the same analysis for diene **8.41** shows that the influence of the lower lying σ–orbitals cause a very large contribution of the double bond π–orbitals to the overall HOMO of the diene.

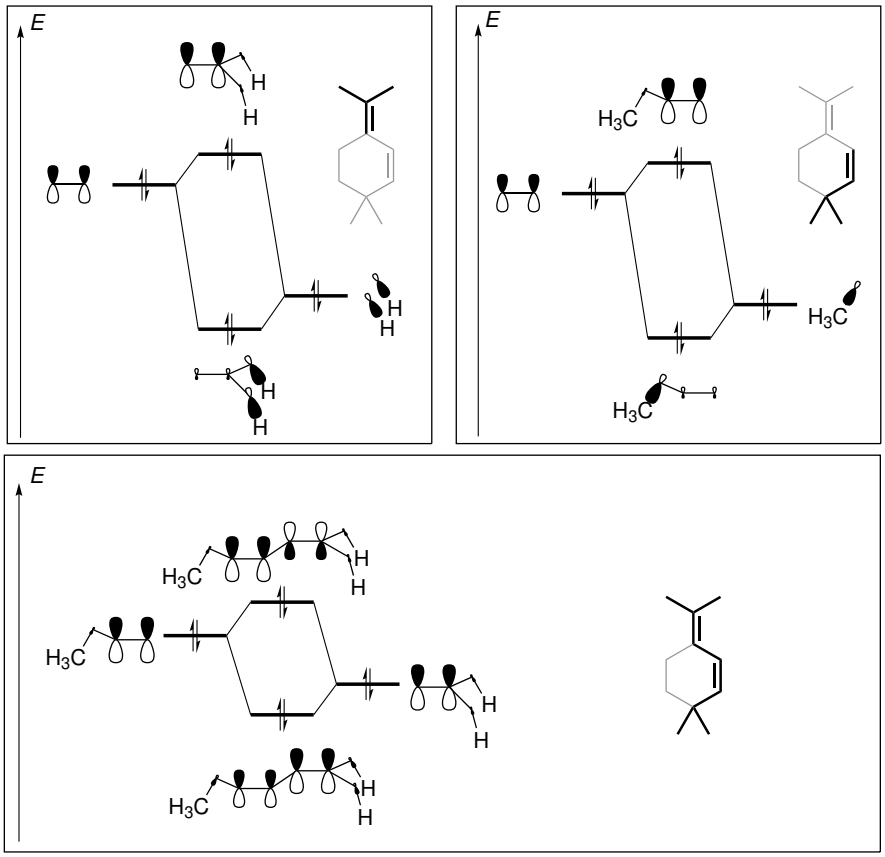

Figure 8.23. – Substituent effect on the HOMO of **8.41**

The example of the phenylthio–substituted diene shows a very different situation (fig. 8.24) as there is only one sulfur atom contributing to the HOMO. Moreover, the phenyl group stabilizes the lone pair, resulting in a larger contribution of the double bond. Combination with the MO of the other double bond then gives an overall HOMO which has a larger contribution from the diene system.

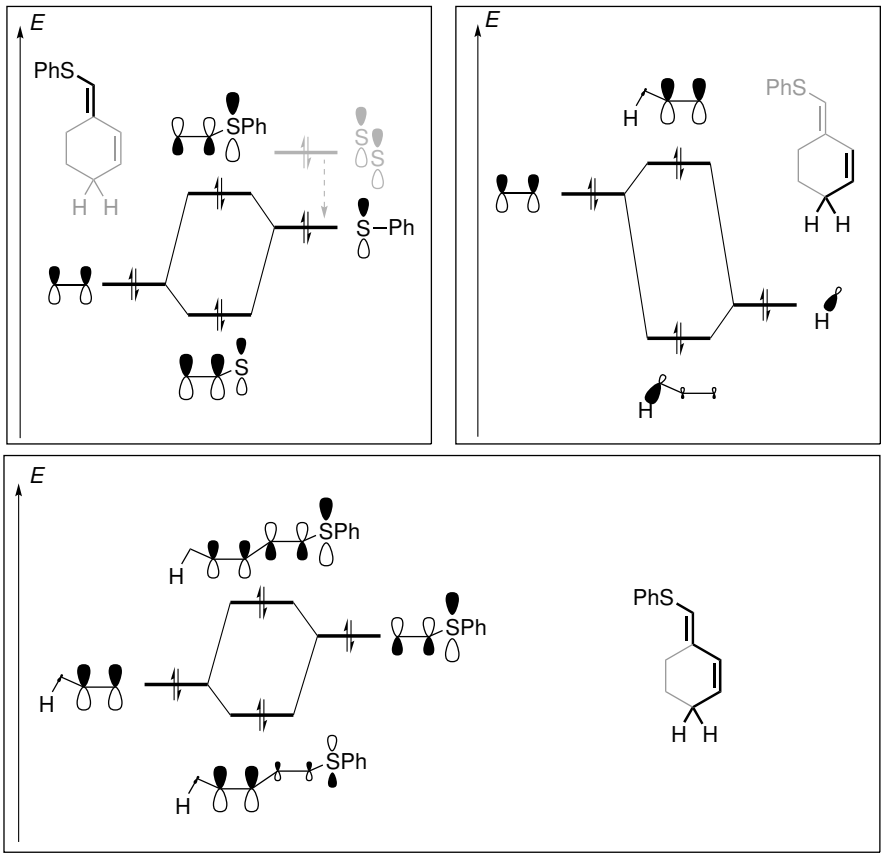

Figure 8.24. – Substituent effect on the HOMO of **8.46**

We can now consider two different geometries for a pre–reactive complex for the reaction of **8.46** and a DHDT cation. The first one involves an interaction with the lobe on the sulfur atom, which gives a complex that can lead to either the cycloadduct **8.51a** or the phenylthioether **8.51c**. An alternative orientation in which the interaction is centered in the middle of the diene π–bonds can then give cycloadduct **8.51b**.

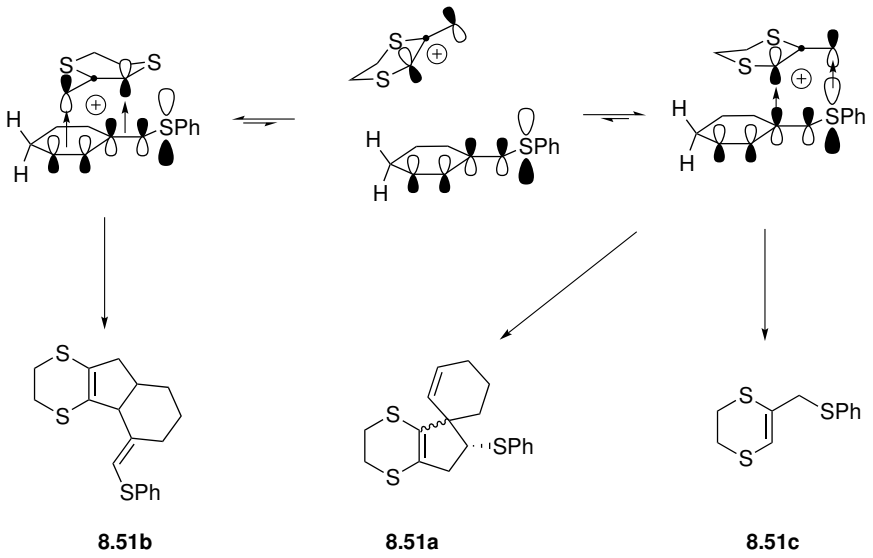

8.51b **8.51a** **8.51c**

Figure 8.25. – Equilibrium between pre–reactive complex and separate reactants **8.46** and DHDT–cation

If we apply this model to the example of diene **8.49** and a DHDT cation we can draw similar conclusions. The sulfur interacting pre–reactive complex can again result in competing cycloadditions and alkylation pathways, whereas the alternative geometry seems very unfavourable because of the steric interaction with the methyl group. This could explain the exclusive formation of **8.50** and **8.51c** in this reaction.

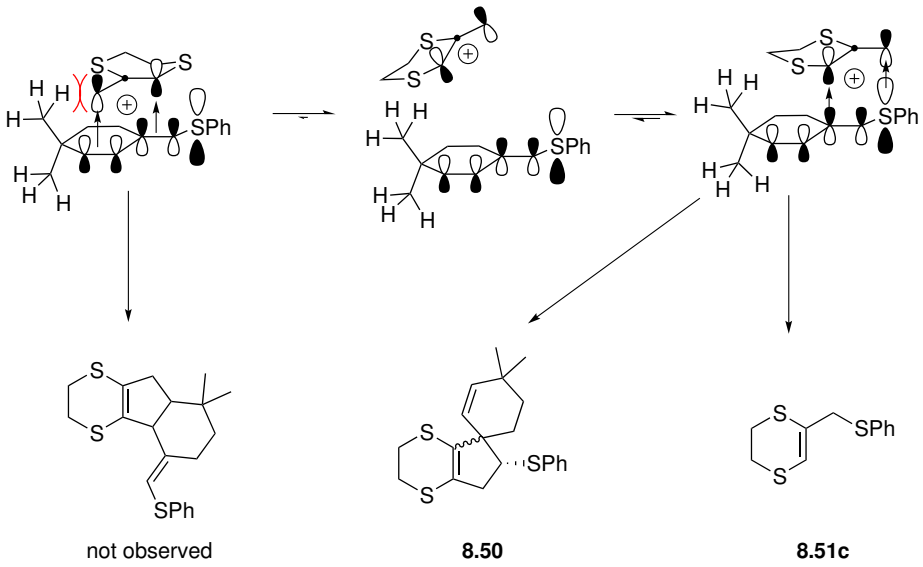

Figure 8.26. – Equilibrium between pre–reactive complex and separate reactants **8.49** and DHDT–cation

8.5. Conclusions

In this chapter we have shown that the feasibility of harvesting furfuryl and/or thienyl alcohols as precursors in (3+2)–cycloaddition is rather limited. However, dihydrodithiin alcohols and their derived cations have proven to be much more reliable reaction partners for these transformations as was shown by Hullaert and Winne. Expanding the scope of this promising reaction with a clear focus on *trans*–locked dienes, has led to attempts to use methylidene cyclohexene–derived dienes together with DHDT for the generation of complex polycyclopentanoids. In these series of experiments we found that blocking the methylidene carbon is essential to avoid premature cationic polymerization of the dienes. These substituents can include methyl groups but more interesting was a thiophenyl group that was introduced, as methyl groups do limit the scope, whereas thiophenyl can be removed afterwards. A major drawback we found, was the occurrence of

cationic attack onto the sulfur atom leading to DHDT deactivation during the time of the reaction.

Interestingly, reactivity descriptors suggested a different regiochemistry with respect to the exocyclic double bond in the case of the thiophenyl substituted dienes. We proposed a model in which the first electrophilic addition step is preceded by a complex in which the sulfur atom of the diene aligns with the cation on DHDT. The resulting proximity of reactive centers could then lead to observed regioisomer.

As this work was only in a preliminary state, we can suggest some points of attention for further research. These can include:

- Enlarging the number of diene partners with blocked methylidene carbons,
- increasing the steric bulk of the thiophenyl substituent as to minimise the attack of the sulfur atom on the DHDT cation

9 Conclusions for the second part

Ever since Diels and Alder reported the smooth (4+2)–cycloaddition between olefins and 1,3–dienes, the development of cycloaddition reactions in general have proven to be a very valuable method in the syntheses of complex carbocyclic molecules. The rationalization of the experimental observations by Woodward and Hoffmann, reported in a series of seminal papers, have provided the organic chemistry community with a set of rules (WH–rules) that have been shown invaluable as a predictive tool for the geometries of cycloaddition transition state geometries. Later work by Susstman enabled rationalization of the energy levels involved in cycloadditions. In chapter 6 we discussed some general aspects of cycloaddition reactions applied to the lesser known examples that produce odd–membered rings ((2+1), (3+2) and (4+3)). The concepts that dictate the selectivities in these transformation are, to a certain extent, common among all three. The discussion whether those additions proceed via stepwise or concerted mechanisms is sometimes subject of debate.

In chapter 2 we investigated a very specific example of a (4+3)–cycloaddition between a furfuryl cation and a 1,3–diene. This reaction has been shown to be very reliable and is found to allow intermolecular cycloaddition between different furfuryl cations and a lot of different dienes. The specific example of the reaction with the sesquiterpene (*R*)-α-phellandrene caught our attention as it was found to proceed with a remarkably high degree of stereoselectivity, something which was also reported in the literature for other cycloaddition reactions and electrophilic additions.

A thorough computational investigation through DFT calculations, revealed that indeed the boundary between concerted and stepwise cycloaddition is a very thin line. The reaction was found to go through two distinct ring–closing steps in which the first step is rate–limiting. The geometry along the reaction coordinate was shown to exhibit a high degree of preorganization, which has been termed a 'closed arrangement' in the recent literature. This proposed model describes the experimental observations quite well. Attempts to design an experiment in which we could predict the stereochemical outcome beforehand, indeed confirmed our model. However, forced stepwise cyclization of the putative intermediate cation, also showed the same selectivity and could not endorse the 'closed arrangement' hypothesis.

We also tried to find evidence for the stereospecificity of the (4+3)–cycloaddition between symmetrical furfuryl cations and 1,3–dienes, but the substrates we chose were very well–suited for this purpose. Although recent literature has shown stereospecific (4+3)–cycloaddition between 1,3–dienes and indolyl cations, future research might focus on investigating alternative substitutions of the furfuryl cation as well as a different set of cycloaddition conditions.

The final chapter 8 focused on investigations into possible applications of allyl cation cycloadditions. We conducted preliminary research into the construction of the carbocyclic core of the natural product family of the scopariusins by employing the aforementioned (4+3)–cycoaddtion between a 1,3–diene and a furfuryl cation. Unoptimised results showed that the scopariusin scaffold could indeed be accessed by this approach. Further optimization as well as method development for the final carbon core decoration might lead to a total synthesis in the future.

In order to expand the toolbox of allyl cation cycloadditions, we started tests in order to be able to perform (3+2)–cycloadditions between sulfur–stabilized alkenes and furfuryl or thienyl cations. These initial attempts have been proven unsuccessful and this route was abandoned. At that time, a very efficient (1+3)–cycloaddition reaction between a dihydrodithiin cation and a a stabilized alkene was developed. Intrigued by

the potency of this reaction with *trans*–locked dienes, we investigated the application of methylidene substituted cyclohexenes. We quickly found that it was very important to block the methylidene carbon to avoid cationic polymerization reactions as the primary reaction. Methyl substituents indeed enables (3+2)–cycloaddition with this type of diene. More interestingly, a phenylthio–substituent was also applicable in this reaction and can, in theory, be removed afterwards. The use of phenylthio–substituted dienes is however compromised by the formation of a side product related to the alkylation of the diene by the dihydrodithiin cation.

The experimental results enabled us to rationalize some reactivity trends in these cycloadditions. We hypothesized that the success of (3+2)–cycloaddition is dependent on the equilibrium between a pre–reactive complex and the diene, as classical nucleophilicity could not explain certain experimental results. The position of the equilibrium is largely dependent on the stability of the pre–reactive complex which in turn depends on the structure of the Highest Molecular Orbital (HOMO) of the diene. This model was able to reconcile some of the seemingly anomalous experimental observations. Future experiments as well as computational studies might indeed reveal the true nature of this very intriguing transformation.

We must trust to nothing but facts: these are presented to us by nature and cannot deceive. We ought, in every instance, to submit our reasoning to the test of experiment, and never to search for truth but by the natural road of experiment and observation.

(A. Lavoisier)

III

EXPERIMENTAL

10 Experimental procedures

10.1. General methods and materials

General Methods Reactions were monitored by thin layer chromatography (TLC) using SIL G-25 UV254 precoated silicagel plates (0.25 mm thickness). The TLC plates were visualized using an anisaldehyde (5 % anisaldehyde in ethanol with 1 % sulfuric acid) solution. Flash column chromatography was performed using BIOSOLVE silica gel (0.063-0.200 mm particle size). 1H NMR and 13C NMR spectra were recorded on a 300 MHz instrument at 300 and at 75 MHz respectively, a 400 MHz instrument at 400 and at 100 MHz respectively, a 500 MHz instrument at 500 and at 125 MHz respectively or a 700 MHz instrument at 700 and at 175 MHz respectively. Chemical shifts (δ) are reported in units of parts per million (ppm), referenced relative to the residual 1H or 13C peaks of the used solvent as internal standards (chloroform-d: δH 7.26 and δC 77). Where given, proton shifts of overlapping signals were determined from a HSQC spectrum. The following abbreviations were used to explain the observed multiplicities: s, singlet; d, doublet; t, triplet; q, quadruplet; quint, quintuplet; sept, septuplet; m, multiplet; br, broadened; AB, signals with clear roofing; band, several overlapping signals. Where given, assignments of resonances were confirmed by standard COSY, HSQC, HMBC and NOESY 2D NMR experiments. Infrared spectra (IR) were recorded on a PERKIN-ELMER 1600 series FTIR spectrometer and reported in wave numbers (cm-1). Samples were prepared as a thin film (neat) on KBr plate or measured through Attenuated Total Reflection (ATR). High Resolution Mass Spectra (HRMS) were recorded on an Agilent Accurate-Mass Quadrupole

Time-of-Flight mass spectrometer.

Materials All chemicals and solvents were purchased and used without any further purification, except dichloromethane, which was distilled from CaH_2 prior to use.

10.2. Reactions from chapter 2

10.2.1. 4-(3-bromo-4-hydroxyphenyl)-2-methylphthalazin-1(2*H*)-one (2.4)

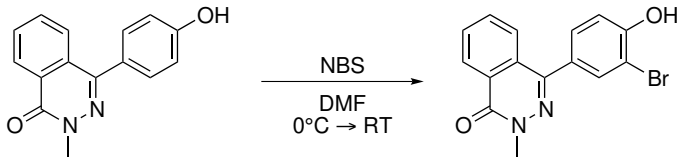

2.3 **2.4**

2.3 (100 mg, 0.4 mmol, 1.0 equiv.) is dissolved in dimethyl formamide (1.5 ml). The mixture is cooled to 0 °C and *N*-bromosuccinimide (71 mg, 0.4 mmol, 1.0 equiv.) is added portion wise and the solution is heated to room temperature and stirred during which a white precipitate was formed. After 3 h the reaction mixture is concentrated *in vacuo* and the resulting residue is purified with flash chromatography (silica, methanol:chloroform 1:99, v/v) to give the title compound **2.4** as a pale yellow solid (10 mg, 0.03 mmol, 8 %).

Formula: $C_{15}H_{12}N_2O_2$;
Molar mass: 252.27 g/mol;
^{1}H-NMR (400 MHz, CD_3OD): δ (ppm) 8.38 (m, 1 H, (O)C−C−C*H*), 7.83–7.68 (band, 3 H, (O)C−C−CH−C*H* + (O)C−C−CH−CH−C*H* + (O)C−C−CH−CH−CH−C*H*), 7.62 (d, 1 H, ^4J = 2.2 Hz, N=C−C−C*H*−CBr−COH), 7.29 (dd, 1 H, ^3J = 8.3 Hz, ^4J = 2.2 Hz, N=C−C−C*H*−CH−COH), 6.98 (d, 1 H, J = 8.3 Hz, N=C−C−CH−C*H*−COH), 3.81 (s, 3 H, CH_3),

10.2.2. 4-Bromo-*N*-(4-nitrophenyl)benzenesulfonamide (2.6)

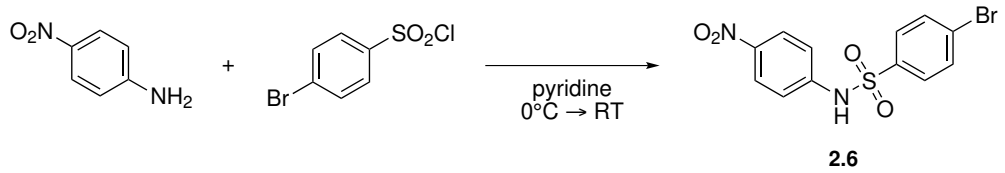

2.6

4-nitroaniline (583 mg, 4.22 mmol, 1.08 equiv.) is dissolved in pyridine (8 ml). The mixture is cooled to 0 °C and 4-bromobenzenesulfonyl chloride (1 g, 3.91 mmol, 1 equiv.) is added portionwise, upon which the mixture turns orange. The reaction is stirred at room temperature for 17 h. After concentration *in vacuo*, the residue is redissolved in a water/ethyl acetate (50/50) mixture. The organic phase is washed with hydrochloric acid (6 × 30 ml, 6 M), water (20 ml), a saturated sodium bicarbonate solution (30 ml) and a saturated sodium chloride solution (40 ml). The organic phase is dried on sodium sulfate, filtered and concentrated *in vacuo*. The crude solid is purified with flash chromatography (silica, ethyl acetate/hexanes 12/88 to 45/55) and recrystallized from *iso*-propanol to yield sulfonamide **2.6** as a pale yellow solid (1.28 g, 3.6 mmol, 92 %).

Yield: 72 %;

Formula: $C_{12}H_9N_2O_4SBr$;

Molar mass: 318.35 g/mol;

^{1}H-NMR (500 MHz, $(CD_3)_2CO$): δ (ppm) 8.20–8.13 (m, 2 H, $O_2N-C=CH$), 7.89–7.82 (m, 2 H, $O_2S-C=CH$), 7.82–7.76 (m, 2 H, $HN-C=CH$), 7.55–7.40 (m, 2 H, $Br-C=CH$),

^{13}C-NMR (125 MHz, $(CD_3)_2CO$): δ (ppm) 144.7 (C), 144.6 (C), 139.6 (C), 133.5 (CH), 129.9 (CH), 128.7 (CH), 126.0 (CH), 119.7 (CH),

HRMS [m/z]: calc'd for $C_{12}H_8N_2O_4SBr^-$, 354.9394; found, 354.9407

10.2.3. 4-Allyl-*N*-(4-nitrophenyl)benzenesulfonamide (2.8)

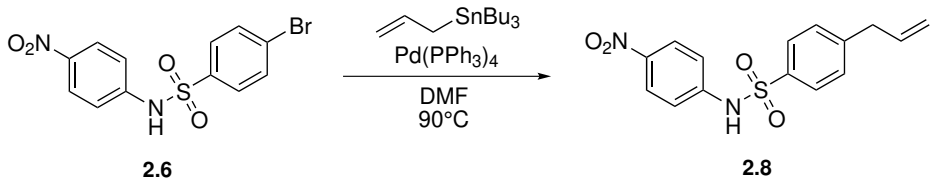

2.6 **2.8**

Sulfonamide **2.6** (1 g, 2.8 mmol, 1 equiv.) is dissolved in dimethylformamide (20 ml) together with tetrakis(triphenylphosphine)palladium (226 mg, 0.2 mmol, 0.09 equiv.). The mixture is extensively purged with nitrogen gas during 30 min. Allyltributylstannane (1.09 ml, 3.5 mmol, 1.25 equiv.) is added and the mixture is purged for another 5 min. The reaction is heated to 90 °C and after stirring for 3.5 h poured into ice water (100 ml). Ethyl acetate (100 ml) is added and the mixture is filtered over a pad of celite. The organic phase is separated and washed with water (30 ml), a saturated sodium bicarbonate solution (30 ml) and a saturated sodium chloride solution (30 ml). After drying on sodium sulfate, the organic phase is concentrated *in vacuo*. The residue is purified with flash chromatography (silica, ethyl acetate/petroleum ether(bp 40-60 °C) 30/70) to yield sulfonamide **2.8** as a viscous oil which is dissolved in methyl-*tert*-butylether and precipitated with petroleum ether(bp 40-60 °C) to yield sulfonamide **2.8** as a pale yellow solid (563 mg, 1.76 mmol, 63 %).

Formula: $C_{15}H_{14}N_2O_4S$;

Molar mass: 318.35 g/mol;

^{1}H-NMR (500 MHz, $(CD_3)_2CO$): δ (ppm) 9.80 (s(br), 1 H, N*H*), 8.20–8.11 (m, 2 H, O_2N−C=C*H*), 7.91–7.82 (m, 2 H, O_2S−C=C*H*), 7.51–7.44 (m, 2 H, HN−C=C*H*), 7.44–7.38 (m, 2 H, H_2C−C=C*H*), 5.93 (ddt, 1 H, $J = 17.0, 10.1, 7.8$ Hz, CH_2−C*H*), 5.08 (ddm(AB), 1 H, $J = 17.0, 1.6$ Hz, CH_2−CH=C*H*H), 5.05 (ddm(AB), 1 H, $J = 10.1, 1.6$ Hz, CH_2−CH=CH*H*), 3.45 (d, 2 H, $J = 7.8$ Hz, CH_2),

^{13}C-NMR (125 MHz, $(CD_3)_2CO$): δ (ppm) 147.4 (C), 145.0 (C), 144.4 (C), 138.1 (C), 137.1 (CH), 130.3 (CH), 128.2 (CH), 126.0 (CH), 119.2 (CH), 117.1 (CH_2), 40.3 (CH_2),

HRMS [*m*/*z*]: [M-H]- calcd. For $C_{15}H_{13}N_2O_4S^-$, 317.0602; found, 317.0606

10.2.4. 4-(4-Hydroxyphenyl)-2-methylphthalazin-1(2*H*)-one (2.3)

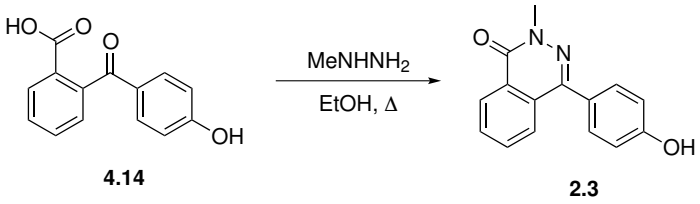

4.14 **2.3**

4.14 (2 g, 7.7 mmol, 1.0 equiv.) is dissolved in ethanol (10 ml). Methyl hydrazine (1.4 ml, 27 mmol, 3.5 equiv.) is added and the solution is refluxed for 5 h after which a yellow precipitate forms. The mixture is cooled and the formed solid is filtered, washed with cold ethanol and dried *in vacuo* to yield phthalazinone **2.3** as a white solid (837 mg, 3.3 mmol, 43 %).

Formula: $C_{15}H_{12}N_2O_2$;

Molar mass: 252.27 g/mol;

^{1}H-NMR (400 MHz, CD_3OD): δ (ppm) 9.82 (s(br), 1 H, −O*H*), 8.34 (m, 1 H, (O)C−C−C*H*), 7.87 (band, 2 H, (O)C−C−CH−C*H* + (O)C−C−CH−CH−C*H*), 7.72 (m, 1 H, (O)C−C−CH−CH−CH−C*H*), 7.41 (m(AB), 2 H, N=C−C−C*H*−CH−COH), 6.93 (m(AB), 2 H, C*H*−C−OH), 3.76 (s, 3 H, CH_3)),

^{13}C-NMR (100 MHz, CD_3OD): δ (ppm) 198.6 (C), 168.9 (C), 163.9 (C), 143.7 (C), 133.4 (CH), 133.3 (CH), 131.3 (CH), 131.0 (C), 130.5 (CH), 130.3 (CH), 128.6 (CH), 116.2 (CH),

HRMS [*m*/*z*]: [M+H]+ calcd. for $C_{15}H_{13}O_4^+$, 253.0972; found, 253.0980;

10.2.5. 4-(4-(Allyloxy)phenyl)-2-methylphthalazin-1(2*H*)-one (2.7)

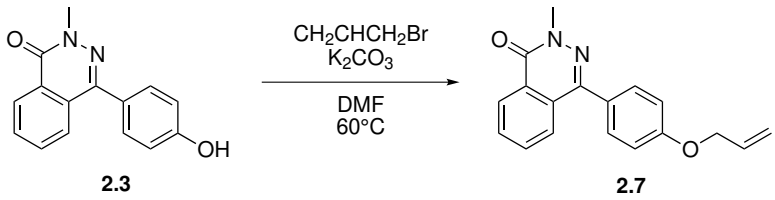

2.3 (0.5 g, 1.98 mmol) was dissolved in dry dimethylformamide (20 mL). Potassium carbonate (1.3 g, 9.9 mmol) was added and the mixture was stirred for 5 min at room temperature. Allyl bromide (850 µL, 9.9 mmol) was added and the reaction was heated to 60 °C until judged completed based on TLC. After cooling to room temperature, water (20 mL) was added and the aqueous phase was extracted with ethyl acetate (3 × 200 mL). The combined organic layers were washed with an aqueous sodium hydroxide-solution (15 %, 60 mL) and a saturated sodium chloride-solution (60 mL). The organic phase was dried on sodium sulfate, filtered and concentrated in vacuo. The resulting yellow solid was recrystallized from 2-propanol to yield **2.7** as an off-white crystalline solid (408.6 mg, 1.4 mmol, 71 %).

Formula: $C_{18}H_{16}N_2O_2$;

Molar mass: 292.34 g/mol;

^{1}H-NMR (400 MHz, $(CD_3)_2CO$): δ (ppm) 8.44–8.37 (m, 1 H, Ar−*H*), 7.90–7.82 (band, 2 H, Ar−*H*), 7.81–7.74 (m, 1 H, Ar−*H*), 7.59–7.54 (m, 2 H, NC−C=C*H*), 7.17–7.10 (m, 2 H, HO−C=C*H*), 6.13 (ddt, 1 H, J = 17.3, 10.5, 5.3 Hz, CH_2−C*H*=CH_2), 5.47 (ddt, 1 H, ^3J = 17.3, 1.5 Hz, ^4J = 1.5 Hz, C=C*H*H), 5.29 (ddt, 1 H, ^3J = 10.5, 1.5 Hz^4J = 1.5 Hz, C=CH*H*), 4.69 (dt, 2 H, ^3J = 5.3 Hz, ^4J = 1.5 Hz, O−CH_2), 3.80 (s, 3 H, CH_3),

^{13}C-NMR (100 MHz, $(CD_3)_2CO$): δ (ppm) 160.2 (C), 159.3 (C), 146.7 (C), 134.5 (CH), 133.6 (CH), 132.1 (CH), 131.7 (CH), 130.2 (C), 129.0 (C), 128.8 (C), 127.5 (CH), 127.4 (CH), 117.6 (CH_2), 115.5 (CH), 69.4 (CH_2), 39.4 (CH_3),

HRMS [*m*/*z*]: [M+H]+ calcd. for $C_{18}H_{17}N_2O_2^+$, 293.1285; found, 293.1292;

10.2.6. 4-(3-((2-Hydroxyethyl)thio)propyl)-N-(4-nitrophenyl)benzenesulfonamide (2.9)

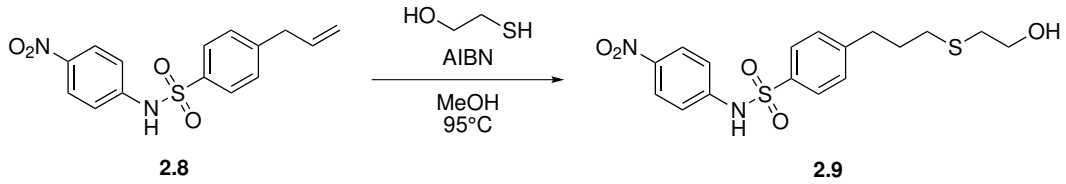

2.8 **2.9**

Sulfonamide **2.8** (100 mg, 314 µmol, 1.0 equiv.) is dissolved in methanol (2 ml) together with *N*,*N*′-azobisbutyronitrile (spatula tip) in a pressure tube. The reaction is heated to 95 °C and stirred. The reaction is monitored with TLC and *N*,*N*′-azobisbutyronitrile is added with 30 min intervals until complete conversion is observed. The crude mixture is concentrated *in vacuo*and the residue is purified with flash chromatography (silica, ethyl actetate/petroleum ether 5/5) to yield alcohol **2.9** as a yellow oil (68 mg, 59 %).

Formula: $C_{17}H_{20}N_2O_5S_2$;

Molar mass: 396.48 g/mol;

^{1}H-NMR (500 MHz, $(CD_3)_2CO$): δ (ppm) 8.18–8.02 (m, 2 H, $O_2N{-}C{=}CH$), 7.83–7.71 (m, 2 H, $O_2S{-}C{=}CH$), 7.31–7.27 (m, 2 H, $HN{-}C{=}CH$), 7.23–7.18 (m, 2 H, $CH_2{-}C{=}CH$), 3.66 (t, 2 H, $J = 5.9$ Hz, $CH_2{-}OH$), 2.74 (t, 2 H, $J = 7.5$ Hz, $Ar{-}CH_2$), 2.68 (t, 2 H, $J = 5.9$ Hz, $S{-}CH_2{-}CH_2OH$), 2.49 (t, 2 H, $J = 7.5$ Hz, $ArCH_2CH_2CH_2$), 1.88 (quint, 2 H, $J = 7.5$ Hz, $CH_2{-}CH_2{-}CH_2$),

^{13}C-NMR (125 MHz, $CDCl_3$): δ (ppm) 147.8 (C), 143.5 (C), 143.3 (C), 136.5 (C), 129.4 (CH), 127.3 (CH), 125.3 (CH), 118.2 (CH), 60.3 (CH_2), 35.0 (CH_2), 34.4 (CH_2), 30.9 (CH_2), 30.5 (CH_2).

HRMS [*m*/*z*]: [M-H]- calcd. for $C_{17}H_{19}N_2O_5S_2^-$, 395.0741; found, 395.0754

10.2.7. *N*-(2-mercaptoethyl)-5-((3a(*S*),4(*S*),6a(*R*))-2-oxohexahydro-1*H*-thieno[3,4-*d*]-imidazol-4-yl)pentanamide (2.10)

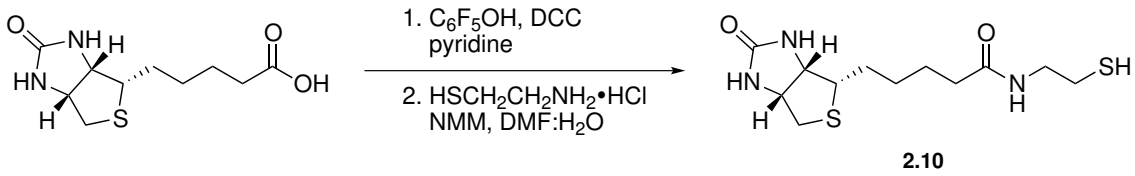

2.10

Biotin (1 g, 4.1 mmol) and pentafluorophenol (773 mg, 4.2 mmol) were dissolved in pyridine (45 mL). The clear solution was cooled to 0 °C upon which a solution of dicyclohexylcarbodiïmide (871 mg, 4.22 mmol) in pyridine (5 mL) was added and the mixture was allowed to heat to room temperature. After overnight stirring, the reaction mixture was filtered and the filtrate was concentrated *in vacuo*. The resulting white solid (1.6 g) was dissolved in a mixture of water and dimethylformamide (210 mL, 1:6 v/v) together with *N*-methylmorpholine (946 µL, 8.6 mL) and cysteamine hydrochloride (443 mg, 3.9 mmol). The resulting mixture was stirred overnight and subsequently concentrated *in vacuo*. The residue was purified by flash chromatography (silica, methanol:dichloromethane 1:7, v/v) to yield **2.10** as a white solid (571 mg, 2 mmol, 49 %) that showed a H-NMR spectrum as those reported in the literature.[147]

Formula $C_{12}H_{21}N_3O_2S_2$;
Molecular weight 303.44 g/mol;

10.2.8. 4-(4-(2-(4-Hydroxypiperidin-1-yl)-2-oxoethoxy)phenyl)-2-methylphthalazin-1-(2*H*)-one (2.11)

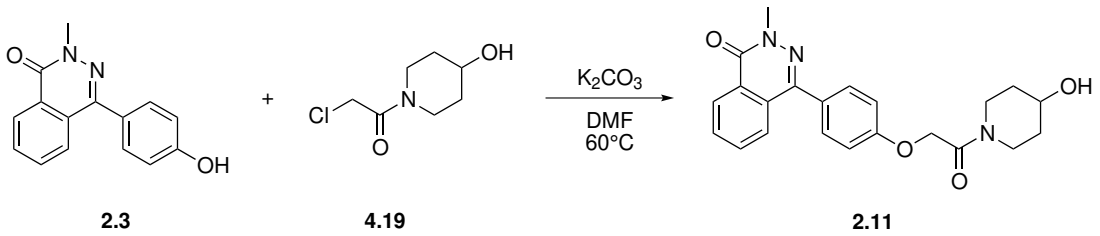

2.3 **4.19** **2.11**

Phthalazinone **2.3** (71 mg, 281 µmol, 1.0 equiv.) and alcohol **4.19** (100 mg, 563 µmol, 2.0 equiv.) are dissolved in dimethylformamide (3 ml). Once complete dissolution is reached, potassium carbonate (78 mg, 563 mmol, 2.0 equiv.) is added upon which the mixture is stirred for 5 min before heating to 60 °C. After 2.5 h, water (150 µl) is added to the reaction mixture. The potassium carbonate is removed by filtration and the filtrate is concentrated *in vacuo*yielding a yellow residue which is purified by flash chromatography (silica, ethyl acetate) to give alcohol **2.11** as a white solid (79.2 mg, 201 µmol, 72 %).

Formula: $C_{22}H_{23}N_3O_4$;

Molar mass: 393.44 g/mol;

^{1}H-NMR (400 MHz, $CDCl_3$): δ (ppm) 8.52 (d(br), 1 H, $J = 7.8$ Hz, Ar$-H$), 7.81–7.7 (band, 3 H, Ar$-H$), 7.6–7.5 (m, 2 H, Ar$-H$), 7.13–7.06 (m, 2 H, Ar$-H$), 4.78 (s, 2 H, O$-CH_2$), 4.05 (ddd, 1 H, $J = 12.8, 6.3, 4.4$ Hz, C$H-$OH), 3.98 (tt, 1 H, $J = 3.9, 3.9$ Hz,), 3.9 (s, 3 H, CH_3), 3.87 (ddd, 1 H, $J = 13.2, 6.0, 3.8$ Hz, piperidine$-H$), 3.34 (tdd, 2 H, $J = 14.0, 8.9, 3.7$ Hz, piperidine$-H$), 2.0–1.85 (m, 2 H, piperidine$-H$), 1.65–1.46 (m), 2 H, piperidine$-H$),

^{13}C-NMR (100 MHz, $CDCl_3$): δ (ppm) 166.0 (C), 159.4 (C), 158.7 (C), 146.5 (C), 132.7 (CH), 131.4 (CH), 129.3 (C), 128.7 (C), 128.1 (C), 127.0 (CH), 126.7 (CH), 114.8 (CH), 67.8 (CH_2), 66.8 (CH), 42.5 (CH_2), 39.5 (CH_2), 39.4 (CH_3), 34.5 (CH_2), 33.8 (CH_2),

HRMS [*m*/*z*]: [M+H]+ calcd. for $C_{22}H_{24}N_3O_4^+$, 394.1761; found, 394.1779;

10.2.9. *N*-(2-((3-((1-(2-(4-(3-methyl-4-oxo-3,4-dihydrophthalazin-1-yl)phenoxy)acetyl)-piperidin-4-yl)oxy)propyl)thio)ethyl)-5-((3a(*S*),4(*S*),6a(*R*))-2-oxohexahydro-1*H*-thieno[3,4-*d*]imidazol-4-yl)pentanamide (2.12)

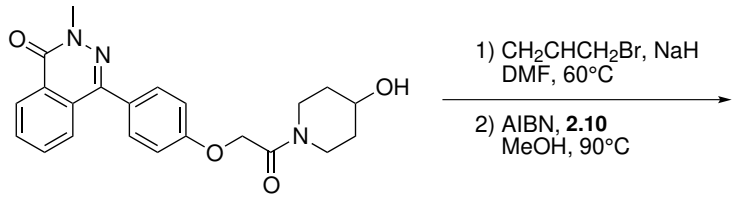

2.11

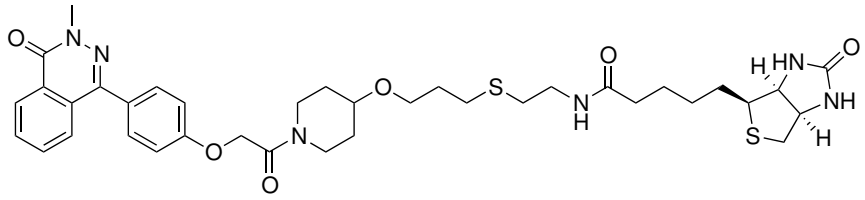

2.12

2.11 (50 mg, 130 µmol, 1.0 equiv.) was dissolved in dry dimethylformamide (500 µl). Sodium hydride (15 mg, 640 µmol, 5.0 equiv.) was added and the mixture was stirred for 30 min at room temperature. Allyl bromide (80 µl, 890 µmol, 7.0 equiv.) was then added and the mixture was heated to 60 °C. After 3 h, a saturated sodium bicarbonate–solution (3 ml) was added and the aqueous phase was extracted with ethyl acetate (3 × 20 ml). The combined organic phases were washed with a saturated sodium chloride–solution (6 ml), dried on sodium sulphate, filtered and concentrated *in vacuo*. A pressure tube was charged with part of the resulting residue (20 mg, 46 µmol), together with **2.10** (70 mg, 230 µmol, 5.0 equiv.) and methanol (100 µl). A catalytic amount of azobisisobutyronitrile was added. The reaction was heated to 90 °C and stirred until judged complete using TLC. The mixture was concentrated *in vacuo* and the residue was purified by preparative HPLC to yield to conjugate **2.12** as a white solid (9 mg, 130 µmol, 28 %)

Formula: $C_{37}H_{48}N_6O_6S_2$;

Molar mass: 736.95 g/mol;

^{1}H-NMR (400 MHz, $CDCl_3$): δ (ppm) 8.54–8.51 (m, 1 H, Ar*H*), 7.81–7.72 (band, 3 H, Ar*H*), 7.55–7.51 (m, 2 H, Ar*H*), 7.12–7.09 (m, 2 H, Ar*H*), 6.40–6.30 (m(br), 1 H, N*H*), 6.13–6.03 (m(br), 1 H, N*H*), 5.27–5.19 (m(br), 1 H, N*H*), 4.78 (s, 2 H, O–CH_2–CO), 4.50 (dd, 1 H, $J = 7.1, 5.1$ Hz, CH_2–C*H*–NHCO), 4.32 (dd, 1 H, $J = 7.1, 4.5$ Hz, C*H*–NHCO), 3.91 (s, 3 H, N–CH_3), 3.88–3.73 (band, 2 H), 3.64–3.36 (band, 7 H), 3.14 (dt(br), 1 H, $J = 7.2, 4.5$ Hz, CH_2CH_2–C*H*–S), 2.91 (dd, 1 H, $J = 13.0, 4.9$ Hz, S–C*H*H–CHNH(CO)), 2.72 (d(br), 1 H, $J = 13.0$ Hz, S–CH*H*–CHNH(CO)), 2.69–2.61 (band, 4 H), 2.22 (t(br), 2 H, S–CH_2–CH_2), 1.90–1.58 (band, 10 H), 1.50–1.40 (m, 2 H);

^{13}C-NMR (75 MHz, $CDCl_3$): δ (ppm) 173.1 (C), 166.1 (C), 159.4 (C), 158.7 (C), 146.6 (C), 132.7 (CH), 131.4 (CH), 130.9 (CH), 129.4 (C), 128.5 (C), 128.2 (C), 127.0 (CH), 126.7 (CH), 114.8 (CH), 73.6 (CH), 67.8 (CH), 66.3 (CH_2), 61.8 (CH), 60.1 (CH), 55.4 (CH), 50.8 (CH), 42.4 (CH_2), 40.6 (CH_2), 39.5 (CH_3), 39.4 (CH_2), 38.4 (CH_2), 35.9 (CH_2), 31.7 (CH_2), 30.5 (CH_2), 29.9 (CH_2), 28.4 (CH_2), 28.1 (CH_2), 25.5 (CH_2),

10.3. Reactions from chapter 3

10.3.1. *N*-(4-acetylphenyl)-5-bromothiophene-2-sulfonamide (3.3)

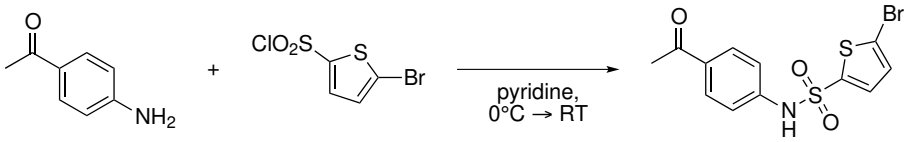

3.3

Procedure (see section 10.2.2): with 1-(4-aminophenyl)ethanone (554 mg, 4.1 mmol, 1.1 equiv.) and 5-bromothiophene-2-sulfonyl chloride (1.0 g, 3.8 mmol, 1.0 equiv.) in pyridine (8 ml) giving **3.3** (1.026 g, 2.85 mmol, 75 %).

Formula: $C_{12}H_{10}BrNO_3S_2$;

Molar mass: 360.25 g/mol;

^{1}H-NMR (400 MHz, $(CD_3)_2CO$): δ (ppm) 8.00–7.91 (m, 2 H, Acyl−C=C*H*), 7.49 (d, 1 H, J = 4.0 Hz, O_2SC=C*H*), 7.44–7.37 (m, 2 H, HNC=C*H*), 7.23 (d, 4.0 H, BrC=C*H*), 2.53 (s, 3 H, CH_3),

^{13}C-NMR (125 MHz, $(CD_3)_2CO$): δ (ppm) 196.6 (C), 142.3 (C), 142.1 (C), 134.5 (C), 134.4 (CH), 132.1 (CH), 130.7 (CH), 120.4 (C), 120.0 (CH), 26.5 (CH_3),

10.3.2. 5-Bromo-*N*-methyl-*N*-(4-nitrophenyl)thiophene-2-sulfonamide (3.4)

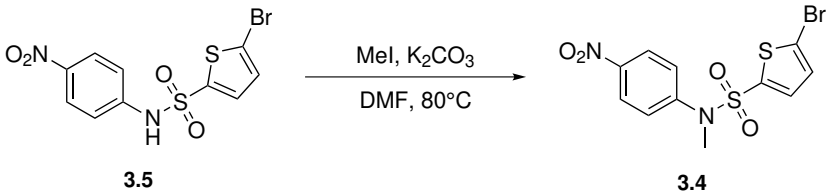

3.5 **3.4**

Endosidin 9 (**3.5**) (100 mg, 275 µmol, 1.0 equiv.) is dissolved in dimethylformamide (700 µL). Potassium carbonate (76 mg, 550 µmol, 2.0 equiv.) is added and the mixture is stirred for 5 min. Methyl iodide (34 µL, 550 µmol, 2.0 equiv.) is added and the reaction is heated to 80 °C and stirred for 1 h. The reaction mixture is cooled down and diluted with ethyl acetate (20 mL) and the organic phase is washed with water (10 mL) and a saturated sodium chloride-solution (7 mL). The organic phase is dried on sodium sulphate, filtered and concentrated in vacuo to yield a yellow solid which is recrystallized from 2-propanol to yield **3.4** as a yellow crystalline solid (100 mg, 95 %).

Formula: $C_{11}H_9BrN_2O_4S_2$;

Molar mass: 377.23 g/mol;

^{1}H-NMR (500 MHz, $(CD_3)_2CO$): δ (ppm) 8.29–8.24 (m, 2 H, $O_2N-C=CH$), 7.62–7.57 (m, 2 H, $MeN-C=CH$), 7.35–7.31 (band, 2 H, Thiophene$-H$), 3.38 (s, 3 H, CH_3),
^{13}C-NMR (125 MHz, $(CD_3)_2CO$): δ (ppm) 147.7 (C), 147.1 (C), 138.0 (C), 134.9 (CH), 132.5 (CH), 127.4 (CH), 125.1 (CH), 121.0 (C), 38.2 (CH_3),
HRMS [*m*/*z*]: [M+OAc]- calcd. For $C_{11}H_8BrN_2O_4S_2^-$, 434.9325; found, 434.9319;

10.3.3. 2-((3-(4-(*N*-(4-nitrophenyl)sulfamoyl)phenyl)propyl)thio)ethyl 5-((3a(*S*),4(*S*),6a(*R*))-2-oxohexahydro-1*H*-thieno[3,4-*d*]imidazol-4-yl)-pentanoate (3.6)

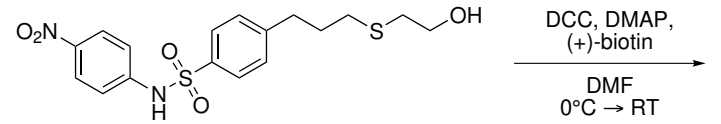

2.9

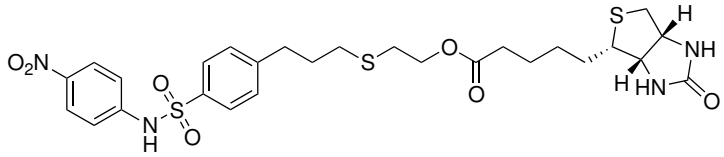

3.6

Alcohol **2.9** (53.2 mg, 144 µmol, 1.5 equiv.) is dissolved in dimethylformamide (0.5 ml) together with biotin (23.5 mg, 96 µmol, 1.0 equiv.) and 4-dimethylaminopyridine (2 mg, 13 µmol, 0.09 equiv.). The mixture is then stirred until complete dissolution and cooled down to 0 °C. *N*,*N*′-dicyclohexylcarbodiimide (23.8 mg, 145 µmol, 1.2 equiv.) is added and the mixture is stirred at the same temperature for another 5 min. After heating the reaction to room temperature it is stirred until judged complete by TLC (3 h). The mixture is concentrated *in vacuo* and purified with flash chromatography (silica, methanol/chloroform 6/94 to 20/80) to yield 63 mg (74 %) of biotin derivative **3.6**.

Formula: $C_{27}H_{34}N_4O_7S_3$;

Molar mass: 622.78 g/mol;

^{1}H-NMR (300 MHz, $CDCl_3$): δ (ppm) 10.88 (s(br), 1 H, N*H*), 8.10–8.02 (m, 2 H, O_2N−C=C*H*), 7.90–7.81 (m, 2 H, O_2S−C=C*H*), 7.39–7.27 (band, 4 H, NH−C=C*H* + CH_2−C=C*H*), 5.90 (s(br), 1 H, HN−C(O)−N*H*), 5.12 (s(br), 1 H, *H*N−C(O)−NH), 4.63 (dd(br), 1 H, J = 7.6, 5.5 Hz, CHNH(CO)NH−C*H*), 4.42 (ddd(br), 1 H, J = 7.5, 5.2, 1.1 Hz, *H*−NH−(CO)−NHCH), 4.18 (t, 2 H, J = 6.4 Hz, C(O)O−CH_2), 3.21 (ddd(br), 1 H, J = 9.2, 5.6, 4.9 Hz, C(O)−NH−CH−C*H*−S), 2.97 (dd, 1 H, J = 13.0, 4.9 Hz, C(O)−NH−CH−C*H*H−S), 2.75 (t, 2 H, J = 6.5 Hz, SCH_2−CH_2−O), 2.74 (d, 1 H, J = 12.2 Hz, C(O)−NH−CH−CH*H*−S), 2.66 (t, 2 H, J = 6.5 Hz, SCH_2−CH_2−O), 2.49 (t, 2 H, J = 7.3 Hz, Ar−CH_2), 2.19 (t, 2 H, J = 7.3 Hz, ArCH_2CH_2CH_2), 1.94 (quint, 2 H, J = 7.3 Hz, ArCH_2CH_2CH_2), 1.77–1.34 (band, 6) H),

^{13}C-NMR (125 MHz, $CDCl_3$): δ (ppm) 173.1 (C), 163.8 (C), 147.5 (C), 144.1 (C), 143.3 (CH), 136.8 (CH), 129.5 (CH), 127.4 (CH), 125.2 (CH_2), 118.1 (CH_2), 64.1 (CH), 62.3 (CH), 60.3 (CH_2), 55.7 (CH_2), 40.6 (CH), 34.1 (CH), 33.6 (CH_2), 31.1 (CH_2), 30.5 (CH), 30.3 (CH), 28.4 (CH_2), 28.3 (CH_2), 24.8 (CH_2),

HRMS [*m*/*z*]: [M-H]- calcd. for $C_{27}H_{33}N_4O_7S_3^-$, 621.1517; found, 621.1512

10.3.4. 2-(hexylthio)ethanol (3.8)

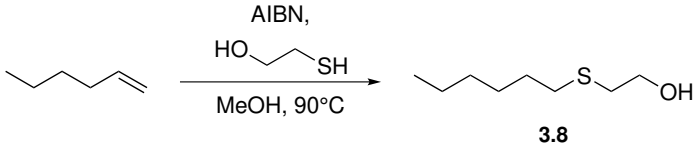

3.8

1-Hexene (742 µL, 5.94 mmol, 1.0 equiv.) and 2-mercaptoethanol (414 µL, 59.4 mmol, 10.0 equiv.) are dissolved in methanol (2 mmol) together with *N*,*N*′-azobisisobutyronitrile (72 mg, 439 µmol, 0.08 equiv.). The mixture is heated to 95 °C and stirred for 1.5 h. After concentration *invacuo* the residue is purified by flash chromatography (silica, ethyl acetate:petroleum ether, 2:3 v/v) to yield thioether **3.8** quantitatively as a colourless oil.

Formula: $C_8H_{18}OS$;

Molar mass: 162.29 g/mol;

^{1}H-NMR (500 MHz, $CDCl_3$): δ (ppm) 3.71 (t, 2 H, J = 5.9 Hz, CH_2–OH), 2.73 (t, 2 H, J = 5.9 Hz, S–CH_2–CH_2OH), 2.52 (t, 2 H, J = 7.4 Hz, S–CH_2–CH_2CH_2), 2.04 (s(br), 1 H, O*H*), 1.58 (quint, 2 H, J = 7.4 Hz, SCH_2–CH_2), 1.38 (quint, 2 H, J = 7.4 Hz, SCH_2CH_2 –CH_2), 1.34–1.23 (band, 4 H, CH_2–CH_2–CH_2–CH_3), 0.89 (t, 3 H, J = 7.0 Hz, CH_3),

^{13}C-NMR (125 MHz, $CDCl_3$): δ (ppm) 60.3 (CH_2), 35.5 (CH_2), 31.8 (CH_2), 31.6 (CH_2), 29.9 (CH_2), 28.7 (CH_2), 22.7 (CH_2), 14.2 (CH_3)

10.3.5. 2-(Hexylthio)ethyl 5-((3a(*S*),4(*S*),6a(*R*))-2-oxohexahydro-1*H*-thieno[3,4-*d*]-imidazol-4-yl)pentanoate (3.7)

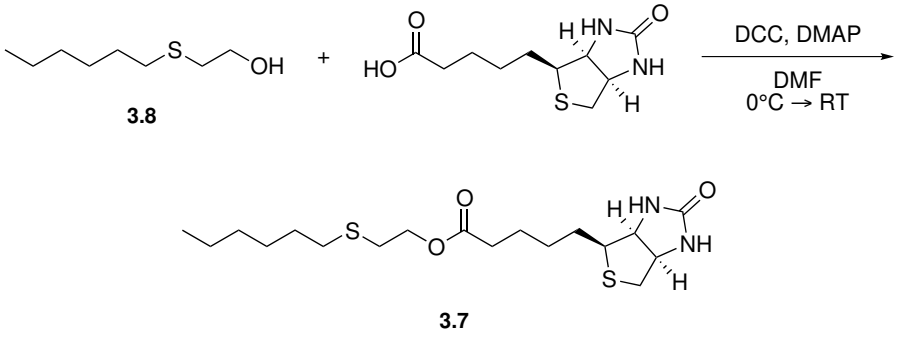

Thioether **3.8** (300 mg, 1.85 mmol, 1.0 equiv.) is dissolved in dimethylformamide (4 mL) together with biotin (452 mg, 1.85 mmol, 1.0 equiv.) and 4-dimethylaminopyridine (20 mg, 165 µmol, 0.09 equiv.). The mixture is then stirred until complete dissolution and cooled down to 0 °C. A solution of *N*,*N*′-dicyclohexylcarbodiimide (458 mg, 2.22 mmol, 1.2 equiv.) in dimethylformamide (2 mL) is added and the mixture is stirred at the same temperature for 1 h, after which it is heated to room temperature and stirred overnight. The mixture is concentrated *in vacuo* and purified with flash chromatography (silica, methanol:chloroform, 1:9 v/v) to yield **3.7** as a white waxy solid (62.9 mg, 9 %).

Formula: $C_{18}H_{32}N_2O_3S_2$;

Molar mass: 388.59 g/mol;

^{1}H-NMR (300 MHz, $CDCl_3$): δ (ppm) 5.58 (s(br), 1 H, N*H*(CO)NH), 5.13 (s(br), 1 H, NH(CO)N*H*), 4.51 (dd(br), 1 H, $J = 7.8, 4.9$ Hz, CHNH(CO)NH−C*H*), 4.32 (dd, 1 H, $J = 7.7, 4.6$ Hz, *H*−NH(CO)NHCH), 4.20 (t, 2 H, $J = 6.9$ Hz, C(O)O−CH_2), 3.16 (ddd(br), 1 H, $J = 8.5, 6.6, 5.0$ Hz, C(O)−NH−CH−C*H*−S), 2.92 (dd, 1 H, $J = 12.9, 5.0$ Hz, C(O)−NH−CH−C*H*H−S), 2.78–2.69 (band, 3 H, C(O)−NH−CH−CH*H*−S + O−CH_2), 2.55 (t, 2 H, $J = 7.3$ Hz, OCH$_2$−CH_2), 2.35 (t, 2 H, $J = 7.3$ Hz, OCH$_2$CH$_2$S−CH_2), 1.76–1.62 (band, 4 H, CH_2), 1.58 (quint, 2 H, $J = 7.5$ Hz, CH_2), 1.51–1.22 (band, 8 H, CH_2), 0.89 (t, 3 H, $J = 6.7$ Hz, *CH*$_3$),

^{13}C-NMR (125 MHz, $CDCl_3$): δ (ppm) 173.5 (C), 163.4 (C), 63.5 (CH_2), 62.1 (CH), 60.2 (CH), 55.5 (CH), 40.7 (CH_2), 33.9 (CH_2), 32.5 (CH_2), 31.6 (CH_2), 30.7 (CH_2), 29.8 (CH_2), 28.7 (CH_2), 28.5 (CH_2), 28.4 (CH_2), 24.9 (CH_2), 22.7 (CH_2), 14.2 (CH_3),

HRMS [*m*/*z*]: [M+H]+ calcd. for $C_{18}H_{33}N_2O_3S_2^+$, 389.1927; found, 389.1933

10.3.6. 5-Bromo-*N*-(3-nitrophenyl)thiophene-2-sulfonamide (3.9)

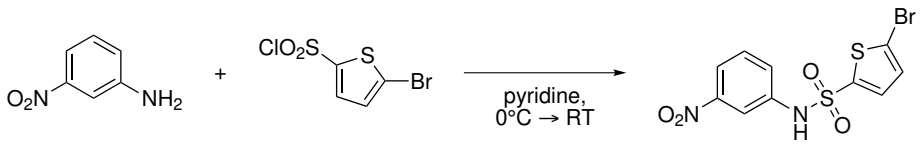

3.9

Procedure (see section 10.2.2): with 3-nitroaniline (1 g, 7.2 mmol, 1.08 equiv.) and 5-bromothiophene-2-sulfonyl chloride (1.75 g, 6.7 mmol, 1.0 equiv.) in pyridine (13 ml) giving **3.9** (1.79 g, 4.9 mmol, 73 %).

Formula: $C_{10}H_8BrNO_2S_2$;

Molar mass: 363.20 g/mol;

^{1}H-NMR (400 MHz, $(CD_3)_2CO$): δ (ppm) 9.80 (s(br), 1 H, N*H*), 8.18 (t(br), 1 H, $J = 2.1$ Hz, $NO_2C{=}CH{-}CH$), 8.03 (ddd, 1 H, $J = 8.0$ Hz, $^4J = 2.1, 1.0$ Hz, $NO_2C{=}CH{-}CNH$), 7.72 (ddd(AB), 1 H, $J = 8.0$ Hz, $^4J = 2.1, 1.0$ Hz, $NHC{=}CH{-}CH$), 7.65 (t(AB), 1 H, $J = 8.0$ Hz, $CH{=}CH{-}CH$), 7.48 (d, 1 H, $J = 4.1$ Hz, $SO_2C{=}CH$), 7.24 (d, 1 H, $J = 4.1$ Hz, $BrC{=}CH$),

^{13}C-NMR (125 MHz, $(CD_3)_2CO$): δ (ppm) 149.8 (C), 141.5 (C), 139.5 (C), 134.6 (CH), 132.3 (CH), 131.7 (CH), 127.3 (CH), 120.8 (C), 120.5 (CH), 115.8 (CH),

ESI-MS [*m*/*z*]: 362.9 ([M-H]-; 100 %)

10.3.7. 4-Bromo-*N*-(4-hydroxyphenyl)benzenesulfonamide (3.10)

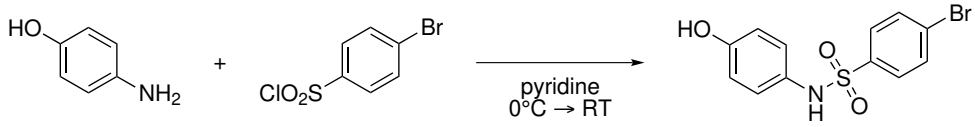

3.10

Procedure (see section 10.2.2): with 4-aminophenol (230 mg, 2.11 mmol, 1.08 equiv.) and 4-bromobenzene-1-sulfonyl chloride (0.5 g, 1.95 mmol, 1.0 equiv.) in pyridine (4 ml) giving **3.10** (359 g, 1.15 mmol, 59 %).

Formula: $C_{11}H_9BrN_2O_2S$;

Molar mass: 313.17 g/mol;

^{1}H-NMR (300 MHz, $(CD_3)_2CO$): δ (ppm) 8.63 (s(br), 1 H, N*H*), 8.34 (s, 1 H, O*H*), 7.73–7.69 (m, 2 H, $O_2SC{=}CH$), 7.63–7.59 (m, 2 H,), 7.00–6.96 (m, 2 H, $HN{-}C{=}CH$), 6.74–6.71 (m, 2) H, $HO{-}C{=}CH$),

^{13}C-NMR (125 MHz, $(CD_3)_2CO$): δ (ppm) 156.5 (C), 140.2 (C), 133.0 (CH), 129.9 (CH), 129.6 (C), 127.6 (C), 126.0 (CH), 116.5 (CH),

HRMS [*m*/*z*]: [M-H]- calcd. for $C_{11}H_8BrN_2O_2S^-$, 325.9492; found, 325.9499;

10.3.8. 4-Bromo-*N*-(pyridin-4-yl)benzenesulfonamide (3.11)

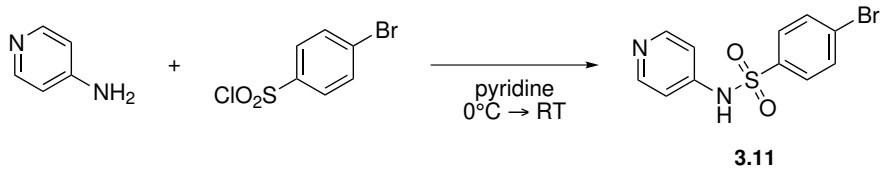

3.11

pyridin-4-amine (199 mg, 2.11 mmol, 1.08 equiv.) is first dissolved in anhydrous pyridine (4 ml). The mixture is cooled to 0°C, and 4-bromobenzene-1-sulfonyl chloride (0.5 g, 1.95 mmol, 1.0 equiv.) is added portionwise over a period of a few minutes. The reaction is then stirred without cooling (at room temperature) for 17 h. After concentration *in vacuo* of the reaction mixture, the residue is taken up in ethyl acetate (25 ml). The organic phase is extracted with small portions of a sodium hydroxide-solution (15 %, 5 ml) to extract acidic material. The combined aqueous phases are finally acidified with hydrochloric acid (6 M), until precipitation occurs. After filtration, the solid is washed with water and dried to give **3.10** (244 g, 1.15 mmol, 40 %).

Formula: $C_{11}H_9BrN_2O_2S$;

Molar mass: 313.17 g/mol;

^{1}H-NMR (300 MHz, $(CD_3)_2SO$): δ (ppm) 12.63 (s(br), 1 H, N*H*), 7.99 (m, 2 H, N=C*H*), 7.74–7.67 (band, 4 H, BrAr−*H*), 6.90 (m, 2 H, HNC=C*H*),

^{13}C-NMR (125 MHz, $(CD_3)_2SO$): δ (ppm) 143.0 (C), 139.5 (C), 131.7 (CH), 128.1 (CH), 124.8 (C), 114.8 (CH), 79.1 (CH),

HRMS [*m*/*z*]: [M+H]+ calcd. for $C_{11}H_{10}BrN_2O_2S^+$, 312.9641; found, 312.9467;

10.3.9. 5-Bromo-*N*-(4-butylphenyl)thiophene-2-sulfonamide (3.12)

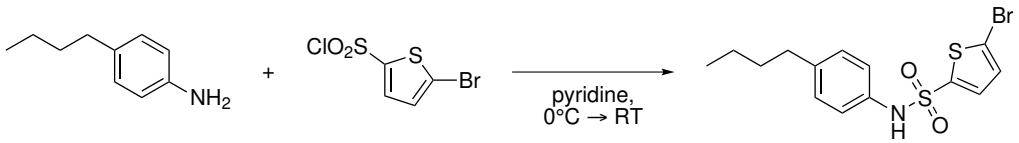

3.12

Procedure (see section 10.2.2): with 4-*n*-butyl aniline (670 µl, 4.2 mmol, 1.08 equiv.) and 5-bromothiophene-2-sulfonyl chloride (1.0 g, 3.9 mmol, 1.0 equiv.) in pyridine (8 ml) giving **3.18** (617 mg, 1.65 mmol, 42 %).

Formula: $C_{14}H_{16}BrNO_2S_2$;

Molar mass: 374.32 g/mol;

^{1}H-NMR (400 MHz, $(CD_3)_2CO$): δ (ppm) 7.19 (d, 1 H, J = 3.9 Hz, $O_2SC{=}CH$), 7.14–7.08 (m, 2 H, $HNC{=}CH$), 7.05–7.00 (m, 2 H, $H_2CC{=}CH$), 6.97 (d, 1 H, J = 3.9 Hz, $BrC{=}CH$), 2.57 (t, 2 H, J = 7.6 Hz, $Ar{-}CH_2$), 1.55 (quint, 2 H, J = 7.6 Hz, $Ar{-}CH_2{-}CH_2$), 1.32 (sext, 2 H, J = 7.6 Hz, $Ar{-}CH_2{-}CH_2{-}CH_2$), 0.91 (t, 3 H, J = 7.6 Hz, $Ar{-}CH_2{-}CH_2{-}CH_2{-}CH_3$),

^{13}C-NMR (125 MHz, $(CD_3)_2CO$): δ (ppm) 142.5 (C), 141.0 (C), 135.6 (C), 133.6 (CH), 131.8 (CH), 130.0 (CH), 122.8 (CH), 119.0 (C), 35.5 (CH_2), 34.4 (CH_2), 22.9 (CH_2), 14.2 (CH_3),

10.3.10. 4-Methyl-*N*-phenylbenzenesulfonamide (3.14)

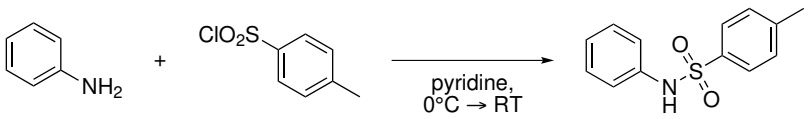

3.14

Procedure (see section 10.2.2): with aniline (0.5 ml, 5.5 mmol, 1.1 equiv.) and 4-methylbenzene-1-sulfonyl chloride (953 mg, 5.0 mmol, 1.0 equiv.) in pyridine (10 ml) giving **3.14** (724 mg, 2.93 mmol, 59 %).

Formula: $C_{13}H_{13}NO_2S$;

Molar mass: 247.31 g/mol;

^{1}H-NMR (400 MHz, $(CD_3)_2CO$): δ (ppm) 8.91 (s(br), 1 H, N*H*), 7.70–7.64 (m, 2 H, O_2SC=C*H*), 7.34–7.28 (m, 2 H, H_3CC=C*H*), 7.27–7.18 (band, 4 H, HNC=C*H* + HNC=CH−C*H*), 7.06 (tt, 1 H, $J = 6.8$ Hz, $^4J = 1.7$ Hz, HNC=CH−CH=C*H*), 2.36 (s, 3 H, CH_3),

^{13}C-NMR (125 MHz, $(CD_3)_2CO$): δ (ppm) 144.4 (C), 138.9 (C), 138.1 (C), 130.4 (CH), 130.0 (CH), 128.0 (CH), 125.2 (CH), 121.5 (CH), 21.3 (CH_3),

10.3.11. *N*-phenylbenzenesulfonamide (3.15)

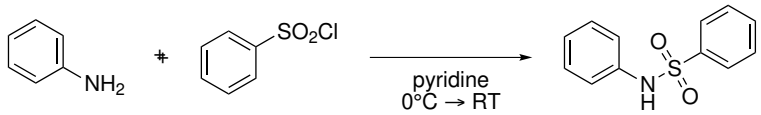

3.15

Procedure (see section 10.2.2): with aniline (0.5 ml, 5.5 mmol, 1.1 equiv.) and benzenesulfonyl chloride (1.13 g, 5.0 mmol, 1.0 equiv.) in pyridine (10 ml) giving the commercially available **3.15** (677 mg, 2.90 mmol, 58 %).

Formula: $C_{12}H_{11}NO_2S$;

Molar mass: 233.29 g/mol;

10.3.12. 5-bromo-*N*-phenylthiophene-2-sulfonamide (3.16)

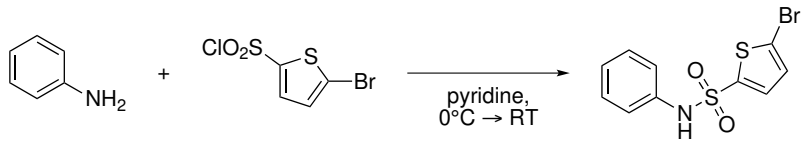

3.16

Procedure (see section 10.2.2): with aniline (193 µl, 2.13 mmol, 1.08 equiv.) and (0.5 g, 1.95 mmol, 1.0 equiv.) in pyridine (4 ml) giving **3.16** (542 mg, 1.6 mmol, 83 %).

Formula: $C_{10}H_8BrNO_2S_2$;

Molar mass: 318.20 g/mol;

^{1}H-NMR (500 MHz, $(CD_3)_2CO$): δ (ppm) 9.21 (s(br), 1 H, N*H*), 7.36–7.30 (band, 3 H), 7.30–7.25 (m, 2 H), 7.20 (d, 2 H, $J = 4.0$ Hz, $O_2S{-}C{=}CH$), 7.19–7.14 (m, 1 H),

^{13}C-NMR (125 MHz, $(CD_3)_2CO$): δ (ppm) 142.4, 138.1, 133.8, 131.9, 130.2, 126.2, 122.3, 119.8,

HRMS [*m*/*z*]: [M-H]- calc'd for $C_{10}H_7BrNO_2S_2^-$, 315.9107; found, 315.9116;

10.3.13. 2-Nitro-*N*-phenylbenzenesulfonamide (3.17)

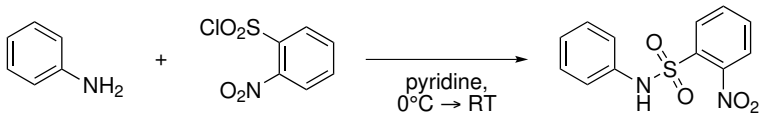

3.17

Procedure (see section 10.2.2): with aniline (0.5 ml, 5.5 mmol, 1.1 equiv.) and 2-nitrobenzene-1-sulfonyl chloride (1.1 g, 5.0 mmol, 1.0 equiv.) in pyridine (10 ml) giving **3.17** (693 mg, 2.5 mmol, 50 %).

Formula: $C_{12}H_{10}N_2O_4S$;

Molar mass: 278.28 g/mol;

^{1}H-NMR (400 MHz, $(CD_3)_2CO$): δ (ppm) 9.03 (s(br), 1 H, N*H*), 8.00–7.93 (band, 2 H, O_2SC=C*H* + O_2NC=C*H*), 7.87 (td, 1 H, $J = 7.7$ Hz, $^4J = 1.5$ Hz, O_2NC=CH−C*H*), 7.77 (td, 1 H, $J = 7.7$ Hz, $^4J = 1.5$ Hz, O_2SC=CH−C*H*), 7.34–7.25 (band, 4 H, HNC=C*H* + HNC=CH−C*H*), 7.20–7.11 (m, 1 H, HNC=CH−CH=C*H*),

^{13}C-NMR (125 MHz, $(CD_3)_2CO$): δ (ppm) 149.4 (C), 137.5 (C), 135.4 (CH), 133.2 (CH), 132.7 (C), 132.0 (CH), 130.2 (CH), 126.4 (CH), 125.8 (CH), 122.9 (CH),

10.3.14. *N*-phenylnaphthalene-1-sulfonamide (3.18)

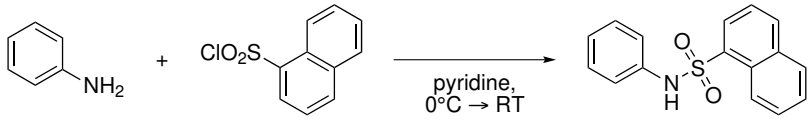

3.18

Procedure (see section 10.2.2): with aniline (0.5 ml, 5.5 mmol, 1.1 equiv.) and naphthalene-1-sulfonyl chloride (1.13 g, 5.0 mmol, 1.0 equiv.) in pyridine (10 ml) giving **3.18** (940 mg, 3.3 mmol, 66 %).

Formula: $C_{16}H_{13}NO_2S$;

Molar mass: 283.35 g/mol;

^{1}H-NMR (400 MHz, $(CD_3)_2CO$): δ (ppm) 9.35 (s(br), 1 H, N*H*), 8.82 (d, 1 H, $J = 8.5$ Hz, Napth−CH_8), 8.26 (dd, 1 H, $J = 8.0$ Hz, $^4J = 0.9$ Hz, Napth−CH_2), 8.16 (d(br), 1 H, $J = 8.0$ Hz, Napth−CH_4), 8.03 (d(br), 1 H, $J = 8.1$ Hz, Napth−CH_5), 7.70 (tm, 1 H, $J = 8.5$ Hz, Napth−CH_7), 7.64 (tm, 1 H, $J = 8.1$ Hz, Napth−CH_6), 7.58 (t(br), 1 H, $J = 8.0$ Hz, Napth−CH_3), 7.18–7.08 (band, 4 H, HNC=C*H* + HNC=CH−C*H*), 7.00–6.92 (m, 1 H, HNC=CH−CH=C*H*),

^{13}C-NMR (125 MHz, $(CD_3)_2CO$): δ (ppm) 138.6 (C), 135.8 (C), 135.3 (CH), 135.2 (C), 131.1 (CH), 130.0 (CH), 129.9 (CH), 128.9 (C), 127.8 (CH), 125.5 (CH), 125.1 (CH), 125.0 (CH), 121.0 (CH),

10.3.15. 2,4,6-Triisopropyl-*N*-phenylbenzenesulfonamide (3.19)

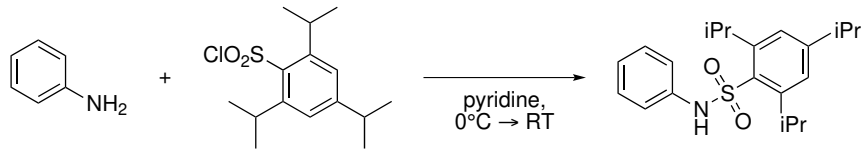

3.19

Procedure (see section 10.2.2): with aniline (0.5 ml, 5.5 mmol, 1.1 equiv.) and 2,4,6-triisopropylbenzene-1-sulfonyl chloride (1.5 g, 5.0 mmol, 1.0 equiv.) in pyridine (10 ml) giving **3.19** (803 mg, 2.23 mmol, 45 %).

Formula: $C_{21}H_{29}NO_2S$;

Molar mass: 359.53 g/mol;

^{1}H-NMR (400 MHz, $(CD_3)_2CO$): δ (ppm) 7.30–7.22 (band, 4 H, CH=C*H*−CH + iPrC=C*H*), 7.20–7.15 (dm, 2 H, J = 7.3 Hz, NHC=C*H*), 7.07 (tm, 1 H, J = 7.3 Hz, HNC=CH−CH =C*H*), 4.23 (sept, 2 H, J = 6.8 Hz, O_2SC=C−C*H*$(CH_3)_2$), 2.92 (sept, 1 H, CH=C−C*H*$(CH_3)_2$), 1.22 (d, 6 H, CH=C−CH(C*H*$_3)_2$), 1.17 (d, 12 H, O_2SC=C −CH(C*H*$_3)_2$),

^{13}C-NMR (125 MHz, $(CD_3)_2CO$): δ (ppm) 153.6 (C), 151.4 (C), 138.6 (C), 134.3 (C), 130.0 (CH), 125.4 (CH), 124.8 (CH), 122.3 (CH), 34.7 (CH), 30.3 (CH), 25.0 (CH_3), 23.8 (CH_3),

10.3.16. 2,4-Dichloro-*N*-phenylbenzenesulfonamide (3.20)

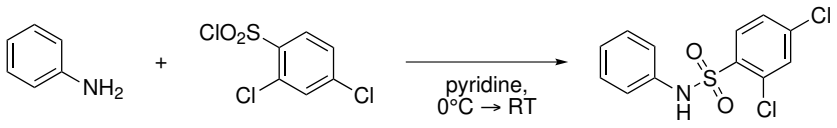

3.20

Procedure (see section 10.2.2): with aniline (350 µl, 3.85 mmol, 1.1 equiv.) and 2,4-dichlorobenzene-1-sulfonyl chloride (855 mg, 3.5 mmol, 1.0 equiv.) in pyridine (7 ml) giving **3.20** (607 mg, 2.0 mmol, 57 %).

Formula: $C_{12}H_9Cl_2NO_2S$;

Molar mass: 302.18 g/mol;

^{1}H-NMR (400 MHz, $(CD_3)_2CO$): δ (ppm) 9.36 (s(br), 1 H, N*H*), 8.06 (d, 1 H, J = 8.6 Hz, $O_2SC{=}CH$), 7.68 (d(br), 1 H, ^4J = 1.9 Hz, ClC=C*H*−CCl), 7.53 (dd(br), 1 H, J = 8.6 Hz, ^4J = 1.9 Hz, ClC=C*H*−CH), 7.30–7.20 (band, 4 H, HNC=C*H* + HNC=CH−C*H*), 7.06 (sept(br), 1 H, J = 4.7 Hz, HNC=CH−CH=C*H*),

^{13}C-NMR (125 MHz, $(CD_3)_2CO$): δ (ppm) 140.1 (C), 137.7 (C), 136.7 (C), 134.1 (CH), 133.4 (C), 132.2 (CH), 130.1 (CH), 128.5 (CH), 125.7 (CH), 121.3 (CH),

10.3.17. 4-Nitro-*N*-phenylbenzenesulfonamide (3.21)

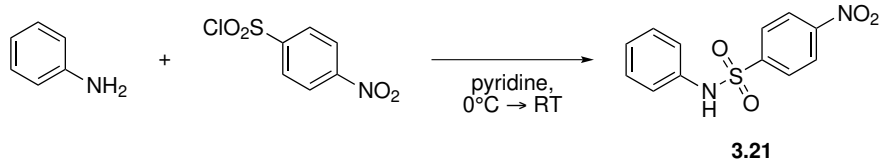

3.21

Procedure (see section 10.2.2): with aniline (0.5 ml, 5.5 mmol, 1.1 equiv.) and 4-nitrobenzene-1-sulfonyl chloride (1.1 g, 5.0 mmol, 1.0 equiv.) in pyridine (10 ml) giving **3.21** (948 mg, 3.5 mmol, 70 %).

Formula: $C_{12}H_{10}N_2O_4S_2$;

Molar mass: 278.28 g/mol;

^{1}H-NMR (400 MHz, $(CD_3)_2CO$): δ (ppm) 8.40–8.34 (m, 2 H, $NO_2C{=}CH$), 8.07–8.00 (m, 2 H, $SO_2C{=}CH$*H*), 7.13 (tt, 1 H, J = 7.3 Hz, ^4J = 1.3 Hz, NHCCH=CH−CH*H*), 7.28 (tm, 2 H, J = 7.3 Hz, CH=C*H*−CH), 7.25 (m, 2 H, NHC=C*H*),

^{13}C-NMR (125 MHz, $(CD_3)_2CO$): δ (ppm) 151.2 (C), 146.3 (C), 137.9 (C), 130.2 (CH), 129.5 (CH), 126.2 (CH), 125.2 (CH), 122.4 (CH),

10.3.18. *N*-phenylmethanesulfonamide (3.22)

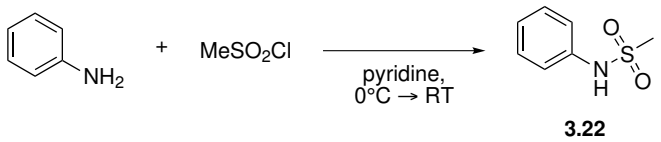

3.22

Procedure (see section 10.2.2): with aniline (0.5 ml, 5.5 mmol, 1.1 equiv.) and methanesulfonyl chloride (390 µl, 5.0 mmol, 1.0 equiv.) in pyridine (10 ml) giving **3.22** (407 mg, 2.38 mmol, 48 %).

Formula: $C_7H_9NO_2S$;

Molar mass: 171.22 g/mol;

^{1}H-NMR (400 MHz, $(CD_3)_2CO$): δ (ppm) 8.53 (s(br), 1 H, N*H*), 7.40–7.30 (band, 4 H, Ar$-H_{ortho,meta}$), 7.20–7.10 (m, 1 H, Ar$-H_{para}$), 2.97 (s, 3 H, CH_3),

^{13}C-NMR (125 MHz, $(CD_3)_2CO$): δ (ppm) 139.5 (C), 130.2 (CH), 125.2 (CH), 121.1 (CH), 39.3 (CH_3),

10.4. Reactions from chapter 4

10.4.1. 2-(4-Hydroxybenzoyl)benzoic acid (4.14)

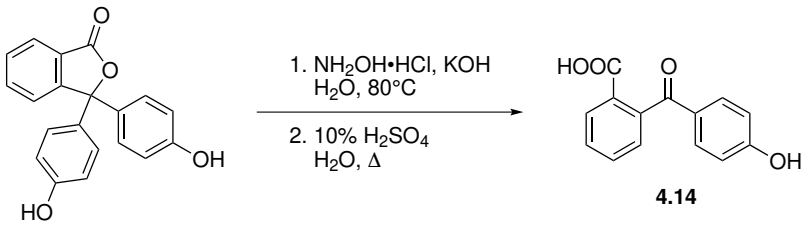

4.14

Phenolphthalein (7 g, 22 mmol, 1.0 equiv.) was dissolved in an aqueous potassium hydroxide–solution (70 ml, 2 mM). Hydroxylamine hydrochloride (1.7 g, 24 mmol, 1.09 equiv.) was added to the purple solution and the mixture was heated to 80 °C. Consumption of phenolphthalein was checked by taking a sample from the reaction mixture which was acidified with acetic acid, until a yellow precipitate was formed. The solid was filtered and potassium hydroxide was added to the filtrate. A colour change to purple indicated the presence of unreacted phenolphthalein. After 1 h the reaction was finished as the test no longer showed colour change. The reaction was cooled to room temperature and ethanol (14 ml) was added. The resulting mixture was then acidified until a yellow precipitate was formed which was filtered and dried in a vacuum oven at 50 °C. The dry solid was dissolved in a warm sulfuric acid-solution (70 ml, 10 %) and the mixture was heated to reflux for 3 h. After cooling to room temperature a precipitate was formed which was filtered and recrystallized from water to yield benzoic acid **4.14** as an off-white crystalline solid (5.2 g, 20 mmol, 91 %).[89]

Formula $C_{14}H_{11}NO_4$

Molecular weight 257.24 g/mol

10.4.2. 2-Chloro-1-(piperidin-1-yl)ethanone (4.18)

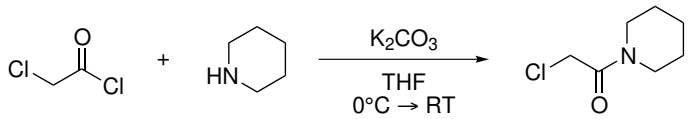

4.18

Piperidine (1.24 g, 15 mmol) and potassium carbonate (2.07 g, 15 mmol) were dissolved in tetrahydrofuran (50 mL) and the mixture was cooled to 0 °C. Chloroacetyl chloride (1.3 mL) was added drop wise, after which the mixture was slowly heated to room temperature. Water (50 mL) was added carefully and the aqueous phase was extracted with

ethyl acetate (3 × 250 mL). The combined organic phases were washed with a saturated sodium bicarbonate-solution (75 mL), an aqueous hydrochloric acid-solution (1 M, 75 mL), and a saturated sodium chloride-solution (75 mL). The organic phase was dried on sodium sulfate, filtered, and concentrated in vacuo to yield 2-chloro-1-(piperidin-1-yl)-ethan-1-one as a pale yellow oil (2.1 g, 13 mmol, 87 %), wihich was used without further purification and had experimental characteristics similar to those reported in the literature.[148]

Formula $C_7H_{12}ClNO$

Molecular weight 161.65 g/mol

10.4.3. 2-Chloro-1-(4-hydroxypiperidin-1-yl)ethanone (4.19)

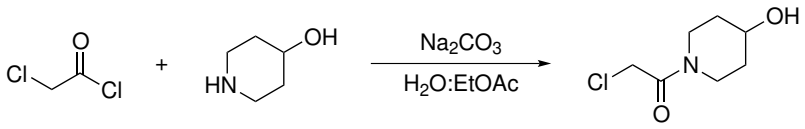

4.19

4-hydroxypiperidine (1 g, 10 mmol, 1.0 equiv.) and potassium carbonate (2.76 g, 20 mmol, 2.0 equiv.) are dissolved in a mixture of ethyl acetate (32 ml) and water (8 ml). Once complete dissolution is reached, chloroacetylchloride (1 ml, 13 mmol, 1.3 equiv.) is added drop wise upon which the mixture is stirred, whilst monitoring by thin-layer chromatography. After 2 h, the reaction is judged complete and methyl-*tert*-butyl ether (10 ml) is added. The resulting mixture is washed with sodium bicarbonate-solution (10 ml) and sodium chloride-solution (10 ml), dried on sodium sulfate, filtered and concentrated *in vacuo*to yield alcohol **4.19** as a yellow oil (403.7 mg, 2.3 mmol, 23 %), which crystallised into off-white crystals after one week storage at −20 °C. The product was used without further purification and showed experimental data as those reported in the literature.[149]

Formula $C_7H_{12}ClNO_2$;

Molecular weight 177.63 g/mol;

10.4.4. 2-Methyl-4-(4-(2-oxo-2-(piperidin-1-yl)ethoxy)phenyl)phthalazin-1(2*H*)-one (4.20)

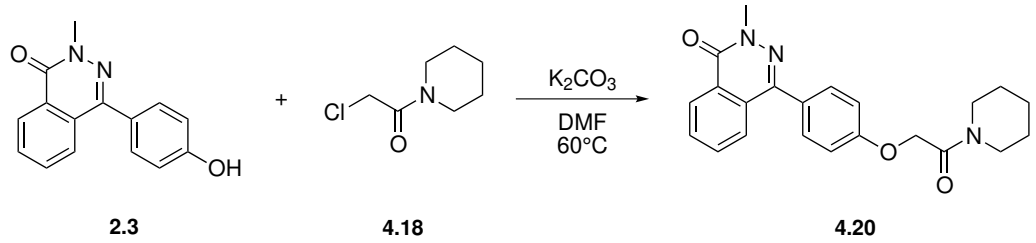

2.3 **4.18** **4.20**

2.3 (250 mg, 0.99 mmol, 1.0 equiv.) and **4.18** (176 mg, 1.1 mmol, 1.1 equiv.) were dissolved in dry dimethylformamide (10 mL). Potassium carbonate (274 mg, 1.98 mg, 2.0 equiv.) was added and the mixture was heated to 60 °C. When judged complete by TLC, water (50 mL) was added upon which a white precipitate was formed. The solid was filtered and recrystallised from 2-propanol to yield **4.20** as a white crystalline solid (324.4 mg, 0.86 mmol, 86 %).

Formula: $C_{22}H_{23}N_3O_3$;

Molar mass: 377.44 g/mol;

^{1}H-NMR (400 MHz, $CDCl_3$): δ (ppm) 8.52 (d(br), 1 H, $J = 7.4$ Hz, Ar$-H$), 7.8–7.7 (band, 3 H, Ar$-H$), 7.55–7.47 (m, 2 H, Ar$-H$), 7.13–7.06 (m, 2 H, Ar$-H$), 4.76 (s, 2 H, O$-CH_2$), 3.90 (s, 3 H, CH_3), 3.58 (dd, 2 H, $J = 6.0, 4.8$ Hz, piperidine$-H$), 3.54 (dd, 2 H, $J = 6.0, 4.8$ Hz, piperidine$-H$), 1.69–1.52 (band, 6 H, piperidine$-H$);

^{13}C-NMR (100 MHz, $CDCl_3$): δ (ppm) 165.9 (C), 159.4 (C), 158.8 (C), 146.6 (C), 132.7 (CH), 131.4 (CH), 130.8 (CH), 129.4 (C), 128.4 (C), 128.2 (C), 127.0 (CH), 126.7 (CH), 114.9 (CH), 67.8 (CH_2), 46.5 (CH_2), 43.3 (CH_2), 39.6 (CH_3), 26.5 (CH_2), 25.6 (CH_2), 24.5 (CH_2);

HRMS [*m*/*z*]: [M+H]+ calcd. for $C_{22}H_{24}N_3O_2^+$, 378.1812; found, 378.1829

10.4.5. 4-(3-Allyl-4-hydroxyphenyl)-2-methylphthalazin-1(2*H*)-one (4.30)

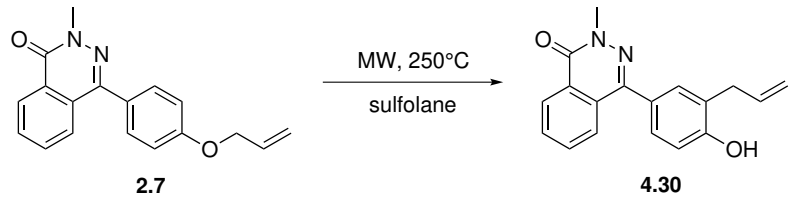

2.7 **4.30**

A microwave vial was charged with **2.7** (250 mg, 0.86 mmol) and sulfolane (5 mL). The mixture was heated in a microwave apparatus (75 W) to 250 °C for 15 min. After cooling to room temperature the mixture was diluted with water (5 mL) upon which a white precipitate was formed. The solid was filtered and recrystallized from a water:ethanol mixture (1:1, v/v) to yield **4.30** derivative as an off-white crystalline solid (195 mg, 0.67 mmol, 78 %).

Formula: $C_{18}H_{16}N_2O_2$;

Molar mass: 292.34 g/mol;

^{1}H-NMR (400 MHz, $(CD_3)_2SO$): δ (ppm) 9.80 (s(br), 1 H, −O*H*), 9.37–8.30 (m, 1 H, Ar−*H*), 7.91–7.83 (band, 2 H, Ar−*H*), 7.74–7.68 (m, 1 H, Ar−*H*), 7.30–7.24 (band, 2 H, Ar−*H*), 7.00–6.94 (m, 1 H, Ar−*H*), 6.00 (ddt, 1 H, $J = 17.0, 10.0, 6.7$ Hz, CH_2−C*H*=CH_2), 5.08 (ddt, 1 H, $^3J = 17.0, 2.1$ Hz, $^4J = 1.5$ Hz, CH=C*H*H), 5.20 (ddt, 1 H, $^3J = 10.0, 2.1$ Hz, $^4J = 1.2$ Hz, CH=C*H*H), 3.76 (s, 3 H, −CH_3), 3.37 (d(br), 2 H, $J = 6.7$ Hz, Ar−CH_2),

^{13}C-NMR (100 MHz, $(CD_3)_2SO$): δ (ppm) 158.2 (C), 155.8 (C), 155.7 (C), 146.1 (C), 136.8 (CH), 133.2 (CH), 131.6 (CH), 130.7 (CH), 128.9 (C), 128.4 (CH), 126.7 (CH), 126.2 (CH), 125.4 (C), 115.7 (CH_2), 114.8 (CH), 39.0 (CH_3), 33.7 (CH_2),

HRMS [*m*/*z*]: [M+H]+ calcd. for $C_{18}H_{17}N_2O_2^+$, 293.1285; found, 293.1286;

10.4.6. 4-(3-Allyl-4-(2-oxo-2-(piperidin-1-yl)ethoxy)phenyl)-2-methylphthalazin-1(2*H*)-one (4.29)

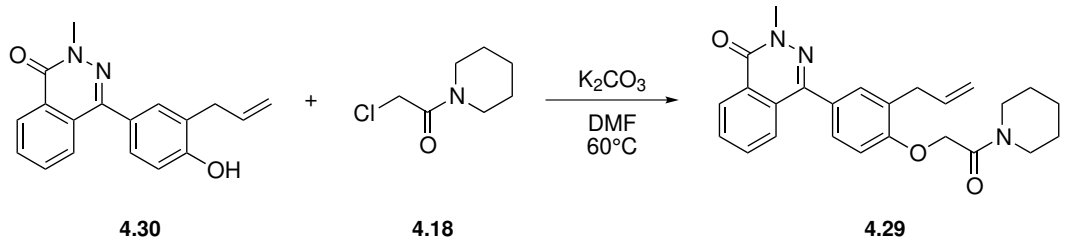

4.30 **4.18** **4.29**

The allylated phenol derivative (150 mg, 0.51 mmol) and yield 2-chloro-1-(piperidin-1-yl)-ethan-1-one (91 mg, 0.56 mmol) were dissolved in dimethylformamide (5 mL). Potassium carbonate (142 mg, 1.03 mmol) was added. The mixture was stirred for 5 min and subsequently heated to 60 °C. After 4 h, water (20 mL) was added and the aqueous layer was extracted with ethyl acetate (3 × 200 mL). The combined organic phases were dried on sodium sulfate, filtered, and concentrated in vacuo to yield a dark yellow oil that solidified upon storage at −20 °C. The off-white solid was recrystallized from 2-propanol to give the **4.29** analog as a white crystalline solid (129.8 mg, 0.31 mmol, 61 %).

Formula: $C_{25}H_{27}N_3O_3$;

Molar mass: g/mol;

^{1}H-NMR (400 MHz, $CDCl_3$): δ (ppm) 8.55–8.50 (m, 1 H, Ar−*H*), 7.80–7.70 (band, 3 H, Ar−*H*), 7.40–7.36 (band, 2 H, Ar−*H*), 7.04 (dm(br), 1 H, $J = 8.6$ Hz, O−C=C*H*), 6.03 (ddt, 1 H, $J = 16.9, 10.1, 6.7$ Hz, CH_2−C*H*=CH_2), 5.11 (ddt, 1 H, $^3J = 16.9, 1.6$ Hz, $^4J = 1.6$ Hz, CH=C*H*H), 5.05 (m, 1 H, CH=CH*H*), 4.78 (s, 2 H, O−C*H*CO), 3.91 (s, 3 H, CH_3), 3.63–3.48 (band, 6 H, piperidine−*H*), 1.72–1.53 (m(br), 4 H, piperidine−*H*),

^{13}C-NMR (100 MHz, $CDCl_3$): δ (ppm) 166.1 (C), 159.4 (C), 156.6 (C), 146.8 (C), 136.3 (C), 132.6 (C), 131.3 (C), 129.5 (C), 128.7 (CH), 128.2 (CH), 128.1 (CH), 127.0 (CH), 126.8 (CH), 116.2 (CH_2), 111.5 (CH_2), 68.2 (CH_2), 46.5 (CH_2), 43.3 (CH_2), 39.6 (CH), 34.2 (CH_2), 26.7 (CH_2), 25.6 (CH_2), 24.5 (CH_2),

HRMS [*m*/*z*]: [M+H]+ calcd. for $C_{25}H_{28}N_3O_3^+$, 418.2125; found, 418.2133.

10.4.7. *N*-(2-((3-(5-(3-methyl-4-oxo-3,4-dihydrophthalazin-1-yl)-2-(2-oxo-2-(piperidin-1-yl)ethoxy)phenyl)propyl)thio)ethyl)-5-((3a(*S*),4(*S*),6a(*R*))-2-oxohexahydro-1*H*-thieno[3,4-*d*]imidazol-4-yl)pentanamide (4.31)

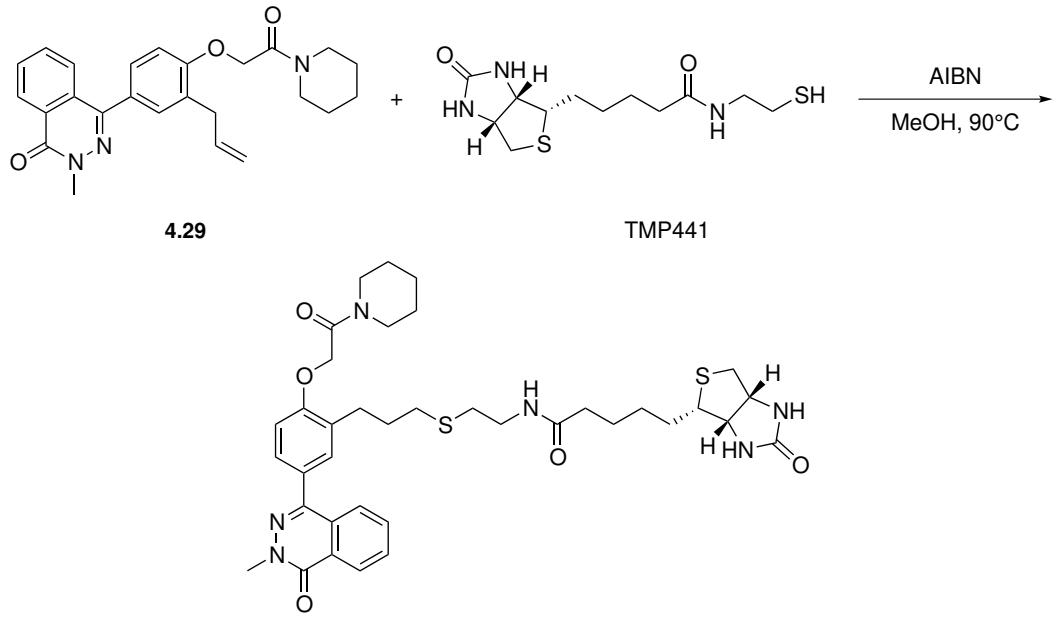

4.29 TMP441

4.31

A pressure tube was charged with **4.29** (165 mg, 0.40 mmol), **2.10** (240 mg, 0.79 mmol) and methanol (0.2 mL). A catalytic amount of azoisobisbutyronitrile was added and the mixture was heated to 90 °C. After 1.5 h, the reaction mixture was concentrated in vacuo and the residue was purified by flash chromatography to yield biotinylated Secdin **4.31** as a white solid (29 mg, 0.04 mg, 10 %).

Formula: $C_{37}H_{47}N_5O_6S_2$;
Molar mass: 721.93 g/mol;

^{1}H-NMR (400 MHz): δ (ppm) 8.58–8.47 (m, 1 H,), 7.85–7.70 (band, 3 H,), 7.45–7.34 (band, 2 H,), 7.00–6.94 (m, 1 H,), 7.80 (s, 2 H,), 4.50 (dd, 1 H, $J = 7.5, 5.2$ Hz,), 4.32 (dd, 1 H, $J = 7.5, 4.6$ Hz,), 3.60 (dd(br), 2 H, $J = 5.5, 5.5$ Hz,), 3.52 (dd(br), 2 H, $J = 5.5, 5.5$ Hz,), 3.44–3.36 (m, 2 H,), 3.14 (td, 1 H, $J = 7.3, 4.4$ Hz,), 2.90 (dd, 1 H, $J = 1.0, 5.0$ Hz,), 2.84 (t, 2 H, $J = 7.3$ Hz,), 2.70 (d, 1 H, $J = 13.0$ Hz,), 2.67 (t, 2 H, $J = 6.6$ Hz,), 2.60 (t, 2 H, $J = 6.9$ Hz,), 2.21 (td, 2 H, $J = 7.2, 5.7$ Hz,), 1.97 (quint, 2 H, $J = 7.14$ Hz,), 1.92–1.35 (band +2O), 18 H,),

10.5. Reactions from chapter 7

10.5.1. (5-Methylfuran-2-yl)(phenyl)methanol (7.4)

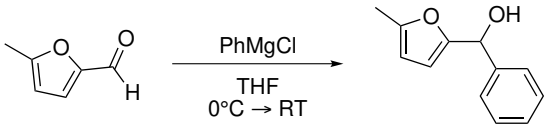

7.4

5-methyl furfural (1.0 g, 9.1 mmol, 1.0 equiv.) was dissolved in tetrahydrofuran (8 mL). The solution was cooled to 0 °C and phenylmagnesium chloride (2.0 M solution in tetrahydrofuran, 5.5 mL, 10.9 mmol, 1.2 equiv.) was added dropwise. The reaction was stirred for 5 min at 0 °C and then heated to room temperature over the course of 0.5 h an left overnight. A saturated ammonium chloride-solution (3 mL) was added and the aqueous phase was extracted with methyl-*tert*-butyl ether (3 × 30 mL). The cmbined organic extracts were dried on sodium sulfate and concentrated *in vacuo*. The crude material was purified by flash chromatography (silica, ethyl acetate:petroleum ether, 1:6 v/v) to yield alcohol **7.4** as a yellow oil (700 mg, 41 %). The product showed experimental properties identical to those found in the literature.[126]

Formula: $C_{12}H_{12}O_2$;

Molar mass: 188.22 g/mol;

10.5.2. 2-(5-Methylfuran-2-yl)propan-2-ol (7.6)

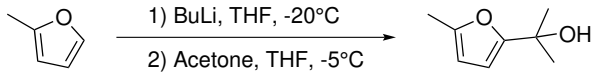

7.6

2-methylfuran (5 g, 60.9 mmol, 1.0 equiv.) is dissolved in dry tetrahydrofuran (38 mL). The solution is cooled to −20 °C and *n*-butyllithium (2.5 M solution in hexane, 27.0 mL, 67.6 mmol, 1.11 equiv.) is added dropwise. The reaction was heated to room temperature over the course of 0.5 h and subsequently cooled to −5 °C. A solution of acetone (5.6 mL, 76.1 mmol, 1.25 equiv.) in tetrahydrofuran (5 mL) was added dropwise and the mixture was again heated to room temperature. When judged complete by thin layer chromatography, a saturated ammonium chloride-solution (10 mL) was added and the aqueous phase was extracted with methyl-*tert*-butyl ether (3 × 100 mL). The combined organic extracts are washed with a saturated sodium chloride-solution (30 mL), dried on sodium sulfate and concentrated *in vacuo*. The crude material was purified with flash chromatography (silica, ethyl acetate:petroleum ether, 7:93 v/v → 12:88 v/v) to yield alcohol **7.6** as a pale yellow oil (4.2 g, 48 %). The product showed experimental properties identical to those found in the literature.[126]

Formula: $C_8H_{12}O_2$;
Molar mass: 140.14 g/mol;

10.5.3. (5-Methylfuran-2-yl)methanol (7.12)

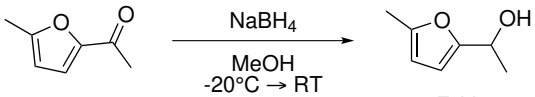

7.11

2-acetyl-5-methyl furan (1.2 g, 10 mmol, 1.0 equiv.) was dissolved in dry methanol (25 mL). The solution was cooled to −20 °C and sodium borohydride (567 mg, 15 mg, 1.5 equiv.) was added portionwise. The reaction was slowly heated to room temperature over the course of 1.5 h and judged complete by thin layer chromatography. A saturated ammonium chloride-solution (12 mL) was added and the biphasic mixture was stirred for 0.5 h. The aqueous phase was extracted with dichloromethane (3 × 100 mL). he combined organic extracts were washed with a saturated sodium chloride-solution (100 mL) dried on sodium sulfate and concentrated *in vacuo*. Alcohol **7.11** was quantitatively isolated as a yellow oil and was used without any further purification, showing experimental properties identical to those found in the literature.[126]

Formula: $C_7H_{10}O_2$;
Molar mass: 126.16 g/mol;

10.5.4. (5-Methylfuran-2-yl)methanol (7.12)

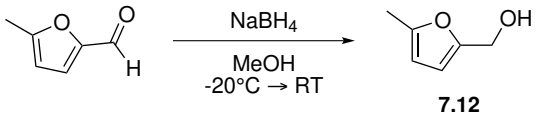

7.12

5-methyl furfural (1.0 g, 9.1 mmol, 1.0 equiv.) was dissolved in dry methanol (25 mL). The solution was cooled to −20 °C and sodium borohydride (515 mg, 13.6 mg, 1.5 equiv.) was added portionwise. The reaction was slowly heated to room temperature over the course of 1.5 h and judged complete by thin layer chromatography. A saturated ammonium chloride-solution (10 mL) was added and the biphasic mixture was stirred for 0.5 h. The aqueous phase was extracted with methyl-*tert*-butyl ether (3 × 100 mL) and the combined organic extracts were dried on sodium sulfate and concentrated *in vacuo*. Alcohol **7.12** was quantitatively isolated as a yellow oil and was used without any further purification, showing experimental properties identical to those found in the literature.[126]

Formula: $C_6H_8O_2$;

Molar mass: 112.13 g/mol;

10.5.5. 1-(5-Methylfuran-2-yl)propan-1-ol (7.13)

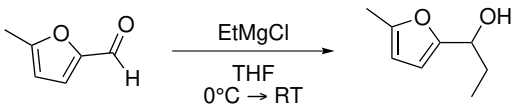

7.13

5-methyl furfural (1.0 g, 9.1 mmol, 1.0 equiv.) was dissolved in dry tetrahydrofuran (8 mL). The solution was cooled to 0 °C and ethylmagnesium bromide (1.0 M solution in tetrahydrofuran, 10.9 mL, 10.9 mmol, 1.2 equiv.) was added dropwise. The reaction was stirred for 5 min at 0 °C and then heated to room temperature over the course of 0.5 h an left overnight. A saturated ammonium chloride-solution (3 mL) was added and the aqueous phase was extracted with methyl-*tert*-butyl ether (3 × 30 mL). The combined organic extracts were dried on sodium sulfate and concentrated *in vacuo*. The crude material was purified by flash chromatography (silica, ethyl acetate:petroleum ether, 1:5 v/v) to yield alcohol **7.13** as a yellow oil (784 mg, 62 %). The product showed experimental properties identical to those found in the literature.[126]

Formula: $C_8H_{12}O_2$;

Molar mass: 140.18 g/mol;

10.5.6. 2-(Benzofuran-2-yl)propan-2-ol (7.14)

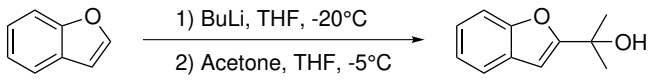

7.14

benzofuran (1.0 g, 8.5 mmol, 1.0 equiv.) is dissolved in dry tetrahydrofuran (5 mL). The solution is cooled to −20 °C and *n*-butyllithium (2.5 M solution in hexane, 3.8 mL, 9.4 mmol, 1.11 equiv.) is added dropwise. The reaction was heated to room temperature over the course of 0.5 h and subsequently cooled to −5 °C. A solution of acetone (780 µL, 10.6 mmol, 1.25 equiv.) in tetrahydrofuran (1 mL) was added dropwise and the mixture was again heated to room temperature. When judged complete by thin layer chromatography, a saturated ammonium chloride-solution (10 mL) was added and the aqueous phase was extracted with methyl-*tert*-butyl ether (3 × 100 mL). The combined organic extracts are washed with a saturated sodium chloride-solution (30 mL), dried on sodium sulfate and concentrated *in vacuo*. The crude material was purified with flash chromatography (silica, ethyl acetate:petroleum ether, 15:85 v/v → 20:80 v/v) to yield alcohol **7.14** as a viscous yellow oil (1.14 g, 76 %). The product showed experimental properties identical to those found in the literature.[126]

Formula: $C_{11}H_{12}O_2$;
Molar mass: 176.21 g/mol;

10.5.7. (4+3)–cycloaddition: general procedure

The alcohol (1.0 equiv.) and diene (2.0 equiv.) are dissolved in dry dichloromethane (0.2 M relative to the alcohol). After cooling to −78 °C, water is added (10.0 equiv.) followed by a solution of titanium chloride (1.24 equiv.) in dichloromethane (300 µl). The reaction mixture is heated to −10 °C over the course of 1.5 h after which a saturated sodium bicarbonate–solution (6 ml) is added all at once. The resulting biphasic mixture is separated and the aqueous phase is extracted two times with methyl *tert*-butyl ether, the combined organic phases are then washed with a saturated sodium chloride–solution after which the organic phase is dried on sodium sulfate, filtered and concentrated *in vacuo*. The resulting residue was purified by flash chromatography eluting with light petroleum ether (bp 60 °C–80 °C).

10.5.8. (4(*R*),7(*S*),10(*R*))-10-isopropyl-2,6,8,8-tetramethyl-7,8-dihydro-4*H*-4,7-ethanocyclohepta[b]furan (7.7)

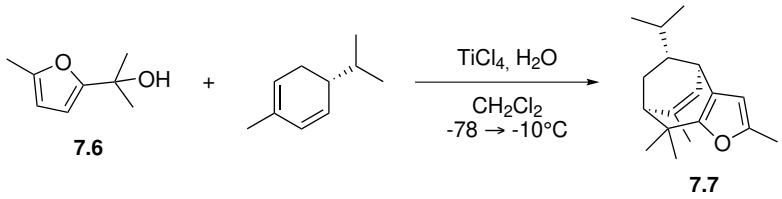

7.6 **7.7**

General procedure (see section 10.5.7): with alcohol **7.6** (147 mg, 1.05 mmol), α-(*R*)-phellandrene (286 mg, 2.10 mmol), titanium(IV)chloride (169 mg, 1.31 mmol), water (128 mg, 10.5 mmol) to give **7.7** as a colorless oil (235 mg, 0.91 mmol, 87 %).

Formula: $C_{18}H_{26}O$;

Molar mass: 258.40 g/mol;

^{1}H-NMR (400 MHz, $CDCl_3$): δ (ppm) 6.01 (d, 1 H, J = 7.0 Hz, Me−C=C*H*), 5.66 (q(br), 1 H, J = 0.9 Hz, Fur−*H*), 2.92 (dd, 1 H, J = 7.5, 0.88 Hz, C=C−C*H*−C=C), 2.22 (ddd, 1 H, J = 14.1, 8.9, 1.1 Hz, CH*H*), 2.19 (d, 3 H, J = 0.9 Hz, Fur−CH_3), 2.04 (d, 1 H, J = 5.7 Hz, $(CH_3)_2$C−C*H*−C=C), 1.85–1.78 (m, 1 H, $(CH_3)_2$C−CH−C*H*), 1.81 (d, 3 H, J = 1.3 Hz, C=C−CH_3), 1.34 (sept, 1 H, J = 6.6 Hz, $(CH_3)_2$−C*H*), 1.31 (s, 3 H, CH_3−C−CH_3), 1.22 (dt, 1 H, J = 14.1, 5.8 Hz, C*H*H), 1.17 (s, 3 H, CH_3−C−CH_3), 0.86 (d, 3 H, J = 6.6 Hz, CH_3−CH−CH_3), 0.82 (d, 3 H, J = 6.6 Hz, CH_3−CH−CH_3)),

^{13}C-NMR (100 MHz, $CDCl_3$): δ (ppm) 153.4 (C), 147.9 (C), 139.0 (C), 129.0 (CH), 124.0 (C), 105.5 (CH), 50.2 (CH), 50.1 (CH), 38.6 (C), 33.9 (CH), 33.3 (CH), 28.3 (CH_3), 27.4 (CH_2), 26.5 (CH_3), 24.4 (CH_3), 20.9 (CH_3), 20.4 (CH_3), 13.5 (CH_3),

HRMS [*m*/*z*]: [M+H]+ calcd. for $C_{18}H_{27}O^+$, 259.2056; found, 259.2055

FT-IR (ν_{max} / cm^{-1}): 2954 (s), 2918 (s), 2879 (s), 1661 (w), 1624 (w), 1575 (m)

(4(*R*),7(*S*),10(*R*))-10-isopropyl-3-((1(*R*),6(*R*))-6-isopropyl-3-methylcyclohex-2-en-1-yl)-2,6,8,8-tetramethyl-7,8-dihydro-4*H*-4,7-ethanocyclohepta[b]furan (7.8)

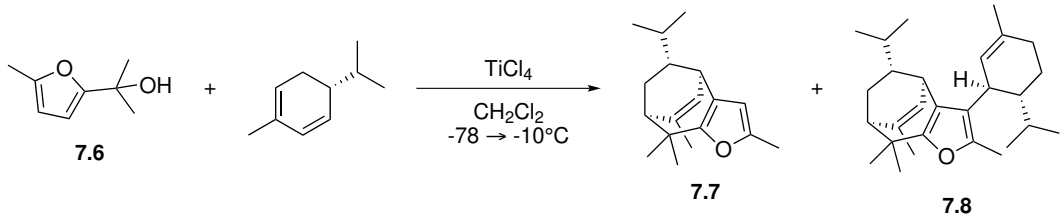

Formula: $C_{28}H_{42}O$;

Molar mass: 394.63 g/mol;

^{1}H-NMR (700 MHz, $CDCl_3$): δ (ppm) 5.89 (d, 1 H, J = 7.0 Hz, C=C*H*), 5.33 (s, 1 H, Fur−CH−C*H*=C), 3.18 (d, 1 H, J = 7.5 Hz, C=C−C*H*−C=C), 3.00 (dm, 1 H, J = 10.7 Hz, Fur−C*H*−C=C), 2.22 (ddd, 1 H, J = 14.1, 8.9, 1.1 Hz, (iPr)−CH−CH*H*−CH−C(CH_3)), 2.1 (d, 3 H, J = 0.8 Hz, Fur−CH_3), 2.10–2.05 (m, 1 H, Fur−CH−C=CCH_3−C*H*axH), 2.08–2.04 (m, 1 H, J = 5.7 Hz, $(CH_3)_2$C−C*H*−C=C), 1.79 (d, 3 H, J = 1.3 Hz, C=CCH_3−CH−C(CH_3)$_2$), 1.74 (dddd, 1 H, J = 12.5, 7.5, 4.8, 2.2 Hz, Fur−CH−CH(iPr)−CHH_{eq}), 1.71 (s(br), 3 H, Fur−CH−C=CCH_3), 1.70–1.64 (m, 1 H, iPr−C*H*−CH−C(CH_3)$_2$), 1.64 (septd, 1 H, J = 7.2, 2.1 Hz, $(CH_3)_2$C*H*−CH−$(CH_2)_2$), 1.42 (ddd, 1 H, J = 12.5, 10.6, 2.1, 2.1 Hz, Fur−CH−C*H*(iPr)), 1.34–1.30 (band, 1 H, Fur−CH−C(iPr)−CH_{ax}H), 1.30–1.28 (band, 1 H, $(CH_3)_2$−C*H*−CHCH_2CHC(CH_3)$_2$),1.29 (s, 3 H, CH_3−C−CH_3), 1.22–1.18 (overlapping band with other isomer, 1 H, (iPr)−CH−C*H*H−CH−C(CH_3)$_2$), 1.15 (s, 3 H, CH_3−C−CH_3), 0.87 (d, 3 H, J = 6.6 Hz, Fur−CH−CH(CH_3)(CH_3)), 0.84 (d, 3 H, J = 6.6 Hz, (CH_3)C(CH_3)−$(CH)_2CH_2$CHC(CH_3)$_2$), 0.81 (d, 3 H, J = 6.6 Hz, (CH_3)(CH_3)−$(CH)_2$−CH_2−CH−C(CH_3)$_2$), 0.78 (d, 3 H, J = 6.6 Hz, Fur−CH−CH(CH_3)(CH_3)),

^{13}C-NMR (175 MHz, $CDCl_3$): δ (ppm) 152.8 (C), 143.7 (C), 138.8 (C), 133.6 (C), 128.9 (CH), 126.2 (CH), 123.3 (C), 118.8 (C), 50.0 (CH), 49.6 (CH), 44.7 (CH), 38.7 (C), 36.3 (CH), 34.3 (CH), 31.0 (CH), 30.9 (CH_2), 28.4 (CH_3), 27.9 (CH_2), 27.0 (CH), 26.8 (CH_3), 25.5 (CH), 24.4

(CH_3), 23.3 (CH), 22.2 (CH_2), 21.8 (CH_3), 21.2 (CH_3), 16.0 (CH_3), 11.9 (CH_3), diagnostic correlation observed in 2D NOESY experiment (700 MHz): 5.89 × 0.81, 5.89 × 3.18, 5.89 × 1.34–1.30, 3.02 × 1.32, 1.42 × 2.08

10.5.9. (4(*R*),7(*R*),8(*S*)/(*R*),10(*R*))-10-isopropyl-2,6,8-trimethyl-7,8-dihydro-4*H*-4,7-ethanocyclohepta[b]furan (7.15)

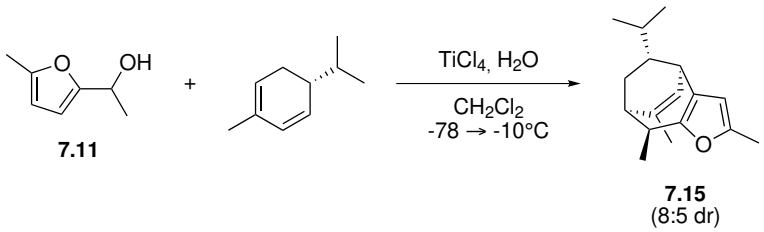

General procedure (see section 10.5.7): with alcohol **7.11** (401 mg, 3.20 mmol), *α*-(*R*)-phellandrene (845 mg, 6.40 mmol), titanium(IV)chloride (728 mg, 3.84 mmol), water (576 mg, 32.0 mmol) to give **7.15** as a colorless oil (362 mg, 1.51 mmol, 47 %) **Major Isomer**

Formula: $C_{17}H_{24}O$;
Molar mass: 244.38 g/mol;

Major Isomer

^{1}H-NMR (400 MHz, $CDCl_3$): δ (ppm) 6.01 (d, 1 H, J = 7.3 Hz, C=C*H*), 5.69 (q(br), 1 H, J = 1.0 Hz, Fur−*H*), 2.99 (qd, 1 H, J = 7.0, 2.4 Hz, Fur−C*H*CH_3), 2.91 (dd, 1 H, J = 7.2, 1.5 Hz, Fur−C*H*−C=C), 2.23–2.19 (m, 1 H, C=C(CH_3)−C*H*), 2.20 (m, 3 H, Fur−CH_3), 2.17 (ddd, 1 H, ^2J = 14.1 Hz, ^3J = 9.3, 1.1 Hz, C*H*H), 1.90–1.80 (overlapping band with other isomer, 1 H, C*H*−iPr), 1.79 (d, 3 H, J = 1.6 Hz, C=C−CH_3), 1.40–1.30 (overlapping band with other isomer, 1 H, $(CH_3)_2$−C*H*), 1.27 (ddd, 1 H, ^2J = 14.1 Hz, ^3J = 6.1, 4.8 Hz, CH*H*), 1.25 (d, 3 H, J = 7.0 Hz, Fur−C(CH_3)), 0.86 (d, 3 H, J = 6.7 Hz, CH_3−C−CH_3), 0.83 (d, 3 H, J = 6.7 Hz, CH_3−C−CH_3)),

^{13}C-NMR (100 MHz, $CDCl_3$): δ (ppm) 151.2 (C), 148.0 (C), 139.1 (C), 125.2 (C), 128.9 (CH), 105.8 (CH), 50.7 (CH), 43.8 (CH), 34.0 (CH), 33.8 (CH), 33.1 (CH), 24.7 (CH_2), 21.6 (CH_3), 21.0 (CH_3), 20.5 (CH_3), 17.5 (CH_3), 13.4 (CH_3),

Minor Isomer

Formula: $C_{17}H_{24}O$;

Molar mass: 244.38 g/mol;

^{1}H-NMR (500 MHz, $CDCl_3$): δ (ppm) 6.07 (d, 1 H, J = 7.3 Hz, C=C*H*), 5.70 (q(br), 1 H, J = 1.0 Hz, Fur−*H*), 2.97 (dd, 1 H, J = 7.2, 1.4 Hz, Fur−C*H*−C=C), 2.89 (qd, 1 H, J = 7.1, 4.0 Hz, C=C(CH_3)−C*H*), 2.40 (dddd(br), 1 H, ^3J = 6.8, 4.0, 1.0 Hz, ^4J = 1.0 Hz, C=C(CH_3)−C*H*), 2.20 (m, 3 H, Fur−CH_3), 1.90 (ddd, 1 H, ^2J = 13.0 Hz, ^3J = 9.2, 1.1 Hz, C*H*H), 1.90–1.80 (band, 1 H, C*H*−iPr), 1.79 (d, 3 H, J = 1.6 Hz, C=C−CH_3), 1.53 (ddd, 1 H, J = 13.0 Hz, CH*H*), 1.40–1.30 (overlapping band with other isomer, 1 H, $(CH_3)_2$−C*H*), 1.19 (d, 3 H, J = 7.1 Hz, Fur−C(CH_3)), 0.86 (d, 3 H, J = 6.8 Hz, CH_3−C−CH_3), 0.81 (d, 3 H, J = 6.8 Hz, CH_3−C−CH_3)),

^{13}C-NMR (125 MHz, $CDCl_3$): δ (ppm) 150.9 (C), 148.1 (C), 136.7 (C), 130.1 (CH), 125.3 (C), 105.7 (CH), 50.7 (CH), 43.5 (CH), 38.9 (CH), 33.8 (CH), 33.3 (CH), 31.8 (CH_2), 24.5 (CH_3), 21.0 (CH_3), 20.6 (CH_3), 19.4 (CH_3), 13.4 (CH_3),

HRMS [*m*/*z*]: [M+H]+ calcd. for $C_{17}H_{25}O^+$, 245.1900; found, 245.1896;

FT-IR (ν_{max}/cm^{-1}): 2955 (s), 2928 (s), 2884 (m), 2868 (m), 1662 (w), 1630 (w), 1574 (m)

10.5.10. (4(*R*),7(*R*),8(*R*)/(*S*),10(*R*))-10-isopropyl-2,6-dimethyl-8-phenyl-7,8-dihydro-4*H*-4,7-ethanocyclohepta[*b*]furan (7.17)

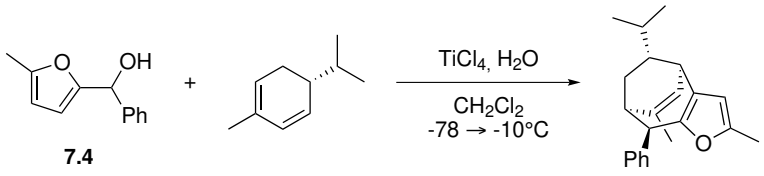

7.17
(10:1 dr)

General procedure (see section 10.5.7): with alcohol **7.4** (70 mg, 0.37 mmol), α-(*R*)-phellandrene (101 mg, 0.74 mmol), titanium(IV)chloride (85 mg, 0.45 mmol), water (67 mg, 3.70 mmol) to give **7.17** as a colourless oil. The crude product showed a diastereomeric ratio of 10:1 by proton NMR integration. Flash chromatography gave a combined yield for both isomers of 87 % with a typically slightly enhanced dr, next to a small fraction enriched in the minor isomer which could be used for its identification.

Formula: $C_{22}H_{26}O$;

Molar mass: 306.45 g/mol;

Major isomer

^{1}H-NMR (500 MHz, $CDCl_3$): δ (ppm) 7.33 (tm, 2 H, J = 7.7 Hz, Ar−H_m), 7.24 (tm, 1 H, J = 6.1 Hz, Ar−H_p), 7.11 (dm, 2 H, J = 6.9 Hz, Ar−H_o), 6.11 (d, 1 H, J = 7.0 Hz, C=C*H*), 5.79 (q(br), 1 H, J = 0.9 Hz, Fur−*H*), 4.28 (d(br), 1 H, J = 3.4 Hz, Ph−C*H*), 3.02 (dd, 1 H, J = 7.1, 1.1 Hz, Fur−C*H*−C=C), 2.44 (dddd, 1 H, J = 6.0, 3.4, 1.1 Hz, ^4J = 1.0 Hz, C=C−C*H*−CH_2), 2.17 (s(br), 3 H, Fur−CH_3), 2.09–2.01 (m, 1 H, iPr−C*H*), 1.89 (d, 3 H, J = 1.7 Hz, C=C−CH_3), 1.88 (ddd, 1 H, J = 13.9, 9.5, 1.1 Hz, C*H*H), 1.39 (qq, 1 H, J = 6.7, 6.7 Hz, CH_3−C*H*−CH_3), 1.08–1.00 (m, 1 H, C*H*H), 0.86 (d, 3 H, J = 6.7 Hz, CH_3−CH−CH_3), 0.79 (d, 3 H, J = 6.7 Hz, CH_3−CH−CH_3)),

^{13}C-NMR (125 MHz, $CDCl_3$): δ (ppm) 148.9 (C), 147.4 (C), 142.6 (C), 138.7 (C), 130.4 (CH), 129.7 (C), 128.5 (CH), 128.2 (CH), 128.0 (CH), 105.7 (CH), 50.7 (CH), 46.5 (CH), 45.9 (CH), 34.0 (CH), 33.3 (CH), 25.3 (CH_2), 21.6 (CH_3), 20.8 (CH_3), 20.4 (CH_3), 13.5 (CH_3),

Minor isomer

^{1}H-NMR (500 MHz, $CDCl_3$): δ (ppm) 7.28–7.23 (band, 2 H, Ar$-H_{meta}$), 7.00–6.97 (m, 2 H, Ar$-H_{ortho}$), 6.05 (d(br), 1 H, J = 7.4 Hz, C=CH), 5.80 (band, 1 H, Fur$-H$), 4.08 (d, 1 H, J = 4.6 Hz, Fur$-$C$H-$Ph), 3.11 (dd, 1 H, J = 7.4, 1.6 Hz, Fur$-$C$H-$C=C), 2.65 (dddd, 1 H, J = 7.1, 4.6, 1.2 Hz, ^4J = 1.0 Hz, C(Ph)$-$C$H-$C=C), 2.19–2.16 (band, 3 H, Fur$-$CH_3), 2.08 (ddd, 1 H, J = 14.0, 11.3, 0.8 Hz, CHH), 1.93–1.85 (band, 1 H, C$H-$iPr), 1.62 (ddd, 1 H, 3.8), 1.40–1.34 (band, 1 H, CH_3-C$H-CH_3$), 1.05 (d, 3 H, J = 1.6 Hz, C=C$-CH_3$), 0.89 (d, 3 H, J = 6.7 Hz, CH_3-C$-CH_3$), 0.85 (d, 3 H, J = 5.7 Hz, CH_3-C$-$CH_3)),
^{13}C-NMR (125 MHz, $CDCl_3$): δ (ppm) 149.0 (C), 147.6 (C), 142.9 (C), 136.4 (C), 129.5 (CH), 128.0 (CH), 127.6 (C), 126.4 (CH), 126.3 (CH), 105.7 (CH), 51.2 (CH), 49.6 (CH), 45.6 (CH), 33.7 (CH), 33.5 (CH), 31.5 (CH_2), 23.3 (CH_3), 21.2 (CH_3), 20.8 (CH_3), 13.5 (CH_3),

HRMS [*m*/*z*]: [M+H]+ calcd. for $C_{17}H_{25}O^+$, 307.2056; found, 307.2053;
FT-IR (ν_{max}/cm^{-1}): 3026 (w), 2954 (s), 2925 (s), 2869 (m), 1631 (w), 1600 (w), 1572 (w)

10.5.11. (4(*R*),7(*R*),8(*S*)/(*R*),10(*R*))-8-ethyl-10-isopropyl-2,6-dimethyl-7,8-dihydro-4*H*-4,7-ethanocyclohepta[*b*]furan (7.18)

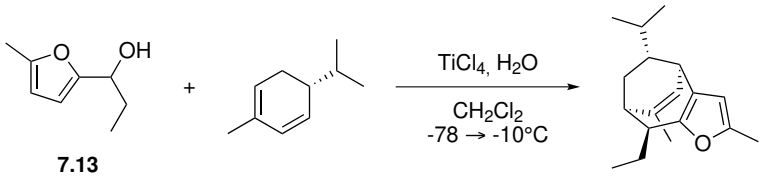

7.13 **7.18** (9:5 dr)

General procedure (see section 10.5.7): with alcohol **7.13** (100 mg, 0.70 mmol), α-(*R*)-phellandrene (191 mg, 1.40 mmol), titanium(IV)chloride (169 mg, 0.88 mmol), water (128 mg,

7.0 mmol) to give **7.18** as a colorless oil (95 mg, 0.37 mmol, 52 %)

Formula: $C_{18}H_{26}O$;

Molar mass: 258.41 g/mol;

Major isomer

^{1}H-NMR (500 MHz, $CDCl_3$): δ (ppm) 6.04 (d, 1 H, J = 7.0 Hz, C=C*H*), 5.69 (s, 1 H, Fur −*H*), 2.91 (d, 1 H, J = 7.0 Hz, C=C−C*H*−C=C), 2.72–2.66 (m, 1 H, C=C−C*H*Et−CH −C=C), 2.43 (dd, 1 H, J = 6.2, 2.7 Hz, C=C−CH−C*H*−C=C), 2.19 (s, 3 H, Fur−CH_3), 2.10 (dd, 1 H, J = 14.0, 9.3 Hz, C(i−Pr)−C*H*H), 2.01 (qd, 1 H, J = 7.4, 5.0 Hz, CH−C*H*H −CH_3), 1.91–1.80 (band3, 1 H), 1.78 (s, 3 H, C=CCH_3), 1.54–1.45 (m, 1 H, CH−CH*H*−CH_3), 1.38 (sept, 1 H, J = 6.6 Hz, CH_3−C*H*−CH_3), 1.24 (ddd, 1 H, J = 14.0, 5.52, 5.52 Hz, C(iPr)CH*H*), 1.06 (t, 3 H, J = 7.4 Hz, CH−CH_2−CH_3), 0.86 (d, 3 H, J = 6.6 Hz, CH_3 −CH−CH_3), 0.83 (d, 3 H, J = 6.6 Hz, CH_3−CH −CH_3)),

^{13}C-NMR (125 MHz, $CDCl_3$): δ (ppm) 151.0 (C), 147.9 (C), 139.0 (C), 129.3 (CH), 125.7 (C), 105.8 (CH), 50.7 (CH), 41.3 (CH), 39.4 (CH), 33.9 (CH), 33.2 (CH), 24.8 (CH_2), 24.2 (CH_2), 21.1 (CH_3), 21.0 (CH_3), 20.5 (CH_3), 13.5 (CH_3), 12.1 (CH_3)

Minor Isomer

^{1}H-NMR (500 MHz, $CDCl_3$): δ (ppm) 6.07 (d, 1 H, J = 7.3 Hz, C=C*H*), 5.70 (s, 1 H, Fur−*H*), 2.98 (d, 1 H, J = 7.3 Hz, C=C−C*H*−C=C), 2.66–2.58 (band, 2 H,), 2.19 (s, 3 H, Fur−CH_3), 1.93–1.81 (band, 3 H,), 1.78 (s, 3 H, C=C−CH_3), 1.59–1.53 (m, 1 H,), 1.44–1.30 (band, 2 H,), 1.09 (t, 3 H, J = 6.6 Hz, CH−CH_2−CH_3), 0.86 (d, 3 H, J = 6.6 Hz, CH_3−CH−CH_3), 0.83 (d, 3 H, J = 6.6 Hz, CH_3−CH−CH_3)),

^{13}C-NMR (125 MHz, $CDCl_3$): δ (ppm) 150.7 (C), 148.1 (C), 136.8 (C), 130.2 (CH), 125.2 (C), 105.8 (CH), 50.9 (CH), 46.5 (CH), 39.2 (CH), 33.9 (CH), 33.4 (CH), 31.7 (CH_2), 26.3 (CH_2), 21.5 (CH_3), 21.0 (CH_3), 20.5 (CH_3), 13.5 (CH_3), 12.4 (CH_3),

HRMS [*m*/*z*]: [M+H]+ calcd. for $C_{18}H_{27}O^+$, 259.2056; found, 259.2059;

FT-IR (ν_{max}/cm^{-1}): 2954 (s), 2928 (s), 2870 (m), 1663 (w), 1630 (w), 1573 (w)

10.5.12. (7(*S*),10(*R*),11(*R*))-11-isopropyl-6,6,8-trimethyl-7,10-dihydro-6*H*-10,7-ethanocyclohepta[*b*]benzofuran (7.19)

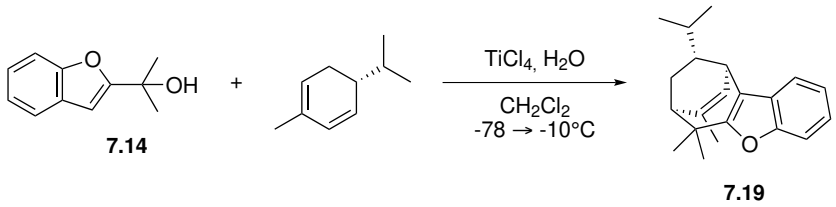

General procedure (see section 10.5.7): with alcohol **7.14** (184 mg, 1.04 mmol), α-(*R*)-phellandrene (282 mg, 2.08 mmol), titanium(IV)chloride (245 mg, 1.30 mmol), water (187 mg, 10.4 mmol) to give **7.19** as a colorless viscous oil (216 mg, 0.74 mmol, 71 %)

Formula: $C_{21}H_{26}O$;

Molar mass: 294.44 g/mol;

^{1}H-NMR (400 MHz, $CDCl_3$): δ (ppm) 7.45–7.42 (m, 1 H, Ar$-H_4$), 7.37–7.34 (m, 1 H, Ar$-H_7$), 7.20–7.14 (band, 2 H, Ar$-H_{5,6}$), 6.08 (d, 1 H, $J = 7.3$ Hz, C*H*=CCH$_3$), 3.41 (dd, 1 H, $J = 7.3, 1.3$ Hz, C=C$-$C*H*$-$C=C), 2.28 (ddd, 1 H, $J = 14.3, 9.0, 1.6$ Hz, (i$-$Pr)CH$-$C*H*H), 2.16 (dt(br), 1 H, $J = 6, 1.3$ Hz, C(CH$_3$)$_2-$C*H*), 1.91–1.85 (m, 1 H, (i$-$Pr)$-$C*H*), 1.86 (d, 3 H, $J = 1.7$ Hz, C=C$-$C*H*$_3$), 1.44 (sept, 1 H, $J = 6.6$ Hz, CH$_3$ $-$C*H*$-$CH$_3$), 1.42 (s, 3 H, C*H*$_3$ $-$C $-$CH$_3$), 1.33 (dt, 1 H, $J = 14.3, 5.8$ Hz, (i$-$Pr)CH$-$CH*H*), 1.29 (s, 3 H, CH$_3$ $-$C $-$C*H*$_3$), 0.94 (d, 3 H, $J = 6.6$ Hz, C*H*$_3$ $-$CH$-$CH$_3$), 0.86 (d, 3 H, $J = 6.6$ Hz, CH$_3-$CH$-$C*H*$_3$)),

^{13}C-NMR (100 MHz, $CDCl_3$): δ (ppm) 158.6 (C), 153.1 (C), 139.6 (C), 128.5 (CH), 127.7 (C), 122.6 (CH), 121.8 (CH), 117.9 (CH), 110.7 (CH), 112.3 (C), 50.1 (CH), 49.7 (CH), 39.0 (C), 33.9 (CH), 30.3 (CH), 28.0 (CH$_3$), 27.6 (CH$_2$), 26.3 (CH$_3$), 24.4 (CH$_3$), 20.9 (CH$_3$), 20.4 (CH$_3$),

HRMS [*m*/*z*]: calc'd for $C_{21}H_{27}O^+$, 295.2056; found, 295.2055;

FT-IR (ν_{max}/cm^{-1}): 2956 (s), 2928 (s), 2888 (s), 1661 (w), 1625 (w), 1611 (w), 1585 (w)

10.5.13. (2-Methylallyl)triphenylphosphonium chloride (7.31)

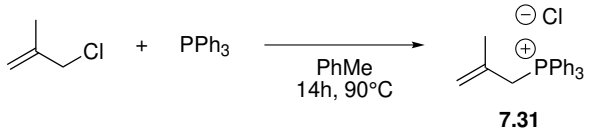

7.31

Methallyl chloride (3.37 ml, 34.5 mmol, 1.0 equiv.) is dissolved in toluene (20 ml) in a pressure tube. Triphenylphosphine (10 g, 38 mmol, 1.1 equiv.) is added and the mixture is heated to 90 °C for 14 h. The formed solids are filtered and washed with toluene and the filtered material was taken up in *iso*-propanol which after concentration *in vacuo* gave the commercially available title compound as a white crystalline solid (2.8 g, 8 mmol, 29 %).

Formula: $C_{22}H_{22}ClP$;

Molar mass: 352.84 g/mol;

10.5.14. 1-(*tert*-Butyl)-4-(2-methylallylidene)cyclohexane (7.30)

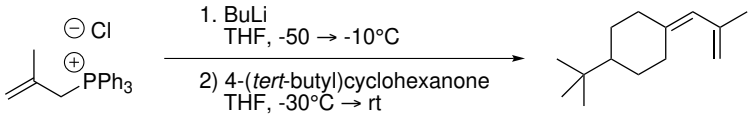

TMP814 **7.30**

The phosphonium salt **7.31** is suspended in tetrahydrofuran (17 ml) and the resulting mixture is cooled down to −50 °C. A *n*-butyllithium–solution (2.28 ml, 2.5 M in hexane) is added dropwise and the reaction is allowed to heat to −10 °C after which it is cooled again to −30 °C. A solution of 4-(*tert*-butyl)cyclohexanone in tetrahydrofuran (0.5 ml) is added and the reaction is heated to room temperature and left stirring overnight. Water (10 ml) is added and the aqueous phase is extracted with *n*-pentane (50 ml) and the organic phase is

washed with a saturated sodium chloride–solution (5 ml). The organic extracts are dried on sodium sulfate, filtered and concentrated *in vacuo*. The resulting residue was purified with flash chromatography (silica, petroleum ether) to give the title diene as a volatile liquid (342 mg, 1.78 mmol, 37 %).

Formula: $C_{14}H_{24}$;
Molar mass: 192.34 g/mol;

Major isomer

^{1}H-NMR (500 MHz, $CDCl_3$): δ (ppm) 5.59 (s(br), 1 H, C=C*H*−C), 4.90 (dq, 1 H, ^3J = 2.6 Hz, ^4J = 1.4 Hz, C=C*H*H), 4.74 (m, 1 H, C=CH*H*), 3.00 (dq, 1 H, J = 13.6, 2.8 Hz, C=C−CH_{ax}H), 2.23 (dq, 1 H, J = 13.9, 3.7 Hz), 2.08 (), 1.92–1.81 (band 2 H), 1.84 (s, 3 H, C=C−CH_3), 1.76 (tm, 1 H, J = 13.6 Hz), 1.19 (tt, 1 H, J = 11.9, 2.8 Hz, tBu−C*H*), 1.10 (td, 1 H, J = 12.2, 3.7 Hz), 1.06–0.93 (band, 2 H), 0.85 (s, 9 H, C(CH_3)$_3$),
^{13}C-NMR (125 MHz, $CDCl_3$): δ (ppm) 142.1 (C), 137.9 (C), 123.7 (CH), 113.7 (CH_2), 48.5 (C), 48.3 (CH), 37.8 (CH_2), 29.5 (CH_2), 29.3 (CH_2), 28.7 (CH_2), 27.6 (CH_3), 23.8 (CH_3),
HRMS [*m*/*z*]: [M+H]+ calcd. for $C_{14}H_{25}^+$, 193.1951; found, 193.1946;

10.5.15. 4′-(tert-Butyl)-2,7,8,8-tetramethyl-4,8-dihydrospiro[cyclohepta[*b*]furan-5,1′-cyclohexane] (7.32)

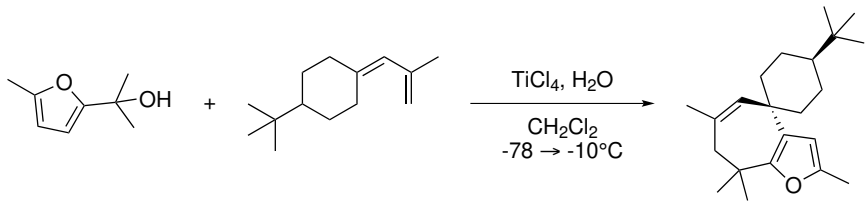

7.6 **7.30** **7.32**

General procedure (see section 10.5.7): with alcohol **7.6** (100 mg, 0.71 mmol), diene **7.30** (275 mg, 1.43 mmol), titanium(IV)chloride (169 mg, 0.89 mmol), water (129 mg, 7.14 mmol)

to give **7.32** as a waxy solid, which was treated with mercaptoethanol and AIBN in methanol at 90 °C for 30 min to give **7.32** (104 mg, 0.33 mmol, 47 %)

Formula: $C_{22}H_{34}O$;

Molar mass: 314.51 g/mol;

^{1}H-NMR (400 MHz, $CDCl_3$): δ (ppm) 5.83 (q(br), 1 H, $^4J = 1.0$ Hz, Fur−*H*), 5.60 (q(br), 1 H, $^4J = 1.5$ Hz, C=C*H*), 2.31 (s, 2 H, $(CH_3)_2C-CH_2$), 2.20 (d(br), 3 H, $^4J = 1.0$ Hz, Fur−CH_3), 1.90 (dm, 2 H, $J = 13.1$ Hz, C−CH_{eq}H−CH_2), 1.84 (d(br), 3 H, $^4J = 1.5$ Hz, C=C−C*H*), 1.61 (d(br), 2 H, $J = 12.2$ Hz, tBuCH−CH_{eq}H), 1.53 (td, 2 H, $J = 13.1, 3.5$ Hz, C−CHH_{ax}−CH_2), 1.28 (td, 2 H, $J = 13.2, 3.2$ Hz, tBuCH−CHH_{ax}), 1.24 (s, 6 H, CH_3−C−CH_3), 1.02 (tt, 1 H, $J = 12.2, 3.2$ Hz), 0.87 (s, 9 H, tBu−*H*),

^{13}C-NMR (125 MHz, $CDCl_3$): δ (ppm) 154.3 (C), 147.3 (C), 133.8 (C), 131.4 (CH), 126.0 (C), 105.2 (CH), 47.9 (CH), 44.1 (CH_2), 39.1 (CH_2), 36.4 (C), 35.7 (C), 32.4 (C), 28.7 (CH_3), 28.4 (CH_3), 27.6 (CH_3), 23.7 (CH_2), 13.4 (CH_3),

HRMS [*m*/*z*]: [M+H$^+$] calc'd for $C_{22}H_{35}O^+$, 315.2682; found, 315.2678;

FT-IR (ν_{max}/cm^{-1}): 2937 (s), 2863 (m), 1666 (w), 1645 (w), 1620 (w), 1591 (w), 1562 (w), 1469 (w), 1445 (m)

10.5.16. 4-Methyl-4-(5-methylfuran-2-yl)pentan-2-one (7.33)

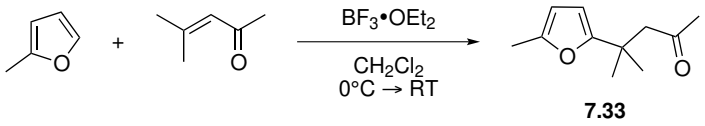

7.33

2-Methylfuran (1.0 g, 12.2 mmol, 1.0 equiv.) and mesityl oxide (1.2 g, 12.2 mmol, 1.0 equiv.) were dissolved in dry dichloromethane (15 ml). The solution is cooled to 0 °C and boron trifluoride etherate (1.65 ml, 13.4 mmol, 1.1 equiv.) is added dropwise. The reaction is heated to room temperature and stirred for 1.5 h after which one more equivalent of

2-methylfuran is added. After 0.5 h, a saturated sodium bicarbonate–solution (10 ml) was added and the aqueous phase was extracted with diethyl ether (3 × 50 ml), dried on sodium sulfate and concentrated *in vacuo*. The crude material was purified by flash chromatography (silica, 5:95 → 7:93 ethyl actetate:petroleum ether, v/v) to give **7.33** as a pale yellow oil (1.4 g, 7.8 mmol, 64 %) showing experimental properties identical as those found in the literature.[150,151]

Formula: $C_{11}H_{16}O_2$;
Molar mass: 180.24 g/mol;

10.5.17. 1-(tert-Butyl)-4-(iodomethylene)cyclohexane (7.34)

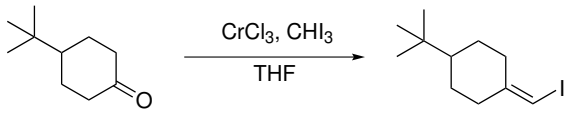

7.34

Flame–dried chromium(II)chloride (6.39 g, 52 mmol, 4.0 equiv.), was dissolved in dry tetrahydrofuran (60 ml). A solution of *tert*-butyl cyclohexanone (2.00 g, 13 mmol, 1.0 equiv.) and iodoform (10.24 g, 26 mmol, 2.0 equiv.) in tetrahydrofuran (30 ml) was carefully added, and the reaction was left overnight. After 23 h the crude mixture filtered over a plug of silica, and the filtrate was washed with water (2 × 10 ml) and a saturated sodium chloride–solution (2 × 10 ml). The organic phase was dried on sodium sulfate, filtered and concentrated *in vacuo*. The crude material was purified by flash chromatography (silica(long column!), petroleum ether) to yield diene **7.34** as a pale pink oil (781 mg, 3 mmol, 23 %)

Formula: $C_{11}H_{19}I$;
Molar mass: 278.17 g/mol;

^{1}H-NMR (400 MHz, $CDCl_3$): δ (ppm) 5.76 (t, 1 H, J = 1.7 Hz, IC−*H*), 2.84–2.70 (m, 1 H, C=C−C*H*H), 2.54 (ddd, 1 H, J = 13.6, 6.6, 3.2 Hz, C=C−C*H*H), 2.08 (td, 1 H, J = Hz, C=C−CH*H*), 1.98–1.74 (band, 3 H, CH_2), 1.18 (tt, 1 H, J = 11.7, 2.5 Hz, tBu−C*H*), 1.12 (band, 2 H, CH_2),

^{13}C-NMR (100 MHz, $CDCl_3$): δ (ppm) 151.4 (C), 121.3 (C), 70.7 (CH), 47.7 (CH), 37.0 (CH_2), 35.8 (CH_2), 32.3 (C), 28.7 (C), 27.7 (CH_2), 27.6 (CH_2), 27.2 (CH_3)

10.5.18. 1-(4-(tert-Butyl)cyclohexylidene)-2,4-dimethyl-4-(5-methylfuran-2-yl)pentan-2-ol (7.35)

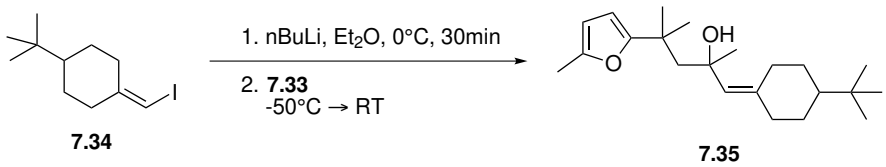

7.34 **7.35**

Diene **7.34** (417 mg, 1.5 mmol, 1.5 equiv.) is dissolved in dry diethyl ether (2 ml). The solution is cooled to 0 °C and *n*-butyllithium (600 µl, 2.5 M in hexane) is added. The reaction is stirred maintaining the temperature at 0 °C or slightly below. After 30 min the mixture is cooled to −50 °C and a solution of **7.33** 180 mg, 1 mmol, 1.0 equiv. in dry diethyl ether (1 ml) is added dropwise. The reaction is heated to room temperature and after 30 min, a saturated ammonium chloride–solution (4 ml) was added. The aqueous phase is extracted with diethyl ether (3 ×20 ml) and the combined organic extracts are dried on sodium sulfate, filtered and concentrated *in vacuo*. The crude material is purified by flash chromatography (silica, ethyl acetate:petroleum ether 5:95, v/v) to yield the acyclic precursor **7.35** (185 mg, 556 µmol, 56 %) as an equimolar mixture of two diastereoisomers.

Formula: $C_{22}H_{36}O_2$;

Molar mass: 332.52 g/mol;

Isomer 1

^{1}H-NMR (500 MHz, $CDCl_3$): δ (ppm) 5.86 (d(AB), 1 H, $J = 3.1$ Hz, $H_3CC{=}CH{=}CH$), 5.83 (dq(br,AB), 1 H, $J = 3.1$ Hz, $^4J = 0.8$ Hz, $H_3CC{=}CH{=}CH$), 5.08 (s(br), 1 H, $HOC{-}CH{=}C$), 3.17 (ddd, 1 H, $J = 13.4, 5.5, 3.0$ Hz, $C{=}C{-}CHH$), 2.26 (s(br), 3 H, $Fur{-}CH_3$), 2.05–1.98 (overlapping band with other isomer, 1 H, $C{=}C{-}CHH$), 1.96–1.85 (overlapping band with other isomer, 1 H, $C{=}C{-}CHH$), 1.83–1.77 (overlapping band with other isomer, 1 H, $C{=}C{-}CH_2{-}CHH$), 1.82–1.75 (overlapping band with other isomer, 1 H, $C{=}C{-}CH_2{-}CHH$), 1.65–1.57 (overlapping band with other isomer, 1 H, $C{=}C{-}CHH$), 1.34 (s, 3 H, $Fur{-}C(CH_3)(CH_3)$), 1.33 (s, 3 H, $Fur{-}C(CH_3)(CH_3)$), 1.16–1.07 (m, 1 H, *tert*$Bu{-}CH$), 1.13 (s, 2 H, $HOC{-}CH_2$), 1.04–0.95 (overlapping band with other isomer, 1 H, $C{=}C{-}CH_2{-}CHH$), 1.00–0.91 (overlapping band with other isomer, 1 H, $C{=}C{-}CH_2{-}CHH$), 0.85 (s, 9 H, $C{-}(CH_3)_3$);

^{13}C-NMR (125 MHz, $CDCl_3$): δ (ppm) 161.0 (C), 150.0 (C), 140.1 (C), 129.2 (CH), 105.9 (CH), 104.4 (CH), 105.9 (CH), 73.9 (C), 54.6 (C), 38.2 (CH_2), 33.0 (C), 29.6 (CH_2), 29.1 (CH_2), 28.3 (CH_2), 27.6 (CH_3),

Isomer 2

^{1}H-NMR (500 MHz, $CDCl_3$): δ (ppm) 5.85 (d(AB), 1 H, $J = 3.2$ Hz, $H_3CC{=}CH{=}CH$), 5.81 (dq(br,AB), 1 H, $J = 3.2$ Hz, $^4J = 0.9$ Hz, $H_3CC{=}CH{=}CH$), 5.03 (s(br), 1 H, $HOC{-}CH{=}C$), 3.17 (ddd, 1 H, $J = 13.4, 5.5, 3.0$ Hz, $C{=}C{-}CHH$), 2.25 (s(br), 3 H, $Fur{-}CH_3$), 2.05–1.98 (overlapping band with other isomer, 1 H, $C{=}C{-}CHH$), 1.96–1.85 (overlapping band with other isomer, 1 H, $C{=}C{-}CHH$), 1.83–1.77 (overlapping band with other isomer, 1 H, $C{=}C{-}CH_2{-}CHH$), 1.82–1.75 (overlapping band with other isomer, 1 H, $C{=}C{-}CH_2{-}CHH$), 1.65–1.57 (overlapping band with other isomer, 1 H, $C{=}C{-}CHH$), 1.33 (s, 3 H, $Fur{-}C(CH_3)(CH_3)$), 1.31 (s, 3 H, $Fur{-}C(CH_3)(CH_3)$), 1.14–1.07 (m, 1 H, *tert*$Bu{-}CH$), 1.16 (s, 2 H, $HOC{-}CH_2$), 1.04–0.95 (overlapping band with other isomer, 1 H, $C{=}C{-}CH_2{-}CHH$), 1.00–0.91 (overlapping band with other isomer, 1 H, $C{=}C{-}CH_2{-}CHH$), 0.83 (s, 9 H, $C{-}(CH_3)_3$);

^{13}C-NMR (125 MHz, $CDCl_3$): δ (ppm) 161.0 (C), 150.1 (C), 140.1 (C), 129.2 (CH), 105.9 (CH), 104.3 (CH), 73.9 (C), 54.8 (C), 38.1 (CH_2), 33.0 (C), 29.6 (CH_2), 29.1 (CH_2), 28.3 (CH_2), 27.6 (CH_3),

10.5.19. Cycloadduct 7.32 from acyclic precursor 7.35

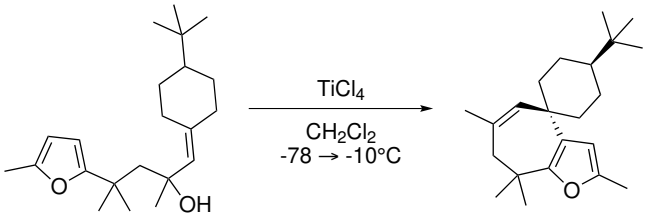

7.35 **7.32**

General procedure (see section 10.5.7): with acyclic precursor **7.35** (52 mg, 156 µmol), titanium(IV)chloride (37 mg, 196 µmol), water (28 mg, 1.56 mmol) to give a crude sample (60 mg) showing **7.32** as the only diastereoisomer (see section 10.5.15).

10.5.20. Penta-1,3-dien-1-ylbenzene (7.37)

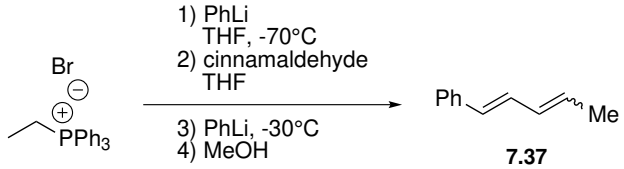

7.37
86:14 *(E):(Z)*

Ethyltriphenylphosphonium bromide (2.82 g, 7.6 mmol, 1.0 equiv.) is suspended in dry tetrahydrofuran (25 ml). Phenyllithium (4.3 ml, 1.8 M in dibutylether, 1.02 equiv.) is added carefully and the reaction is cooled to −70 °C upon which a solution of cinnamaldehyde (1

g, 7.6 mmol, 1.0 equiv.) in tetrahydrofuran () is added dropwise. The mixture is stirred for 5 min and subsequently heated to −30 °C followed by a second addition of phenyllithium (5 ml, 1.8 M in dibutylether, 1.17 equiv.). Again, the reaction is stirred for 5 min followed by addition of methanol (1.1 ml). The mixture is heated to room temperature and stirred for 2 h after which it is poured into water (100 ml). The aqueous phase is extracted with diethyl ether (2 ×100 ml), the combined organic phases dried on sodium sulfate, filtered and concentrated *in vacuo*. The crude material is purified by flash chromatography (silica, petroleum ether) to yield diene **7.37** (397 mg, 2.8 mmol, 36 %) as a 86:14–mixture of (*E*):(*Z*) isomers. The product showed experimental properties comparable to those found in the literature.[152]

Formula: $C_{11}H_{12}$;
Molar mass: 144.21 g/mol;

10.5.21. Dodeca-5,7-diene (7.38)

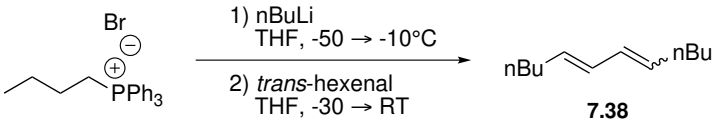

7.38

Butyltriphenylphosphonium bromide (5.1 g, 12.7 mmol, 1.2 equiv.) is suspended in dry tetrahydrofuran (35 ml) and the suspension is cooled to −50 °C. Butyllithium (5.1 ml, 2.5 M in hexane, 1.2 equiv.) is added dropwise and the reaction is heated to −10 °C and subsequently cooled again to −30 °C. A solution of hex-2-enal (1 g, 10.6 mmol, 1.0 equiv.) in tetrahydrofuran (5 ml) is added and the reaction is heated to room temperature. A saturated sodium bicarbonate–solution (20 ml) is added and the aqueous phase is extracted with pentane (2 × 50 ml). The combined organic phases are washed with a saturated sodium chloride–solution (2 × 20 ml), dried on silica, filtered and concentrated *in vacuo*. The

crude material is purified by flash chromatography (silica, pentane) to give diene **7.38** as a colorless oil (526 mg, 3.8 mmol, 36 %) that showed experimental properties comparable to those found in the literature.[153]

Formula: $C_{12}H_{22}$;

Molar mass: 166.30 g/mol;

10.5.22. 1,3,3-Trimethyl-2-(prop-1-en-1-yl)cyclohex-1-ene (7.39)

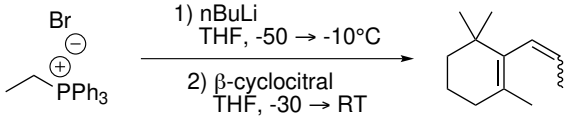

7.39
7:93 *(E)*:*(Z)*

β-cyclocitral (1.0 g, 6.6 mmol) and ethyltriphenylphosphonium bromide (2.5 g, 6.6 mmol) were transformed into diene **7.39** (21 %, 83 %m–solution in pentane) (7:93 (*E*):(*Z*)) following the procedure as for **7.37** but by using butyllithium instead of phenyllithium.

Major isomer

Formula: $C_{12}H_{20}$;

Molar mass: 164.29 g/mol;

^{1}H-NMR (400 MHz, $CDCl_3$): δ (ppm) 5.87 (d(br), 1 H, $J = 11.5$ Hz, C=C−C*H*=CHMe), 5.58 (dq, 1 H, $J = 11.5, 6.8$ Hz, C=C−CH=C*H*Me), 1.96 (tdd, 2 H, $J = 6.3, 2.1, 0.7$ Hz, C=C−CH_2−CH_2), 1.66–1.58 (m, 2 H, CH_2), 1.51 (s(br), 3 H, CH_2−C(CH_2)=C), 1.47 (d, 3 H, $J = 6.8$ Hz, C=CH(CH_3)), 1.49–1.40 (m, 2 H, CH_2), 0.95 (s, 6 H, H_3C−C−CH_3),

^{13}C-NMR (100 MHz, $CDCl_3$): δ (ppm) 134.9 (C), 128.3 (CH), 127.6 (C), 126.5 (CH), 39.2 (CH_2), 34.1 (C), 31.9 (CH_2), 28.3 (CH_3), 21.0 (CH_3), 19.4 (CH_2), 14.4 (CH_3),

Minor isomer

Signals of the minor isomer largely overlapped with those from the major isomer, except for the distinct signal: 5.37 (dq, 1 C, $J = 15.8, 6.3$ Hz); In which the scalar coupling of 15.8 Hz pointed at an (*E*)–isomer and which allowed for the determination of the (*E*):(*Z*)–ratio.

10.6. Reactions from chapter 8

10.6.1. 2,4,7,7-Tetramethyl-5,6,7,8,9,10-hexahydro-4*H*-benzo[3,4]cyclohepta[1,2-*b*]-furan (8.5)

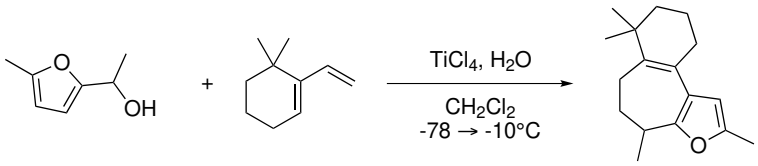

7.11 **8.4** **8.5**

General procedure (see section 10.5.7): with alcohol **7.11** (200 mg, 1.59 mmol), diene **8.4** (433 mg, 3.18 mmol), titanium(IV)chloride (377 mg, 1.99 mmol), water (286 mg, 15.9 mmol) to give **8.5** as a colorless oil (70 mg, 287 mmol, 18 %).

Formula: $C_{17}H_{24}O$;
Molar mass: 244.32 g/mol;

Major isomer

^{1}H-NMR (400 MHz, $CDCl_3$): δ (ppm) 5.92 (q(br), 1 H, $J = 1.0$ Hz, Fur$-H$), 3.07 (, 1 H, $J =$ Hz, Fur$-CH-CH_3$), 2.33 (s(br), 3 H, Fur$-CH-CH_3$), 2.26–2.18 (band, 2 H, $(Me)_2CCH_2CH_2-CH_2$), 2.21–2.16 (m, 1 H, H_3CCHCH_2-CHH), 2.14–2.06 (m, 1 H, H_3CCHCH_2-CHH), 1.87 (dddd, 1 H, $J = 13.5, 9.2, 6.7, 1.0$ Hz, $H_3CCH-CHH$), 1.70–1.61 (band, 2 H, $(Me)_2CCH_2-CH_2-CH_2$), 1.13–1.44 (m, 1 H, $H_3CCH-CHH$), 1.50–1.42 (band, 2 H, $(Me)_2C-CH_2-CH_2CH_2$),

1.25 (d, 3 H, $J = 6.7$ Hz, FurCH−CH_3), 1.04 (s, 3 H, H_3C−CCH$_3$), 1.04 (s, 3 H, H$_3$CC −CH_3),

^{13}C-NMR (125 MHz, $(CD_3)_2CO$): δ (ppm) 153.8 (C), 149.0 (C), 142.5 (C), 122.2 (C), 121.6 (C), 105.6 (CH), 39.3 (CH_2), 35.5 (C), 35.1 (CH), 33.9 (CH_2), 29.9 (CH_2), 28.0 (CH_3), 27.8 (CH_3), 25.9 (CH_2), 21.0 (CH_3), 19.7 (CH_2), 13.4 (CH_3)

10.6.2. 5,6-Dihydro-1,4-dithiine-2-carbaldehyde (8.34)

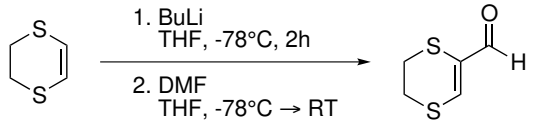

8.34

2,3-Dihydro-1,4-dithiine (1 g, 8.4 mmol, 1.0 equiv.) is dissolved in dry tetrahydrofuran (15 ml) and the solution is cooled to −78 °C. *n*-Butyllithium (4 ml, 2.5 M in hexane) is added and the reaction is stirred at the same temperature for 2 h after which dimethylformamide (930 µl, 12.6 mmol, 1.5 equiv.) is added carefully. The mixture is heated to room temperature over the course of 2 h and then quenched by adding a saturated sodium bicarbonate–solution (15 ml). The aqueous phase is extracted with diethyl ether (3 ×70 ml) and the combined organic extracts are washed with a saturated sodium chloride–solution (20 ml), dried on sodium sulfate, filtered and concentrated *in vacuo*. The crude material is purified by flash chromatography (silica, ethyl acetate:petroleum ether 1:4, v/v) to give the aldehyde **8.34** as a yellow oil (1.05 g, 7.2 mmol, 86 %) showing experimental properties identical to those reported in the literature.[154]

Formula: $C_5H_6OS_2$;

Molar mass: 148.25 g/mol;

10.6.3. (5,6-dihydro-1,4-dithiin-2-yl)methanol (8.31)

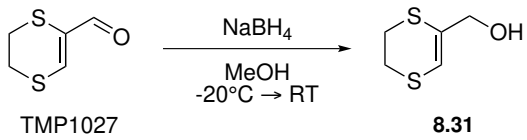

TMP1027 **8.31**

The aldehyde **10.1** (0.5 g, 3.4 mmol, 1.0 equiv.) is dissolved in dry methanol (8 ml) and the mixture is cooled to −20 °C. Sodium borohydride (193 g, 5.1 mmol, 1.5 equiv.) is added portion wise and the reaction is allowed to warm to room temperature. After 1.5 h, the reaction is cooled to 0 °C and a saturated sodium bicarbonate–solution (10 ml) is added upon which the mixture is stirred for 1.5 h. The aqueous mixture is extracted with methyl-*tert*-butyl ether (3 × 100 ml) and the combined organic extracts are dried on sodium sulfate, filtered and concentrated *in vacuo*. The resulting residue was purified with flash chromatography (silica, ethyl acetate:petroleum ether, 1:4 v/v) to give the title compound as a pale yellow oil (470 mg, 3.2 mg, 94 %) that showed experimental properties identical to those reported in the literature.[146]

Formula: $C_5H_8OS_2$;
Molar mass: 148.25 g/mol;

10.6.4. Olefination conditions E

Methyltriphenylphosphonium bromide (1.2 equiv.) was suspended in dry tetrahydrofuran (0.7 M)[1] and the suspension was cooled to −78 °C. A solution of *n*-butyllithium in hexane (2.5 M, 1.2 equiv.) was added dropwise and the mixture was gently heated to 0 °C. After cooling to −50 °C, a solution of the enone (1.0 equiv.) in tetrahydrofuran (2 M) was added dropwise and the heterogeneous mixture was heated to room temperature.

[1] relative to the limiting reagent

Petroleum ether was added and the precipitates were allowed to settle at 4 °C for 12 h. After filtration over a pad of celite the solution was carefully concentrated *in vacuo* and the crude material was filtered over a plug of silica eluting with pentane.

10.6.5. Olefination conditions F

Isopropyltriphenylphosphonium iodide (1.2 equiv.) was suspended in dry tetrahydrofuran (0.7 M)[2] and the suspension was cooled to 0 °C. A solution of *n*-butyllithium in hexane (2.5 M, 1.5 equiv.) was added dropwise and the mixture was gently heated to room temperature. After stirring for 30 min, a solution of the enone (1.0 equiv.) in tetrahydrofuran (2 M) was added dropwise and the mixture was refluxed for 3 h. After cooling to room temperature, petroleum ether was added and the precipitates were allowed to settle at 4 °C for 12 h. After filtration over a pad of celite the solution was carefully concentrated *in vacuo* and the crude material was filtered over a plug of silica eluting with pentane.

10.6.6. 3-Methylenecyclohex-1-ene (8.35)

8.35

Olefination Conditions E (section 10.6.4): with 2-cyclohexenone (1 g, 10 mmol) to give the diene **8.35** (71 mg (8m%–solution in pentane), 754 µmol, 8 %) that showed experimental properties identical to those found in the literature.[155]

Formula: C_7H_{10};
Molar mass: 94.15 g/mol;

[2] relative to the limiting reagent

10.6.7. 1-Methyl-3-methylenecyclohex-1-ene (8.36)

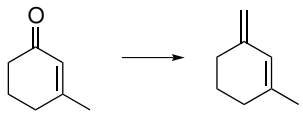

8.36

Olefination conditions E (section 10.6.4): with 3-methylcyclohex-2-enone (2 g, 18.2 mmol) to give diene **8.36** as a volatile liquid (839 mg, 7.76 mmol, 43 %) showing experimental properties identical to those found in the literature.[156]

Formula: C_8H_{12};

Molar mass: 108.18 g/mol;

10.6.8. 3-Methylenecyclohept-1-ene (8.37)

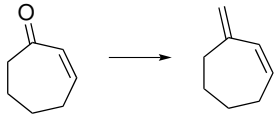

8.37

Olefination conditions E (section 10.6.4): with 3-cycloheptenone (0.5 g, 4.5 mmol) to give diene **8.37** as a volatile liquid (270 mg, 2.52 mmol, 56 %) showing experimental properties identical to those found in the literature.[157]

Formula: C_8H_{12};

Molar mass: 108.18 g/mol;

10.6.9. (*S*)-5-isopropyl-2-methylcyclohex-2-enone (8.39)

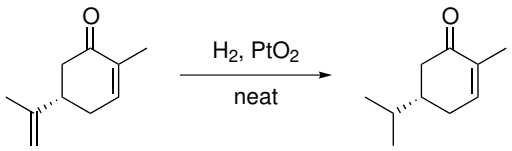

(+)-carvone **8.39**

Platinum(II)oxide (45 mg, 0.2 mmol, 0.2 equiv.) is added to 15.7 ml of (+)-carvone (100 mmol, 1.0 equiv.). The reaction is put under hydrogen atmosphere and conversion is followed by H-NMR spectroscopy. After 20 h, the catalyst is run over a small pad of silica, eluting with ethyl acetate, to give **8.39** as light brown oil in quantitative yield that showed experimental properties identical to those found in the literature.[158]

Formula: $C_{10}H_{16}O$;
Molar mass: 152.23 g/mol;

10.6.10. (*S*)-4-isopropyl-1-methyl-6-methylenecyclohex-1-ene (8.38)

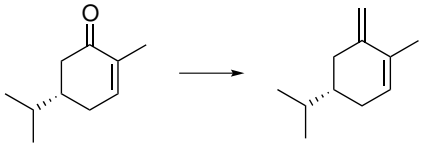

8.39 **8.38**

Olefination conditions E (section 10.6.4): with **8.39** (1 g, 6.6 mmol) to give diene **8.38** as a volatile liquid (675 mg, 4.49 mmol, 68 %).

Formula: $C_{11}H_{18}$;
Molar mass: 150.26 g/mol;

10.6.11. 6-(Dibromomethylene)-3,3-dimethylcyclohex-1-ene (8.40)

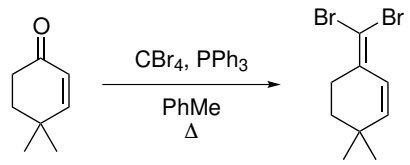

8.40

Tetrabromomethane (5.3 g, 10.1 mmol, 2.0 equiv.) is dissolved in toluene (40 ml). Triphenylphosphine) (8.5 g, 32.22 mmol, 4.0 equiv.) and 4,4-dimethylcyclohex-2-en-1-one (1 g, 8.05 mmol, 1.0 equiv.) is added and the mixture is refluxed for 18 h. After cooling to room temperature, the suspension is filtered over a pad of celite and the solids are thoroughly washed with cold petroleum ether. A cooling–filtration cycle is repeated three times. The filtrate is concentrated *in vacuo* and the residue is purified with flash chromatography (silica, petroleum ether) to give diene **8.40** in a near quantitative yield. The material showed experimental properties as those reported in the literature.[159]

Formula: $C_9H_{12}Br_2$;
Molar mass: 280.00 g/mol;

10.6.12. 3,3-Dimethyl-6-(propan-2-ylidene)cyclohex-1-ene (8.41)

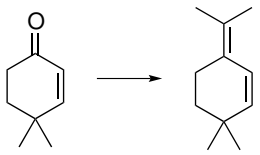

8.41

Olefination conditions F (section 10.6.5): with 4,4-dimethyl-2-cyclohexenone (410 g, 3.3 mmol) to give the diene **8.41** (355 mg (8m%–solution in pentane), 1.9 mmol, 56 %)

Formula: $C_{11}H_{18}$;

Molar mass: 150.26 g/mol;

^{1}H-NMR (400 MHz, $CDCl_3$): δ (ppm) 6.31 (d, 1 H, J = 10.1 Hz CH=C*H*), 5.46 (d, 1 H, J = 10.1 Hz C*H*=CH), 2.34 (t(br), 2 H, J = 6.5 Hz C=C–CH_2), 1.78 (s, 3 H, CH_3), 1.75 (s, 3 H, CH_3), 1.50 (t(br), 2 H, J = 6.5 Hz C=CCH_2–CH_2), 1.01 (s, 6 H, CH_3–C–CH_3),

^{13}C-NMR (100 MHz, $CDCl_3$): δ (ppm) 138.8 (C), 137.1 (CH), 127.1 (CH), 126.2 (C), 122.8 (C), 36.9 (CH_2), 29.0 (CH_3), 23.3 (CH_2), 20.5 (CH_3), 19.5 (CH_3),

10.6.13. Trimethyl((phenylthio)methyl)silane (8.48)

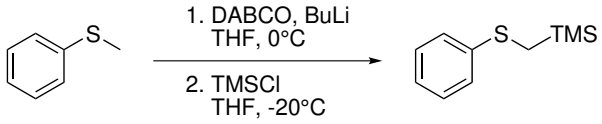

8.48

Thioanisole (2.01 g, 16.2 mmol, 1.0 equiv.) and 1,4-Diazabicyclo[2.2.2]octane (1.82 g, 16.2 mmol, 1.0 equiv.) are dissolved in tetrahydrofuran (24 ml). The mixture is cooled to 0 °C and *n*-butyllithium (6.9 ml, 2.5 M in hexanes) over a period of 12 min. The reaction is stirred at the same temperature for 1 h during which slight precipitation could be observed. After cooling to −20 °C, chlorotrimethylsilane (2.25 ml, 17.8 mmol, 1.1 equiv.) is added and the mixture is slowly heated to room temperature. The reaction is quenched by addition of a saturated ammonium chloride–solution (12 ml) and water (50 ml). The aqueous phase is extracted with diethyl ether (3 ×100 ml), the combined organic extracts are dried on sodium sulfate, filtered and concentrated *in vacuo* to give the commercial silane **8.48** as a pale yellow oil (3.2 g, purity 91 %).[160–163]

Formula: $C_{10}H_{16}SSi$;

Molar mass: 196.38 g/mol;

10.6.14. (Cyclohex-2-en-1-ylidenemethyl)(phenyl)sulfane (8.46)

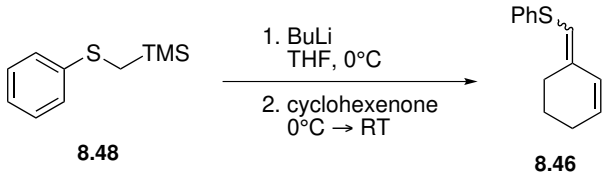

8.48 **8.46**

8.48 (1.02 g, 5.2 mmol, 1.0 equiv.) is dissolved in tetrahydrofuran (15 ml) and the solution is cooled to 0 °C. *n*-Butyllithium (2.3 ml, 2.5 M in hexane) is added and the reaction is stirred for 1 h after which cyclohex-2-en-1-one (0.5 g, 5.2 mmol, 1.0 equiv.) is added dropwise. The mixture is heated to room temperature and stirred for 30 min. The reaction is quenched by pouring the mixture into a saturated ammonium chloride–solution (25 ml). The aqueous phase is extracted with diethyl ether (3 ×25 ml) and the combined organic extracts are then washed with a sodium hydroxide–solution (15 %, 10 ml) and a saturated sodium chloride–solution (10 ml). The organic phase is dried on sodium sulfate, filtered and concentrated *in vacuo*. The crude material is purified by flash chromatography (silica, petroleum ether) to yield diene **8.46** as a colorless oil (783 mg, 3.6 mmol, 70 %) that showed experimental properties comparable to those reported in the literature.[164]

Formula: $C_{13}H_{14}S$;
Molar mass: 202.32 g/mol;

10.6.15. ((4,4-Dimethylcyclohex-2-en-1-ylidene)methyl)(phenyl)sulfane (8.49)

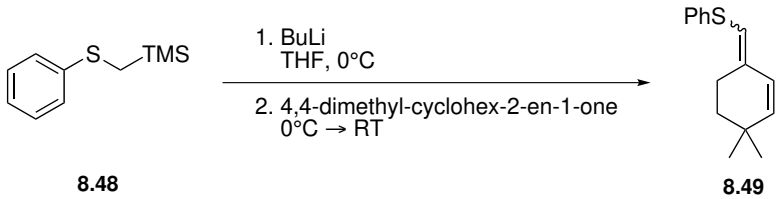

8.48 **8.49**

Procedure as for **8.46** () with: **8.48** (982 mg, 5 mmol, 1.0 equiv.) and 4,4-dimethyl-cyclohex-2-en-1-one (745 mg, 5 mmol, 1.0 equiv.) to yield diene **8.49** as a colorless oil (870.5 mg, 3.8 mmol, 76 %) that showed experimental properties comparable to those reported in the literature.[164]

Formula: $C_{15}H_{18}S$;

Molar mass: 230.37 g/mol;

(*E*)–isomer

^{1}H-NMR (400 MHz, $CDCl_3$): δ (ppm) 7.38–7.25 (overlapping band with other isomer, 4 H, Ar$-H_{ortho,meta}$), 7.20 (dd, 1 H, $^3J = 6.6$ Hz, $^4J = 1.3$ Hz, Ar$-H_{para}$), 6.50 (dd, 1 H, $^3J = 10.1$ Hz, $^4J = 0.9$ Hz, C=C $-$C*H*=C), 5.91 (m, 1 H, PhS$-$C*H*), 5.70 (dd, 1 H, $^3J = 10.1$ Hz, $^4J = 1.5$ Hz, C =C $-$CH =C*H*), 2.53–2.43 (overlapping band with other isomer, 2 H, PSC =C $-$CH_2), 1.60–1.54 (overlapping band with other isomer, 2 H, PSC =CH_2 $-$CH_2), 1.06 (s, 6 H, H_3C$-$C$-$CH_3);

^{13}C-NMR (100 MHz, $CDCl_3$): δ (ppm) 142.3 (CH), 138.9 (C), 137.1 (C), 128.9 (CH), 128.8 (CH), 125.8 (CH), 121.7 (CH), 115.4 (CH), 36.9 (CH_2), 32.6 (C), 28.9 (CH_3), 28.6 (CH_2),

(*Z*)–isomer

^{1}H-NMR (400 MHz, $CDCl_3$): δ (ppm) 7.38–7.25 (overlapping band with other isomer, 4 H, Ar $-H_{ortho,meta}$), 7.17 (dd, 1 H, $^3J = 6.5$ Hz, $^4J = 1.6$ Hz, Ar $-H_{para}$), 6.05 (m(br), 1 H, PhS $-$C*H*), 6.00 (d, 1 H, $J = 9.7$ Hz, C =C $-$C*H* =C), 5.55 (d, 1 H, $J = 9.7$ Hz, C =C $-$CH =C*H*), 2.53–2.43 (overlapping band with other isomer, 2 H, PSC =C $-$CH_2), 1.60–1.54 (overlapping band with other isomer, 2 H, PSC =CH_2 $-$CH_2), 1.05 (s, 6 H, H_3C$-$C$-$CH_3);

^{13}C-NMR (100 MHz, $CDCl_3$): δ (ppm) 139.1 (CH), 137.8 (C), 136.5 (C), 128.7 (CH), 128.3 (CH), 126.1 (CH), 125.8 (CH), 118.7 (CH), 36.0 (CH_2), 32.0 (C), 28.8 (CH_3), 23.6 (CH_2),

(*Z*)–isomer

HRMS [*m*/*z*]: [M+H]+ calcd. for $C_{15}H_{19}S^+$, 231.1202; found, 231.1195

10.6.16. 2-(Cyclohex-2-en-1-ylidene)-1,3-dithiane (8.52)

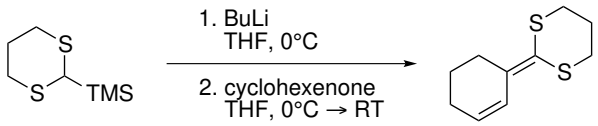

8.52

Procedure as for **8.46** with: (1,3-dithian-2-yl)trimethylsilane (160 mg, 0.83 mmol, 1.0 equiv.) and cyclohex-2-en-1-one (100 mg, 1 mmol, 1.2 equiv.) to yield diene **8.52** as a coulorless oil (72 mg, 0.29 mmol, 35 %) which showed experimental properties comparable to those found in the literature.[165]

Formula: $C_{10}H_{14}S_2$;
Molar mass: 198.35 g/mol;

10.6.17. 3+2–Cycloaddition: general procedure

(5,6-Dihydro-1,4-dithiin-2-yl)methanol (74 mg, 0.5 mmol, 1.0 equiv.) and the diene (0.75 mmol, 1.5 equiv.) were dissolved in dry dichloromethane (5 mL). The solution was cooled to −78 °C and a solution of trifloroacetic acid (76 µL, 1 mmol, 2.0 equiv.) in dichloromethane (0.5 mL) was added dropwise. The reaction was then heated slowly to room temperature and monitored by thin layer chromatography. When judged complete, the reaction was finished by adding a saturated sodium bicarbonate-solution (5 mL). The aqueous phase was extracted with dichloromethane (2 × 5 mL) and the combined extracts were washed with a saturated sodium chloride-solution (5 mL). After drying on sodium sulfate the organic phase was concentrated *in vacuo*. The crude material was with purified flash chromatography (silica, ethyl acetate:petroleum ether, 1:9 v/v).

10.6.18. 4,4,6′,6′-Tetramethyl-2′,3′,6′,7′-tetrahydrospiro[cyclohex[2]ene-1,5′-cyclopenta-[*b*][1,4]dithiine] (8.44)

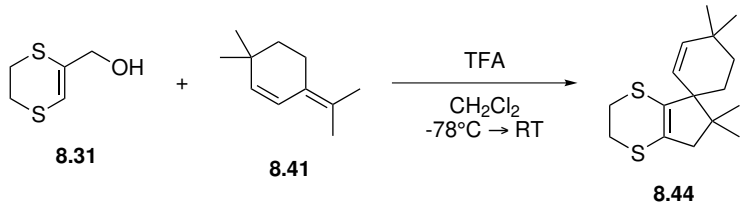

3+2–Cycloaddition procedure (section 10.6.17):

Yield: 68 %;

Formula: $C_{16}H_{24}S_2$;

Molar mass: 280.49 g/mol;

^{1}H-NMR (400 MHz, $CDCl_3$): δ (ppm) 5.59 (d(AB), 1 H, J = 10.2 Hz, HC=C*H*), 5.28 (d(AB), 1 H, J = 10.2 Hz, *H*C=CH), 3.17–3.09 (band, 4 H, S−CH_2CH_2−S), 2.30 (d(AB), 1 H, J = 14.7 Hz, SC−C*H*H), 2.16 (d(AB), 1 H, J = 14.7 Hz, SC−CH*H*), 1.70–1.56 (band, 3 H, $(Me)_2$C−CH_2−C*H*H), 1.52–1.41 (m, 1 H, $(Me)_2$C−CH_2−CH*H*), 1.03 (s, 3 H, CH_3), 1.01 (s, 3 H, CH_3), 0.99 (s, 3 H, CH_3), 0.96 (s, 3 H, CH_3),

^{13}C-NMR (100 MHz, $CDCl_3$): δ (ppm) 139.4 (CH), 128.8 (C), 127.0 (CH), 120.0 (C), 56.1 (C), 50.4 (CH_2), 43.8 (C), 34.8 (CH_2), 30.8 (C), 29.6 (CH_3), 29.3 (CH_3), 27.2 (CH_2), 27.1 (CH_2), 25.0 (CH_3), 24.7 (CH_3), 24.0 (CH_2)

HRMS [*m*/*z*]: [M+H]+ calc'd for $C_{16}H_{25}S_2^+$, 281.1392; found, 281.1403;

10.6.19. (1(*S*),6′(*R*))-6′-(phenylthio)-2′,3′,6′,7′-tetrahydrospiro[cyclohex[2]ene-1,5′-cyclopenta[*b*][1,4]dithiine] (8.51a) & ((*E*))-5-((phenylthio)methylene)-3,4b,5,6,7,8,8a,9-octahydro-2*H*-indeno[1,2-*b*]-[1,4]dithiine (8.51b)

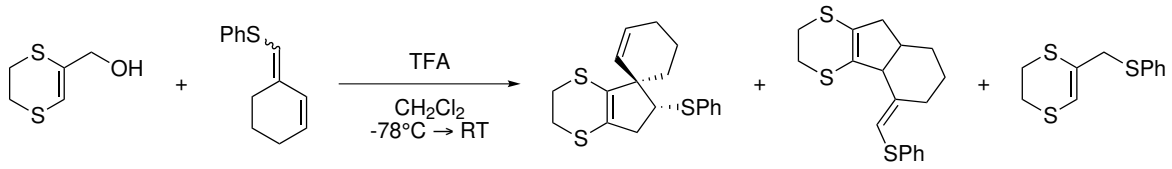

8.31 **8.46** **8.51a** (2:1 dr) **8.51b** (rac) **8.51c**

General procedure (see section 10.6.17): with DHDT–alcohol **8.31** (74 mg, 0.5 mmol), diene **8.46** (162 mg, 0.75 mmol) to give, after FC, a mixture of **8.51a** (14 %, 2:1 dr), **8.51b** (26 %) and **8.51c** (13 %). The percentages were determined from a purified sample (81 mg) by proton NMR integration. **8.51a**:

Formula: $C_{18}H_{20}S_3$;

Molar mass: 332.55 g/mol;

Major isomer

^{1}H-NMR (400 MHz, $(CD_3)_2CO$): δ (ppm) 5.97 (dt, 1 H, $J = 9.8, 3.7$ Hz, $CH_2{-}CH{=}CH$), 5.34 (dt, 1 H, $J = 9.8, 1.9$ Hz, $CH_2{-}CH{=}CH$), 3.62 (t, 1 H, $J = 7.5$ Hz, PhS$-CH$), 3.21–3.07 (overlapping band with other isomers, 4 H, S$-CH_2CH_2-$S), 2.87–2.56 (overlapping band with other isomers, 2 H, PhSCH$-CH_2$), 2.97–1.89 (m, 2 H, C=C$-CH_2$);

HSQC: 5.97 × 131.8, 5.34 × 131.2

Minor isomer

Formula: $C_{18}H_{20}S_3$;

Molar mass: 332.55 g/mol;

^{1}H-NMR (400 MHz, $(CD_3)_2CO$): δ (ppm) 6.02 (dt, 1 H, J = 10.3, 3.7 Hz, CH_2−CH=C*H*), 5.58 (dt, 1 H, J = 10.3, 1.9 Hz, CH_2−C*H*=CH), 3.59 (t, 1 H, J = 7.4 Hz, PhS−C*H*), 3.21–3.07 (overlapping band with other isomers, 4 H, S−CH_2CH_2−S), 2.87–2.56 (overlapping band with other isomers, 2 H, PhSCH−CH_2), 2.07–1.95 (m, 2 H, C=C−CH_2),
HSQC: 5.97 × 131.8

8.51b:

^{1}H-NMR (400 MHz, $CDCl_3$): δ (ppm) 7.44–7.13 (overlapping band with other isomers, 5 H, Ar−*H*); 6.08 (d(br), 1 H, J = 1.5 Hz, C=C*H*), 3.44 (d(br), 1 H, J = 6.7 Hz, C=C −C*H* −C =C), 3.21–3.07 (overlapping band with other isomers, 4 H, S−CH_2CH_2 −S), 2.73 (ddd, 1 H, J = 5.0, 3.7, 1.2 Hz, PhSC =C−C*H*H), 2.69–2.60 (overlapping band with other isomers, 2 H, H_2CSC=C−C*H*H), 2.40 (, 1 H, H_2CSC=CCH_2 −C*H*), 1.93–1.80 (overlapping band with other isomers, 1 H, PhSC=C −CH*H*), 1.76–1.66 (overlapping band with other isomers, 1 H, PhSC =CCH_2−CH*H*), 1.70–1.62 (overlapping band with other isomers, 1 H, H_2CSC =CCH_2CH −C*H*H), 1.41–1.31 (m, 1 H, H_2CSC =CCH_2CH −CH*H*), 1.33–1.22 (m, 1 H, PhSC =CCH_2−C*H*H);
HSQC: 6.08 × 117.7, 3.44 × 57.1, 2.73 × 27.4, 2.69–2.60 × 43.8, 2.40 × 37.8, 1.93–1.80 × 27.4, 1.76–1.66 × 24.4, 1.70–1.62 × 29.2, 1.41–1.31 × 29.2, 1.33–1.22 × 24.4

Alkylation product **8.51c**:

Formula: $C_{11}H_{12}S_3$;
Molar mass: 240.41 g/mol;

IUPAC: 5-((phenylthio)methyl)-2,3-dihydro-1,4-dithiine;
Formula: $C_{11}H_{12}S_3$;
Molar mass: 240.41 g/mol;
^{1}H-NMR (400 MHz, $CDCl_3$): δ (ppm) 7.44–7.13 (overlapping band with major products, 5 H, Ar−*H*); 5.99 (s(br), 1 H, C=C*H*), 3.63 (d, 1 H, J = 0.9 Hz, C=C−CH_2−SPh), 3.21–3.08 (overlapping band with major products, 4 H, S−CH_2CH_2−S);

HSQC: 5.99 × 113.0, 3.63 × 43.5

10.6.20. (1(*S*),6′(*R*))-4,4-dimethyl-6′-(phenylthio)-2′,3′,6′,7′-tetrahydrospiro[cyclohex-[2]ene-1,5′-cyclopenta[*b*][1,4]dithiine] (8.50)

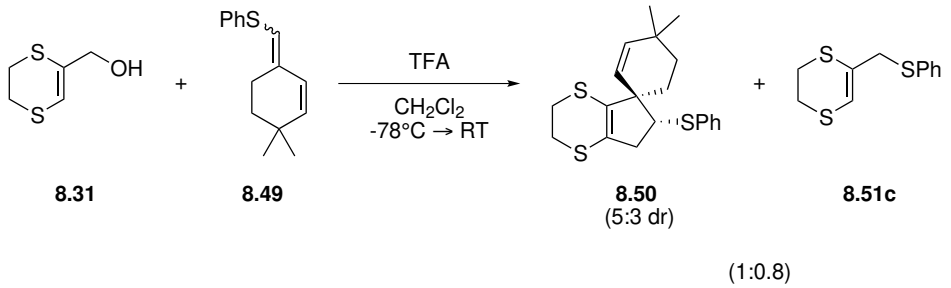

General procedure (see section 10.6.17): with DHDT–alcohol **8.31** (74 mg, 0.5 mmol), diene **8.49** (173 mg, 0.75 mmol) to give, after FC, a mixture of **8.50** (26 %, 5:3 dr) and **8.51c** (21 %). The percentages were determined from a purified sample (73 mg) by proton NMR integration.

8.50:

Formula: $C_{20}H_{24}S_3$;
Molar mass: 360.60 g/mol;

Major isomer

^{1}H-NMR (400 MHz, $CDCl_3$): δ (ppm) 5.67 (d(AB), 1 H, J = 9.9 Hz, $(Me)_2C{-}CH{=}C$), 5.18 (d(AB), 1 H, J = 9.9 Hz, $(Me)_2C{-}CH{=}CH$), 3.64 (dd, 1 H, J = 9.3, 7.6 Hz, PhS−C*H*), 3.21–2.08 (overlapping band with other isomer, 4 H, S−CH_2−CH_2−S), 2.68 (dd, 1 H, J = 15.1, 7.6 Hz, PhSCH−C*H*H), 2.60 (dd, 1 H, J = 15.1, 9.3 Hz, PhSCH−CH*H*), 2.10–2.01 (m, 1 H, $(Me)_2C{-}CHH$), 1.83–1.59 (overlapping band with other isomer, 3 H, $(Me)_2C{-}CHH{-}CH_2$), 1.03 (s), 3 H, $H_3C{-}C{-}CH_3$), 1.02 (s, 3 H, $H_3C{-}C{-}CH_3$);

HSQC: 5.67 × 142.1, 5.18 × 128.6, 3.64 × 55.8, 2.68 × 43.2, 2.60 × 43.2, 1.03 × 29.1

Minor isomer

^{1}H-NMR (400 MHz, $CDCl_3$): δ (ppm) 5.71 (d(AB), 1 H, J = 10.0 Hz, $(Me)_2C-CH{=}C$), 5.41 (d(AB), 1 H, J = 10.0 Hz, $(Me)_2C-CH{=}CH$), 3.59 (t, 1 H, J = 7.6 Hz, $PhS-CH$), 3.21–2.08 (overlapping band with other isomer, 4 H, $S-CH_2-CH_2-S$), 2.82 (dd, 1 H, J = 15.3, 7.6 Hz, $PhSCH-CHH$), 2.65 (dd, 1 H, J = 15.1, 7.6 Hz, $PhSCH-CHH$), 1.97–1.88 (m, 1 H, $(Me)_2C-CHH$), 1.83–1.59 (overlapping band with other isomer, 3 H, $(Me)_2C-CHH-CH_2$), 0.95 (s), 3 H, $H_3C-C-CH_3$);
HSQC: 5.71 × 141.4, 5.41 × 125.1, 3.59 × 55.1, 2.82 × 44.3, 2.65 × 44.3, 1.97–1.88 × 30.0, 0.95 × 29.5

HRMS [*m*/*z*]: [M+H]+ calcd. for $C_{20}H_{25}S_3^+$, 361.1113; found, 361.1108

8.51c

See **8.51** section 10.6.19

Bibliography

[1] Beutler, B.; Du, X.; Hoebe, K. From Phenomenon to Phenotype and from Phenotype to Gene: Forward Genetics and the Problem of Sepsis. *The Journal of Infectious Diseases* **2003**, *187*, S321–S326.

[2] Moresco, E. M. Y.; Li, X.; Beutler, B. Going forward with genetics: Recent technological advances and forward genetics in mice. *American Journal of Pathology* **2013**, *182*, 1462–1473.

[3] Mendel, G. Versuche über Pflanzen-Hybriden. *Verhandlungen des naturforschenden Vereines in Brünn, Bd. IV* **1866**, 3–47.

[4] Morrison, K. L.; Weiss, G. A. The origins of chemical biology. *Nature Chemical Biology* **2006**, *2*, 3–6.

[5] Anonymous, A Community of Chemists and Biologists. *Nature Chemical Biology* **2005**, *1*, 3.

[6] Ostler, E. L. Chemical Biology is..... *Chemistry Central journal* **2007**, *1*, 5.

[7] Corre, C.; Challis, G. L. Heavy Tools for Genome Mining. *Chemistry and Biology* **2007**, *14*, 7–9.

[8] Challis, G. L. Genome mining for novel natural product discovery. *Journal of Medicinal Chemistry* **2008**, *51*, 2618–2628.

[9] Jensen, P. R. Natural Products and the Gene Cluster Revolution. *Trends in Microbiology* **2016**, *24*, 968–977.

[10] Ward, A.; Allenby, N. Genome mining for the search and discovery of bioactive compounds: The Streptomyces paradigm. *FEMS Microbiology Letters* **2018**,

[11] Crick, F. Central Dogma of Molecular Biology. *Nature* **1970**, *227*, 561–563.

[12] Alonso, J. M.; Ecker, J. R. Moving forward in reverse: genetic technologies to enable genome-wide phenomic screens in Arabidopsis. *Nature reviews. Genetics* **2006**, *7*, 524–536.

[13] Nowak, M. A.; Boerlijst, M. C.; Cooke, J.; Smith, J. M. Evolution of genetic redundancy. *Nature* **1997**, *388*, 167–171.

[14] Stockwell, B. R. Chemical genetics: ligand-based discovery of gene function. *Nature reviews. Genetics* **2000**, *1*, 116–125.

[15] Kawatani, M.; Osada, H. Affinity-based target identification for bioactive small molecules. *MedChemComm* **2014**, *5*, 277–287.

[16] Schenone, M.; Dančík, V.; Wagner, B. K.; Clemons, P. a. Target identification and mechanism of action in chemical biology and drug discovery. *Nature chemical biology* **2013**, *9*, 232–240.

[17] Bunnage, M. E.; Chekler, E. L. P.; Jones, L. H. Target validation using chemical probes. *Nature chemical biology* **2013**, *9*, 195–199.

[18] Sakamoto, S.; Kabe, Y.; Hatakeyama, M.; Yamaguchi, Y.; Handa, H. Development and application of high-performance affinity beads: Toward chemical biology and drug discovery. *Chemical Record* **2009**, *9*, 66–85.

[19] Ito, T.; Ando, H.; Suzuki, T.; Ogura, T.; Hotta, K.; Imamura, Y.; Yamaguchi, Y.; Handa, H. Identification of a primary target of thalidomide teratogenicity. *Science (New York, N.Y.)* **2010**, *327*, 1345–1350.

[20] Chen, G.; Heim, A.; Riether, D.; Yee, D.; Milgrom, Y.; Gawinowicz, M. A.; Sames, D. Reactivity of functional groups on the protein surface: Development of epoxide probes for protein labeling. *Journal of the American Chemical Society* **2003**, *125*, 8130–8133.

[21] Tsukiji, S.; Miyagawa, M.; Takaoka, Y.; Tamura, T.; Hamachi, I. Ligand-directed tosyl chemistry for protein labeling in vivo. *Nature Chemical Biology* **2009**, *5*, 341–343.

[22] Molina, D. M.; Jafari, R.; Ignatushchenko, M.; Seki, T.; Larsson, E. A.; Dan, C.; Sreekumar, L.; Cao, Y.; Nordlund, P. Monitoring drug target engagement in cells and tissues using the cellular thermal shift assay. *Science* **2013**, *341*, 84–87.

[23] Lomenick, B. *et al.* Target identification using drug affinity responsive target stability (DARTS). *Proceedings of the National Academy of Sciences* **2009**, *106*, 21984–21989.

[24] Overington, J. P.; Al-Lazikani, B.; Hopkins, A. L. How many drug targets are there? *Nature Reviews Drug Discovery* **2006**, *5*, 993–996.

[25] Ziegler, S.; Pries, V.; Hedberg, C.; Waldmann, H. Target identification for small bioactive molecules: Finding the needle in the haystack. *Angewandte Chemie - International Edition* **2013**, *52*, 2744–2792.

[26] Hicks, G. R.; Raikhel, N. V. Small molecules present large opportunities in plant biology. *Annual review of plant biology* **2012**, *63*, 261–282.

[27] Hicks, G. R.; Raikhel, N. V. Plant chemical biology: are we meeting the promise? *Frontiers in Plant Science* **2014**, *5*, 1–5.

[28] Rojas-Pierce, M.; Titapiwatanakun, B.; Sohn, E. J.; Fang, F.; Larive, C. K.; Blakeslee, J.; Cheng, Y.; Cuttler, S.; Peer, W. A.; Murphy, A. S.; Raikhel, N. V. Arabidopsis P-Glycoprotein19 Participates in the Inhibition of Gravitropism by Gravacin. *Chemistry and Biology* **2007**, *14*, 1366–1376.

[29] Noutoshi, Y.; Okazaki, M.; Kida, T.; Nishina, Y.; Morishita, Y.; Ogawa, T.; Suzuki, H.; Shibata, D.; Jikumaru, Y.; Hanada, A.; Kamiya, Y.; Shirasu, K. Novel Plant Immune-Priming Compounds Identified via High-Throughput Chemical Screening Target Salicylic Acid Glucosyltransferases in Arabidopsis. *The Plant Cell* **2012**, *24*, 3795–3804.

[30] Botté, C. Y. *et al.* Chemical inhibitors of monogalactosyldiacylglycerol synthases in Arabidopsis thaliana. *Nature Chemical Biology* **2011**, *7*, 834–842.

[31] Dejonghe, W.; Russinova, E. Target identification strategies in plant chemical biology. *Frontiers in Plant Science* **2014**, *5*, 1–11.

[32] Taunton, J.; Hassig, C. A.; Schreiber, S. L. A mammalian histone deacetylase related to the yeast transcriptional regulator Rpd3p. *Science* **1996**, *272*, 408–411.

[33] Kim, Y. K.; Chang, Y.-T. Tagged library approach facilitates forward chemical genetics. *Molecular bioSystems* **2007**, *3*, 392–397.

[34] Ahn, Y. H.; Chang, Y. T. Tagged small molecule library approach for facilitated chemical genetics. *Accounts of Chemical Research* **2007**, *40*, 1025–1033.

[35] Mitsopoulos, G.; Walsh, D. P.; Chang, Y. T. Tagged library approach to chemical genomics and proteomics. *Current Opinion in Chemical Biology* **2004**, *8*, 26–32.

[36] Chamni, S.; He, Q.-l.; Dang, Y.; Bhat, S.; Liu, J. O.; Romo, D. Diazo reagents with small steric footprints for simultaneous arming/SAR studies of alcohol-containing natural products via O-H insertion. *ACS chemical biology* **2011**, *6*, 1175–1181.

[37] Peddibhotla, S.; Dang, Y.; Liu, J. O.; Romo, D. Simultaneous arming and structure/activity studies of natural products employing O-H insertions: an expedient and versatile strategy for natural products-based chemical genetics. *Journal of the American Chemical Society* **2007**, *129*, 12222–12231.

[38] Zhou, C.-Y.; Li, J.; Peddibhotla, S.; Romo, D. Mild arming and derivatization of natural products via an In(OTf)$_3$-catalyzed arene iodination. *Organic letters* **2010**, *12*, 2104–2107.

[39] Yamaguchi, J.; Yamaguchi, A. D.; Itami, K. C-H bond functionalization: emerging synthetic tools for natural products and pharmaceuticals. *Angewandte Chemie (International ed. in English)* **2012**, *51*, 8960–9009.

[40] Li, J.; Cisar, J. S.; Zhou, C.-Y.; Vera, B.; Williams, H.; Rodríguez, A. D.; Cravatt, B. F.; Romo, D. Simultaneous structure-activity studies and arming of natural products by C-H amination reveal cellular targets of eupalmerin acetate. *Nature chemistry* **2013**, *5*, 510–517.

[41] Fiori, K. W.; Du Bois, J. Catalytic intermolecular amination of C-H bonds: method development and mechanistic insights. *Journal of the American Chemical Society* **2007**, *129*, 562–568.

[42] Zalatan, D. N.; Du Bois, J. Understanding the differential performance of $Rh_2(esp)_2$ as a catalyst for C-H amination. *Journal of the American Chemical Society* **2009**, *131*, 7558–7559.

[43] Kanoh, N.; Kumashiro, S.; Simizu, S.; Kondoh, Y.; Hatakeyama, S.; Tashiro, H.; Osada, H. Immobilization of Natural Products on Glass Slides by Using a Photoaffinity Reaction and the Detection of Protein–Small-Molecule Interactions. *Angewandte Chemie* **2003**, *115*, 5742–5745.

[44] Kanoh, N.; Honda, K.; Simizu, S.; Muroi, M.; Osada, H. Photo-cross-linked small-molecule affinity matrix for facilitating forward and reverse chemical genetics. *Angewandte Chemie (International ed. in English)* **2005**, *44*, 3559–3562.

[45] Vallès-Miret, M.; Bradley, M. A generic small-molecule microarray immobilization strategy. *Tetrahedron Letters* **2011**, *52*, 6819–6822.

[46] Kanoh, N.; Nakamura, T.; Honda, K.; Yamakoshi, H.; Iwabuchi, Y.; Osada, H. Distribution of photo-cross-linked products from 3-aryl-3-trifluoromethyldiazirines and alcohols. *Tetrahedron* **2008**, *64*, 5692–5698.

[47] Valot, G.; Garcia, J.; Duplan, V.; Serba, C.; Barluenga, S.; Winssinger, N. Diversity-oriented synthesis of diverse polycyclic scaffolds inspired by the logic of sesquiterpene lactones biosynthesis. *Angewandte Chemie (International ed. in English)* **2012**, *51*, 5391–5394.

[48] Chen, M. S.; White, M. C. A predictably selective aliphatic C-H oxidation reaction for complex molecule synthesis. *Science (New York, N.Y.)* **2007**, *318*, 783–787.

[49] Chen, K.; Baran, P. S. Total synthesis of eudesmane terpenes by site-selective C-H oxidations. *Nature* **2009**, *459*, 824–828.

[50] Chen, M. S.; White, M. C. Combined effects on selectivity in Fe-catalyzed methylene oxidation. *Science (New York, N.Y.)* **2010**, *327*, 566–571.

[51] Moteki, S. a.; Usui, A.; Zhang, T.; Solorio Alvarado, C. R.; Maruoka, K. Site-selective oxidation of unactivated C(sp^3)-H bonds with hypervalent iodine(III) reagents. *Angewandte Chemie (International ed. in English)* **2013**, *52*, 8657–8660.

[52] Dondoni, A. The emergence of thiol-ene coupling as a click process for materials and bioorganic chemistry. *Angewandte Chemie (International ed. in English)* **2008**, *47*, 8995–8997.

[53] Khripach, V.; Zhabinskii, V.; De Groot, A. Twenty years of brassinosteroids: Steroidal plant hormones warrant better crops for the XXI century. *Annals of Botany* **2000**, *86*, 441–447.

[54] Divi, U. K.; Krishna, P. Brassinosteroid: a biotechnological target for enhancing crop yield and stress tolerance. *New Biotechnology* **2009**, *26*, 131–136.

[55] Vriet, C.; Russinova, E.; Reuzeau, C. Boosting crop yields with plant steroids. *The Plant cell* **2012**, *24*, 842–857.

[56] Noguchi, T.; Fujioka, S.; Choe, S.; Takatsuto, S.; Tax, F. E.; Yoshida, S.; Feldmann, K. A. Biosynthetic Pathways of Brassinolide in Arabidopsis. *Plant Physiology* **2000**, *124*, 201–210.

[57] Kim, B. K.; Fujioka, S.; Takatsuto, S.; Tsujimoto, M.; Choe, S. Castasterone is a likely end product of brassinosteroid biosynthetic pathway in rice. *Biochemical and Biophysical Research Communications* **2008**, *374*, 614–619.

[58] Kim, T.-W.; Wang, Z.-Y. Brassinosteroid signal transduction from receptor kinases to transcription factors. *Annual review of plant biology* **2010**, *61*, 681–704.

[59] Schumacher, K.; Chory, J. Brassinosteroid signal transduction: still casting the actors. *Current opinion in plant biology* **2000**, *3*, 79–84.

[60] Clouse, S. D. Brassinosteroid signal transduction: from receptor kinase activation to transcriptional networks regulating plant development. *The Plant cell* **2011**, *23*, 1219–1230.

[61] Hothorn, M.; Belkhadir, Y.; Dreux, M.; Dabi, T.; Noel, J. P.; Wilson, I. a.; Chory, J. Structural basis of steroid hormone perception by the receptor kinase BRI1. *Nature* **2011**, *474*, 467–471.

[62] Wang, Z. Y.; Seto, H.; Fujioka, S.; Yoshida, S.; Chory, J. BRI1 is a critical component of a plasma-membrane receptor for plant steroids. *Nature* **2001**, *410*, 380–383.

[63] De Smet, I.; Voß, U.; Jürgens, G.; Beeckman, T. Receptor-like kinases shape the plant. *Nature Cell Biology* **2009**, *11*, 1166–1173.

[64] Sorkin, A.; Von Zastrow, M. Endocytosis and signalling: Intertwining molecular networks. *Nature Reviews Molecular Cell Biology* **2009**, *10*, 609–622.

[65] Irani, N. G. *et al.* Fluorescent castasterone reveals BRI1 signaling from the plasma membrane. *Nature chemical biology* **2012**, *8*, 583–589.

[66] Geldner, N.; Hyman, D. L.; Wang, X.; Schumacher, K.; Chory, J. Endosomal signaling of plant steroid receptor kinase BRI1, Supplemental Data5. **2007**, 1598–1602.

[67] Kaksonen, M.; Roux, A. Mechanisms of clathrin-mediated endocytosis. *Nature Reviews Molecular Cell Biology* **2018**, *19*, 313–326.

[68] Dejonghe, W.; Mishev, K.; Russinova, E. The brassinosteroid chemical toolbox. *Current Opinion in Plant Biology* **2014**, *22*, 48–55.

[69] De Rybel, B. *et al.* Chemical Inhibition of a Subset of Arabidopsis thaliana GSK3-like Kinases Activates Brassinosteroid Signaling. *Chemistry and Biology* **2009**, *16*, 594–604.

[70] Asami, T.; Min, Y. K.; Nagata, N.; Yamagishi, K.; Takatsuto, S.; Fujioka, S.; Murofushi, N.; Yamaguchi, I.; Yoshida, S. Characterization of brassinazole, a triazole-type brassinosteroid biosynthesis inhibitor. *Plant physiology* **2000**, *123*, 93–100.

[71] Sekimata, K.; Kimura, T.; Kaneko, I.; Nakano, T.; Yoneyama, K.; Takeuchi, Y.; Yoshida, S.; Asami, T. A specific brassinosteroid biosynthesis inhibitor, Brz2001: Evaluation of its effects on Arabidopsis, cress, tobacco, and rice. *Planta* **2001**, *213*, 716–721.

[72] Sekimata, K.; Han, S. Y.; Yoneyama, K.; Takeuchi, Y.; Yoshida, S.; Asami, T. A specific and potent inhibitor of brassinosteroid biosynthesis possessing a dioxolane ring. *Journal of Agricultural and Food Chemistry* **2002**, *50*, 3486–3490.

[73] Oh, K.; Yamada, K.; Asami, T.; Yoshizawa, Y. Synthesis of novel brassinosteroid biosynthesis inhibitors based on the ketoconazole scaffold. *Bioorganic and Medicinal Chemistry Letters* **2012**, *22*, 1625–1628.

[74] Rozhon, W.; Husar, S.; Kalaivanan, F.; Khan, M.; Idlhammer, M.; Shumilina, D.; Lange, T.; Hoffmann, T.; Schwab, W.; Fujioka, S.; Poppenberger, B. Genetic Variation in Plant CYP51s Confers Resistance against Voriconazole, a Novel Inhibitor of Brassinosteroid-Dependent Sterol Biosynthesis. *PLoS ONE* **2013**, *8*.

[75] Dejonghe, W. Endomembrane trafficking and brassinosteroid signaling from a small molecule perspective . Ph.D. thesis, 2015.

[76] Li, J. J. *Progress in Heterocyclic Chemistry*; Elsevier Masson SAS, 2000; Vol. 12; pp 37–56.

[77] Schmid, S. L. ATP is required for receptor-mediated endocytosis in intact cells. *The Journal of Cell Biology* **1990**, *111*, 2307–2318.

[78] Dejonghe, W. *et al.* Mitochondrial uncouplers inhibit clathrin-mediated endocytosis largely through cytoplasmic acidification. *Nature Communications* **2016**, *7*, 11710.

[79] Sandvig, K. Acidification of the cytosol inhibits endocytosis from coated pits. *The Journal of Cell Biology* **2004**, *105*, 679–689.

[80] Mishev, K. *et al.* Nonselective Chemical Inhibition of Sec7 Domain-Containing ARF GTPase Exchange Factors. *The Plant Cell* **2018**, *30*, 2573–2593.

[81] Kahn, R.; Volpicelli-Daley, L.; Bowzard, B.; Shrivastava-Ranjan, P.; Li, Y.; Zhou, C.; Cunningham, L. Arf family GTPases: roles in membrane traffic and microtubule dynamics. *Biochemical Society Transactions* **2005**, *33*, 1269.

[82] Yorimitsu, T.; Sato, K.; Takeuchi, M. Molecular mechanisms of Sar/Arf GTPases in vesicular trafficking in yeast and plants. *Frontiers in Plant Science* **2014**, *5*, 1–12.

[83] Donaldson, J. G.; Jackson, C. L. ARF family G proteins and their regulators: roles in membrane transport, development and disease. *Nature Reviews Molecular Cell Biology* **2011**, *12*, 362–375.

[84] Beck, R.; Ravet, M.; Wieland, F. T.; Cassel, D. The COPI system: Molecular mechanisms and function. *FEBS Letters* **2009**, *583*, 2701–2709.

[85] Bonifacino, J. S.; Lippincott-Schwartz, J. Coat proteins: shaping membrane transport. *Nature Reviews Molecular Cell Biology* **2003**, *4*, 409–414.

[86] Rosquete, M. R.; Davis, D. J.; Drakakaki, G. The Plant Trans-Golgi Network: Not Just a Matter of Distinction. *Plant Physiology* **2018**, *176*, 187–198.

[87] Nebenfuhr, A. Brefeldin A: Deciphering an Enigmatic Inhibitor of Secretion. *PLANT PHYSIOLOGY* **2002**, *130*, 1102–1108.

[88] Langhans, M.; Förster, S.; Helmchen, G.; Robinson, D. G. Differential effects of the brefeldin A analogue (6R)-hydroxy-BFA in tobacco and Arabidopsis. *Journal of Experimental Botany* **2011**, *62*, 2949–2957.

[89] Hardcastle, I. R. *et al.* Small-molecule inhibitors of the MDM2-p53 protein-protein interaction based on an isoindolinone scaffold. *Journal of medicinal chemistry* **2006**, *49*, 6209–6221.

[90] Friedlaender, P. Ueber eine Reaction des Phenolphtaleïns. *Berichte der deutschen chemischen Gesellschaft* **1893**, *26*, 172–179.

[91] Hubacher, M. H. The Preparation of 2-(4-Hydroxybenzoyl)-benzoic Acid. *Journal of the American Chemical Society* **1946**, *68*, 718–719.

[92] Orndorff, W. R.; Murray, M. R. R. A NEW CLASS OF PHTHALEINS—MIXED PHTHALEINS—FORMED BY HEATING p-HYDROXYBENZOYL-o-BENZOIC ACID WITH PHENOLS. *Journal of the American Chemical Society* **1917**, *39*, 679–697.

[93] Orndorff, W. R.; Yang, S. T. The structure of phenolphthalein oxime. *Journal of the American Chemical Society* **1923**, *45*, 1926–1933.

[94] Diels, O.; Alder, K. Synthesen in der hydroaromatischen Reihe; 1. Mitteilung: Anlagerungen von "Di-en"-kohlenwasserstoffen. *Liebigs Annalen der Chemie* **1928**, *460*, 98–122.

[95] Gothelf, K. V.; Jørgensen, K. A. Asymmetric Metal-catalyzed 1 , 3-Dipolar Cycloaddition Reactions. *Chemical Reviews* **1998**, *98*, 863–909.

[96] Woodward, R. B.; Hoffmann, R. Stereochemistry of Electrocyclic Reactions. *Journal of the American Chemical Society* **1965**, *87*, 395–397.

[97] Zimmerman, H. E. On Molecular Orbital Correlation Diagrams, the Occurrence of Möbius Systems in Cyclization Reactions, and Factors Controlling Ground- and Excited-State Reactions. I. *Journal of the American Chemical Society* **1966**, *88*, 1564–1565.

[98] Sustmann, R. Orbital energy control of cycloaddition reactivity. *Pure and Applied Chemistry* **1974**, *40*, 569–593.

[99] Fleming, I. *Molecular Orbitals and Organic Chemical Reactions*; John Wiley & Sons, Ltd: Chichester, UK, 2010; pp 1–57.

[100] Sustmann, R. A simple model for substituent effects in cycloaddition reactions. II. The diels-alder reaction. *Tetrahedron Letters* **1971**, *12*, 2721–2724.

[101] Fukui, K.; Yonezawa, T.; Shingu, H. A Molecular Orbital Theory of Reactivity in Aromatic Hydrocarbons. *The Journal of Chemical Physics* **1952**, *20*, 722–725.

[102] Huisgen, R. First Two-step 1,3-Dipolar Cycloadditions: Nonstereospecificity. *Journal of the American Chemical Society* **1986**, *108*, 6401–6402.

[103] Nicolaou, K. C.; Snyder, S. a.; Montagnon, T.; Vassilikogiannakis, G. The Diels-Alder reaction in total synthesis. *Angewandte Chemie (International ed. in English)* **2002**, *41*, 1668–1698.

[104] Brieger, G.; Bennett, J. N. The intramolecular Diels-Alder reaction. *Chemical Reviews* **1980**, *80*, 63–97.

[105] Hoffmann, N. Photochemical reactions as key steps in organic synthesis. *Chemical Reviews* **2008**, *108*, 1052–1103.

[106] Lee-Ruff, E.; Mladenova, G. Enantiomerically Pure Cyclobutane Derivatives and Their Use in Organic Synthesis. *Chemical Reviews* **2003**, *103*, 1449–1484.

[107] Bach, T. Stereoselective Intermolecular [2 + 2]-Photocycloaddition Reactions and Their Application in Synthesis. *Synthesis* **2002**, *1998*, 683–703.

[108] Ebner, C.; Carreira, E. M. Cyclopropanation Strategies in Recent Total Syntheses. *Chemical Reviews* **2017**, *117*, 11651–11679.

[109] Bourissou, D.; Guerret, O.; Gabbaï, F. P.; Bertrand, G. Stable Carbenes. *Chemical Reviews* **2000**, *100*, 39–92.

[110] Rauk, A. *Orbital Interaction Theory of Organic Chemistry*; John Wiley & Sons, Inc.: New York, USA, 2000.

[111] Fleming, I. *Molecular Orbitals and Organic Chemical Reactions*; John Wiley & Sons, Ltd: Chichester, UK, 2009.

[112] Huisgen, R. 1,3-Dipolar Cycloadditions. Past and Future. *Angewandte Chemie International Edition in English* **1963**, *2*, 565–598.

[113] Mandal, D. K. *Pericyclic Chemistry*; Elsevier, 2018.

[114] Gerard, B.; Jones, G.; Porco, J. A. A biomimetic approach to the rocaglamides employing photogeneration of oxidopyryliums derived from 3-hydroxyflavones. *Journal of the American Chemical Society* **2004**, *126*, 13620–13621.

[115] Masuya, K.; Domon, K.; Tanino, K.; Kuwajima, I. Highly regio- and stereoselective [3+2] cyclopentanone annulation using a 3-(alkylthio)-2-siloxyallyl cationic species. *Journal of the American Chemical Society* **1998**, *120*, 1724–1731.

[116] Domon, K. M. K.; Tanino, K.; Kuwajima, I. A New Synthetic Method for Cyclopentanones via Formal [3+2] Cycloaddition Reaction. *Synlett* **1996**, *1996*, 157–158.

[117] Yamazaki, S.; Fujitsuka, H.; Takara, F.; Inoue, T. Utilization of selenium-directed [2 + 2] cycloadditions: concise synthesis of (±)-fragranol. *J. Chem. Soc., Perkin Trans. 1* **1994**, 695–700.

[118] Yamazaki, S.; Fujitsuka, H.; Yamabe, S.; Tamura, H. Selenium-directed stereoselective [2 + 2] cycloaddition reactions promoted by Lewis acids: a novel zwitterionic intermediate. *The Journal of Organic Chemistry* **1992**, *57*, 5610–5619.

[119] Fort, A. W. Capture of a Favorskii Intermediate by Furan. *Journal of the American Chemical Society* **1962**, *84*, 4979–4981.

[120] Cramer, C. J.; Barrows, S. E. Quantum Chemical Characterization of Cycloaddition Reactions between the Hydroxyallyl Cation and Dienes of Varying. **1998**, *3263*, 5523–5532.

[121] Cramer, C. J.; Barrows, S. E. Quantum chemical characterization of cycloaddition reactions between 1,3-butadiene and oxyallyl cations of varying electrophilicity. *Journal of Physical Organic Chemistry* **2000**, *13*, 176–186.

[122] Hoffmann, H. M. R. The Cycloaddition of Allyl Cations to 1,3-Dienes: General Method for the Synthesis of Seven-Membered Carbocycles. New Synthetic Methods(40). *Angewandte Chemie International Edition in English* **1984**, *23*, 1–19.

[123] Harmata, M.; Wacharasindhu, S. The [4 + 3]-Cycloaddition/Quasi-Favorskii Process. Synthesis of the Carbocyclic Core of Tricycloclavulone. *Organic Letters* **2005**, *7*, 2563–2565.

[124] Harmata, M. The (4 + 3)-cycloaddition reaction: simple allylic cations as dienophiles. *Chem. Commun.* **2010**, *46*, 8886–8903.

[125] Pattenden, G.; Winne, J. M. An intramolecular [4+3]-cycloaddition approach to rameswaralide inspired by biosynthesis speculation. *Tetrahedron Letters* **2009**, *50*, 7310–7313.

[126] Winne, J. M.; Catak, S.; Waroquier, M.; Van Speybroeck, V. Scope and mechanism of the (4+3) cycloaddition reaction of furfuryl cations. *Angewandte Chemie (International ed. in English)* **2011**, *50*, 11990–11993.

[127] Denoo, B. Biomimetische geneesmiddelenontwikkeling : studie van de oxidatieve variatie van polycyclische koolstofskeletten. 2012.

[128] Houk, K.; Paddon-Row, M.; Rondan, N.; Wu, Y.; Brown, F.; Spellmeyer, D.; Metz, J.; Li, Y.; Loncharich, R. Theory and modeling of stereoselective organic reactions. *Science* **1986**, *231*, 1108–1117.

[129] Molander, G. A.; Czakó, B.; St. Jean, D. J. A general route toward the synthesis of the cladiellin skeleton utilizing a SmI2-mediated cyclization. *Journal of Organic Chemistry* **2006**, *71*, 1172–1180.

[130] Oh, J.; Lee, C.-R.; Chun, K. H. A one–pot convenient procedure for the synthesis of *C*-glycoside via cycloaddition of dichloroketene to glycol and dechlorination of the cycloadduct. *Synthetic Communications* **2002**, *32*, 2349–2353.

[131] Guo, Y.; Zhang, Y.; Xiao, M.; Xie, Z. Biomimetic Syntheses of Callistrilones A-E via an Oxidative [3 + 2] Cycloaddition. *Organic Letters* **2018**, *20*, 2509–2512.

[132] Thorat, S. S.; Palange, M. N.; Kontham, R. Four-Step Total Synthesis of (+)-Yaoshanenolides A and B. *ACS Omega* **2018**, *3*, 7036–7045.

[133] Okamoto, K.; Hayashi, T.; Rawal, V. H. Simple chiral diene ligands provide high enantioselectivities in transition-metal-catalyzed conjugate addition reactions. *Organic Letters* **2008**, *10*, 4387–4389.

[134] Eyring, H. The Activated Complex in Chemical Reactions. *The Journal of Chemical Physics* **1935**, *3*, 107–115.

[135] Eschenmoser, A.; Ruzicka, L.; Jeger, O.; Arigoni, D. Eine stereochemische Interpretation der biogenetischen Isoprenregel bei den Triterpenen. *Helvetica Chimica Acta* **1955**, *38*, 1890–1904.

[136] Eschenmoser, A.; Arigoni, D. Revisited after 50 years: The 'stereochemical interpretation of the biogenetic isoprene rule for the triterpenes'. *Helvetica Chimica Acta* **2005**, *88*, 3011–3050.

[137] Krenske, E. H.; Houk, K. N.; Harmata, M. Origin of Stereoselectivity in the (4 + 3) Cycloadditions of Chiral Alkoxy Siloxyallyl Cations with Furan. *Organic Letters* **2010**, *12*, 444–447.

[138] Krenske, E. H.; Houk, K. N.; Harmata, M. Computational Analysis of the Stereochemical Outcome in the Imidazolidinone-Catalyzed Enantioselective (4 + 3)-Cycloaddition Reaction. *The Journal of Organic Chemistry* **2015**, *80*, 744–750.

[139] Kouridaki, A.; Montagnon, T.; Kalaitzakis, D.; Vassilikogiannakis, G. Using singlet oxygen to synthesise the CDE-ring system of the pectenotoxins. *Organic and Biomolecular Chemistry* **2013**, *11*, 537–541.

[140] Han, X.; Li, H.; Hughes, R. P.; Wu, J. Gallium(III)-catalyzed three-component (4+3) cycloaddition reactions. *Angewandte Chemie - International Edition* **2012**, *51*, 10390–10393.

[141] Callebaut, B.; Hullaert, J.; Van Hecke, K.; Winne, J. M. An Intramolecular Cycloaddition Approach to the Kauranoid Family of Diterpene Metabolites. *Organic Letters* **2019**, *21*, 310–314.

[142] Hullaert, J.; Laplace, D. R.; Winne, J. M. A Three-Step Synthesis of the Guaianolide Ring System. *European Journal of Organic Chemistry* **2014**, *2014*, 3097–3100.

[143] Laplace, D. R.; Verbraeken, B.; Van Hecke, K.; Winne, J. M. Total synthesis of (+/-)-frondosin B and (+/-)-5-epi-liphagal by using a concise (4+3) cycloaddition approach. *Chemistry - A European Journal* **2014**, *20*, 253–262.

[144] Zhou, M.; Geng, H.-c.; Zhang, H.-b.; Dong, K.; Wang, W.-g.; Du, X.; Li, X.-N.; He, F.; Qin, H.-B.; Li, Y.; Pu, J.-X.; Sun, H.-D. Scopariusins, A New Class of ent -Halimane Diterpenoids Isolated from Isodon scoparius , and Biomimetic Synthesis of Scopariusin A and Isoscoparin N. *Organic Letters* **2013**, *15*, 314–317.

[145] Katritzky, A. R.; Serdyuk, L.; Xie, L.; Ghiviriga, I. Efficient Syntheses of 2-Functionalized Thiophenes, Cyclopent[b]thiophenes, and Polysubstituted Benzo[b]thiophenes from 2-(Benzotriazol-1-ylmethyl)thiophenes. *Journal of Organic Chemistry* **1997**, *62*, 6215–6221.

[146] Hullaert, J.; Winne, J. M. (5,6-Dihydro-1,4-dithiin-2-yl)methanol as a Versatile Allyl-Cation Equivalent in (3+2) Cycloaddition Reactions. *Angewandte Chemie - International Edition* **2016**, *55*, 13254–13258.

[147] Roling, O.; Wendeln, C.; Kauscher, U.; Seelheim, P.; Galla, H. J.; Ravoo, B. J. Layer-by-layer deposition of vesicles mediated by supramolecular interactions. *Langmuir* **2013**, *29*, 10174–10182.

[148] Joshi, M. C.; Wicht, K. J.; Taylor, D.; Hunter, R.; Smith, P. J.; Egan, T. J. In vitro antimalarial activity, β-haematin inhibition and structure-activity relationships in a series of quinoline triazoles. *European Journal of Medicinal Chemistry* **2013**, *69*, 338–347.

[149] Wessig, P.; Möllnitz, K. Nanoscale molecular rods with a new building block for solubility enhancement. *Journal of Organic Chemistry* **2008**, *73*, 4452–4457.

[150] Francke, W.; Reith, W. 2,9-dioxabicyclo[4.2.1]Nonan - darstellung, massenspektroskopie und umlagerung eines neuen heterocyclischen systems. *Tetrahedron Letters* **1981**, *22*, 2029–2032.

[151] Dujardin, G.; Poirier, J. M. Michael addition of aromatic heterocyclic compounds to α, β-unstaurated ketones – 3-oxalkylation of furans, insoles and thiophenes. *Bulletin de la Societe chimique de France* **1994**, *131*, 900–909.

[152] Dong, D.-J.; Li, Y.; Wang, J.-Q.; Tian, S.-K. Tunable stereoselective alkene synthesis by treatment of activated imines with nonstabilized phosphonium ylides. *Chemical Communications* **2011**, *47*, 2158–2160.

[153] Baeckvall, J. E.; Schink, H. E.; Renko, Z. D. A stereocontrolled organopalladium route to 2,5-disubstituted pyrrolidine derivatives. Application to the synthesis of a venom alkaloid of the ant species Monomorium latinode. *The Journal of Organic Chemistry* **1990**, *55*, 826–831.

[154] Caputo, R.; Ferreri, C.; Isita, P.; Longobardo, L.; Mastroianni, D.; Palumbo, G. Chemistry of Ethanediyl S,S-Acetals - 4. Promising Way to Cis-Substituted Olefins, Stereoselectively from Carbonyl Compounds. *Synthetic Communications* **1992**, *22*, 1345–1350.

[155] Adam, W.; Alt, C.; Braun, M.; Denninger, U.; Zang, G. Central and Lateral Bicyclo [1.1.0] butane Bond Cleavage with Subsequent Wagner-Meerwein Rearrangements

or Carbene Formation in the 185-nm Photolysis of. *Journal of the American Chemical Society* **1991**, *113*, 4563–4571.

[156] Eilbracht, P.; Jelitte, R.; Trabold, P. Regioselective synthesis of substituted bicyclo[3.2.1]oct-3-ene-2,8-diones via double carbonylation of 1,3-cyclohexadienes. *Chemische Berichte* **1986**, *119*, 169–181.

[157] Groenewold, G. S.; Gross, M. L. Reaction of the Vinyl Methyl Ether Cation Radical and 1,3-Butadiene: A Two-step Cycloaddition. *Journal of the American Chemical Society* **1984**, *106*, 6575–6579.

[158] Wang, Z.-Y.; Bai, M.-Y.; Oh, E.; Zhu, J.-Y. Brassinosteroid signaling network and regulation of photomorphogenesis. *Annual review of genetics* **2012**, *46*, 701–724.

[159] Hopf, H.; Kämpen, J.; Bubenitschek, P.; Jones, P. G. En route to 7,7,8,8-tetraethynyl-p-quinodimethane (TEQ). *European Journal of Organic Chemistry* **2002**, 1708–1721.

[160] Corey, E. J.; Seebach, D. Phenylthiomethyllithium and Bis(phenylthio)methyllithium. *The Journal of Organic Chemistry* **1966**, *31*, 4097–4099.

[161] Kocienski, P. J. Phenylthiomethyltrimethylsilane : a new formyl anion synthon. *Tetrahedron Letters* **1980**, *21*, 1559–1562.

[162] Eberhardt, G. G.; Butte, W. A. A Catalytic Telomerization Reaction of Ethylene with Aromatic Hydrocarbons. *The Journal of Organic Chemistry* **1964**, *29*, 2928–2932.

[163] Screttas, C. G.; Eastham, J. F. Alkyllithium-Amine Crystalline Complexes. *Journal of the American Chemical Society* **1965**, *87*, 3276–3277.

[164] East, M. B.; Ager, D. J. A Comparison of the Reactions of [(Phenylthio)(trimethylsilyl)methyl]lithium with a,β-Unsaturated Ketones and Those of Other Acyl Anion Equivalents Containing Sulfur. *Journal of Organic Chemistry* **1986**, *51*, 3983–3992.

[165] Seebach, D.; Kolb, M.; Grobel, B. ß er Anwendungsbreite zur Herstellung von Keten-thioacetalen. *Chemische Berichte* **1973**, *106*, 2277–2290.

Nederlandstalige samenvatting

1. Inleiding

Dit doctoraatswerk kan onderverdeeld worden in drie onderscheiden delen. In een eerste deel wordt ingegaan op een discipline die we *chemische biologie* noemen, een interdisciplinair onderzoeksdomein op de grens tussen chemie en biologie. De uitdagingen voor beide wetenschappen zijn in deze niet min. We beschrijven het ontwikkelen van strategieën om de synthese van kleine moleculaire tools te stroomlijnen en passen deze verder toe in twee heel specifieke contexten in het systeem–biologisch onderzoek in planten.

Een tweede deel is eerder fundamenteel van aard en gaat dieper in op een klasse van organisch chemische transformaties die we cycloaddities noemen. Mechanistische inzichten in dit type van reacties is van groot belang om de uitkomst en de mogelijke toepassingen van deze omzettingen beter te kunnen begrijpen. De hoofdstukken in dit deel beschrijven gedetailleerde experimentele en theoretische studies naar twee specifieke voorbeelden van dit soort reacties: (4+3)– en (2+3)–cycloaddities.

Het derde deel beschrijft alle experimentele details die belangrijk zijn om de conclusies in dit werk te ondersteunen.

2. KLEINE MOLECULEN IN BIOLOGISCH ONDERZOEK: ONDERZOEK NAAR BRASSINOSTEROIDE SIGNALISATIE EN MEMBRAAN TRAFIEK IN PLANTEN

2.1. Chemische biologie

Biologie is geëvolueerd van een heel beschrijvende wetenschap naar een discipline die in staat is om in te grijpen in biologische systemen en voorspellingen te kunnen doen over hoe systemen zullen evolueren. De era van de genetica heeft ons in staat gesteld om heel nauwkeurig te kunnen bepalen wat de bouwstenen van cellen zijn, maar de inzichten in hoe deze bouwstenen samenwerken en interageren is nog altijd gefragmenteerd en speculatief.

Essentieel in de vooruitgang van deze inzichten is de ontwikkeling van een discipline die men chemische biologie noemt. Kleine organische moleculen worden hier gebruikt om door interactie met proteïnen en andere biosystemen, de cel te verstoren waardoor biologen inzicht kunnen krijgen in de manier waarop de cel functioneert. Deze aanpak heeft een aantal voordelen ten opzichte van de klassieke genetische methoden en wordt daarom meer en meer toegepast.

Chemische biologie steunt op het gebruik van kleine organische moleculen en derivaten daarvan die binden met eiwitten in de cel. Deze verstoring zorgt voor een verandering in uiterlijke kenmerken (het fenotype) die gelinkt zijn aan een veranderde functie van de betrokken eiwitten.

Kleine organische moleculen met interessante activiteit moeten in de regel aangepast en getuned worden om optimaal gebruikt te kunnen worden als biologische tool. Deze aanpassingen dienen onder andere voor het verbeteren van hun activiteit, maar veel belangrijker is het introduceren van zogenaamde afiniteitsmatrices om te komen tot affiniteitsprobes. Deze stellen ons in staat om het eiwit dat bindt met de organische molecule (het ligand) te isoleren en karakteriseren (fig. 1). Als affiniteitsmatrix wordt vaak gebruik gemaakt van biotine omdat dit ons in staat stelt om de volledige probe te immobiliseren

op een streptavidinekolom.

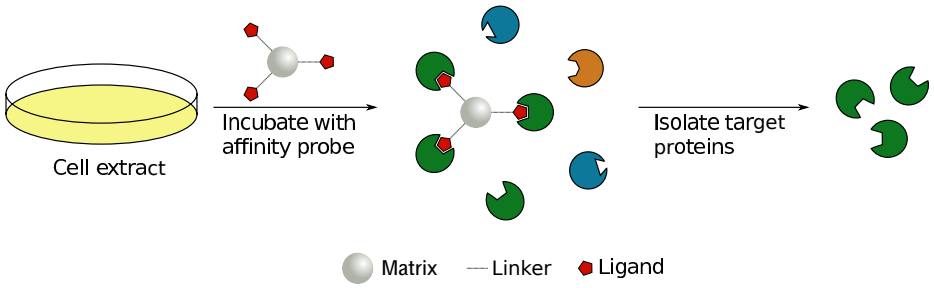

Figure 1. – General scheme for affinity purification

Het aanpassen van kleine organische moleculen stelt de chemicus voor soms heel grote uitdagingen en er zijn twee verschillende strategieën die gevolgd kunnen worden om te komen tot die aanpassingen. Ofwel wordt de molecule helemaal opnieuw opgebouwd en worden er in dit proces strategische wijzigingen in de structuur geïntroduceerd (doel–gebaseerde derivatisatie), ofwel zoekt de chemicus manieren om de molecule zoals hij bestaat aan te passen (diversiteit–gebaseerde derivatisatie) (fig. 2).

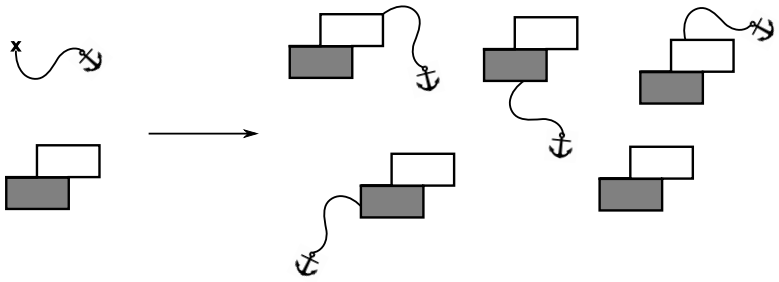

(a) Diversiteit–gebaseerde derivatisatie

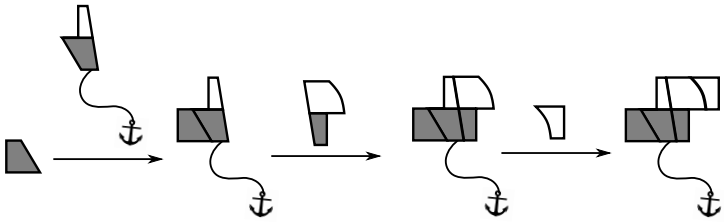

(b) Doel–gebaseerde derivatisatie

Figure 2. – Verschillende derivatisatiestrategieën

Het spreekt voor zich dat de tweede optie veruit de meest interessante is maar wel de meest uitdagende want men kan alleen bouwen op de inherente reactiviteit van moleculaire structuur. Het opnieuw opbouwen van de molecule is dan wel de meest veelzijdige manier om nieuwe structurele elementen in te bouwen, deze hersynthese doorvoeren neemt soms veel tijd beslag en kan op termijn vrij duur worden.

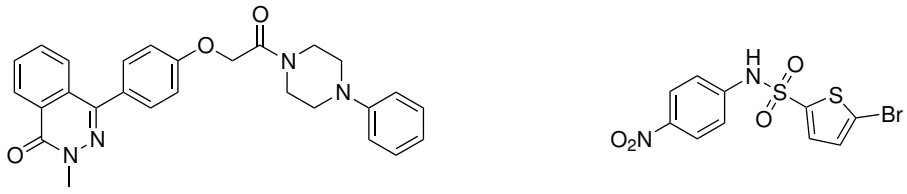

Secdin (SCD) Endosidin9 (ES9)

Figure 3. – Bio–actieve kleine moleculen als basis voor een algemene derivatisatiestratgeie

In dit doctoraatswerk hebben we onze focus gelegd op twee kleine organische moleculen die geïdentificeerd waren in fenotypische screens in planten (fig. 3), waarin men moleculen selecteert op basis van interessante uiterlijke kenmerken die ze veroorzaken na toediening. De strategie die we ontwikkelden was dan ook op maat van deze twee specifieke producten en bestond erin om de moleculen te voorzien van een allylgroep. We vonden dat de allylgroep een heel geschikte chemische eenheid bleek te zijn omdat het ons toelaat om heel wat verschillende chemische transformaties mee uit te voeren (fig. 4).

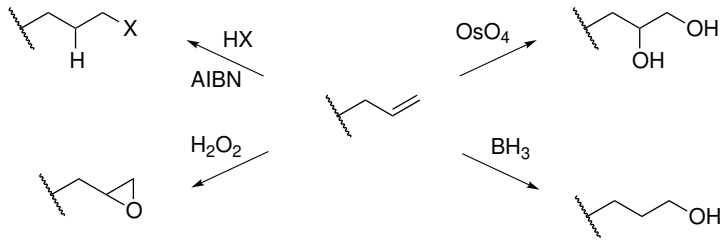

Figure 4. – Mogelijkheden van de allylgroep

2.2. Op zoek naar een specifieke inhibitor van endocytose in planten

Het labo van prof. Russinova doet al geruime tijd onderzoek naar het brassinosteroide signalisatie pad in *Arabidopsis thaliana*. Dit biochemisch mechanisme is verantwoordelijk voor communicatie tussen de buitenkant van de cel en de celkern. Signalen in de vorm van planthormonen worden aan de buitenkant van de cel opgevangen en doorgegeven aan de celkern door een cascade van biochemische interacties tussen verschillende eiwitten. In de kern worden dan bepaalde genen vertaald in eiwitten die onder andere functies vervullen in planteigenschappen zoals: zaadopbrengst, biomassa, stressresistentie, enz. Biologen hebben een link aangetoond met een ander biochemisch pad genaamd endocytose dat verantwoordelijk is voor het transport van essentiële onderdelen tussen

de buitenkant van de cel en verschillende intracelullaire componenten. Het onderliggend mechanisme voor deze connectie bleek echter nog onduidelijk.

Een kleine organische molecule, Endosidin9 (ES9, (fig. 3)), waarvan aangetoond was dat het een effect had op endocytose en bijgevolg ook op het brassinosteroide signalisatie pad, diende in dit onderzoek als startpunt voor de zoektocht naar nieuwe derivaten met een betere activiteit en ook voor de ontwikkeling van een affiniteitsprobe om het cellulair target van ES9 te vinden. De vooropgestelde strategie stelde ons inderdaad in staat om een functionele probe (fig. 5) te ontwikkelen die ons inderdaad een eerste indicatie gaf van een mogelijk eiwit dat interageerde met ES9. Dit eiwit bleek clathrine te zijn en is essentieel voor endocytose.

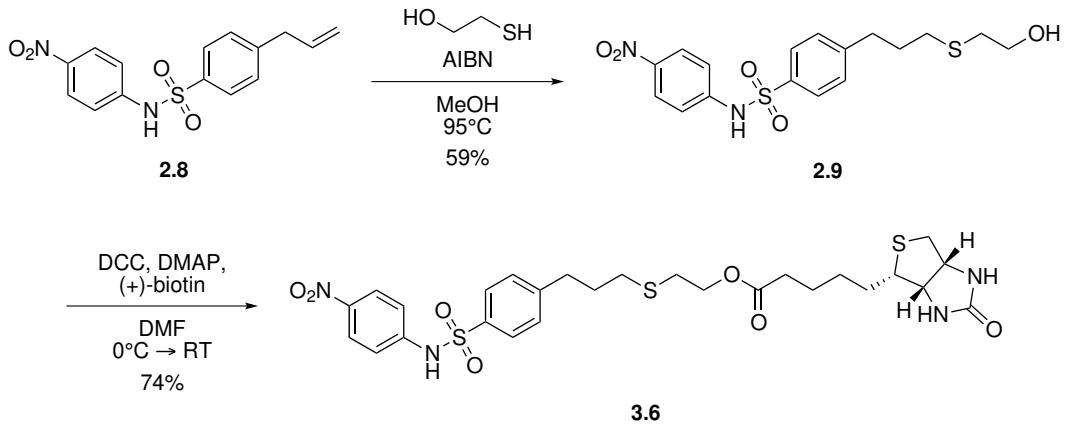

Figure 5. – Affiniteitsprobe gebaseerd op ES9

Opvallend was echter dat ES9 een welbepaalde niet–specifieke activiteit (protonofoor) vertoonde in de zin dat het elektrische potentialen over verschillende celmembranen verstoort. De structuur van ES9 verklaarde de protonofore aangezien het een zuur proton bevat en bovendien heel erg hydrofoob is. Op die manier kan het zowel in geladen als ongeladen toestand doorheen de membranen bewegen en de protonenbalans aan beide

zijden verstoren wat uiteindelijk leidt tot veranderingen in de elektrochemische potentiaal over deze membranen (fig. 6).

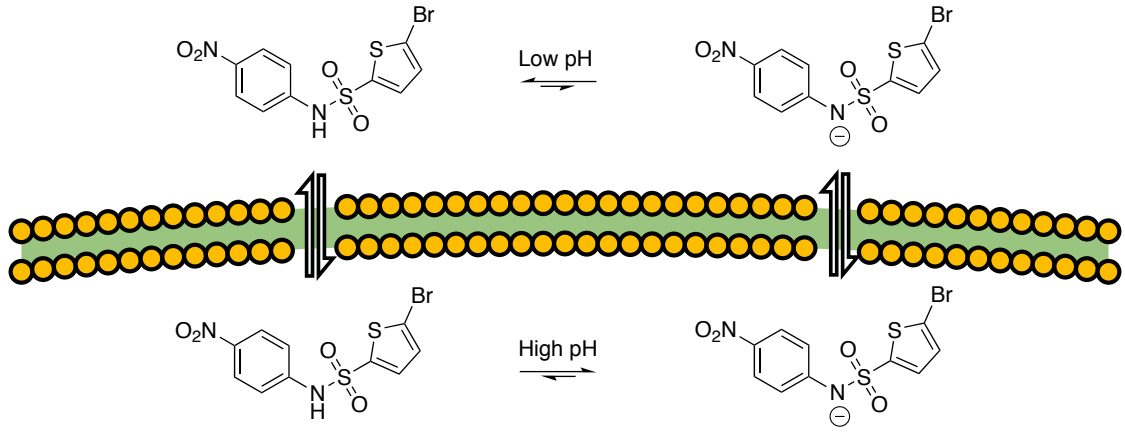

Figure 6. – Protonofoor in actie

Hoewel een relevant eiwit kon geïsoleerd worden dat mogelijks bond met ES9, was het moeilijk om beide activiteiten volledig los te koppelen van elkaar. Om die reden werd tijd geïnvesteerd om een derivaat te ontwikkelen dat specifiek interageerde met het gevonden eiwit. Door de p$K_a$van het proton van ES9 te beïnvloeden door de nitro–groep te verwijderen, konden we inderdaad een analoog vinden (ES9-17) dat nog steeds bond met het vooropgestelde target clathrine maar niet de protonofore eigenschappen vertoonde.

We konden aantonen dat ES9-17 specifiek de functie van clathrine inhibeert en bovendien de enige specifieke inhibitor is van endocytose in planten.

2.3. Op zoek naar het eiwittarget van secdin

Een tweede onderzoeksproject draaide rond de molecule Secdin die eveneens geïdentificeerd was in het labo van prof. Russinova. Secdin bleek ook endocytose te beïnvloeden,

en bijgevolg dus ook het brassinosteroide signalisatie pad. De strategie om allylgroepen te introduceren bleek hier ook de beste optie te zijn. Op die manier konden drie generaties affiniteitsprobes ontwikkeld worden, waarbij met elke generatie een verbetering van de affiniteit beoogd werd (figs. 7 to 9).

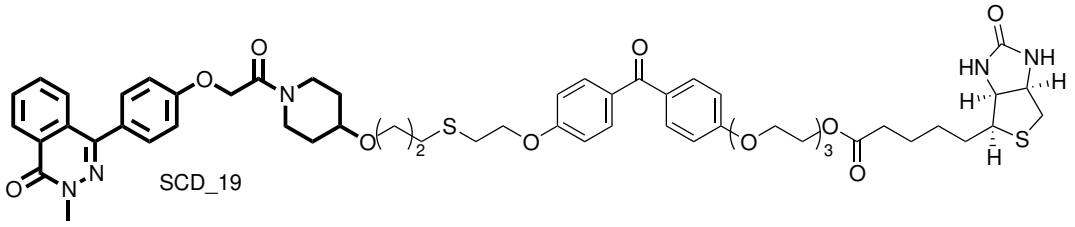

4.25

Figure 7. – Eerste generatie

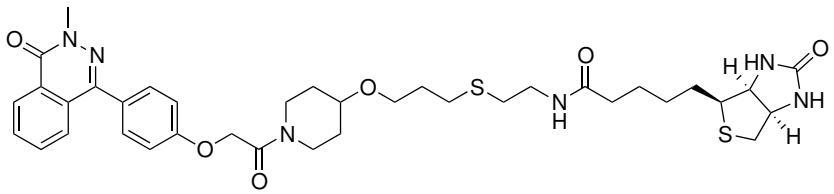

2.12

Figure 8. – Tweede generatie

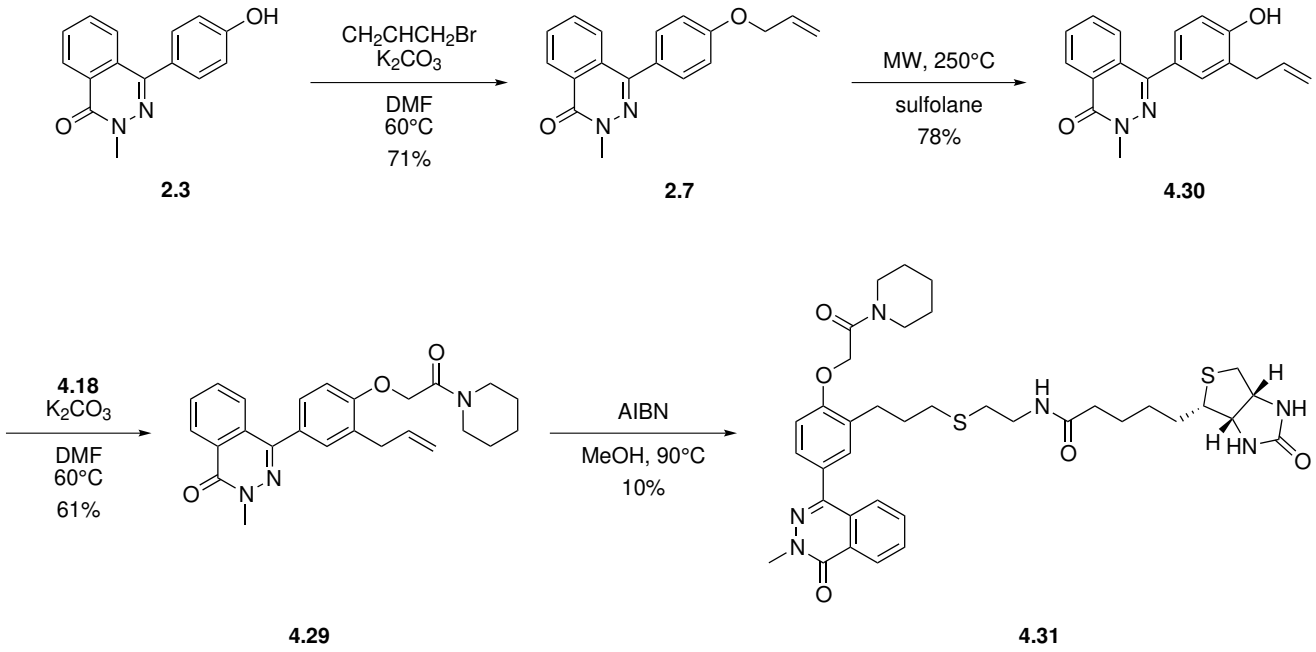

Figure 9. – Derde generatie

Experimenten in planten hebben uiteindelijk aangetoond dat Secdin bindt met *guanine–exchange factors* (GEF). Deze eiwitten spelen een belangrijke rol bij de activatie/deactivatie cyclus van de *adenosine–ribosylation factor* (ARF) familie van GTPasen. De actieve toestand van ARF eiwitten initiëren onder andere het rekruteren van *coat* eiwitten die essentieel zijn voor endocytose.

3. Kationische cycloaddities: mechanistische rationalisatie van selectiviteit en toepassing in het genereren van complexe carbocyclische verbindingen

3.1. Inleiding: cycloaddities en hun mechanismes

Cycloaddities zijn een van de meest waardevolle reacties in de toolbox van de organische chemist. Het zijn heel efficiënte processen waarbij in een enkele stap twee bindingen

gevormd worden door twee onverzadigde reactiepartners met elkaar te laten reageren. De meeste van de goed gedocumenteerde cycloadditie (zoals de Diels–Alder reactie) verlopen via mechanismes die zich goed laten voorspellen en rationaliseren. Cycloadditie verlopen ofwel via een geconcerteerd of een stapsgewijs mechanisme (fig. 10). Let wel, geconcerteerd en pericyclisch zijn geen synoniemen van elkaar. Terwijl geconcerteerd betekent dat beide bindingen tegelijk gevormd worden, betekent pericyclisch dat de reactie verloopt via een transitietoestand waarin de elektronen een gesloten kring vormen. Een pericyclisch proces is per definitie dus altijd geconcerteerd terwijl dit omgekeerd niet zo is.

De wetmatigheden die deze eigenschappen bepalen werden uitvoerig bestudeerd en gerapporteerd door onder andere Woodward, Hoffmann en Susstman. De eerste twee ontwikkelden de zogenaamde Woodward–Hoffmann regels die voorspellen of een cycloadditie kan verlopen via een geconcerteerd dan wel een stapsgewijs proces. Het is *a priori* heel moeilijk om uit maken of een cycloadditie stapsgewijs dan wel geconcerteerd verloopt, maar de reactie–uitkomst kan wel al deels verraden welke van de twee het geweest moet zijn. Geconcerteerde processen verlopen in de regel veel selectiever wat betreft stereochemische uitkomst en het optreden van nevenreacties.

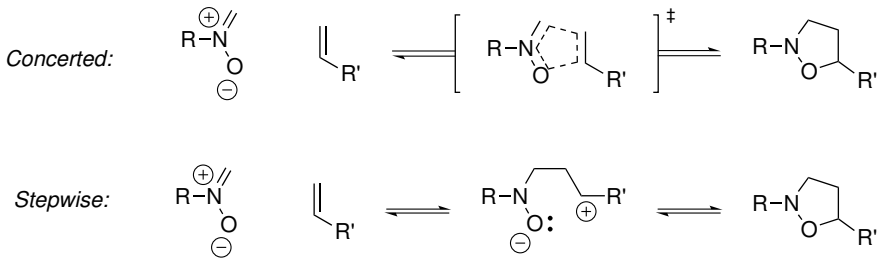

Figure 10. – Geconcerteerde en stapsgewijze additie van nitronen en olefinen

3.2. Stereoselectiviteit in stapsgewijze (4+3)–cycloaddities van furfuryl kationen

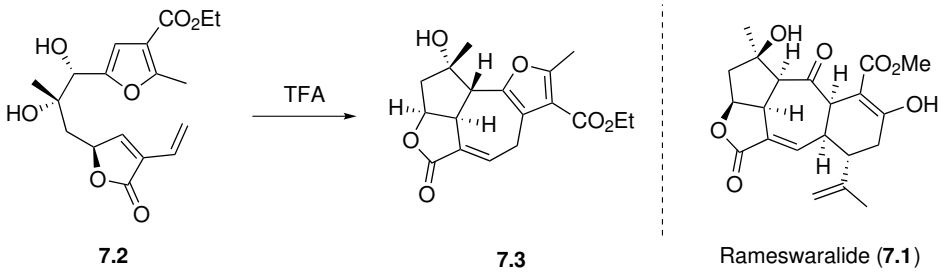

Figure 11. – Onverwachte dehydratieve (4+3)–cycloadditie in de totaalsynthese van Rameswaralide

In 2009 rapporteerden Pattenden en Winne een nieuwe dehydratieve (4+3)–cycloheptannulatie tussen een furfuryl alcohol en een 1,3–dieen, tijdens synthetische studies naar het diterpeen rameswaralide (fig. 11). Deze omzetting verloopt via de vorming van een furfuryl kation dat gegenereerd kan worden door zowel Brønstedt als Lewis zuren (fig. 12).

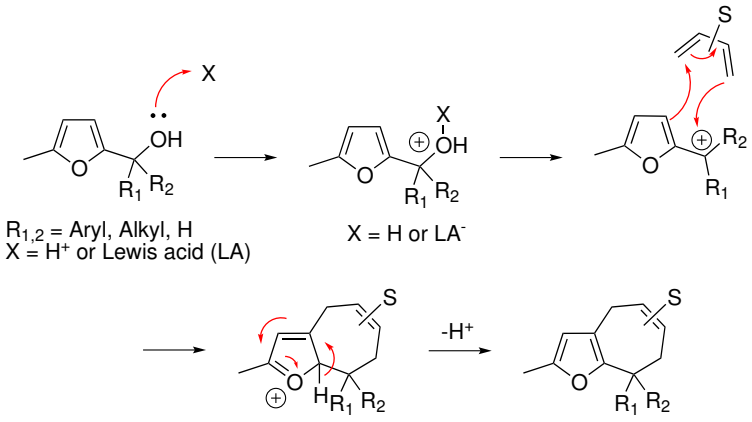

Figure 12. – Algemeen verloop van de (4+3)–cycloadditie tussen een furfurylkation en een 1,3–dieen

Opmerkelijk was de heel brede toepasbaarheid van deze reactie wat betreft de mogelijke dieen–reactiepartners.

Tijdens het thesisonderzoek van de auteur, werd een heel efficiënte en stereoselectieve reactie waargenomen tussen een tertiair furfuryl kation en α–fellandreen, een sesquiterpeen (fig. 13).

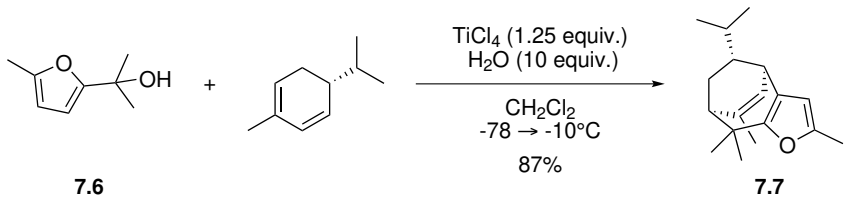

Figure 13. – Selectieve reactie tussen een furfurylkation en fellandreen

Eerder theoretisch onderzoek had uitgewezen dat deze reactie mogelijks verloopt via een stapsgewijs reactiepad, wat zou betekenen dat het optreden van nevenreacties heel waarschijnlijk is en dat bovendien niet kan verwacht worden dat de stereoselectiviteit erg groot zal zijn; hoewel fellandreen in de literatuur beschreven wordt als heel selectief te zijn, ook in stapsgewijze processen. Dit spoorde ons aan om een theoretische studie te doen, in samenwerking met het *Center for Molecular Modeling*, om de dynamische details van deze opmerkelijk omzetting bloot te leggen. Uit deze studie bleek dat deze cycloadditie verloopt langs een stapsgewijs reactiepad, maar met een duidelijk gepreorganiseerd karakter (fig. 14).

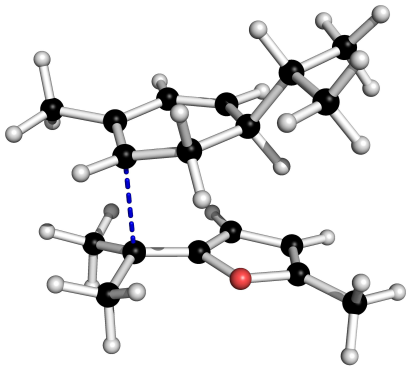

Figure 14. – Gepreorganiseerde geometrie van stapswijze omzetting

Dit betekent dat de geometrie van de snelheidsbepalende stap, hoewel niet geconcerteerd, toch heel compact is en op die manier, althans geometrisch, vergelijkbaar met die van een geconcerteerd proces. Dit gegeven stelt ons in staat om op zijn minst de selectiviteit van deze omzetting te rationaliseren, gezien de inherente stabiliteit van het kation dat doorheen de reactiecoördinaat loopt.

3.3. Toepassingen van allylkation cycloaddities en verdere mechanistische beschouwingen

Een furfurylkation kan beschouwd worden als een gestabiliseerd allylkation. We hebben een poging ondernomen om deze reactieve precursor te gebruiken om het skelet van het natuurproduct scopariusine op te bouwen. Hoewel het basisskelet relatief toegankelijk bleek te zijn, bleek de verdere decoratie van de koolstofkern vrij moeilijk te zijn.

De toepasbaarheid van de (4+3)–cycloadditie tussen furfurylkationen en 1,3–diënen is in onze groep al meerdere keren aangetoond. Deze heeft echter het nadeel dat de furan slechts beperkt kan aangewend worden om andere structurele elementen te introduceren. Zo is de synthese van naakte koolstofskeletten bijvoorbeeld niet vanzelfsprekend. Om die reden werd in onze groep gezocht naar een andere gestabiliseerde allylkation precursor,

die ons toelaat om het heterocyclisch fragment na reactie te verwijderen. Verschillende testen resulteerden in de identificatie van dihydrodithiin (DHDT) methanol als geschikte kation precursor (fig. 15).

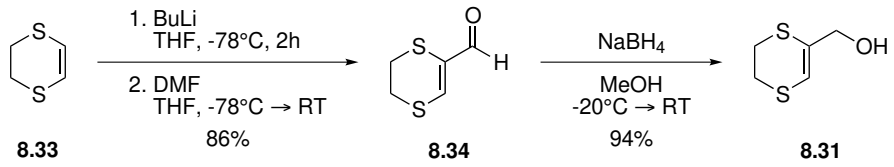

Figure 15. – Synthese van DHDT methanol

De reactie tussen het DHDT kation en een 1,3–dieen bleek echter voornamelijk aanleiding te geven tot een (3+2)–cycloadditie, wat resulteert in cyclopentanoide koolstofskeletten. Deze reactie werd in ons labo verder ontwikkeld tot een veelbelovende synthesemethode. De competitie tussen (4+3)– en (3+2)–cycloadditie was het meest uitgesproken in het geval van zogenaamde *trans*–locked diënen. Deze kunnen niet roteren rond de enkelvoudige koolstof–koolstof binding die de twee π–systemen met elkaar verbindt en kunnen om geometrische redenen geen aanleiding geven tot (4+3)–cycloadducten.

We hebben onze focus gelegd op deze *trans–locked* diënen om de dynamica van deze omzetting beter te kunnen begrijpen. In het bijzonder hebben we gebruik gemaakt van methylideen–gebaseerde diënen die vrij eenvoudig bereid kunnen worden uit verschillende cyclohexenonen (fig. 16a). De *exo*–methylideen koolstof zorgde echter voor een hoge gevoeligheid voor polymerisatie tijdens de kationische cycloadditie; blokkeren van deze positie is dus noodzakelijk gebleken (fig. 16b).

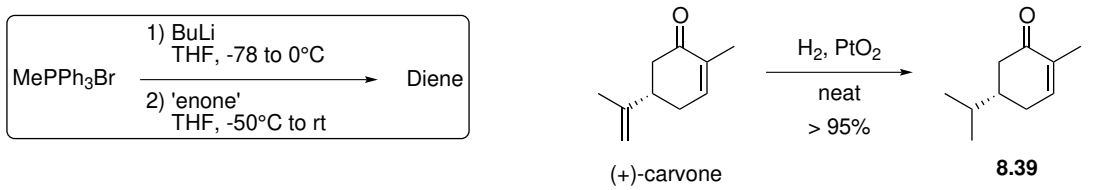

8.35
8%
from cyclohex-2-enone

8.36
43%
from 3-methylcyclohex-2-enone

8.37
28%
from cyclohept-2-enone

8.38
68%
from **8.39**

(a) Methylideen–cyclohexeen diënen

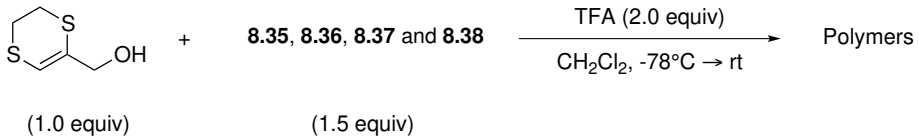

(b) Poging tot (3+2)–cycloadditie reactie

Figure 16. – Eerste testen met methylideen–cyclohexeen gebaseerde diënen

De aard van substitutie toont echter een niet–voor de hand liggend effect op de reactiviteit van deze dienen. Substitutie met broom atomen of een dithiaan–groep geeft geen cycloadditie terwijl twee methylgroepen wel een reactief dieen geven (fig. 16a). Substitutie met een thiofenylgroep geeft ook aanleiding tot cycloadditie, zij het wel met een lager rendement en de vorming van een nevenproduct in de vorm van een nucleofiel additieproduct van het DHDT kation met de thiofenylzwavel (fig. 17).

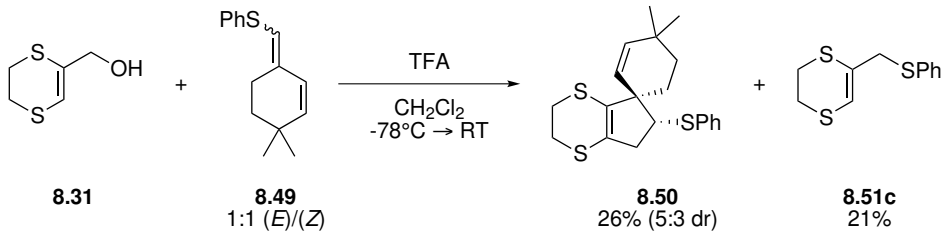

8.31 **8.49** 1:1 (*E*)/(*Z*) **8.50** 26% (5:3 dr) **8.51c** 21%

Figure 17. – Cycloadditie met een thiofenyl–gebaseerd methylideen dieen

Deze trend in reactiviteit suggereert een effect op de energetische grondtoestand van het dieen, eerder dan een invloed op de nucleofiele eigenschappen.

Onze huidige hypothese houdt in dat de vorming van een pre–reactief complex essentieel is voor de verder cycloadditiereactie. Verschillende substituenten hebben een verschillende invloed op de orbitaalbijdrage van de π–binding tot het moleculair orbitaal. Een kleine bijdrage (zoals bij broom of dithiaan) zal aanleiding geven tot een moeizame vorming van het pre-reactief complex; grotere bijdragen (zoals bij methylgroepen en thiofenyl) verhogen die bijdrage waardoor het complex wel gevormd kan worden en verder cycloadditie mogelijk wordt.

Appendices

Curriculum Vitae

EDUCATION

- Ghent University — Doctor of Science: Chemistry, 2013-2018
- Ghent University — Master of Science in Chemistry, 2010-2012
  Thesis: Biomimetic drug development via oxidative variation of polycyclic hydrocarbons
- Ghent University — Bachelor of Science in Chemistry, 2007-2010
  Bachelorproject: Synthetic studies towards Frondosin B based on a furfuryl cation cycloaddition

RESEARCH

1. PhD, UGhent — 2013-2018 (Organic Synthesis lab - Prof. Dr. Johan Winne)
   - 2015-2018: Teaching assistant (AAP)
   - 2013-2014: PhD fellow

   Subjects:
   - Small molecules as tools for biology research: interrogating brassinosteroid signaling and membrane trafficking in plants
   - Cationic cycloadditions: mechanistic rationale of their selectivity and applications in the generation of complex carbocyclic scaffolds

2. Master dissertation, UGhent — 2011-2012 (Prof. Dr. Pierre De Clercq & Prof. Dr. Johan Winne)

3. Publications

   - Disruption of clathrin-mediated endocytosis in Arabidopsis through small molecule inhibition of clathrin heavy chain function, Nature Chemical Biology, 2019
   - Nonselective chemical inhibition of ARF GEFs in Arabidopsis through likely targeting the Sec7 domain, The Plant Cell, 2018
   - Selectivity in stepwise (4+3) cycloadditions of furfuryl cations: stereocontrol by highly organized transition states in a nonstop cycloaddition mechanism (in review)
   - Heterocycles as Moderators of Allyl Cation Cycloaddition Reactivity, Synlett, 2017, 28, 2345-2352
   - Co-author of two chapters from: Endomembrane trafficking and brassinosteroid signaling from a small molecule perspective, Wim Dejonghe, 2015 (PhD dissertation)

SERVICE

- AAP representative in the departmental council of the department of organic and macromolecular chemistry — 2015-2018
- Member of the First Intervention Team — 2015-2018 Coordination during evacuations, First Aid, safety control in research laboratories
- Deputy AAP representative in the Commission for the Quality control of eduction in the Faculty of Sciences — 2017-2018 Cluster Chemie/Chemistry - Biochemie & Biotechnologie/Biochemistry & Biotechnology - Bioinformatics - Plant Biotechnology - Biosafety in Plant Biotechnology

- AAP representative in the commission for the educational program of chemistry — 2015-2018

Publications

- Disruption of clathrin-mediated endocytosis in Arabidopsis through small molecule inhibition of clathrin heavy chain function, Nature Chemical Biology, 2019 (accepted)
- Nonselective chemical inhibition of ARF GEFs in Arabidopsis through likely targeting the Sec7 domain, The Plant Cell, 2018
- Selectivity in stepwise (4+3) cycloadditions of furfuryl cations: stereocontrol by highly organized transition states in a nonstop cycloaddition mechanism, (*in review*)
- Heterocycles as Moderators of Allyl Cation Cycloaddition Reactivity, Synlett, 2017, 28, 2345-2352

Selectivity in stepwise (4+3) cycloadditions of furfuryl cations: stereocontrol by highly organized transition states in a nonstop cycloaddition mechanism

Dietmar Hertsen,[a],† Bram Denoo,[b],† Oykum Naz Avci,[c] Veronique Van Speybroeck,[a] Johan M. Winne,[b],* Saron Catak[a,c],*

Abstract: Furfuryl cations are reliable three-carbon dienophiles for a wide range of conjugated dienes and can be generated from simple furan-2-methanol derivatives (furfuryl alcohols) as versatile organic building blocks for the elaboration of complex fused-ring systems. The mechanism of this orbital symmetry-allowed oxyallyl-type (4+3) cycloaddition can be considered either as a *concerted* or a *stepwise* carbocationic process. In this work, we have examined the highly selective intermolecular furfuryl cation cycloadditions of (*R*)-α-phellandrene from a joint experimental and theoretical perspective, in order to gain insight into the factors which govern the stereoselectivity. We have found that these reactions proceed *via* a stepwise mechanism with a highly pre-organized transition state for the first step, thus reconciling the stepwise mechanism with the experimentally observed high selectivities, and offering a new general explanation as similar pathways were identified with a range of diene reaction partners.

Introduction

Cycloadditions such as the well-known Diels-Alder reaction,[1] and 1,3-dipolar cycloadditions,[2] are highly useful synthetic processes in which two unsaturated reaction partners can be joined together at the ends of their π-systems (Scheme 1a,b). The resulting net transformation of two weaker π-bonds (e.g. carbon-carbon π bonds) into two stronger σ-bonds (e.g. carbon-carbon σ-bonds) gives a formidable driving force to the process, that can even overcome significant ring strain, providing access to a wide variety of ring systems.[1-3] Insight into the reaction mechanism of these established synthetic methods has been instrumental in their wide adoption as synthetic strategies.[3] The mechanism of any cycloaddition reaction can either be a concerted (pericyclic) or a stepwise process. Stepwise cycloadditions are not controlled by the orbital symmetry concepts developed by Woodward and Hoffmann, but are also more prone to undergo side reactions since they involve non-cyclised high-energy radical and/or ionic intermediate adducts (Scheme 1, right hand structures). Indeed, while most pericyclic cycloadditions are expected to give high levels of stereoselectivity and -specificity because of their highly ordered transition states, stepwise cycloadditions have often been associated with lower yields and lower selectivity.[4] This can be rationalized by premature termination reactions, or the competition of different cyclization modes and divergent pathways from the initially formed high energy intermediate.[5] The (4+2) and 1,3-dipolar (3+2) cycloaddition methods mentioned above mostly proceed through pericyclic concerted mechanisms. Conversely, (4+3) cycloadditions of (oxy)allyl cations and conjugated dienes (Scheme 1c), an iso-electronic reaction giving seven-membered ring adducts, are often more likely to proceed through a stepwise cationic cycloaddition pathway.[6] Although allyl cation cycloadditions have found several useful applications in the synthesis of seven-membered rings,[7] compared to their iso-electronic counterparts, these methods indeed often give rise to low levels of efficiency and stereoselectivity, hindering their wide implementation in synthetic chemistry.

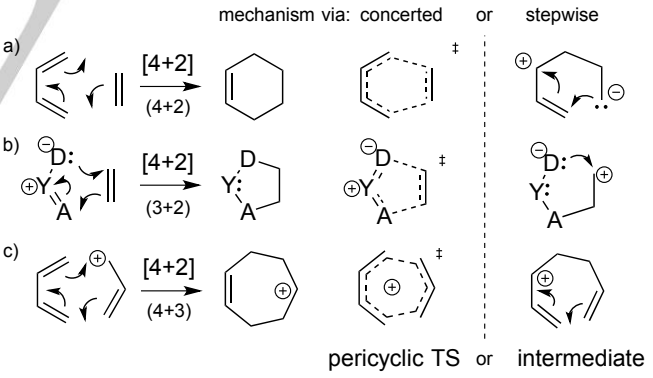

Scheme 1. Three six-electron cycloaddition reactions that can either proceed through a pericyclic or a stepwise mechanism: a) Diels-Alder reactions; b) 1,3-dipolar cycloadditions: A=donor atom, D=acceptor atom, Y=central atom; c) allyl cation [4π+2π] cycloadditions.

[a] Dietmar Hertsen, Oykum Naz Avci, Veronique Van Speybroeck, Saron Catak
Center for Molecular Modeling, Ghent University, Tech Lane Ghent Science Park Campus A, Technologiepark 903, 9052 Zwijnaarde, Belgium.
E-mail:
[b] Bram Denoo, Johan M. Winne
Organic Synthesis Research Group, Department of Organic and Macromolecular Chemistry, Ghent University, Krijgslaan 281(S4), 9000 Gent, Belgium.
[c] Bogazici University, Department of Chemistry, Bebek, Istanbul, 34342, Turkey.
(†) These authors contributed equally to this manuscript.
(*) Corresponding author

Supporting information for this article is given via a link at the end of the document.

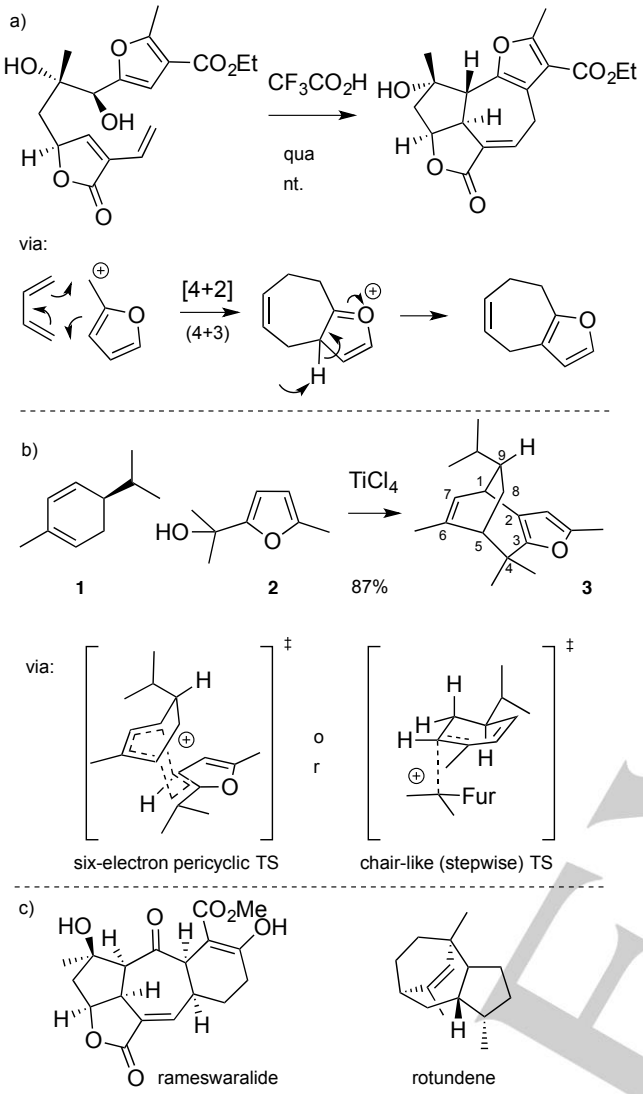

Scheme 2. a) Intramolecular dehydrative annulation of a furfuryl aclohol and a conjugated diene via a formal (4+3) cycloaddition pathway leading to a single diastereomer; b) intermolecular cycloaddition of a furfuryl cation with (*R*)-α-phellandrene **1** giving a single diastereomeric cycloheptanoid adduct via either a concerted or a stepwise mechanism; c) structures of two cycloheptanoid polycyclic natural product.

In 2009, Pattenden and Winne reported an unexpected, but very efficient and highly stereoselective intramolecular dehydrative cycloheptannulation between a furfuryl alcohol and a diene moiety (Scheme 2a).[8] The reaction can be rationalized by the generation of a furfuryl cation (upon treatment with acid), followed by a (4+3) cycloaddition with the diene, in which the furfuryl cation serves as a classical oxyallyl-type cation.[9] In a pericyclic process, this reaction could also constitute an example of a [6+4] ten-electron concerted cycloaddition.[10] Later investigations showed that furfuryl alcohols are, in fact, highly reliable reaction partners in intermolecular dehydrative (4+3) cycloadditions, with a substrate scope with regard to the diene that considerably expands that of classical oxyallyl cations.[11] Furthermore, the furfuryl cations can be easily generated from the corresponding alcohols under diverse conditions, and the yields and selectivities were found to be high. As a result, this enabling synthetic method has been used quite a few times in the total synthesis of complex polycyclic natural products or analogues thereof.[12] The mechanism of the furfuryl cation cycloadditions has been probed by DFT calculations in some preliminary studies,[9,11] indicating competing stepwise and asynchronous concerted reaction pathways.[13] In a model substrate, the stepwise pathway was calculated to be favored by at least 12 kJ/mol over the pericyclic process.[11]

The combined computational and experimental study reported in the current article was inspired by our observation that (*R*)-α-phellandrene **1** reacts with furfuryl alcohols in a completely regio- and stereoselective manner (see example for furfuryl alcohol **2** in Scheme 2b), giving a one-step asymmetric entry into an oxa-analog of the tricyclic ring system found in the natural sesquiterpene rotundene (Scheme 2c).[14] Although such levels of stereoselectivity or stereoinduction by remote stereogenic centers have been previously observed in a number of intramolecular reactions of furfuryl cations (cf Scheme 2a),[8,12b-d,f] the selectivity of this intermolecular reaction is quite striking. Two competing classical explanations can be put forward (Scheme 2b): either the reaction proceeds through a highly ordered concerted or pericyclic transition state that facilitates the stereoinduction for these substrates, or via a stepwise reaction in which the initial addition of the furfuryl cation to the cyclohexadiene ring system is completely stereocontrolled through steric and stereo-electronic factors, e.g. favouring an 'axial' attack on the diene, achieving a maximum staggering of allylic bonds relative to forming bonds.[15] However, the combined synthetic and in-depth computational study reported herein reveals a more convoluted situation, and also offers new insight into the factors that govern the reaction mechanism of these synthetically useful cycloadditions.

Results and Discussion

Stereoselective synthesis of bicyclo[2.2.3]nonanes through (4+3) cycloadditions of (*R*)-α-phellandrene

The bicyclo[2.2.3]nonane cycloheptannulation products **3**-**7** were readily obtained from phellandrene **2** and a range of furfuryl alcohols in synthetically useful yields, and with complete stereoinduction of the isopropyl group on the newly formed bonds (Scheme 2b and 3a). As mentioned above, when (R)-α-phellandrene **1** is reacted with the symmetrically substituted furfuryl alcohol **2**, the expected bridged cycloadduct **3** is obtained as a single diastereomer in good yield, after some optimization of conditions (Scheme 2b, see SI for optimization study). Using the same optimized reaction conditions, three unsymmetrically substituted furfuryl alcohols all gave the expected cycloadducts **4**, **5** and **6**, albeit as mixtures of two diastereomers with respect to the third new stereocenter at the C-4 position of the bicyclononane, deriving from the asymmetrically substituted furan carbinol position (Scheme 3a). In all cases, the same major stereoisomer at C-4 was observed via diagnostic nOe-contacts, with the selectivity increasing with the steric bulk of the R-group (Me, Et, Ph). The same diastereoselectivity trends have in fact

been observed in the corresponding furfuryl cation cycloadditions with 1,3-cyclohexadiene.[11] When compared to cyclohexadiene, the yields obtained with α-phellandrene are somewhat lower, which can be explained by the increased acid-sensitivity of the diene (leading to proton-mediated addition and oligomerisation reactions). A benzofuran-derived alcohol gave the expected tetracyclic product **7** as a single diastereomer.

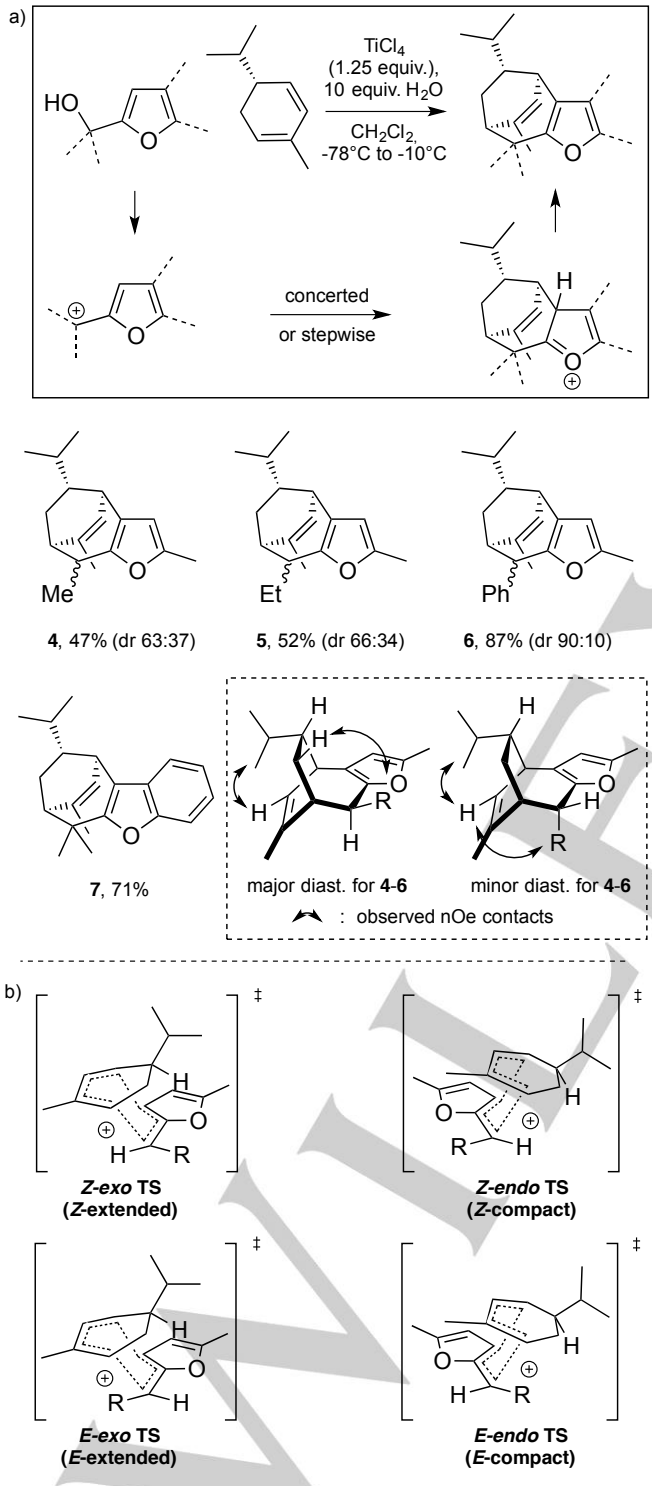

Scheme 3. a) Stereoselective (4+3) cycloadditions of (*R*)-(-)-phellandrene **1** with a range of furfuryl alcohols; b) four possible concerted TSs for the cycloaddition reaction.

For the reactions of asymmetrically susbstituted furfuryl cations, no less than 16 geometrically distinct concerted transition states can be considered for the formation of adducts like **4**, **5** or **6**. From these 16 possibilities, half can be discarded based on the exclusive regioselectivity observed in these reactions of phellandrene. Of the remaining eight, four more can be excluded which would lead to the incorrect stereo-relationship between the isopropyl substiutuent and the ringface where the furan bridge is added (*trans*- or *cis*- attack on phellandrene). Thus, in order to explain the observed reaction products, four different approaches between the reactant diene and furfuryl cation remain plausible (Scheme 3b). These diastereomerically related alternative approaches of diene and furfuryl cation also give rise to four possible different diastereomers of the initial cycloaddition product, which ultimately fall into one of only two possible final reaction products, via deprotonation and rearomatization of the furan ring, i.e. the observed diastereomers. Using the nomenclature proposed by Hoffmann for oxyallyl-type (4+3) cycloadditions, these four diastereomeric transition states (TS's) can be designated as 'extended' or 'compact' TS geometries, or as 'exo' or 'endo' TS's, respectively, in accordance with their analogous descriptors in Diels-Alder reactions (Scheme 4).[16] In the compact (endo) TS's, the π-systems of the furfuryl cation and phellandrene are superimposed on each other and thus in close proximity, wherein the overall conformation of the forming cycloheptenyl cation is boat-like. In the extended (exo) TS's, the reacting π-systems are facing away from each other and are on opposing sides of the plane formed by the incipient carbon-carbon σ-bonds, corresponding to a chair-like conformation of the forming cycloheptenyl cation. In (4+3) cycloadditions, a preference for exo or endo TS's have both been observed depending on electronic and steric factors. Also with furfuryl cations, both extended and compact addition modes have been observed experimentally.[11,12a] Taking into account the preference for a *Z*-configuration of the furfuryl cations derived from alcohols **4**-**6**, the experimentally observed diastereoselectivity would correspond to an extended or exo approach of the diene, via the Z-exo TS. In order to check this rationalization, and to gain further insight into the factors that govern the remarkable selectivity in these processes, we performed a detailed computational study on these reactions using Density Functional Theory (DFT) calculations to obtain the geometries and energies of the various stationary points along the potential energy surface of the reaction between phellandrene and furfuryl cations.

Computational study of phellandrene-furfuryl cation cycloadditions

The cycloaddition reaction between (*R*)-α-phellandrene **1** and the symmetrically substituted furfuryl alcohol **2**, proceeding via cation **I** (Scheme 4), was chosen as the first system to be investigated by DFT calculations in order to understand its stereoselectivity.[17] Both concerted (**1** + **I** → **III**) and stepwise (**1** + **I** → **II** → **III**) pathways were taken into account (Scheme 4). A concerted transition state was located between furfuryl cation **I** and phellandrene **1**, however, similar to the one in our previous study of 1,3-cyclohexadiene (CHD),[11] it was shown to be considerably higher in energy than the stepwise pathway (See SI sections 5, 6 for details of concerted profiles).

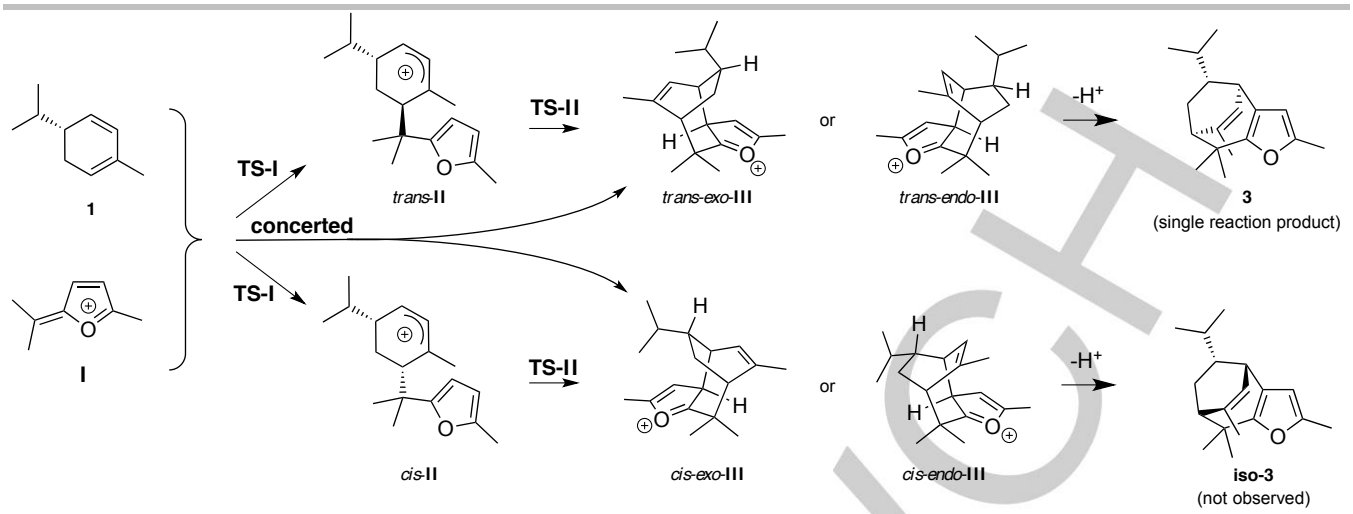

Scheme 4. Stepwise and concerted pathways for the cycloaddition reaction between (*R*)-phellandrene **1** and the furfuryl cation **I**, derived from furfuryl alcohol **2**.

In the stepwise mechanism, outlined in Scheme 4, the two new bonds of the bicyclic oxonium intermediate **III** are formed during two subsequent reactions rather than in a single concerted TS. In the first step, an allyl cation intermediate **II** with a pendant furan ring is generated. Two distinct modes of attack can lead to the formation of either ***trans*-II** or ***cis*-II** as an initial intermediate. In both cases, however, multiple approaches are possible between the reactants, resulting in several different conformations of **TS-I** and the resulting cation intermediates **II.** The interconversion between different *cis* or *trans* conformations by the rotation around the forming C-C bond is relatively slow, since the rotational barriers are significant with respect to the kinetic barrier of the first step (SI2). Initially, we selected four pre-organized transition states **TS-I** with geometries that correspond to those expected for concerted transition states, with a slightly larger distance between the atoms of the bond that will be formed in the second step. These pre-organized TS's will be indicated using the *exo*/*endo* nomenclature usually preserved for concerted cycloadditions: *cis*-*exo*-**TS-I**, *cis*-*endo*-**TS-I,** *trans*-*exo*-**TS-I** and *trans*-*endo*-**TS-I** (Figure 1). As noted above, **TS-I** is not a priori restricted to these four conformations.

In the second step (**II** → **III**), only four stereoisomers of **III** can be formed via four distinct transition states (**TS-II**), as the reaction product is a rigid ring system. As these four transition states resemble those of concerted reactions, we adopt the same *exo*/*endo* nomenclature for **TS-II** and **III**. After the formation of **III** via a stepwise (4+3) cycloaddition, a highly exothermic deprotonation restores the aromaticity of the furan ring and leads to the final products **3** and iso-**3**. Only the *trans* pathway via intermediate *trans*-*exo*-**III** or *trans*-*endo*-**III** can lead to the experimentally observed product **3**, however. It is assumed that the final deprotonation step is not rate-limiting.

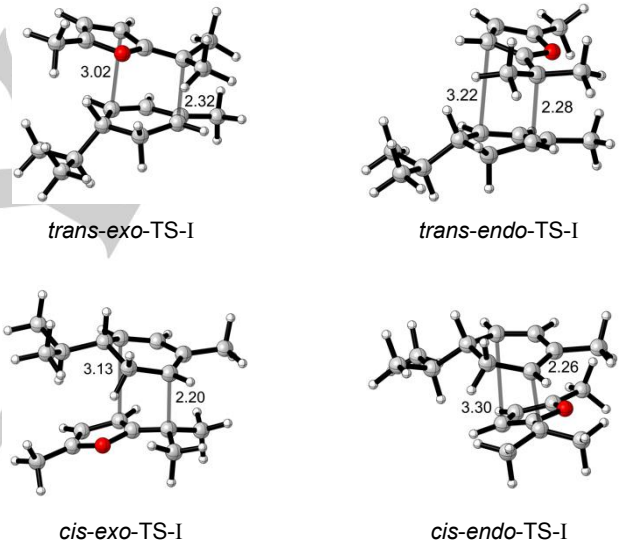

Figure 1. Pre-organized **TS-I** for the cycloaddition between phellandrene **1** and furfuryl alcohol **2** (M06-2X/6-31+G(d,p), IEF-PCM (CH_2Cl_2, ε = 8.93), distances in Å).

In order to understand the experimental outcome of the cycloaddition between **1** and **2**, we initially limited our analysis to the four pre-organized intermediates of **II** and the transition states **TS-I** leading to these 'closed arrangement' intermediates. The Gibbs free energies of every pre-organized **TS-I** and **TS-II** with respect to the separate reactants **1** and **I** can be found in Table 1. It can be seen that the formation of *trans* intermediates is kinetically favored, since the free energy barriers are consistently higher for the *cis* intermediates. More significantly, the barriers for the formation of the *trans*-*exo*-**III** intermediate are at least 10 kJ/mol lower than those for other systems for both reaction steps. Finally, the *trans*-*exo*-**III** intermediate is the most stable intermediate **III**. These findings are in line with the experimental formation of **3**.

Table 1. Gibbs free energies of the stepwise cycloaddition between phellandrene **1** and furfuryl alcohol **2** via a pre-organized **TS-I** (M06-2X/6-31+G(d,p), 298 K, 1 atm, IEF-PCM (CH_2Cl_2, ε = 8.93), Gibbs free energies in kJ/mol w.r.t. the separate reactants **1** and **I**).

		TS-I	II	TS-II	III
trans	*exo*	62.4	25.0	34.2	8.2
	endo	73.3	32.3	52.6	17.0
cis	*exo*	77.8	43.7	50.5	14.5
	endo	86.7	46.0	61.5	19.2

From Table 1, it can be concluded that the first step is the rate-limiting step regardless of the stereochemical pathway, even though the aromaticity of the furan is lost in the second step (G(**TS-II**) – G(**TS-I**) ≥ 20.7 kJ/mol). Our assumption that the rate-determining step has a pre-organized transition state **TS-I**, may cause computational artefacts. Therefore, other possible **TS-I** conformations were taken into account. For every pre-organized **TS-I**, a relaxed potential energy surface scan corresponding to a rotation around the forming bond was carried out (Figure 2). The obtained local minima were then re-optimized as transition states and the Gibbs free energies of these new **TS-I** geometries were determined. These conformational scans established the pre-organized *trans*-*exo*-**TS-I** as the most stable of all *trans*-TS's by at least 10.6 kJ/mol. The most stable *cis*-**TS-I** is 13.8 kJ/mol higher in Gibbs free energy than *trans*-*exo*-**TS-I**.

In the stereoselective reaction of **1** and **2** yielding **3**, the most stable, rate-determining transition state *trans*-*exo*-**TS-I** is highly pre-organized: the length of the forming bond is 2.32 Å, while the distance between the atoms of the bond that will be formed in the second step is only 3.02 Å (Figure 3). Due to this pre-organization, no conformational rearrangement is necessary between the product of the first step and the pre-reactive complex of the second one. Not only does the most stable **TS-I** lead to the most stable isomer of **III**, no rotational Gibbs free energy barrier has to be crossed during the second step. As for **TS-I**, relatively high rotational barriers were found for intermediate *trans*-*exo*-**II**, stereochemically locking this intermediate (SI2). Hence, this cycloaddition is a stereocontrolled, stepwise reaction which proceeds via a series of conformationally rigid cationic intermediates and transition states, a scenario that somewhat defies the classical distinction between stepwise and pericyclic cycloadditions. The closest analogy in classical organic chemistry is perhaps the term 'nonstop reaction' which was introduced by Eschenmoser, Ruzicka, Jeger and Arigoni in their seminal 'biogenetic isoprene rule for triterpenes'-paper.[18] There it is introduced to explain the outcome of cationic polycyclizations through a mechanism involving a series of conformationally well-defined 'nonclassical' carbocationic intermediates. The term nonstop reaction has never been widely used and subsequently became obscured by the debate between concerted and stepwise mechanisms in polyene cyclizations.[18b] However, a 'nonstop cycloaddition' seems to be a highly adequate term for the reaction between phellandrene and furfuryl cations in view of our findings.

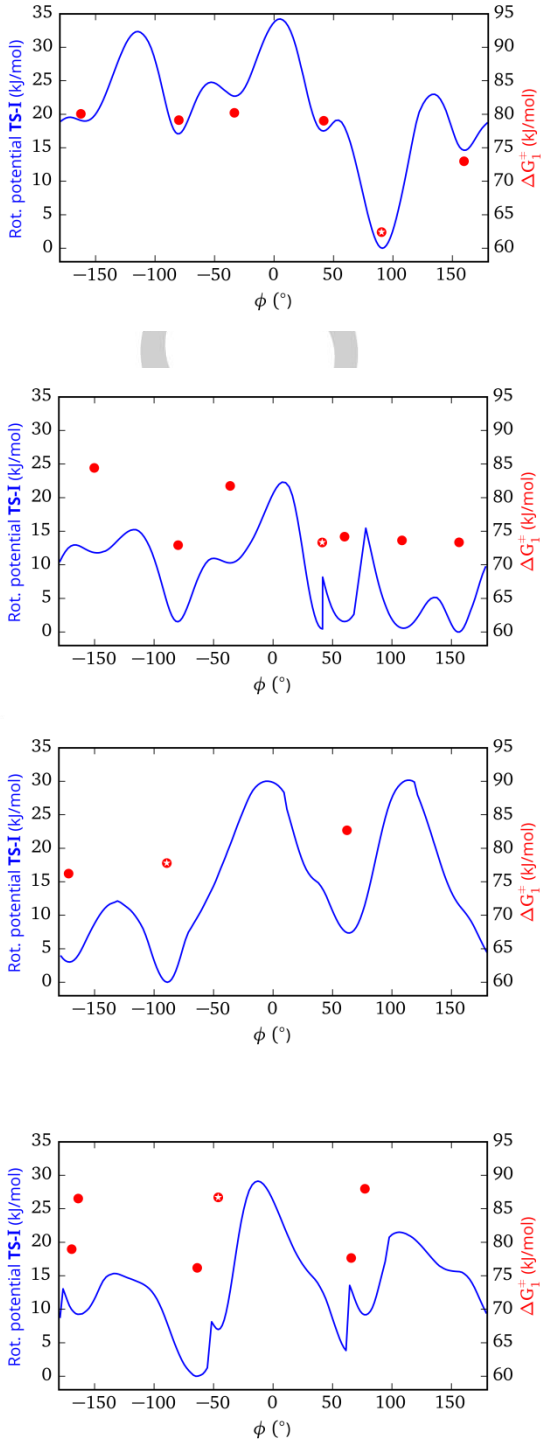

Figure 2. Relaxed, rotational scans around the forming bond of pre-organized **TS-I** (blue, electronic energy with respect to the lowest minimum) and the Gibbs free activation energy of the re-optimized transition states (red, with respect to the separate reactants **1** and **I**, closed arrangement TS as ✪). (M06-2X/6-31+G(d,p), energies in kJ/mol, forming bonds constrained at the distance in Figure 1, Gibbs free energies at 298 K, 1 atm and IEF-PCM (CH_2Cl_2, ε = 8.93)).

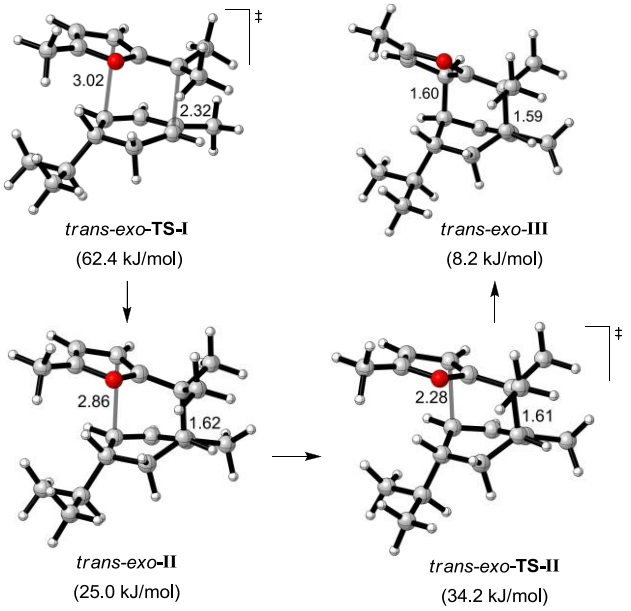

Figure 3. Structural pre-organization in the kinetically favorable pathway of the reaction between phellandrene **1** and furfuryl alcohol **2** (M06-2X/6-31+G(d,p), Gibbs free energies with respect separate reactants **1** and **I**, 298 K, 1 atm, IEF-PCM (CH_2Cl_2, ε = 8.93), distances in Å).

Pre-organized TS's for stepwise cycloadditions that structurally resemble concerted TS's have been observed in DFT calculations on cationic (4+3) cycloadditions with a furan diene by Houk and Harmata et al. and were termed 'closed arrangement' transition states.[19] These TS's have been rationalized by electrostatic stabilization of developing partial charges in the diene π-system. Similar 'closed arrangement' TS's have been found for the (4+3) cycloaddition of indolyl cations with cyclopentadiene, although these were not studied in detail.[20]

From the calculations described above, it is clear that the reaction of phellandrene **1** and furfuryl alcohol **2** is a stepwise reaction whose stereoselectivity can be explained kinetically by a rate-determining first step with a highly organized transition state, structurally similar to that of an asynchronous pericyclic reaction. It must be noted that the thermodynamically favored product iso-**3** is different from the kinetic product **3** (ΔΔG = 5.1 kJ/mol).

Intrigued by the insight DFT calculations have provided in the reactivity of phellandrene with the simple furfuryl alcohol **2**, we turned to the more complex reaction of an asymmetrical furfuryl alcohol (1-(5-methylfuran-2-yl)ethan-1-ol), leading to cycloadduct **4** (Scheme 3). Since the furfuryl cation **IV** has only one methyl substituent, an additional stereogenic center is present. Two pathways with pre-organized transition states can lead to the experimentally observed products (4*S*)-*trans*-**4** (major product) and (4*R*)-*trans*-**4** (minor product), via the (*Z*)-furfuryl cation **IV** or its strained (E)-isomer, respectively (Scheme 5).
For the stepwise mechanism, there are eight instead of four pre-organized pathways because of the extra stereocenter. Hence, eight pre-organized **TS-IV** conformations were located, corresponding to eight cationic cycloaddition products **VI**. (Scheme 5, a full overview can be found in SI 3a). Table 2 gives an overview of the Gibbs free energies of the species in these pre-organized, stepwise pathways. The reaction of furfuryl cation **IV** is both faster and more exergonic than that of the symmetrically subsituted furfuryl cation **I** (Table 1). This could be expected, since secondary carbocations (**IV**) are less stable than tertiary carbocations (**I**).

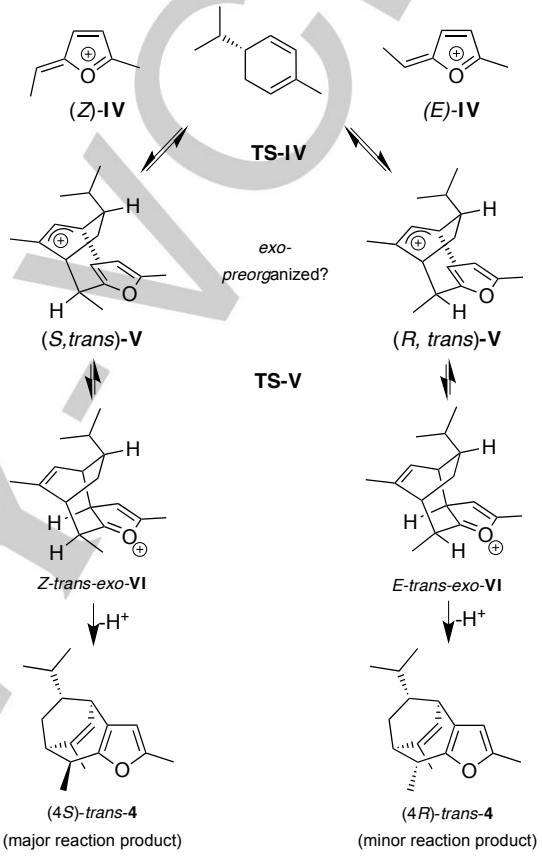

Scheme 5. Proposed stepwise reaction mechanism of the cycloaddition between phellandrene **1** and 1-(5-methylfuran-2-yl)ethan-1-ol via the corresponding *E*- or *Z*-furfuryl cations **IV**.

The experimentally observed major reaction product (4*S*)-*trans*-**4** can be formed via the most favorable rate-limiting transition state (*Z*)-*trans*-*exo*-**TS-IV** (Table 2). Interestingly, the *trans*-*exo* pathway is preferred both for (*Z*)-**IV** and (*E*)-**IV**, yielding the major ((4*S*)-*trans*-**4**) and minor product ((4*R*)-*trans*-**4**), respectively. This preference is smaller for (*E*)-**IV**. Nevertheless, the formation of the non-observed *cis* products (4*R*)-*cis*-**4** ($\Delta G^{\ddagger}$= 43.0 kJ/mol) and (4*S*)-*cis*-**4** ($\Delta G^{\ddagger}$= 42.9 kJ/mol) via the *Z* pathway is kinetically more favorable than that of the minor product (4*R*)-*trans*-**4** via (*Z*)-trans-endo-**TS-IV** ($\Delta G^{\ddagger}$= 45.4 kJ/mol). The calculated energy difference between these barriers is quite small, but the experiment establishes that no *cis*-isomers of **4** are formed. An alternative interpretation of these data, then, would involve a non-Curtin-Hammett scenario wherein the formation of the furfuryl cations **IV** is irreversible. The final product ratio is then a reflection of the initial ratio of (Z)-**IV** and (E)-**IV** (3.8 kJ/mol higher in Gibbs free

energy), which each react via their preferred *trans-exo* pre-organized TS's. This interpretation also explains the increasing selectivity in the synthesis of bicyclononanes **4**-**6**, since the *E*/*Z* energy difference will be more pronounced for furfuryl cations with sterically more demanding substituents (Scheme 3). Again, a full rotational scan around the forming bond in all pre-organized **TS-IV**s was performed to check for other conformations. The transition states leading to the major ((*Z*)-*trans*-*exo*-**TS-IV**) and minor product ((*E*)-*trans*-*exo*-**TS-IV**) are clearly pre-organized (Figure 4). A full overview can be found in SI 3b.

Table 2. Gibbs free energies of the stepwise cycloaddition between furfuryl cations **IV** and phellandrene **1** via a pre-organized **TS-IV** (M06-2X/6-31+G(d,p), 298 K, 1 atm, IEF-PCM (CH_2Cl_2, ε = 8.93), Gibbs free energies in kJ/mol w.r.t. the separate reactants **1** and (*Z*)-**IV**).

			TS-IV	V	TS-V	VI	product
Z	*trans*	*exo*	32.2	-18.8	-3.0	-30.7	(4*S*)-*trans*-**4**
		endo	45.4	-11.0	13.6	-18.9	(4*R*)-*trans*-**4**
	cis	*exo*	43.0	0.0	14.3	-20.3	(4*R*)-*cis*-**4**
		endo	42.9	6.9	19.9	-23.6	(4*S*)-*cis*-**4**
E	*trans*	*exo*	40.8	-2.9	-3.0	-24.5	(4*R*)-*trans*-**4**
		endo	43.3	-15.3	15.2	-16.0	(4*S*)-*trans*-**4**
	cis	*exo*	52.3	11.3	15.0	-19.0	(4*S*)-*cis*-**4**
		endo	54.6	-0.6	21.8	-16.6	(4*R*)-*cis*-**4**

The kinetic and the thermodynamic products of the reaction between **1** and 1-(5-methylfuran-2-yl)ethan-1-ol via intermediates **IV**, **V** and **VI** are not the same, in line with the reaction between **1** and **2** (Figure 5). The *cis* isomers of **4** are more stable than the *trans* isomers, although they were not found experimentally. Furthermore, the minor product (4*R*)-*trans*-**4** is more stable than the major product (4*S*)-*trans*-**4**. This confirms that the reaction proceeds under kinetic control.

From the computational results described above, it is clear that TS's for the initial addition of a furfuryl cation to phellandrene **1** are often pre-organized into a closed arrangement, leading to a highly organized non-concerted reaction pathway best described as a nonstop cycloaddition. In order to assess the generality of this phenomenon, we checked if a similar reaction profile can be found in the reaction of furfuryl alcohol **2** with the more generic diene isoprene (2-methylbutadiene), which is the least substituted diene that has been reacted with furfuryl alcohols so far (Figure 6).[11] Experimentally, this reaction proceeds in a completely regioselective fashion, although an excess of diene is required to achieve good yields, to compensate for isoprene oligomerisation.

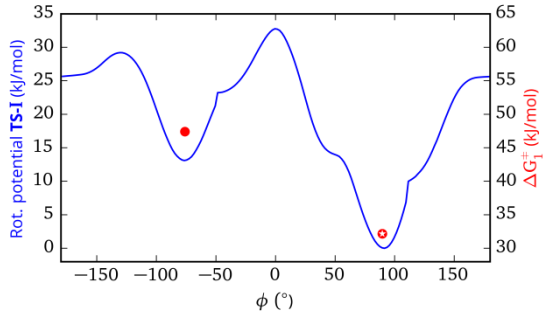

(a) Rotation around the forming bond in *Z*-*trans*-*exo*-**TS-IV**

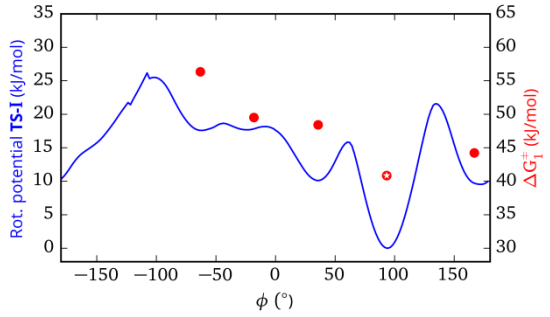

(b) Rotation around the forming bond in *E*-*trans*-*exo*-**TS-IV**

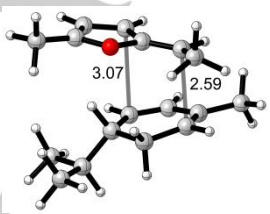

(a) *Z*-*trans*-*exo*-**TS-IV** ( )

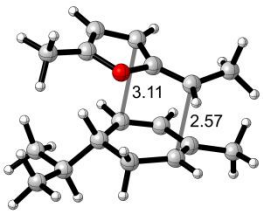

(d) *E*-*trans*-*exo*-**TS-IV** ( )

Figure 4. (a), (b) Relaxed, rotational scans of the pre-organized **TS-I** of the reaction between **1** and **IV** around the forming bond (blue, electronic energy with respect to the lowest minimum) and the Gibbs free activation energy of the re-optimized transition states (red, with respect to the separate reactants **1** and **IV**, closed arrangement TS as). (c), (d) Geometries of the pre-organized TSs. (M06-2X/6-31+G(d,p), energies in kJ/mol, Gibbs free energies at 298 K, 1 atm and IEF-PCM (CH_2Cl_2, ε = 8.93)).

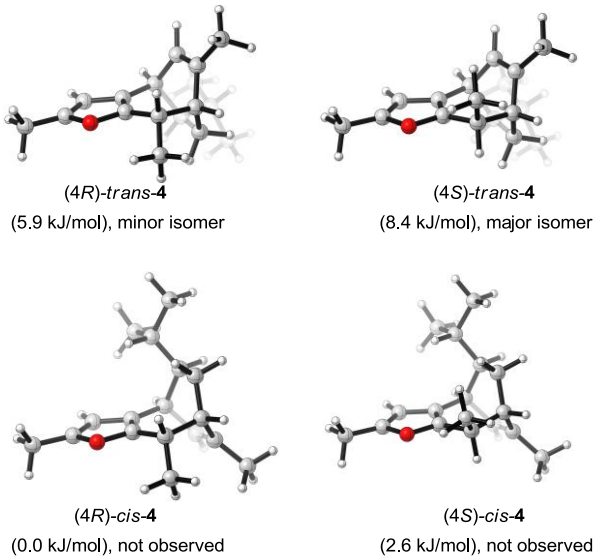

Figure 5. Structures and relative product stabilities of the cycloaddition products **4** of the reaction between **1** and **IV** (M06-2X/6-31+G(d,p), 298 K, 1 atm, relative Gibbs free energies in kJ/mol).

In the reactions of isoprene and cation **I**, derived from furfuryl alcohol **2**, we again found two pre-organized transition states, an *exo*-TS and an *endo*-TS. As for phellandrene, the *exo*-addition is energetically favored, and a full rotational profile also indicates a clear preference for a 'closed arrangement' in this highly organized stepwise TS. This result indicates that the preference for pre-organized TS's is not a steric effect, but that it may be a general effect in furfuryl cation cycloadditions.

Finally, we decided to re-visit our previous study on the cycloaddition of a furfuryl cation with 1,3-cyclohexadiene (CHD),[11] where our computational efforts had focused on determining whether the reaction was concerted or stepwise in nature, but not on the preferred conformation of the first stepwise TS, which was reported as non-organized. In light of the findings of the present study, we located a new 'pre-organized' TS1 for the aforementioned stepwise cycloaddition reaction, which was shown to be lower in energy than the non-organized TS1 reported in 2011.[11] Figure 7 shows the previously reported concerted (69.4 kJ/mol) and non-organized TS1 (52.7 kJ/mol), and the newly located pre-organized TS1 (41.4 kJ/mol). This finding is in line with the insights gained from the current study that propose stepwise cycloadditions of furfuryl cations proceed via pre-organized transition states.

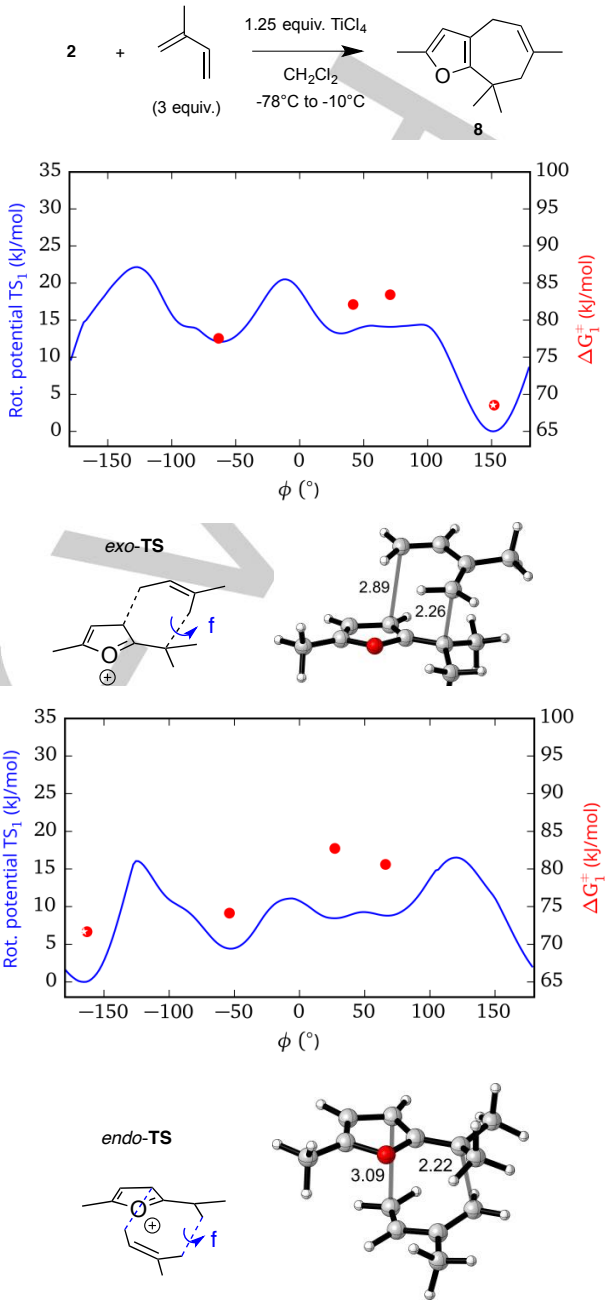

Figure 6. Reaction of **2** with isoprene. Relaxed, rotational scans of the pre-organized TS of the first cycloaddition step between 2 and 2-methylbutadiene around the forming bond (blue, electronic energy with respect to the lowest minimum) and the Gibbs free activation energy of the re-optimized transition states (red, with respect to the separate reactants, closed arrangement TS shown as ✪). 3D structure of the closed arrangement TS shown. (M06-2X/6-31+G(d,p), energies in kJ/mol, Gibbs free energies at 298 K, 1 atm and IEF-PCM (CH_2Cl_2, ε = 8.93), critical distances in Å).

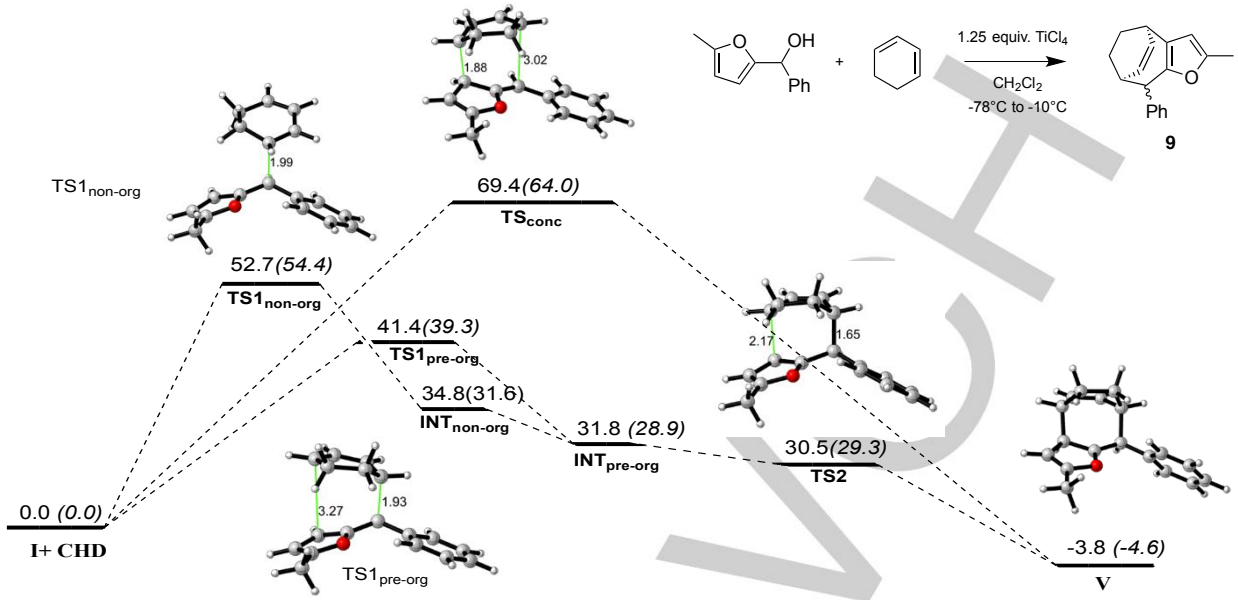

Figure 7. Concerted versus stepwise (pre-organized and non-organized) reaction profiles for the cycloaddition of a furfuryl cation with CHD.[11] (Free energies in kJ mol^{-1} at the M06-2X/6-31+G(d,p)//B3LYP/6-31+G(d,p) level of theory, IEFPCM (ε = 8.93, dichloromethane) results in parentheses, distances in Å).

Conclusions

The reactions of furfuryl alcohols and phellandrene proceed through a stepwise cycloaddition under kinetic control, with a rate-determining initial addition step between the diene and the furfuryl cation. The energetically preferred TS (>10 kJ/mol) for this electrophilic addition shows a closed arrangement molecular geometry, closely resembling that of the subsequent intermediates and TS. The structural pre-organization emulates that found in typical pericyclic concencerted cycloaddition TS's. This TS geometry is found to be responsible for the high stereoselectivity of the process, as well as for the intrinsic *exo*-selectivity of the cycloaddition. The resulting mechanism also explains the relatively high efficiency of these stepwise cationic reactions, a reaction type that is usually prone to undergo side reactions.

The 'pre-organized' stepwise reaction profiles show a very similar degree of organization to their concerted counterparts, leading to high stereoselectivities. It is suggested that the term 'nonstop reaction', borrowed from cationic polycyclizations, may be a more adequate way to describe this type of mechanism.

Finally, the detailed mechanistic profile described herein helps to explain why furfuryl cations have been quite useful as synthetic tools compared to some other (oxy)allyl cations. From this mechanistic picture, a few conclusions can be drawn in line with experimental observations: (i) non-coordinating solvents are favored, (ii) loosely interacting counterions are favored, (iii) reactions should be performed at low temperatures to limit rotational freedom, and (iv) compared to pericyclic cycloadditions, relatively small changes in the substrates or reaction conditions can have significant effects, as the pre-organized TSs are only 10-20 kJ/mol favored over pathways following a non-controlled addition step, opening up alternative pathways. We expect that similar pre-organized nonstop cycloaddition mechanisms can be found in reactions of related allyl-type cations, and investigations along those lines are currently ongoing.

Experimental and computational methods

All Density Functional Theory (DFT) calculations have been performed with the Gaussian software package[21] using the M06-2X functional[22] and the 6-31+G(d,p) basis set. The solvent environment has been taken into account by the inclusion of an IEF Polarizable Continuum Model IEF-PCM (CH_2Cl_2, ε = 8.93). The nature of minima (products, reactants, intermediates) and first-order saddle points (transitions states) was verified via frequency calculations. Gibbs free energies were calculated within the harmonic oscillator approximation at 298 K and 1 atm. Transition states were connected with their respective reactants and products via Intrinsic Reaction Coordinate (IRC) calculations.[23] Relaxed potential energy surface scans of transition states were performed by constraining the length of the forming bond and increasing a dihedral angle around that bond with steps of two degrees, while the other internal coordinates were relaxed after each increment. The obtained electronic energies make up the rotational potential. The minima of the rotational potential were then re-optimized as transition states.

Full experimental details and characterization of all new compounds can be found in the ESI, together with copies of the original proton and carbon NMR spectra.

Acknowledgements

The computational resources and services used were provided by Ghent University (Stevin Supercomputer Infrastructure). The authors thank the Belgian Program on Interuniversity Attraction Poles (IAP) initiated by the Belgian State and the Special Research Fund (BOF) of Ghent University. B.D. thanks Ghent University for financial support.

Keywords: keyword 1 • keyword 2 • keyword 3 • keyword 4 • keyword 5

§ The relative rate of formation of the two cations (*Z*)- and (*E*)-IV is relatively hard to model accurately, but it is highly likely that the more stable (*Z*)-isomer is also formed more readily from the alcohol starting material. The calculated difference in free energy for both isomers of **IV** is 8.9 kJ/mol.

[1] K. C. Nicolaou, S. A. Snyder, T. Montagnon, G. Vassilikogiannakis, *Angew. Chem. Int. Ed.* **2002**, *41*, 1668–1698.
[2] K. V. Gothelf, K. A. Jørgensen, *Chem. Rev.* **1998**, ***98***, 863
[3] N. Nishiwaki, Methods and Applications of Cycloaddition Reactions in Organic Syntheses, John Wiley & Sons, Inc., Hoboken, New Jersey, **2014**.
[4] R. Huisgen, G. Mloston, E. Langhals, *J. Am. Chem. Soc.*, **1986**, *108*, 6401–6402.
[5] M. Harmata, C. Huang, P. Rooshenas, P. R. Schreiner, *Angew. Chem. Int. Ed.* **2008**, *47*, 8696–8699.
[6] a) C. J. Cramer, S. E. Barrows, *J. Phys. Org. Chem.* **2000**, *13*, 176–186; b) C. J. Cramer, S. E. Barrows, *J. Org. Chem.* **1998**, *63*, 5523-5532.
[7] a) M. Harmata, *Chem. Commun.* **2010**, *46*, 8886–8903; b) M. Harmata, *Chem. Commun.* **2010**, *46*, 8904–8922
[8] G. Pattenden, J. M. Winne, *Tetrahedron Lett.* **2009**, *50*, 7310–7313.
[9] B. Lygo, M. J. Palframan, G. Pattenden, *Org. Biomol. Chem.*, **2014**, *12*, 7270-7278.
[10] J. H. Rigby, *Org. React.* **1997**, *49*, 331.
[11] J. M. Winne, S. Catak, M. Waroquier, V. Van Speybroeck, *Angew. Chem. Int. Ed.* **2011**, *50*, 11990.
[12] a) Liu, Z. Sun, S. Li, K. Xiang, Y. Zhang, Y. Li, *RSC Adv.* **2016**, *6*, 26954–26958; b) D. R. Laplace, J. M. Winne, *Synlett*, **2015**, 467–470; c) Y. Li, M. J. Palframan, G. Pattenden, J. M. Winne, *Tetrahedron*, **2014**, *70*, 7229–7240; d) J. Hullaert, D. R. Laplace, J. M. Winne, *Eur. J. Org. Chem.* **2014**, 3097–3100; e) D. R. Laplace, B. Verbraeken, K. Van Hecke, J. M. Winne, *Chem. Eur. J.* **2014**, *20*, 253–262; f) M. J. Palframan, G. Pattenden, *Tetrahedron Lett.* **2013**, *54*, 324–328; g) J. Zhang, L. Li, Y. Wang, W. Wang, J. Xue, Y. Li, *Org. Lett.* **2012**, *14*, 4528–4530.
[13] M. J. Palframan, G. Pattenden, *Synlett* **2013**, *24*, 2720-2722.
[14] S.K. Paknikar, O. Motl, K.K. Chakravarti, *Tetrahedron Lett.* **1977**, *18*, 2121–2124.
[15] K. N. Houk, M. N. Paddon-Row, N. G. Rondan, Y.-D. Wu, F. K. Brown, D. C. Spellmeyer, J. T. Metz, Y. Li, R. J. Loncharich, *Science*, **1986**, *231*, 1108-1117.
[16] H. M. R. Hoffmann, *Angew. Chem. Int. Ed. Eng.* **1984**, *23*, 1.
[17] a) L. R. Domingo, J. A. Sáez, J. A. Joule, L. Rhyman and P. Ramasami, *J. Org. Chem.*, **2013**, *78*, 1621–1629; b) S. Xie, S. A. Lopez, O. Ramström, M. Yan and K. N. Houk, *J. Am. Chem. Soc.*, **2015**, *137*, 2958–66; c) A. Patel, Z. Chen, Z. Yang, O. Gutiérrez, H. Liu, K. N. Houk and D. A. Singleton, *J. Am. Chem. Soc.*, **2016**, *138*, 3631–3634.
[18] a) A. Eschenmoser, L. Ruzicka, O. Jeger, D. Arigoni, *Helv. Chim. Acta* **1955**, *38*, 1890; b) A. Eschenmoser, D. Arigoni, *Helv. Chim. Acta* **2005**, *88*, 3011-3050.
[19] a) E. H. Krenske, K. N. Houk, M. Harmata, *J. Org. Chem.* **2015**, *80*, 744-750; b) E. H. Krenske, K. N. Houk, M. Harmata *Org. Lett.* **2010**, *12*, 444-447.
[20] X. Han, H. Li, R. P. Hughes, J. Wu, *Angew. Chem. Int. Ed.* **2012**, *51*, 10390–10393.
[21] M. Frisch, G. Trucks, H. Schlegel, G. Scuseria, M. Robb, J. Cheeseman, G. Scalmani, V. Barone, B. Mennucci and G. Petersson, Gaussian, Inc., Wallingford, CT 2010.
[22] Y. Zhao and D. G. Truhlar, *Theor. Chem. Acc.* **2008**, *120*, 215-241.
[23] K. Fukui, *Acc. Chem. Res.* **1981**, *14*, 363-368.

Entry for the Table of Contents (Please choose one layout)

Layout 1:

FULL PAPER

Text for Table of Contents

((Insert TOC Graphic here: max. width: 5.5 cm; max. height: 5.0 cm))

*Author(s), Corresponding Author(s)**

Page No. – Page No.

Title

Layout 2:

FULL PAPER

((Insert TOC Graphic here; max. width: 11.5 cm; max. height: 2.5 cm))

*Author(s), Corresponding Author(s)**

Page No. – Page No.

Title

Text for Table of Contents